EFFECTIVE DESIGN AND CONTROL OF FULL DEPTH RECLAIMED PAVEMENTS

by

Peter James Salah

Submitted in partial fulfilment of the requirements
for the degree of Master of Applied Science

at

Dalhousie University
Halifax, Nova Scotia
July 2013

TABLE OF CONTENTS

LIST OF TABLES

LIST OF FIGURES

ABSTRACT

The traditional method of repairing damaged roads in Atlantic Canada has been to place a hot mix asphalt overlay over the existing road. Though this method provides a new, smooth wearing surface to drive on, it is merely a short term fix. With time, the cracks in the original pavement will reflect to the surface of the new pavement, resulting in failure of the overlay. An alternative option gaining more prominence is the use of a Full Depth Reclamation (FDR) technique, which involves pulverizing the flexible pavement, along with a portion of the underlying layer. This material is then stabilized and recompacted to produce a new base layer that is free of damage.

Though FDR has been used for a number of years, there are still problems with variability in the strength of the materials in some projects. It is hypothesized that some of these problems are due to variability and poor quality in the reclaimed materials. It is believed that current pulverization methods contribute to the variability being observed in these materials. Two FDR projects employing different pulverization control methods were studied to examine how the consistency of the reclaimed materials can be improved through the use of a Ground Penetrating Radar (GPR) survey to map the variability in the depth of the pavement. Controlling the thickness ratio of asphalt concrete to granular base materials being pulverized was shown to improve the consistency of materials, properties, and performance.

The second phase of this research project studied how improving the gradation of the reclaimed materials with the addition of a crusher dust might result in improved performance of stabilized base materials, in this case stabilized with expanded asphalt. The effect of construction variability on the improved materials was also studied by varying both the moisture content, and asphalt content from optimum conditions, as might be expected during construction. Results indicated that the quality of the stabilized FDR materials can be significantly improved by bringing the material gradation closer to the theoretical maximum density gradation. The performance of the stabilized materials can be affected by both the mixing moisture content, and the asphalt content used during stabilization. This suggests that effective quality control, and stricter specifications on the constructed product would result in more reliable, effective FDR pavements.

LIST OF ABBREVIATIONS AND SYMBOLS USED

a, b, c	Master curve shift factor calibration values
AASHTO	American Association of State Highway and Transportation Officials
ADT	Average daily traffic
$(ADT)_o$	Average daily traffic at the start of the design period
A_1	Amplitude of surface reflection
A_2	Amplitude of reflection at the surface of the base layer
a_i	Structural coefficient for layer i
A_m	Amplitude of reflection off copper plate
a(T)	Master curve shift factor, as a function of temperature
B_D	Bulk density
BSM	Bitumen stabilized material
°C	Degrees Celsius
C	Laboratory field adjustment factor
c	Speed of light in free space, 0.3 m/ns
C_1, C_2	Depth factors
CBR	California Bearing Ratio
CD	Crusher dust
d	Selected sieve size
D	Maximum particle size
D_i	Thickness of layer i
d_{spec}	Specimen diameter
|E*|	Dynamic modulus
$ELTS_i$	Effective long term stiffness value of layer i
ESAL	80 kN equivalent single-axle load
ER	Expansion ratio
°F	Degrees Fahrenheit
FDR	Full Depth Reclamation
g	Gram, 10^{-3} kg
G	Growth factor

GPR	Ground Penetrating Radar
GWT	Ground water table depth
h	Layer thickness
h_{ac}	HMA layer thickness
h_{spec}	Specimen height
HL	Half life
HMA	Hot Mix Asphalt
Hz	Hertz
I_1, I_2	Constants for resilient modulus calculations, based on gauge length
ITS	Indirect tensile strength
ITS_{dry}	Dry indirect tensile strength
ITS_{wet}	Soaked indirect tensile strength
K_0	Coefficient of earth pressure at rest
k_1	Confining pressure correction factor
k'_1	Layer thickness effect correction factor
kg	Kilogram
km	Kilometre, 10^3 m
kN	Kilonewton, 10^3 N
kPa	KiloPascal, kN/m^2
L	Lane distribution factor
lb	Pound force
L_{samp}	Sample length
LVDT	Linear Variable Differential Transducers
M	Mix factor
m	Metre
MC_{red}	Reduction of moisture content from optimum mixing moisture content
m_i	Drainage coefficient
mm	Millimetre, 10^{-3} m
MPa	MegaPascal, N/mm^2
M_R	Resilient modulus
M_{spec}	Mass of specimen

MTD	Maximum relative theoretical density
N	Newton
n	Grading coefficient, usually taken as 0.45
NCHRP	National Cooperative Highway Research Program
$N_{f,allow}$	Number of load applications to cause fatigue failure in an HMA layer
N_r	Number of load applications
ns	Nanosecond, 10^{-9} seconds
OMC	Optimum moisture content of an untreated material
P	Percentage by mass of material passing sieve size "d"
PC	Portland cement
$P_{contact}$	Contact load
PN	Pavement number
PSI	Pavement serviceability index
psi	Pounds per square inch
P_{max}	Maximum applied load
RAP	Reclaimed asphalt product
S_0	Standard deviation for a given level of reliability
$S_{contact}$	Contact stress
S_{max}	Maximum applied stress
SN	Structural Number
T	Temperature
t	Percentage of trucks in the ADT
t_2	Two-way travel time, ns
t_f	Number of 80 kN single-axle load applications per truck
t_{spec}	Specimen thickness
TSR	Tensile strength ratio
V	Electromagnetic pulse velocity through material in question
V_a	Air voids
V_b	Effective asphalt cement content
VMA	Voids in the mineral aggregate
W_{samp}	Sample width

W_c	Water content
Y	Design period in years
z	Depth below ground surface
Z_R	Normal deviate for a given reliability level
α	Difference between maximum and minimum |E*|
β_1	Calibration factor. 1.673 for unbound granular materials. 1.35 for subgrade materials
β_2	Material property factor
β, γ	Parameters describing master curve sigmoidal function
γ	Unit weight of material
ΔPSI	Change in pavement serviceability index during design period
δ	Minimum value of |E*|
δ_a	Permanent deformation of the layer
δ_{avg}	Average recoverable deformation
δ_h	Recoverable horizontal deformation
ε	Dielectric constant of material in question
$\|\varepsilon^*\|$	Average strain magnitude
ε_1	Dielectric constant of surface material
ε_2	Dielectric constant of base material
ε_p	Accumulated plastic strain at N_r repetitions of load
ε_r	Resilient strain of the HMA at the mid depth of the layer
ε_t	Horizontal tensile strain at the bottom of the HMA layer
ε_v	Vertical strain at the midpoint of the layer
$\frac{\varepsilon_0}{\varepsilon_r}$	Material property factor
θ	Friction angle of granular material
θ_{inv}	Stress invariant
μ	Poisson's ratio
Π	Pi
ρ	Material property factor

$\|\sigma^*\|$	Stress magnitude
σ_1	Major principal stress applied to BSM layer from mechanistic-empirical analysis
$\sigma_{1,f}$	Major principal stress at failure from triaxial testing of BSM
σ_3	Minor principal stress applied to BSM layer from mechanistic-empirical analysis
σ_r	Radial stress
σ_t	Tangential stress
σ_z	Vertical stress
τ_{max}	Peak shear stress
ω	Loading frequency
ω_r	Reduced frequency at master curve reference temperature

Acknowledgements

I would like to thank my supervisory committee: my supervisor, Dr. Nouman Ali, for his guidance, encouragement and support. Dr. Chris Barnes, for the countless hours spent planning, discussing, and reviewing my work. Dr. George Jarjoura for graciously taking the time to review this thesis.

I would also like to thank the Dalhousie Civil Technicians: Brian Kennedy, Jesse Keane, and Blair Nickerson for always being available at a moment's notice to solve whatever problems arose.

Completing a research project of this nature also required assistance, cooperation, and expertise from a number of companies. I would like to thank these companies for their contributions which made this research project possible:

- **AMEC -** For giving me access to their lab foaming equipment, as well as their technician's time and expertise teaching me how to use the equipment properly.

- **General Liquids Canada** - For providing free use of their Asphalt Pavement Analyzer, and their technicians time to help complete testing with it.

- **Industrial Cold Milling -** For providing the opportunity to run a Ground Penetrating Radar survey on their construction project, and supplying the materials used in this research project.

- **LVM Maritime Testing -** For giving me unlimited access to their lab facilities to complete a significant amount of material preparation and testing.

- **McAsphalt Industries -** For donating the asphalt cement used in this project.

CHAPTER 1: INTRODUCTION

A deteriorating network of aging roads and highway infrastructure continues to pose a serious problem to all levels of government throughout North America. In Canada, Dunlavy et al. (2009) estimated there are over 400 000 km of two-lane equivalent paved roads which require continual funding to maintain. Although this network of roads across the country is an important component of the national economy, necessary maintenance has been continually deferred, and annual highways budgets are well short of what is required. Mirza (2007) found that at the municipal level, an extra $21.7 billion above the $7.3 billion spent in 2005 was required to maintain and upgrade existing transportation infrastructure.

Barnes (2008) stated that the problems with roadways are not purely budget related. Many roads were constructed based on dated design methods. Empirical design methods that may not have accurately reflected the true behaviour of the materials have been commonly used for many years. This issue, compounded by rising traffic levels and increased tire pressures, has led to the premature failure of many asphalt concrete pavements.

The cause of this increasing discrepancy between required and applied maintenance is a combination of several factors. Poor planning and maintenance strategies, insufficient investment, and inadequate designs have all contributed to the progressive deterioration of the national pavement network. It has become clear that the current infrastructure maintenance model is unsustainable.

While this thesis does not attempt to address the issue directly, a brief explanation of the factors that lead to damaged pavements requiring rehabilitation will be presented. The drawbacks of conventional pavement rehabilitation strategies will be also briefly discussed. The main focus of this thesis is on a rehabilitation option involving a Full Depth Reclamation (FDR) technique, which will be presented in detail. FDR is a

rehabilitation strategy that utilizes recycled materials, eliminates all existing damage in a pavement structure, and leads to a strengthened base layer.

Effectively designing and controlling the quality of these FDR pavements was the focus of the research project, and the research program and results will be detailed. If used effectively and successfully, FDR could play a large role in helping address the deteriorating infrastructure issues discussed in an economical fashion.

1.1 Scope of the Problem

A number of factors contribute to the accumulation of damage in a pavement. Repeated loads, excessive loads, poor materials or construction, and varying environmental conditions can all be contributing factors. The cause of distress can typically be established based on the type of damage; whether it is a form of cracking, distortion, or disintegration.

As described in Huang (2004) and Roberts et al. (1996), cracking in an asphalt pavement can appear in a number of forms. The types of cracks that can appear in an asphalt pavement include:

- alligator cracking
- transverse cracking
- longitudinal cracking
- block cracking
- reflection cracking
- slippage cracking

A crack in an asphalt pavement could indicate the pavement has experienced structural failure. The crack could also allow water to infiltrate the pavement materials which, combined with cycles of freezing and thawing, and repeated loads, would lead to the progressive deterioration of the layer. Cracks are also a functional concern as they could affect smoothness and rideability. The ability of a vehicle to safely and efficiently travel on the asphalt pavement is impacted by the level of cracking in the layer. These concerns make it important to address cracking issues in asphalt pavements.

Cracking can be caused by pavement stress from repeated axle load applications, moisture conditions, temperature fluctuations, poor construction, and a number of other issues. To determine the root cause of the crack, a thorough pavement distress survey must be completed.

Distortion occurs when the pavement surface experiences plastic deformations. Rutting and shoving are examples of pavement distortion. Huang (2004) described rutting as a depression in the wheel path caused by further densification of the Hot Mix Asphalt (HMA), overstressed subgrade soil, or where a shear failure has occurred. Roberts et al. (1996) stated that shoving is the result of shear flow between layers often caused by an unstable mix, or slippage between layers. While distortion is mainly a functional concern affecting rideability, it could also lead to safety concerns. Ruts in the pavement could fill with water after a rainfall, resulting in the potential for hydroplaning. Severe ruts could also lead to structural failure. Therefore it is important to rehabilitate pavements with excessive plastic deformation.

Disintegration of the HMA layer can be caused by improper material properties such as poor gradation or low density. Ravelling, a form of disintegration, is due to dislodgement of the aggregate particles. It is caused by a number of factors such as an overly thick coating of fine dust on the aggregate, segregated areas of the road with low fines content, or low in-place density of the HMA surface layer. Excessive wear on the surface from repeated traffic loads could also lead to deterioration. This process is accelerated when there are loose particles on the pavement surface that act as an abrasive. Stripping of the asphalt cement from the surface of the aggregate is also a common cause of disintegration, as there is a loss of bond between aggregates and asphalt cement. Disintegration can lead to problems such as ponding water, reduced skid resistance, and loose aggregate being thrown up by the tires of moving vehicles. It is important to identify and address disintegration issues in asphalt pavements.

The cause of damage should be established prior to proceeding with rehabilitation of the pavement. If a thorough distress survey is completed, the root cause of the problem can

be determined, and the design of the rehabilitated pavement can take into account these issues to ensure that the same problem will not reoccur.

Conventional rehabilitation strategies may include complete reconstruction, a "mill-and-fill" approach, placing an HMA overlay over the existing pavement, or using an inverted section design. Although complete reconstruction is the most effective approach, it is also the most costly option as it involves removing and rebuilding the entire pavement structure. A "mill-and-fill" approach entails pulverizing the asphalt layer and placing a fresh HMA layer over the milled surface. This is an effective option when the damage is limited to the asphalt concrete, and not the underlying layers.

Placing an HMA overlay over the existing pavement is a common approach, though it is not generally an effective rehabilitation strategy. If placed at the right time, before the existing pavement is excessively damaged, it can lengthen the service life of the pavement. If an overlay is placed over a heavily damaged asphalt pavement, as is commonly done, this will only temporarily solve the problem. The existing damage results in a localized reduction in stiffness leading to stress concentrations in the overlay. With time, the existing damage in the original pavement will propagate to the surface of the new pavement, known as reflective cracking. The HMA overlay strategy may appear the most appealing given the lower initial cost and quick results, but it is not sustainable in its current form.

An inverted section design, often referred to as a "gravel sandwich" approach, involves milling a portion of the existing pavement, and placing a thick layer of Type 1 gravel on the milled surface. An HMA layer is then constructed on top of the gravel layer. While this method can effectively minimize the risk of reflective cracking, it is not always a feasible option due to the large increase in elevation of the roadway caused by the addition of the gravel and new HMA layer over the old pavement.

Given the worsening quality of numerous rural highways in Nova Scotia and across Canada, there is a strong need for a reliable, cost effective pavement rehabilitation

method. There is also a need for a more sustainable rehabilitation method. Holt et al. (2009) noted that the conventional rehabilitation strategies described require non-renewable resources including quarried aggregates, asphalt cement, and fuel for transportation. The waste materials from construction also require large amounts of space in landfills. These environmental concerns, combined with the performance and financial concerns previously described, have led to the increased use of an FDR approach.

FDR is a pavement rehabilitation method that has been used with success in regions around the world for a number of years. The FDR process has been, and continues to be the subject of much research work as it provides an environmentally friendly, cost-effective means of rehabilitating old roads.

The process involves pulverizing the full depth of the flexible pavement layer, along with a portion of the underlying granular base, adding a binder to the pulverized materials, and then recompacting it to produce a new, stabilized base layer. This base layer, which is free from any previously existing damage, can then be surfaced using HMA or another material to act as a wearing surface. If done properly, the end result is a damage free, strengthened base to support traffic loading.

While the FDR process has the potential to be an important part of an agencies overall rehabilitation strategy, poor performance on some FDR sections has limited its use. It is believed that variability in the properties of the pulverized materials could lead to inconsistent performance of some FDR sections. A reliable design procedure is also important in ensuring the performance of the FDR materials. The Wirtgen Group (2010) and the Asphalt Academy (2009) have published design guides that detail the mix design, structural design, and construction of FDR pavements. Many agencies use these guidelines in specifying standard procedures for FDR projects; however it is believed that a high tolerance in specifications on the end product could have a negative impact on the quality of the FDR sections.

Scullion et al. (2003) in a survey of districts in Texas found some agencies reported that a combination of longitudinal and transverse cracking was leading to increased and unacceptable pavement roughness on some Portland cement stabilized FDR sections. Barnes (2010) stated that some of the Portland cement stabilized FDR projects in Nova Scotia have experienced centreline, transverse, and shoulder edge cracking. As a result of these problems, the Nova Scotia department of Transportation and Infrastructure Renewal have continued to review the viability of continuing with Portland cement stabilized FDR projects.

Alternatively, some FDR pavements, when compared to conventional maintenance strategies, have exhibited superior performance. Lane & Kazmierowski (2012) reporting on a section completed near Wawa, Ontario found that ten years after construction, the expanded asphalt stabilized FDR section continues to perform very well with minimal cracking and an extremely low degree of roughness. This project serves as evidence that when constructed properly, FDR has to potential to be a superior, economical alternative to conventional rehabilitation strategies. Other reports of successful FDR projects supporting this claim have appeared in literature including a number of projects in California reported by Jones et al. (2008), and projects in Minnesota reported by Eller & Olson (2009).

Taking into consideration the benefits of utilizing an effective FDR rehabilitation strategy, a research project was launched to further investigate the FDR process. A reliable mix design method, coupled with the ability to better control the consistency of the pulverized material, could greatly improve the quality of the FDR pavements. FDR, used in conjunction with conventional rehabilitation strategies where appropriate, could then become a more prominent and effective rehabilitation option.

1.2 Research Objectives

This research project was part of a larger overall study of FDR materials. The work completed in conjunction with this study examined the effect of blend ratio, or the

thickness ratio of reclaimed asphalt to total material pulverized, on the quality of the FDR materials. The objective of this research project was to build upon previously completed work and develop a more effective method of designing these pavement materials and controlling the quality of the end product. To accomplish these objectives, the work would be completed in two phases.

The first phase of this research project would involve studying a method of controlling the consistency of pulverized FDR aggregates. To do this, a Ground Penetrating Radar (GPR) survey was completed on a section of Route 790 near Lepreau, New Brunswick that was scheduled to be rehabilitated. The GPR survey would provide information on pavement thicknesses, and the section could then be divided into different subsections of pulverization depths to maintain an approximately consistent blend ratio. Samples taken from various sections within this construction project would then be subjected to a series of tests to evaluate the consistency of the pulverized material.

The second phase of this research project would involve examining the impact of using corrective aggregate on these pulverized materials to improve the gradation and associated properties. Expanded asphalt stabilized FDR mixes would be tested with the gradation as pulverized, and after having been improved with corrective aggregate. One of the goals of this research project was also to study the effect of construction variability on the performance of the mix. This was examined by varying the asphalt content and moisture conditions from the theoretically optimum values.

Accomplishing these research objectives would result in a better understanding on how to control, and improve the quality of FDR pavements. The ability to produce higher quality FDR pavements could lead to the more widespread use of this alternative rehabilitation strategy.

1.3 Report Outline

Chapter 2 of this report presents a review of full depth stabilized base design and practice. This review includes information on the selection of FDR as a rehabilitation strategy, relevant material properties, mix and thickness design, construction, and performance evaluation.

Chapter 3 details the laboratory testing program used to complete the research objectives of this project.

Chapter 4 presents the results from both phases of the research program, as well as a discussion of the results.

Chapter 5 summarizes a series of pavement analyses completed to describe the research results in a practical way. Specifically, a standard pavement design was completed for each FDR mix so that the different minimum design requirements could be compared. From these pavement designs, a basic cost analysis was completed. A Mechanistic-Empirical analysis was also completed on a separate pavement structure to evaluate the variation in service life of pavements using each FDR mix.

Chapter 6 offers conclusions and recommendations deducted from this study, as well as recommendations for future research.

CHAPTER 2: REVIEW OF FDR PAVEMENT DESIGN AND PRACTICE

This chapter details the current state of knowledge on the FDR process. Material properties, stabilizer options, mix design methods, construction processes, and methods of predicting performance will be discussed. While the report includes information on a variety of topics related to all types of FDR pavements, emphasis is placed on subjects relevant to expanded asphalt stabilized FDR, as that was the focus of this research project.

2.1 Background

Rehabilitation using FDR is often used in areas where virgin materials may not be readily available, or where the existing pavement and subgrade has experienced substantial damage. With this technique, the full depth of flexible pavement, along with a predetermined amount of underlying granular materials, is pulverized. This material is then stabilized, and recompacted. If done successfully, the end result is a damage free, strengthened base layer, which is then overlain with a layer to act as a wearing surface. With the ability to recycle material, remove existing damage, and construct a strengthened base layer, the FDR approach appears to be a more sustainable approach to maintaining pavement systems when compared to conventional rehabilitation strategies.

2.1.1 Candidates

Proper road selection is critical in ensuring success with the FDR process. The original pavement should be evaluated to determine the cause of distress. For simple surface defects or deformations, hot in-place or cold in-place recycling may be adequate. Hot in-place recycling is a process in which the surface is softened with heat, scarified, and recompacted. Stroup-Gardiner (2011) stated that this approach is most effective in repairing distresses near the surface of the asphalt concrete layer. Cold in-place recycling is a similar process; however the asphalt concrete remains at its current temperature when

it is pulverized. Cold in-place recycling is effective in repairing distresses occurring in the upper 2 to 4 inches of the asphalt concrete layer; however it does not address deeper distresses or subgrade issues.

Kearney & Huffman (1999) described roads with deep cracks, potholes, and particularly those with subgrade problems as good candidates for FDR. Halsted (2010) offered the following guidelines on when it is appropriate to use FDR:

- full depth patching required over greater than 15-20 % of the surface area
- greater structural capacity required
- existing distress indicating problem is a function of base or subbase failure
- existing damage so serious that a simple resurfacing approach will not address the problems

In addition to evaluating the original cause of distress, traffic levels should also be considered. Chemical stabilizers, for example, require varying amounts of time to gain strength. This could pose problems on high volume roadways where it is not feasible to keep traffic off while the material cures. Other stabilizers or rehabilitation methods should be investigated in these situations. The decision to use FDR as a rehabilitation method should be made after considering all relevant factors, and ensuring it is the most appropriate option.

2.1.2 Advantages

There are numerous advantages to using FDR as opposed to using other pavement rehabilitation methods. Both environmental and financial benefits are realized when FDR is used. When compared to other pavement rehabilitation methods, FDR provides structural benefits as well.

Since the entire depth of flexible pavement as well as a portion of the base layer is pulverized, all existing damage is removed. Ruts, cracks, and any other damage in the existing pavement will be eliminated when the materials are pulverized and recompacted. When HMA overlays or other recycling methods are used, existing damage may not be

completely removed and the remaining damage may lead to a localized reduction in stiffness resulting in stress concentrations in the overlay around the existing cracks. These high stress concentrations eventually lead to new cracks forming and propagating to the surface of the new layer.

Environmental benefits are the result of a reduction in the need for virgin aggregates, and elimination of waste materials. This has factored into the decision to use FDR in many areas, where good quality aggregate may not be readily available. There is also a reduction in emissions which are generally associated with the transportation of both new and waste materials.

Financial savings are the result of reduced trucking costs and virgin aggregate requirements. Aside from financial savings due to reduced aggregate requirements, there are also financial savings related to the reduced need for asphalt cement. Depending on the stabilization method chosen, the amount of asphalt cement used could be substantially reduced, or altogether eliminated. Given the instability in the cost of asphalt cement, this is extremely beneficial. Figure 2-1 shows that, even since 2006, the cost of asphalt cement per tonne in Nova Scotia has been increasing, and is volatile. These are trends that are unlikely to change.

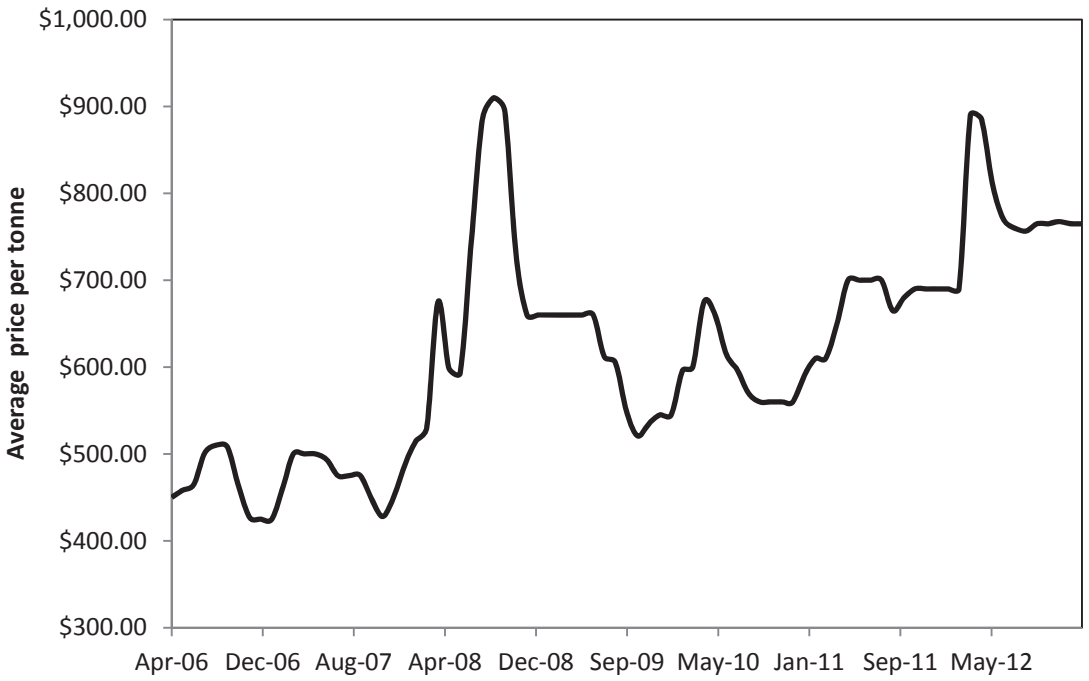

Figure 2-1 PG58-28 asphalt cement rack price over time in Nova Scotia (adapted from NSTIR, 2013)

Marquis (2007) stated that construction costs can be reduced by as much as 25 to 50 percent compared to conventional rehabilitation methods. The actual amount of savings would vary depending on a number of factors including proximity of the section to nearby quarries, stabilization method, and quality of the materials being reclaimed. If constructed successfully, the combination of structural, environmental, and financial benefits make FDR an economical rehabilitation strategy.

2.2 Material Properties

The performance of the FDR base is largely affected by the physical properties of the recycled materials. Testing on the material prior to, and following stabilization is necessary to understand how the material will behave in service.

2.2.1 Unbound Material Tests

Unbound material tests include gradation, moisture-density relationship, maximum relative theoretical density, resilient modulus, direct shear, and California Bearing Ratio (CBR). These tests are described in further detail in the following sections.

2.2.1.1 Gradation

Gradation plays a large role in the strength, stiffness, and moisture susceptibility of the stabilized material. Maximizing density is important in FDR pavements, as these materials rely on inter-granular contact to transfer loads. A tightly compacted FDR pavement outperforms one with low compaction and a high air void content, as it has increased load transfer ability and reduced stresses exerted on the subgrade.

The Asphalt Academy (2009) stated that the gradation resulting from pulverization is affected by a number of factors including:

- degree of oxidation of the reclaimed material
- existing pavement thickness
- original asphalt mix
- geometry and amount of cracking
- condition of bonding between any overlays
- equipment
- asphalt temperature during recycling process

The optimum gradation to achieve maximum particle packing can be computed using Equation 2.1, presented by Roberts et al. (1996), which was first developed by Fuller and Thompson in 1907. This equation utilized a grading coefficient, n, of 0.5. This was later modified by the Federal Highways Administration in the 1960s to use a grading coefficient of 0.45. The size distribution produced by this equation should minimize the Voids in the Mineral Aggregate (VMA), maximizing density, strength, modulus, stability, and a number of other properties.

$$P = \left(\frac{d}{D}\right)^n \text{ x } 100 \qquad \textbf{[2.1]}$$

where:

P = percentage by mass of material passing sieve size "d"
d = selected sieve size
D = maximum particle size
n = grading coefficient, usually taken as 0.45 (Roberts et al., 1996)

An example of the optimal gradation is shown in Figure 2-2. Equation 2.1 was applied to a theoretical mix with a maximum particle size of 25 mm, which is typical of FDR projects, and the resulting ideal gradation is shown. Although particles larger than 25 mm can be found in FDR materials after pulverization, it is typically required that these oversize particles be removed from the surface of the work, as these oversize aggregates would have a negative impact on the quality of the compacted base, making it difficult to compact to a high density.

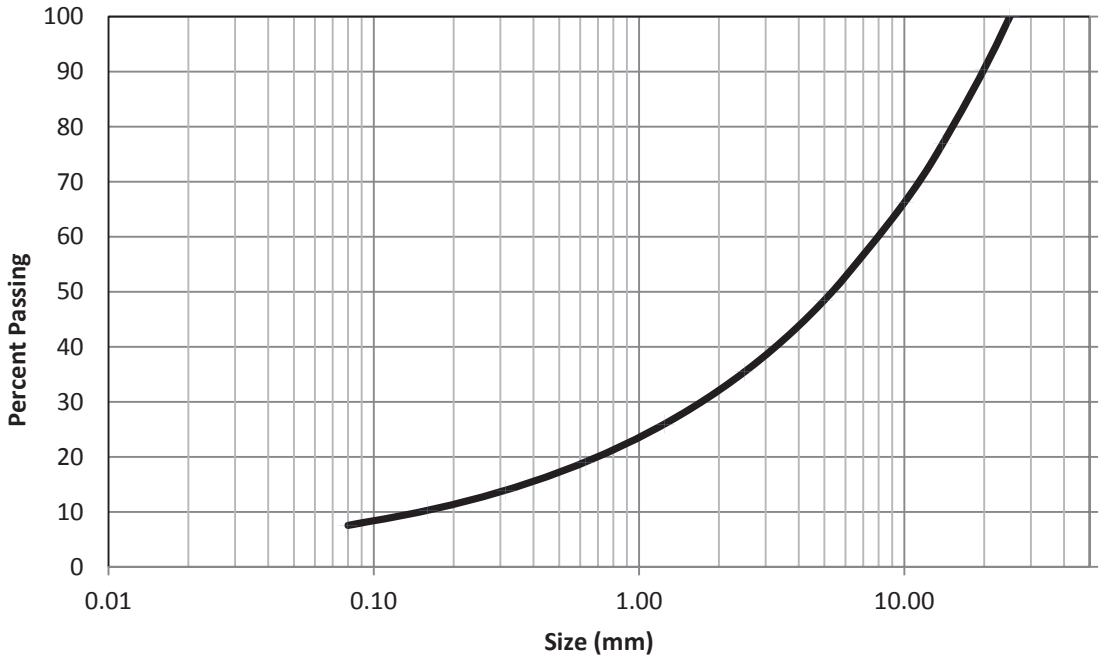

Figure 2-2 Optimal size distribution of a material with a 25 mm maximum particle diameter

A review by Dewar (2002) noted that multiple researchers have criticized the ideal gradation approach, stating that the approach only considers size distribution, and not the shape and texture of the particles. It is also difficult to replicate these gradations in the field. Therefore while this relationship has been found to produce a size distribution optimal for particle packing, it is often more feasible to establish gradation limits, in which the targeted gradation of a material falls within a limited range of values.

Most state agencies do not have a rigorous specification on gradations. Often times only the maximum particle size, percent passing the 5 mm sieve, and percent passing the 0.080 mm sieve are regulated, though tighter restrictions on size distribution would likely improve the end product. In Nova Scotia, the specifications shown in Table 2-1 are placed on the gradations of expanded asphalt stabilized FDR.

Table 2-1 Nova Scotia grading specifications for expanded asphalt FDR mixes (NSTIR, 2012)

Sieve Designation (mm)	Cumulative Percent Passing
40.0	98 - 100
25.0	95 - 100
5.0	35 - 65
0.630	15 - 40
0.080	7 - 15

Reflective of the variability often found in the gradations of the pulverized materials, there is a high tolerance for variability in the specified gradation requirements. This has likely contributed to the poor performance of some of the FDR pavements. While individual agencies are often relatively lenient in the gradation specifications of FDR materials, Wirtgen Group (2010) offered guidance on specific gradation limits for expanded asphalt stabilized materials, which are shown in Figure 2-3. Materials with a size distribution falling within these limits are described as the most suitable for expanded asphalt stabilization.

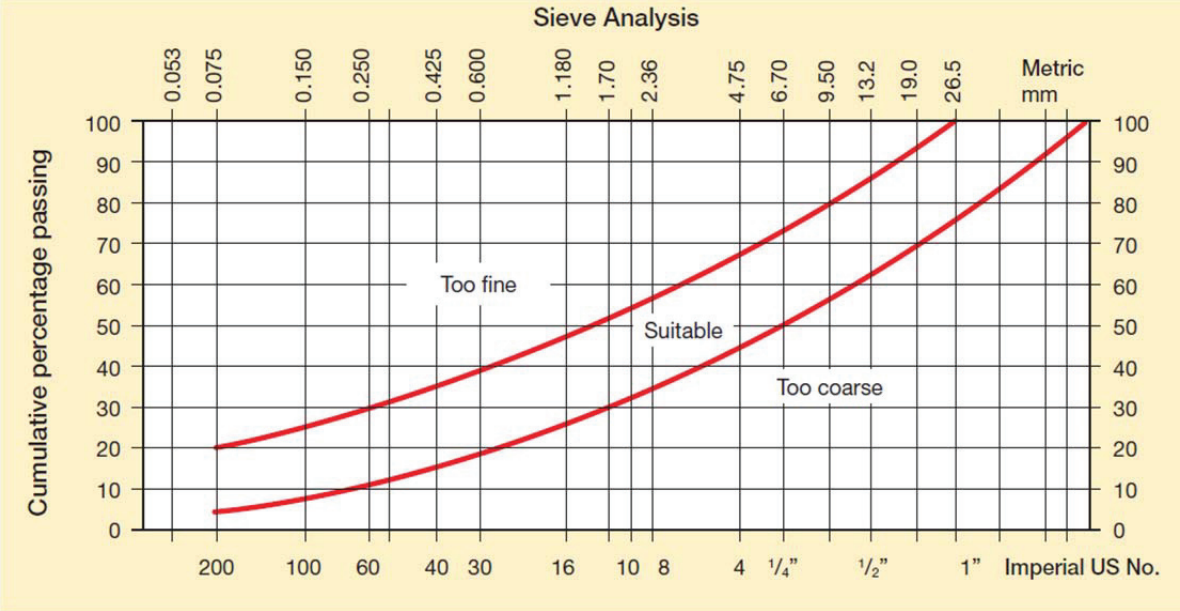

Figure 2-3 Recommended FDR gradation limits for expanded asphalt stabilization (Wirtgen Group, 2010)

It is not clear whether these limits are based on a size distribution of the unbound FDR materials after the asphalt cement has been extracted, or if it is based on the conglomerate particles that would exist in the material with old asphalt cement binding finer particles together. This is an issue which will be re-examined in Section 4.1.1. Based on the information available, it is evident that more research is needed on the effect of gradation on FDR, and how to better control it.

2.2.1.2 Moisture-Density Relationship

The in-place density of the FDR base has a large effect on the performance of the layer. The moisture-density relationship must be determined in order to establish optimum moisture content and maximum dry density for placement. Coduto (1999) in describing the effect of increasing moisture content stated that the water would provide lubrication to soften particles and reduce surface tension in the soil. With too much water, there is very little air left in the soil, thus making it difficult to compact, since the extra moisture keeps particles apart. For these reasons, a typical moisture-density curve will be as

shown in Figure 2-4, and this is why testing must be done to determine the optimum moisture content.

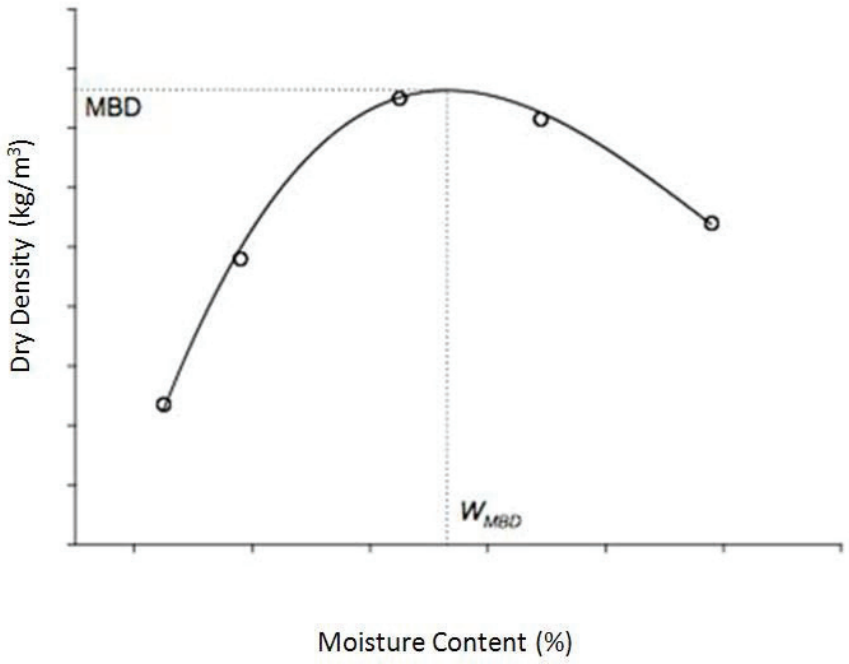

Figure 2-4 Typical soil moisture-density relationship (adapted from University of British Columbia, 2011)

If the layer is not sufficiently compacted, problems with permanent deformation and moisture damage can be expected (Geiger et al., 2007). Optimum density can be determined by following procedures outlined in either ASTM D698 for standard Proctor effort, or ASTM D1557 for modified Proctor effort, depending on the specifications.

2.2.1.3 Maximum Relative Theoretical Density

The Maximum Relative Theoretical Density (MTD) provides a measure of the maximum possible density of the materials, with zero air voids between the particles. This MTD provides a reference for determining the actual amount of air voids in the field compacted mix, compared to the maximum dry density determined from moisture-density testing which serves as a target density during compaction.

2.2.1.4 Granular Resilient Modulus

The resilient modulus of granular materials is analogous to Young's modulus in elastic materials. It is a measure of the amount of resilient, or recoverable, strain in a material subjected to a repeated load. Granular resilient modulus can be determined in the laboratory using the AASHTO T307 test procedure. This test subjects the material to different stress states by varying the confining pressure and applied loads in order to simulate the physical conditions of a granular material underneath a flexible pavement layer. The test configuration is shown in Figure 2-5.

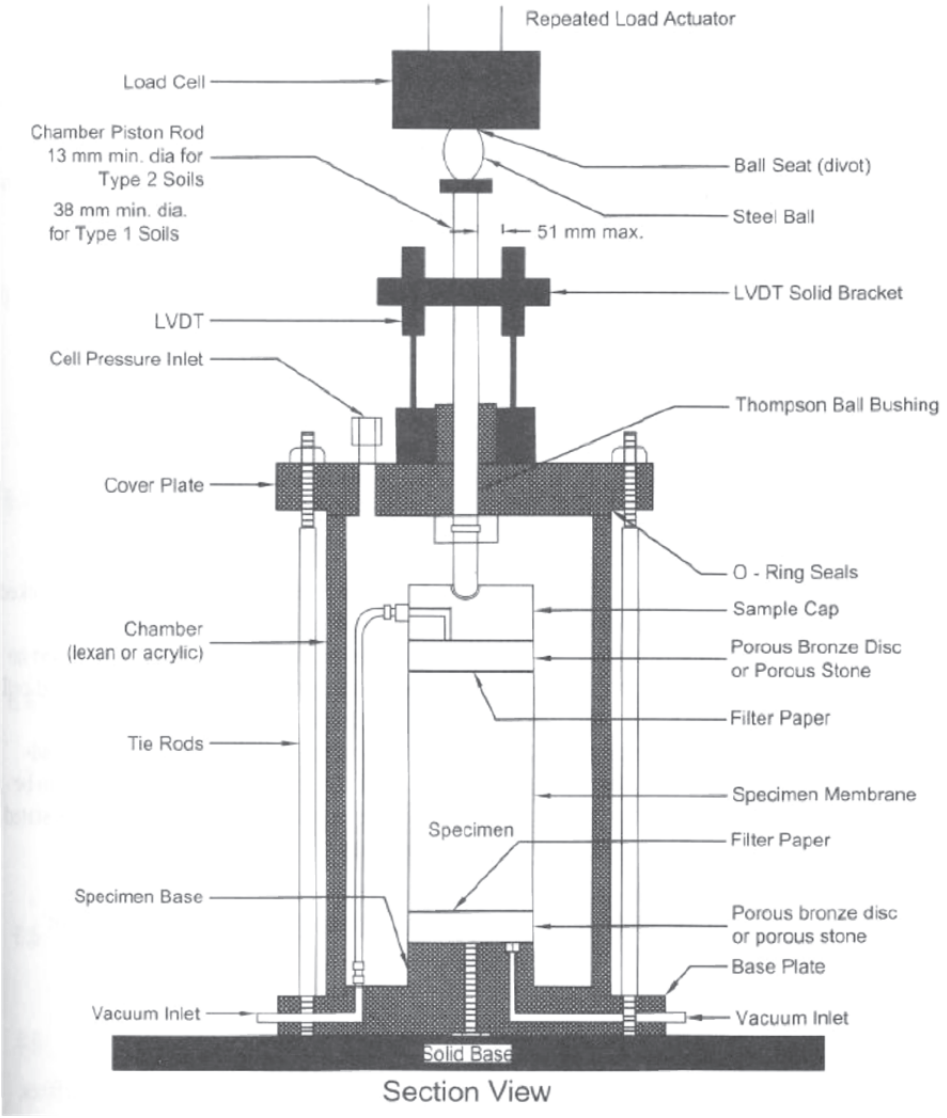

Figure 2-5 Granular resilient modulus test configuration (AASHTO, 2007b)

A cylindrical specimen 150 mm in diameter, 300 mm in height, and contained by a rubber membrane is placed in a triaxial chamber. Different methods can be used to compact the sample, however vibratory compaction has proven to give satisfactory results. Air is used to apply a confining pressure to the sample within the membrane, and a servo-hydraulic loading machine applies repeated compressive haversine load pulses. The different loads, as specified by AASHTO T307, are applied for 0.1 seconds followed by a 0.9 second rest period. Two Linear Variable Differential Transducers (LVDT's) are used to measure axial deformation. Once all test sequences have been completed, Equation 2.2 is used to calculate resilient modulus for each value of stress invariant as a combination of confining pressure and applied load.

$$M_R = \frac{(S_{max} - S_{contact}) * L_{samp}}{\delta_{avg}} \quad \textbf{[2.2]}$$

where:

M_R	= resilient modulus	(MPa)
S_{max}	= maximum applied stress	(MPa)
$S_{contact}$	= contact stress	(MPa)
L_{samp}	= sample length	(mm)
δ_{avg}	= average recoverable deformation	(mm)

The stress invariant is a measure of the combined effect of the normal stresses applied to the material at a selected point in the pavement system. The stress invariant can be calculated using Equation 2.3, as provided in Huang (2004), and this value can be used to select the combination of confining pressure and applied load in testing which best represents the expected service loading conditions. Evaluating the stress state of the material in service allows for the most appropriate resilient modulus value for design to be chosen.

$$\theta_{inv} = \sigma_z + \sigma_r + \sigma_t + \gamma z(1 + 2K_0) \quad \textbf{[2.3]}$$

where:

θ_{inv}	= stress invariant	(MPa)
σ_z	= vertical stress	(MPa)
σ_r	= radial stress	(MPa)
σ_t	= tangential stress	(MPa)
γ	= unit weight of material	(N/mm^3)
z	= depth below ground surface	(mm)
K_0	= coefficient of earth pressure at rest	

Sequences are provided for testing to be done on either base or subgrade materials. The AASHTO T307 test standard gives 15 testing sequences for each type of material.

2.2.1.5 Direct Shear Test

The direct shear test provides a measure of the shear strength of the material under different applied stresses. From the test results, the friction angle can also be determined. The test is completed on the apparatus shown in Figure 2-6. A sample is compacted into a large 12" x 12" box which is split in the centre, allowing the upper portion and lower portion to move relative to one another. The method of compaction used can vary, with kneading or tamping methods being acceptable. The sample is compacted in layers to a specified density, determined by measuring the mass of material used, and the volume of the shear box. The entire sample is subjected to a confining stress, accomplished by applying a normal (vertical) load on the box, and the lower portion is subjected to a constant horizontal displacement, forcing the sample to shear.

Figure 2-6 Direct shear testing apparatus

The applied load is recorded at intervals of one reading per minute, and the maximum load achieved is noted. Coduto (1999) stated that, unlike other materials such as steel or concrete, there is no specific rupture point in these materials. The test is often completed when the shear machine reaches its maximum displacement capacity, as some shear resistance always remains in the material, regardless of the amount of displacement. The peak shear stress at maximum displacement is determined by dividing load by area, as shown in Equation 2.4.

$$\tau_{max} = \frac{P_{max}}{L_{samp} * W_{samp}} \quad \textbf{[2.4]}$$

where:

τ_{max}	= peak shear stress	(kPa)
P_{max}	= maximum applied load	(kN)
L_{samp}	= sample length	(m)
W_{samp}	= sample width	(m)

Tests are done with a confining pressure of 50 kPa, 98.1 kPa, and 150 kPa applied. The maximum shear stress from each can be plotted versus confining pressure to form a straight line relationship. An example of this relationship is shown in Figure 2-7.

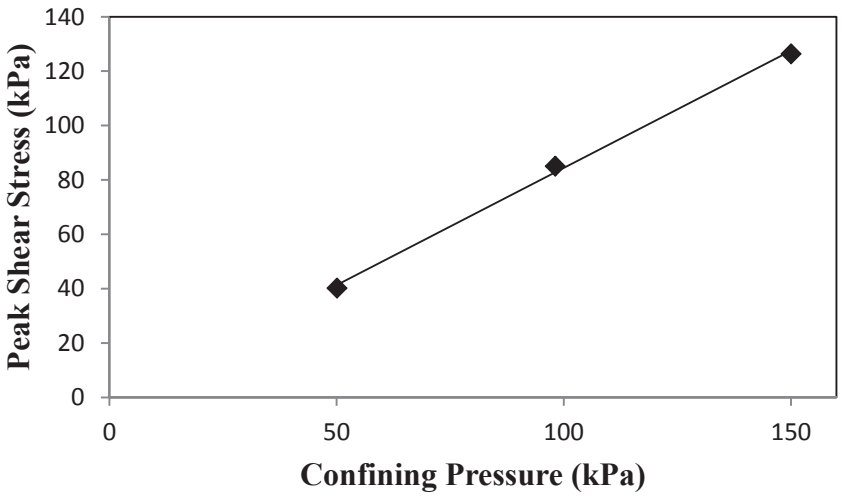

Figure 2-7 Relationship between confining pressure and maximum shear stress

This relationship is defined as the Mohr-Coulomb failure criterion. The straight line can be projected beyond the test data, with the intercept indicating the level of cohesiveness in the material. The slope of the straight line is the friction angle, θ, of the material (Coduto, 1999). The peak shear stress and the friction angle are important parameters in evaluating the strength of soils, and the Mohr-Coulomb failure criterion allows the test data to be related to the expected field conditions.

2.2.1.6 California Bearing Ratio

The CBR test is used to establish a relative measure of the strength of a granular material. Although the CBR value is an empirical number, correlations have been made between CBR and material performance, specifically the resilient modulus. This has made the CBR a common, and typically effective, value used in evaluating material quality. CBR is determined by measuring the amount of load required to force a piston to penetrate 0.1

inches and 0.2 inches into a compacted soil, while moving at a constant rate of displacement. Figure 2-8 shows the sample before and after the test has been completed.

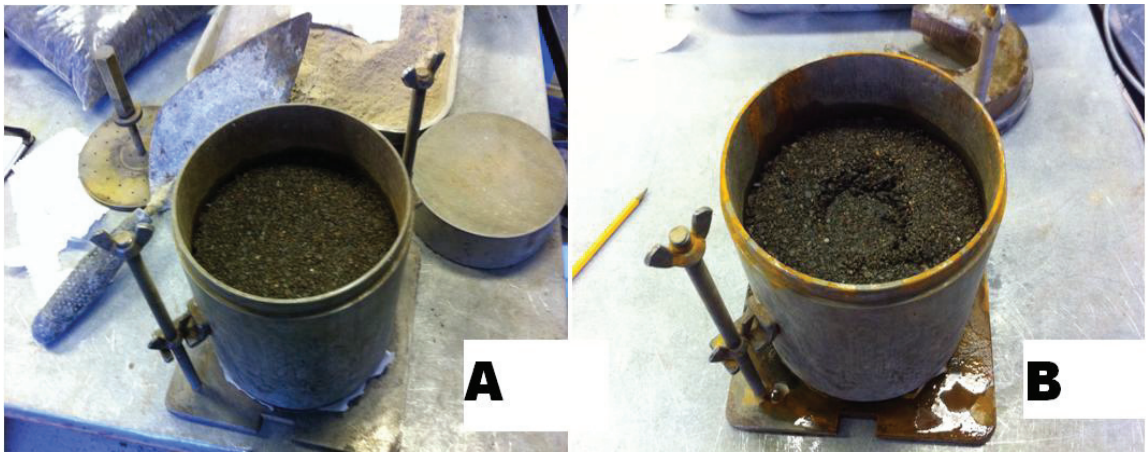

Figure 2-8 CBR sample (A) after compaction and (B) after testing

CBR can be found under both dry and soaked conditions, with the soaked CBR being the result after the compacted sample has been kept underwater for a period of 96 hours. The piston used is 49.63 mm in diameter, and 101.6 mm long. ASTM International (2007a) defined the CBR value itself as the percentage of strength of the material in question, to that of a standard material of well-graded crushed stone.

2.2.2 Stabilized Material Tests

Bound material tests include bulk density, Indirect Tensile Strength (ITS), resilient modulus, dynamic modulus, and rutting potential. These tests are described in further detail in the following sections.

2.2.2.1 Bulk Density

The bulk density of the material is a volumetric measurement, providing information on the level of compaction of the compacted specimen. The bulk density of the specimen is

the sample mass divided by volume. Equation 2.5, provided by Wirtgen Group (2010), is used to determine bulk density.

$$B_D = \frac{4 * M_{Spec}}{\Pi * d_{spec}{}^2 * h_{spec}} * 10^6 \quad \textbf{[2.5]}$$

where:

B_D	= bulk density	(kg/m^3)
M_{spec}	= mass of specimen	(g)
d_{spec}	= specimen diameter	(mm)
h_{spec}	= specimen height	(mm)

The bulk density is used to evaluate the consistency between samples compacted from the same mix. It can also be compared to the MTD of the material to estimate the air void content in the compacted specimen.

2.2.2.2 Indirect Tensile Strength

The ITS test is commonly used in both HMA and expanded asphalt mix designs. It is a popular test due to its simplicity, and short testing time. ASTM International (2007b) stated that the ITS test is used as a measure of the relative strength of a material, as well as to estimate the potential for rutting or cracking. The resistance of a mix to moisture damage can also be determined when testing is completed on both soaked and dry samples.

The ITS test as outlined in ASTM D6931 involves applying a compressive load along the vertical diametrical plane through two 12.7 mm wide loading strips, curved to match the 101.6 mm diameter specimen. This loading configuration results in a tensile force developing perpendicular to the load which forces the sample to split apart, as shown in Figure 2-9.

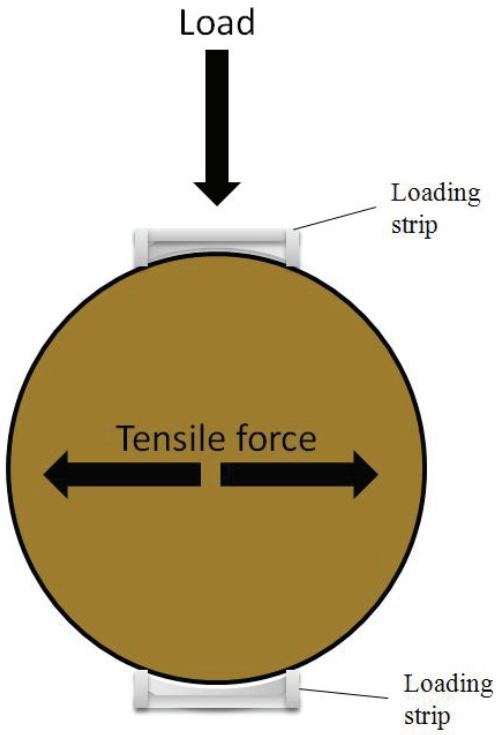

Figure 2-9 ITS load configuration

Load is applied at a uniform rate of displacement of 50.8 mm/minute, and the load at failure is recorded. ITS is then determined from Equation 2.6 (ASTM International, 2007b).

$$ITS = \frac{2000 * P_{max}}{\Pi * h_{spec} * d_{spec}} \quad \textbf{[2.6]}$$

where:

ITS	= indirect tensile strength	(kPa)
P_{max}	= maximum applied load	(N)
h_{spec}	= specimen height	(mm)
d_{spec}	= specimen diameter	(mm)

ITS can be determined under dry (ITS_{dry}) or soaked (ITS_{wet}) conditions. The ratio of ITS_{wet} to ITS_{dry} is known as the Tensile Strength Ratio (TSR), and can be used as a design criterion. A high TSR indicates the mix is not greatly affected by moisture, and is

therefore specified by agencies to ensure a pavement would not be excessively damaged when the material was saturated and subjected to loads.

In Nova Scotia, and typical of other jurisdictions, the specifications require minimum values of 300 kPa, 150 kPa, and 50 percent for ITS_{dry}, ITS_{wet} and TSR respectively. The ITS test is typically completed at 25°C, but can be performed at a range of temperatures as required.

2.2.2.3 Resilient Modulus

Similar to the granular resilient modulus, the resilient modulus is a measure of the stiffness of a material, and is one of the most important properties in designing a new pavement system, as well as evaluating the quality of an existing system. A material with a higher resilient modulus will exhibit less deformation under a given load than that with a lower resilient modulus. The distribution of loads in a system is also a function of this stiffness, and measured by the modular ratio, defined as the ratio of modulus between two adjacent layers (Geiger et al., 2007).

The resilient modulus of in-service pavements can be found using a back calculation technique following deflection testing (Huang, 2004). Lytton (1989) stated that the Falling Weight Deflectometer is the best device available for deflection testing, as it best simulates the magnitude and duration of moving loads, providing the most accurate results.

The laboratory determination of resilient modulus of stabilized material is determined using a similar configuration as that used with the ITS test. A repeated compressive load is applied along the vertical diametrical axis, resulting in a strain developing perpendicular to the load due to the indirect tensile force. A haversine load pulse, as shown in Figure 2-10, is repeatedly applied to the specimen. The load, approximately 10 to 20 percent of the ultimate ITS, is applied for 0.1 seconds followed by a rest period of 0.9 second, and the resulting displacement from the applied load is recorded.

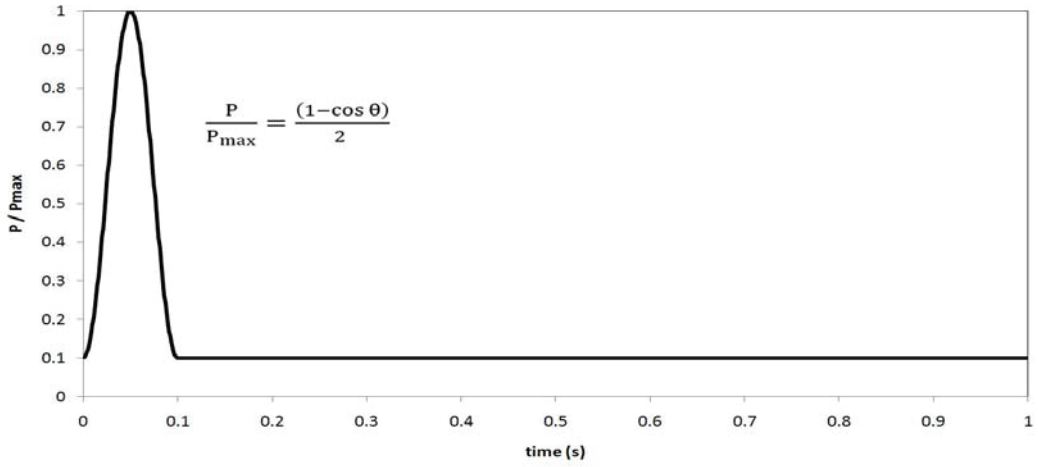

Figure 2-10 Haversine load pulse

Four strain gauges, as shown in Figure 2-11, are typically used to measure both horizontal and vertical deformation so that Poisson's Ratio (μ) can be calculated. For this research project, only two gauges were used to measure horizontal deformation, and Poisson's Ratio was estimated.

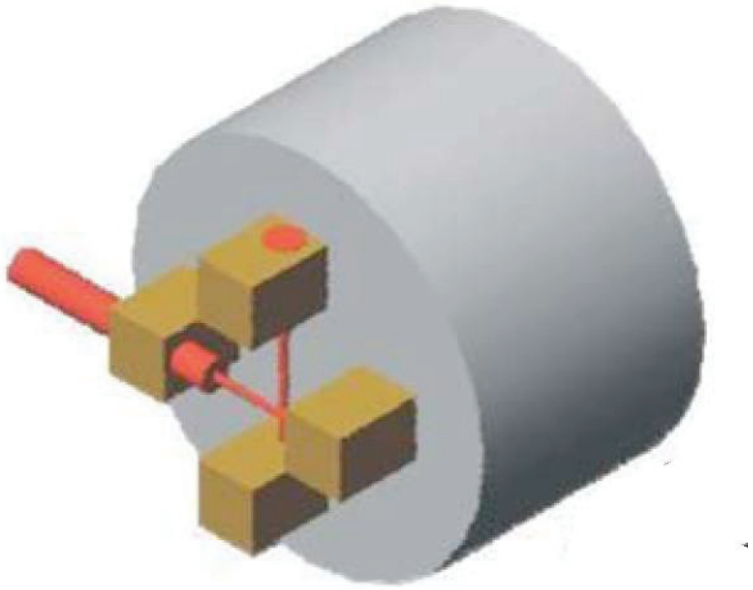

Figure 2-11 Resilient modulus test strain gauge configuration (ASTM International, 2009)

Christensen & Bonaquist (2004) described the disadvantage of using this setup, which is the assumption of isotropic behaviour, meaning the direction of testing and orientation of the particles are assumed to have no effect on the mechanical properties of the mix. In reality, there appears to be substantial anisotropic behaviour in the HMA materials, suggesting the direction of compaction may have an effect on its mechanical properties. Luo & Lytton (2010) stated that because of this anisotropy, testing done perpendicular to the direction of compaction may not yield results representative of field conditions.

Following testing, the load and horizontal displacement results are plotted and Equation 2.7, given in ASTM International (2009), is used to determine resilient modulus.

$$M_R = \frac{P_{max} - P_{contact}}{\delta_h * t_{spec}} * (I_1 - I_2 * \mu) \quad \textbf{[2.7]}$$

where:

M_R	= resilient modulus	(MPa)
P_{max}	= maximum applied load	(N)
$P_{contact}$	= contact load	(N)
δ_h	= recoverable horizontal deformation	(mm)
t_{spec}	= specimen thickness	(mm)
I_1, I_2	= given constant values, based on gauge length	
μ	= Poisson's ratio	

Liu & Li (2010) stated that resilient modulus is influenced by a number of factors including asphalt content, and temperature. The amount of asphalt cement in a mix, as well as the stiffness of the asphalt cement itself, have a large effect on the resilient modulus of the material. The resilient modulus varies greatly with temperature, with materials exhibiting a higher resilient modulus at lower temperatures. In order to study the effect of temperature on resilient modulus, testing can be completed at a number of temperatures; though to minimize the effect of permanent deformation, testing should first be completed at the lower temperatures.

2.2.2.4 Dynamic Modulus

The dynamic modulus test, described in AASHTO TP62, is used as one of the inputs of the National Cooperative Highway Research Program (NCHRP) Mechanistic-Empirical Pavement Design Guide. The dynamic modulus provides information on how a cylindrical specimen behaves when subjected to a continuous sinusoidal load of varying frequencies. From this information, the response of the material under any traffic load such as a highway with a high loading frequency, or an intersection with low loading frequency, can be determined. A test setup as shown in Figure 2-12 is used. One of the benefits to dynamic modulus testing is that the modulus is measured in the direction of compaction, representative of field conditions.

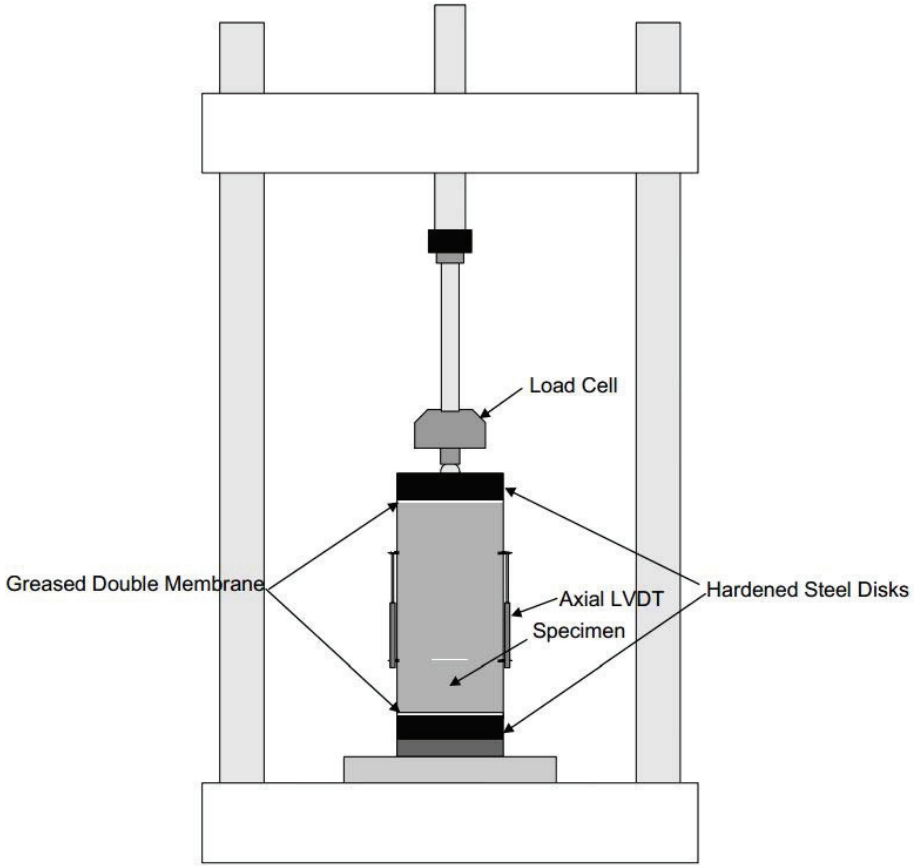

Figure 2-12 Dynamic modulus test configuration (AASHTO, 2007a)

The AASHTO TP62 test standard specifies a sample 101.6 mm in diameter and 150 mm in height. Axial strain is measured using between 2 and 4 equally spaced strain gauges. The sinusoidal load is applied to obtain axial strains between 50 and 150 microstrain and loading frequencies used range between 0.1 Hz and 25 Hz. The sample is tested at these frequencies at temperatures between -10°C and 54°C. Testing is completed on a servo-hydraulic testing machine using an environmental chamber for maintaining temperature, as shown in Figure 2-13.

Figure 2-13 Dynamic modulus testing machine and environmental chamber

Due to the viscoelastic nature of the material, there will be a phase lag between the peak stress and the peak strain. Data analysis is completed to filter the data, determine this phase lag, and determine stress and strain magnitude. Once this analysis is complete, Equation 2.8 can be used to compute the dynamic modulus.

$$|E^*(\omega)| = \frac{|\sigma^*|}{|\bar{\varepsilon}^*|} \quad \textbf{[2.8]}$$

where:

|E*(ω)| = dynamic modulus for loading frequency ω (kPa)
|σ*| = stress magnitude (kPa)
|ε*| = average strain magnitude

The dynamic modulus results obtained at different frequencies and temperatures are plotted and shifted to form a smooth curve, known as the master curve for the material. The master curve gives modulus data for all frequencies at a reference temperature, typically taken as 21.1°C (70°F), values which can then be shifted to any temperature of interest. Witczak & Bari (2004) proposed using a sigmoidal function, as shown in Equation 2.9, to describe the shifted modulus data.

$$\log(|E^*|) = \delta + \frac{\alpha}{1+e^{\beta-\gamma(\log \omega_r)}} \quad \textbf{[2.9]}$$

where:

|E*| = dynamic modulus (MPa)
ω_r = reduced frequency (Hz)
δ = minimum value of |E*|
α = difference between maximum and minimum |E*|
β, γ = parameters describing shape of sigmoidal function

The shift factor used to shift data between the reference temperature and the temperature of interest is given by NCHRP (2004), as shown in Equation 2.10.

$$a(T) = \frac{\omega}{\omega_r} \quad \textbf{[2.10]}$$

where:

a(T)	= shift factor, as a function of temperature	
ω	= frequency at temperature of interest	(Hz)
ω_r	= frequency at reference temperature	(Hz)

An equation must be developed to describe the shift factor as a function of temperature. Witczak & Bari (2004) recommended using a second order polynomial relationship to describe the shift factor as a function of temperature, developed in degrees Fahrenheit, as shown in Equation 2.11.

$$\log[a(T)] = aT^2 + bT + C \quad \textbf{[2.11]}$$

where:

a(T)	= shift factor, as a function of temperature	
a, b,c	= calibration factors	
T	= temperature of interest	(°F)

Cross & Jakatimath (2007) stated that the sigmoidal function should be fit to the shifted modulus data using non-linear least squares regression, and simultaneously solving the δ, α, β, and γ values of Equation 2.9, as well as the a, b, and c values of Equation 2.11. Figure 2-14 is an example of master curve construction, where the original data is shifted to form a smooth curve.

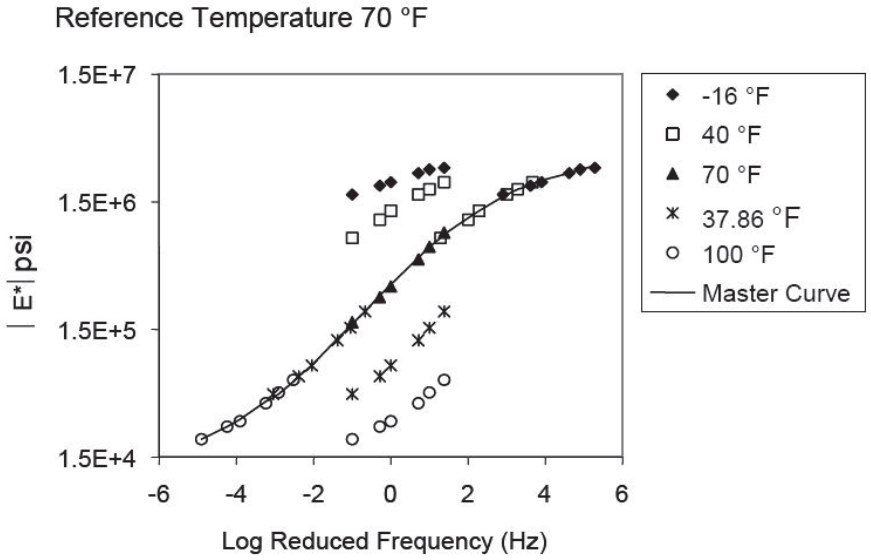

Figure 2-14 Dynamic modulus master curve construction (NCHRP, 2004)

Terrel et al. (1974) observed that the modulus of an HMA mix dropped considerably as temperature increased and loading frequency decreased. The study found that modulus was affected by both loading frequency and test temperature, and that as the asphalt content increased, the mix became more susceptible to changes in temperature

2.2.2.5 Rutting Potential

Excessive rutting is a common cause of failure in pavements. Huang (2004) described a rut as a surface depression in a wheel path which gradually increases in depth when subjected to repeated loads. Rutting in pavements lead to safety concerns as water could pool in the surface depression after a rainfall, and lead to vehicles hydroplaning. White et al. (2002) described rutting as being caused by a combination of mixture instability, and insufficient structural capacity. Rutting in pavement could therefore be indicative of a structural failure in either the HMA surface layer, or an underlying granular layer.

Roberts et al. (1996) stated that rutting can be caused by a number of factors including overstressed subgrade soil, or where shear failure has occurred. Liu & Li (2010) stated that rutting in a well constructed pavement is only caused by further densification of the

material, and shear flow. The definition of what constitutes a failure due to rutting varies depending on the agency. The Asphalt Institute limits allowable rut depth in design to 12.7 mm (Huang, 2004).

Testing for rutting potential is done on a 150 mm diameter, 75 mm high specimen using the Asphalt Pavement Analyzer wheel tracking device. Samples are subjected to loading at a rate of one cycle per second, and the rut depth per cycle is recorded and plotted. An example of a sample after testing is shown in Figure 2-15. The AASHTO T340 test standard describes the detailed test procedure.

Figure 2-15 Sample after rutting test

Kandhal & Cooley (2002) noted that the Asphalt Pavement Analyzer rutting test was not a fundamental test to evaluate permanent deformation in a mix, meaning the results could not be directly correlated to field performance. The results from the rutting test are primarily used to compare the rutting potential of specific mixes and, based on experience, they can also be used for mix design acceptance. Johnston et al. (2005) stated that the maximum allowable rutting depth for mix acceptance is typically set by the

state agencies depending on local conditions and past experience; however a maximum rut depth of 5 mm after 8000 cycles is a criterion that has been used.

Liu & Li (2010) cited a number of studies that have concluded temperature has a large effect on rutting depth. As temperature increases, the viscosity of the asphalt cement decreases, thereby reducing rutting resistance. Therefore, in addition to factors such as shear strength and in-place density, rutting resistance is a function of both asphalt content, and temperature. While limited guidance exists on predicting the rut depth of expanded asphalt stabilized FDR materials, models have been developed to predict the rutting depth of HMA pavements. One such model is presented in Section 2.6.2.1 of this report.

Testing with the Asphalt Pavement Analyzer is typically done at the high temperature of the Superpave performance graded asphalt cement. This temperature is the average seven day maximum temperature the pavement is expected to experience in service.

2.3 Stabilizers

There are many stabilizers available for use with FDR projects. A stabilizer should be chosen based on the existing material properties, expected construction and load conditions, cost and environment. TxDOT (2005) described the following as some of the properties that can be improved upon with the use of stabilizers:

- increase durability and strength
- reduce plasticity index
- reduce dust during construction
- adjust moisture content
- reduce moisture susceptibility

The type of additive used can be mechanical, bituminous, or chemical. Table 2-2 includes a sample of the types of stabilizers available. In addition to being used individually, additives can be used in tandem to improve multiple properties.

Table 2-2 FDR stabilization options

Stabilization Method	Additive
Mechanical	Granular materials
Bituminous	Expanded asphalt Emulsified asphalt
Chemical	Portland Cement Fly ash Calcium chloride

2.3.1 Mechanical Stabilization

Mechanical stabilization refers to the addition of granular materials to the pulverized material. This may be done to improve gradation, increase strength or for other reasons (Kearney & Huffman, 1999). This method alone is not common because when even small amounts of chemical or bituminous stabilizers are used, strength generally increases significantly (Wen et al., 2004). It can however be used strategically to improve the quality of a material for use with other additives which may have specific gradation requirements.

2.3.2 Bituminous Stabilization

Bituminous stabilizers affect the materials by working as an adhesive to bind the reclaimed materials together. Rather than causing a chemical reaction, the asphalt cement coats and binds the particles together. Muthen (1998) stated that bituminous stabilization increases shear strength and stiffness while reducing fatigue and moisture susceptibility. In cold mixing processes, expanded asphalt or emulsified asphalt may be used.

2.3.2.1 Expanded Asphalt

Expanded (foamed) asphalt is a process in which hot asphalt cement is mixed with small quantities of cold water spray resulting in foaming and expansion when the liquid is changed to vapour, and trapped by the asphalt bubbles. This process takes place in the expansion chamber of the mixing machine, and is illustrated in Figure 2-16. The expanded asphalt is then mixed with aggregate and the water quickly (within a minute) vaporizes. What is left is aggregate coated with the asphalt cement, which regains its original adhesive properties (Muthen, 1998).

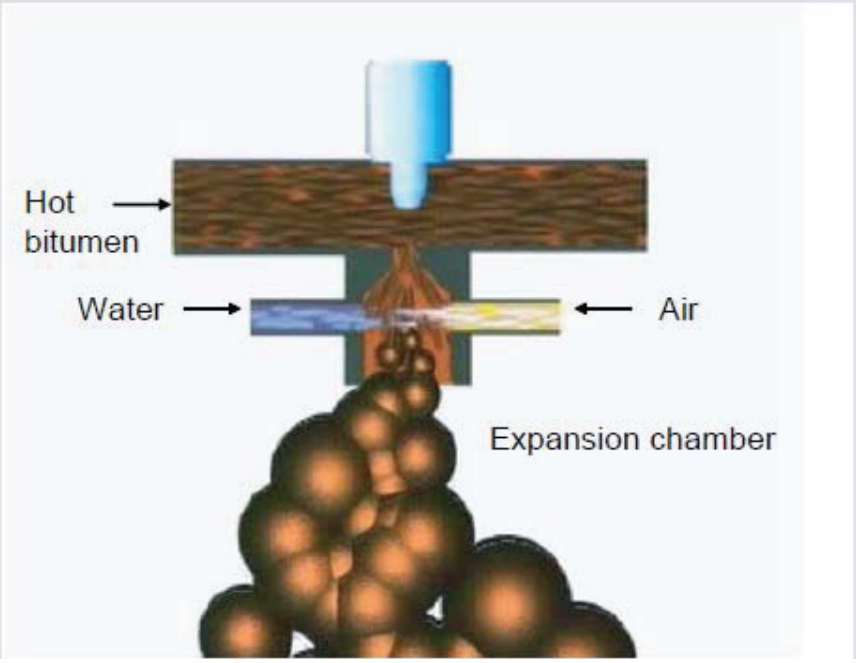

Figure 2-16 Expanded asphalt production in expansion chamber (Asphalt Academy, 2009)

Aggregates are not completely coated with asphalt cement when using expanded asphalt. The Asphalt Academy (2009) described asphalt cement dispersion as primarily taking place among the finer particles in the material. This makes it important to have a grading that minimizes VMA, as previously described in Section 2.2.1.1. The relationship given in Equation 2.1 is particularly important for percent passing the 2.36 mm sieve, as this is primarily where asphalt cement droplets disperse within the mix. The end result of an

expanded asphalt process is a mix with finer particles coated in asphalt cement and coarser particles essentially "spot-welded" together.

Two important factors in selecting asphalt cement for use in an expanded asphalt FDR mix are the expansion ratio and the half life. Wirtgen Group (2010) described the expansion ratio as the ratio of the maximum volume of the asphalt cement relative to its original volume prior to foaming. The expansion ratio provides an indication of how well the asphalt cement will disperse in the mix, with better dispersion occurring with increased expansion ratio.

The half life of the asphalt cement is defined as the time required for the foamed asphalt cement to reduce to half of the maximum volume achieved during foaming. As with expansion ratio, this value should also be maximized as this will maximizes the mixing time available (Kim et al., 2007). Testing is completed prior to acceptance of asphalt cement for use in expanded asphalt mixes to determine the temperature and water content which optimize the expansion ratio and half life.

2.3.2.2 Emulsified Asphalt

Emulsified asphalt is a mixture of asphalt cement, water, and an emulsifying agent. The mix contains small droplets of asphalt cement suspended in water. The emulsifying agent gives the asphalt cement an electric charge causing the different asphalt cement droplets to repel one another, and become attracted to an aggregate of the opposite charge. Once mixed, the asphalt reacts with the surface of the aggregate, when the emulsion is said to have "broken", and dissociates from the water, which evaporates from the mixture. After the water evaporates, the emulsion has then "set", with a film of asphalt cement remaining on the aggregate structure (Roberts et al. 1996).

Anionic or cationic asphalt emulsions are available. The anionic asphalt emulsion has a negative charge and is suited for use with aggregates bearing a positive charge. Cationic asphalt emulsion has a positive charge, and is suited for use with aggregates bearing a

negative charge. The electrical charge of many aggregates is typically negative, though this must be confirmed prior to selecting an emulsion type by evaluating the mineral composition of the aggregate. ASTM D3628 provides guidance on the types of emulsion available, and selecting the appropriate grade to use.

Aggregates are not completely coated with asphalt when using emulsified asphalt. The Asphalt Academy (2009) described asphalt cement dispersion as taking place preferentially amongst the finer particles in the material, but with some larger particles being partially coated. There is a chemical bond between the asphalt cement and the aggregate which is a result of using the emulsifying agent, which caused the electrical charge leading to the attraction.

2.3.3 Chemical Stabilization

Chemical stabilizers affect the materials by altering the particle structure leading to improved properties. One of the disadvantages of using chemical stabilizers is that the materials must cure to gain strength, which could mean keeping traffic off the road for a period of time after construction.

2.3.3.1 Portland Cement

When Portland cement is used to stabilize FDR materials, strength increases when the Portland cement is combined with water and allowed to hydrate. Taylor et al. (2007) described the chemical reaction between the water and the Portland cement during the hydration process starting with the dissolution of the Portland cement grains. Chemical reactions between the water and calcium silicates in the Portland cement lead to the formation of calcium and hydroxide ions, as well as the generation of heat. Once the system becomes saturated with the calcium and hydroxide ions, calcium silicate hydrate and calcium hydroxide compounds form. These compounds crystallize and mesh together. It is this system of connected crystals that provide strength to the material.

When FDR is stabilized with Portland cement, the aggregate materials are bound together by the cement-water paste formed during hydration, strength increases, and moisture susceptibility decreases (TxDOT, 2005). The amount of cement used in stabilizing the FDR materials must be controlled. Halsted (2010) stated that during the mix design process, the cement content should be chosen as the minimum amount required to reach a 7 day unconfined compressive strength between 2.1 and 2.8 MPa. If too much cement is used, the FDR material is likely to experience shrinkage cracking, which would ultimately reflect to the surface of the HMA wearing course (Sebesta et al., 2011).

In addition to controlling the amount of cement used in the mix, a process known as microcracking, further explained in Section 2.5.4, is also sometimes used during construction to reduce the risk of shrinkage cracking. Along with the bitumen stabilization options, Portland cement is a common stabilization technique used in FDR pavements.

2.3.3.2 Fly Ash

Fly ash is a by-product of coal combustion in electric or steam plants (Hensley et al., 2007). The effect of fly ash depends on the composition of fly ash used, which in turn depends on the coal combustion process used. Fly ash can alter particle structure, increase shrink/swell resistance, and decrease moisture susceptibility (TxDOT, 2005). There are two types of fly ash available, classified according to their chemical composition:

- Class CS: Self-setting fly ash
- Class FS: Fly ash requiring activator such as lime or cement

The American Coal Ash Association (2003) described the main difference in chemical composition between the two classes of fly ash. Class CS fly ash contains greater than 20 percent calcium oxide, also known as lime, while Class FS fly ash contains less than 10 percent calcium oxide. As a result, the Class CS fly ash is a "self-setting" fly ash which will react with water to form cementitious compounds, similar to those described in

Section 2.3.3.1, while the Class FS fly ash requires the addition of lime or cement to activate the chemical reaction (American Coal Ash Association, 2003).

ASTM International (2011) stated that the use of fly ash to stabilize FDR is efficient and economical, with improved modulus and resistance to plastic deformation resulting from its use.

2.3.3.3 Calcium Chloride

Calcium chloride can be used as a substitution for water on FDR projects. Mishra (N.D.) stated that, with calcium chloride, the moisture content of the materials could be better controlled, resulting in the ability maintain the optimum moisture content, and achieve maximum density. Kandhal & Mallick (1997) stated that the calcium chloride lowers the freezing point of the FDR materials, thereby reducing the effect of repeated freeze-thaw cycles.

2.4 Design Procedure

A thorough design procedure involves analysis of the existing road condition and traffic levels, material testing, mixture design, and structural design. The general design sequence to be followed is shown in Table 2-3. The process is an iterative process, so different designs may have to be considered and compared. The most efficient design is selected.

Table 2-3 FDR design procedures (Jones et al, 2009)

Stage	Steps
Desktop Study	• Review as-built plans • Photo logs • Pavement condition report • Traffic data • Maintenance report
Preliminary Site Investigation	• Visual assessment • Subgrade material sampling/preliminary testing
Detailed Site Investigation	• Subgrade stiffness assessment • Visual assessment of drainage system • Layer thickness and properties assessment • Material sampling and testing • Life-cycle cost
Mixture and thickness design	• Perform mix design for chosen stabilizer and thickness design for pavement system

A desktop study, preliminary and detailed site investigation should be completed prior to testing the mix design. It is during these stages that the decision is made to use FDR, as well as what may be required for a stabilizer. Further information and guidance on these steps is available in literature, including the Mechanistic-Empirical Pavement Design Guide published by NCHRP (2004). The focus of the following sections is first on determining the design traffic, which would be used in pavement design. Mix design and thickness design methods for expanded asphalt stabilized FDR, the focus of this research project, are then presented.

2.4.1 Design Traffic

To accurately design any pavement, it is important to have an estimate of the predicted traffic levels throughout the design life. The number of load cycles a pavement is expected to experience throughout its service life should be determined prior to mix or thickness design. It is important to note that the number of cycles refers to the number of 80 kN single axle load applications, also known as Equivalent Single Axle Load (ESAL).

This is a fixed loading type of design, meaning the predicted number of cycles is based on a pavement only being loaded by a standard 80 kN single axle load, whereas the levels of loading, and amount of damage from actual traffic would vary a great deal. To account for this, factors are used to relate the damage from various levels of loading to that of a standard ESAL. As presented in Huang (2004), Equation 2.12 is commonly used to estimate the design traffic. This equation utilizes a truck factor that standardizes the damage from different trucks relative to the damage from an ESAL.

$$\mathrm{ESAL} = (\mathrm{ADT})_o(t)(T_f)(G)(L)(365)(Y) \qquad \textbf{[2.12]}$$

where:

ESAL = number of equivalent single-axle load applications
$(ADT)_o$ = average daily traffic at the start of the design period
t = percentage of trucks in the average daily traffic (ADT)
T_f = number of 80 kN single-axle load applications per truck
G = growth factor
L = lane distribution factor
Y = design period (years)

Truck factor and lane distribution factor can be determined from tables developed by the Asphalt Institute, or AASHTO. Percent trucks, average daily traffic, and growth factor should be based on actual traffic data, and growth models for the area.

The design traffic determined from Equation 2.12 is used to predict the service life of the pavement system, and to aid in a life-cycle cost analysis. It is important to establish what the traffic loads will be so that this information can be incorporated into the design process.

2.4.2 Mix Design

The mix design procedures described in this report are for expanded asphalt stabilized FDR mixes, the focus of this research project. At this time, there are no standardized

procedures available for designing these mixes, though the methods followed by different agencies are similar, based on design guides published by Wirtgen Group (2010) and the Asphalt Academy (2009). Wirtgen Group (2010) described three types of mix design procedures available:

- Level 1: Low traffic levels
- Level 2: Intermediate traffic levels
- Level 3: High traffic levels / Lab studies

Level 1 mix designs utilize 100 mm diameter, 63.5 mm high specimens and basic curing procedures. Samples are made using a standard Marshall compaction procedure by applying 75 blows per side with a 4.536 kg mass freefalling 457.2 mm. Samples are placed in an oven at 40°C immediately after compaction, and allowed to cure for 72 hours. ITS testing is then completed on the samples. Level 1 mix designs are acceptable for pavements with traffic levels of up to 3 million ESALs.

Level 2 mix designs use 150 mm diameter, 127 mm high specimens, and a curing procedure that better simulates field conditions. These samples are made in Proctor moulds using a vibratory compaction method. The Asphalt Academy (2009) recommended that the samples be cured for 20 hours at 30°C, and then be placed in a sealed bag and cured for an additional 48 hours at 40°C. This curing procedure results in moisture contents in the specimens which represent the long term equilibrium moisture content the material would achieve in service. ITS testing is then completed on the samples. Level 2 mix designs are acceptable for pavements with traffic levels of up to 6 million ESALs.

Level 3 mix designs use 150 mm diameter, 300 mm high specimens, a curing procedure that simulates field conditions, and more advanced test procedures. Samples are made using a vibratory compaction method. As with level 2 testing, the Asphalt Academy (2009) recommended curing the samples for 20 hours at 30°C, followed by placing the samples in a sealed bag and curing them for an additional 48 hours at 40°C. After curing, triaxial testing is completed on the samples to assess the shear strength of the mix. Level

3 mix designs are acceptable for pavements with traffic levels above 6 million ESALs, as well as for laboratory studies.

In order to replicate procedures often followed in practice, the procedures outlined in this research project are based on level 1 testing.

2.4.2.1 FDR with Expanded Asphalt

When designing an FDR mix to be stabilized with expanded asphalt, the first step involves initial testing on untreated materials. Field sampling in the form of cores and test pits is carried out, with materials being taken to the laboratory. These materials are crushed, and a sieve analysis carried out on the reclaimed asphalt product (RAP) and base material. The materials are then blended together at a specified ratio, known as the blend ratio, which is the thickness ratio of RAP to granular materials. It is typically chosen based on the average thickness of the pavement, and the gradations of the materials. To blend the materials in the lab, the material densities must be known so that the appropriate mass ratio can be applied in combining the two products. The optimum moisture content and maximum dry density of the blended material is then found according to modified Proctor compaction effort methods specified in ASTM D1557.

Just as testing must be done on the aggregates prior to stabilization, the asphalt cement foaming properties must also be determined. The Asphalt Academy (2009) recommended testing the asphalt cement at temperatures between 150°C and 200°C. The asphalt cement should be foamed in a steel bucket with water contents between 2 and 4 percent by mass of asphalt cement, and the resulting expansion ratio and half-life recorded. These results are plotted, and the asphalt cement temperature and water content which optimizes these properties is recorded.

Ruckel et al. (1983) stated that the size of the bucket used for testing has an effect on the test results. When the FDR materials are expected to be between 10°C and 25°C, Wirtgen Group (2010) recommended a minimum half-life of 6 seconds and minimum

expansion ratio of 10 when spraying 500 g of foamed asphalt cement into a 20 litre steel measuring drum, though specific requirements may vary with individual agencies. Figure 2-17 demonstrates the relationship between expansion ratio, half-life, and water content. In this example, the optimum water content was selected as equal distance from the minimum acceptable half-life and minimum acceptable expansion ratio, at 3.0 percent.

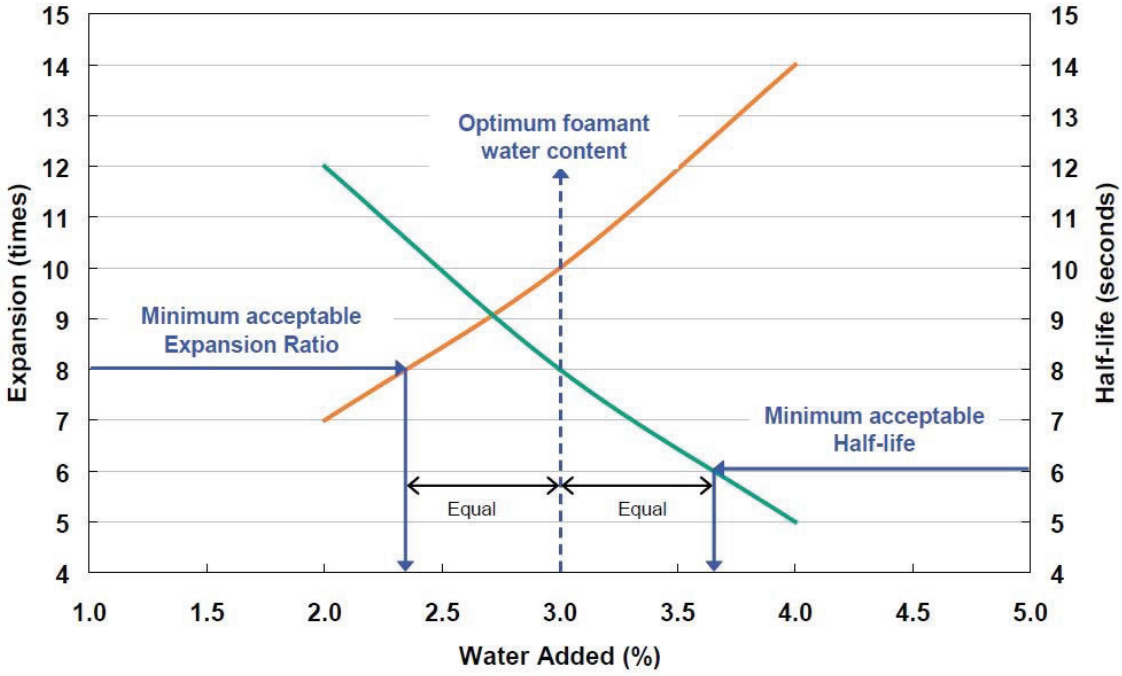

Figure 2-17 Typical expansion ratio and half life versus water content relationship (Asphalt Academy, 2009)

After the aggregates and the asphalt cement have been characterized, the material is stabilized and tested. The mixing moisture content is typically scaled back to between 65 and 85 percent of the optimum moisture content, to account for the extra moisture added in foaming. Wirtgen Group (2010) recommended a reduction based on the optimum moisture content of the material, using the formula given in Equation 2.13.

$$MC_{red} = (0.3 * OMC) - 0.6 \quad \textbf{[2.13]}$$

where:

MC_{red} = reduction of moisture content from optimum mixing moisture content
OMC = optimum mixing moisture content

Foaming and mixing takes place in commercially available pieces of equipment which simulate field conditions, such as the Wirtgen WLB-10S laboratory plant and WLM-30 pugmill mixer shown in Figure 2-18. Wirtgen Group (2010) recommended mixing the material at asphalt contents between 1 percent and 5 percent by mass of material.

Figure 2-18 Wirtgen WLB-10S laboratory plant and WLM-30 pugmill mixer (Wirtgen Group, 2010)

After mixing, specimens 101.6 mm in diameter, and approximately 63.5 mm in height are compacted using the Marshall compaction method, applying 75 blows per side. The samples must then be cured. It is during the curing process that samples gain strength. Jones et al. (2008) found that the materials only gained strength through the loss of moisture. In that study, samples were sealed immediately after compaction to prevent moisture loss, and tested at regular intervals. Six months after compaction, the samples had gained an insignificant amount of strength.

Prior to curing, immediately after compaction, the strength of the foamed asphalt materials is low. Fu et al. (2010) described the curing mechanisms of foamed asphalt mixes in detail, which are shown visually in Figure 2-19. The mix initially contains water, asphalt cement droplets, and aggregate (Figure 2-19A). After compaction the asphalt cement and aggregate are in close contact, however a film of water remains, separating the asphalt cement from the aggregates (Figure 2-19B & C). Once the moisture has been removed, the asphalt cement can fully bond with the aggregates (Figure 2-19D). With the bond formed between the asphalt cement and aggregates, the reintroduction of water (Figure 2-19E), while still having an impact on strength, will not be as severe as the effect of the initial moisture in the mix.

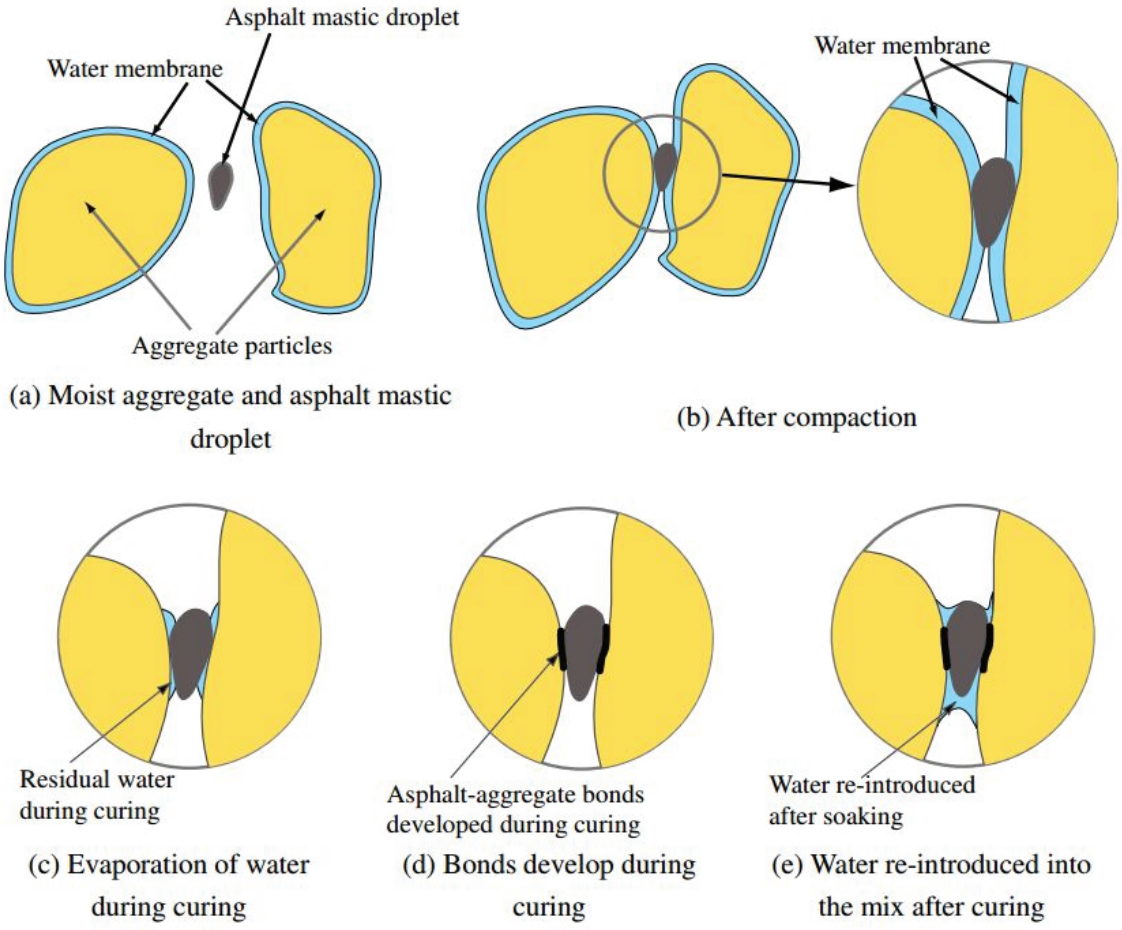

Figure 2-19 Curing process in foamed asphalt mixes (Fu et al., 2010)

Jones et al. (2008) stated that the curing temperature did not appear to be of significant importance provided excessive temperatures, especially above 50°C which would affect the viscosity of the asphalt cement, were not used. The target is a temperature which induces evaporation of the moisture while limiting the effect on the asphalt cement. Ruckel et al. (1983) proposed a curing procedure, commonly used today, to simulate approximately the first 30 days of field curing under dry conditions. In this procedure, samples are extracted from the moulds immediately after compaction, and placed in a forced-draft oven at 40°C for 72 hours to cure. This procedure has been found to provide an acceptable representation of the long term strength of the foamed FDR materials.

After the curing period, 3 specimens from each mix are placed in a water bath at 25°C, and 3 specimens are set aside for 24 hours. Following this 24 hour period, ITS testing is done on the soaked and dry samples of each mix. The relationship between ITS_{wet} and ITS_{dry} is shown in Figure 2-20. The mix must meet minimum soaked and dry strength requirements. There is also a requirement on TSR, which is the ratio of ITS_{wet} to ITS_{dry}.

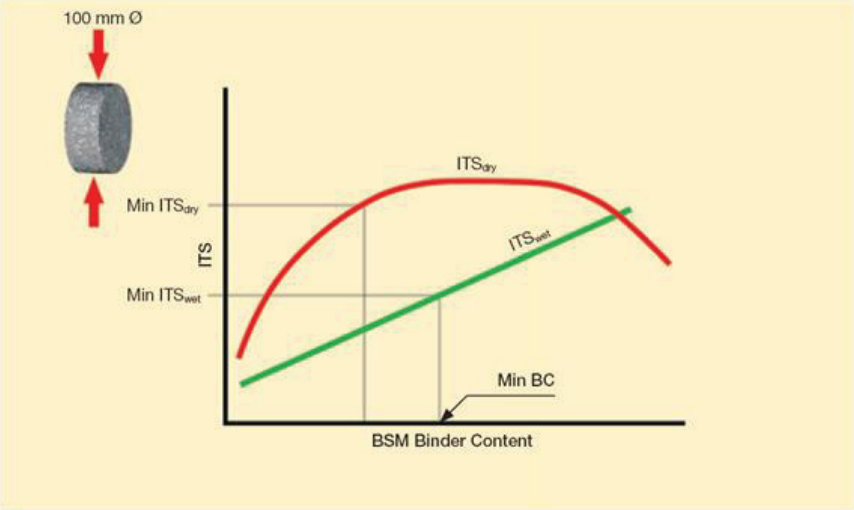

Figure 2-20 Typical TSR relationship (Wirtgen Group, 2010)

From a plot of the ITS results, the minimum asphalt content to satisfy all requirements is selected. In Nova Scotia, and typical of other jurisdictions, a minimum ITS_{dry} of 300 kPa, ITS_{wet} of 150 kPa, and TSR of 50 percent is required.

2.4.3 Thickness Design

The following section details several thickness design methods available for expanded asphalt stabilized FDR pavements. Huang (2004) described a structural number approach developed and published by AASHTO in 1961, and subsequently revised several times, that can be used for stabilized materials. Wirtgen Group (2010) identified two methods for the thickness design of stabilized materials: the Pavement Number approach, and deviator-stress ratio method. In addition, some state agencies reported using a set thickness approach. These design options are detailed in the following sections. A newer approach being used with other pavements involves following a Mechanistic-Empirical design method. Despite the advantages of this method, there is limited guidance on its use with regards to expanded-asphalt stabilized FDR, therefore it will not be discussed in this section.

2.4.3.1 Structural Number Approach

AASHTO developed the Structural Number method originally based on the AASHO road test and later modified with experience. In this method, the minimum thickness of each layer is chosen based on the thickness required to protect the layer below (Huang, 2004). Structural Number is determined based on the material properties and pavement service conditions. The resilient modulus of the material, expected moisture conditions, design traffic, acceptable damage levels based on pavement serviceability index (PSI), and level of reliability in design are all factored into the Structural Number calculation.

The first step is to determine the minimum Structural Number required. This is done for each layer in the pavement system using Equation 2.14 from AASHTO (1993).

$$\log(\text{ESAL}) = Z_R S_0 + 9.36\log(SN+1) - 0.20 + \frac{\log\left[\frac{\Delta PSI}{(4.2-1.5)}\right]}{0.4+\frac{1094}{(SN+1)^{5.19}}} + 2.32\log(M_R) - 8.07 \quad \textbf{[2.14]}$$

where:

ESAL = predicted number of ESALs, defined in Equation 2.12
Z_R = normal deviate for given level of reliability
S_0 = standard deviation for given level of reliability
SN = Structural Number
ΔPSI = change in pavement serviceability index during design period
M_R = effective resilient modulus (psi)

The normal deviate is selected based on the design reliability required. Huang (2004) provided values for standard normal deviate at different levels of reliability for flexible pavements, which are shown in Table 2-4. The standard deviation is typically selected as 0.45 for flexible pavements, a value based on the AASHO road tests.

Table 2-4 Standard normal deviate at different reliability levels (Huang, 2004)

Reliability (%)	**Standard normal deviate (Z_R)**	**Reliability (%)**	**Standard normal deviate (Z_R)**
50	0.000	93	-1.476
60	-0.253	94	-1.555
70	-0.524	95	-1.645
75	-0.674	96	-1.751
80	-0.841	97	-1.881
85	-1.037	98	-2.054
90	-1.282	99	-2.327
91	-1.340	99.9	-3.090
92	-1.405	99.99	-3.750

The change in pavement serviceability index (ΔPSI) is based on the amount of damage in a pavement the specifying agency is willing to tolerate. A newly constructed HMA

pavement typically has an initial PSI of 4.2. AASHTO (1993) recommended using a terminal PSI of 2.5 for the design of major highways, and 2.0 for lower volume highways. Therefore a ΔPSI of 1.7 should be used for major highways, and ΔPSI of 2.2 should be used for lower volume highways.

The effective resilient modulus is the modulus value for each material in the pavement system selected as being representative of the anticipated field performance, taking into consideration seasonal variations. The value may be based on laboratory testing which represents predicted stress and moisture conditions accurately, or by other means such as deflection testing, or using design tables.

Once the required Structural Number has been determined, Equation 2.15, as presented in AASHTO (1993), can be rearranged to solve for the minimum thickness, in inches, of each layer. This value is the minimum thickness to effectively protect the layer below.

$$SN = \sum a_i D_i m_i \qquad \textbf{[2.15]}$$

where:

SN	= Structural Number	
a_i	= structural coefficient for layer i	
D_i	= thickness of layer i	(inches)
m_i	= drainage coefficient	

The drainage coefficient only applies to unstabilized granular base and subbase materials. It is chosen based on the quality of drainage, and the expected moisture conditions in the area. Huang (2004) stated that the quality of the drainage is measured by the length of time for water to be removed, based on material permeability. The percentage of time the pavement structure will be exposed to excessive moisture levels is also a consideration in selecting the drainage coefficient. Tables are available in AASHTO (1993) to estimate these values.

Layer coefficient is chosen based on the quality of the material. The AASHTO design guide includes correlation charts between layer coefficient and different material properties. Figure 2-21(a) relates the resilient modulus of an untreated base with properties such as CBR, R-value, and triaxial shear testing.

- The CBR, described in Section 2.2.1.6, is a relative measure of the ability of a granular material to resist load applied through a piston.

- The R-value is a measure of the horizontal pressures induced when a vertical pressure is applied to a sample in a closed-system.

- The triaxial shear test is a test in which a confining pressure is applied to a sample contained in a rubber membrane, and a shear stress subsequently applied until the material fails. Similar to the direct shear test described in Section 2.2.1.5, the triaxial shear test can be completed at a number of confining pressures in order to develop the Mohr-Coulomb failure criterion.

Figure 2-21(b) presents a relationship between the structural coefficient of a bituminous treated material and either resilient modulus or Marshall stability. Figure 2-21(c) presents a relationship between layer coefficient and either modulus or 7-day unconfined compressive strength.

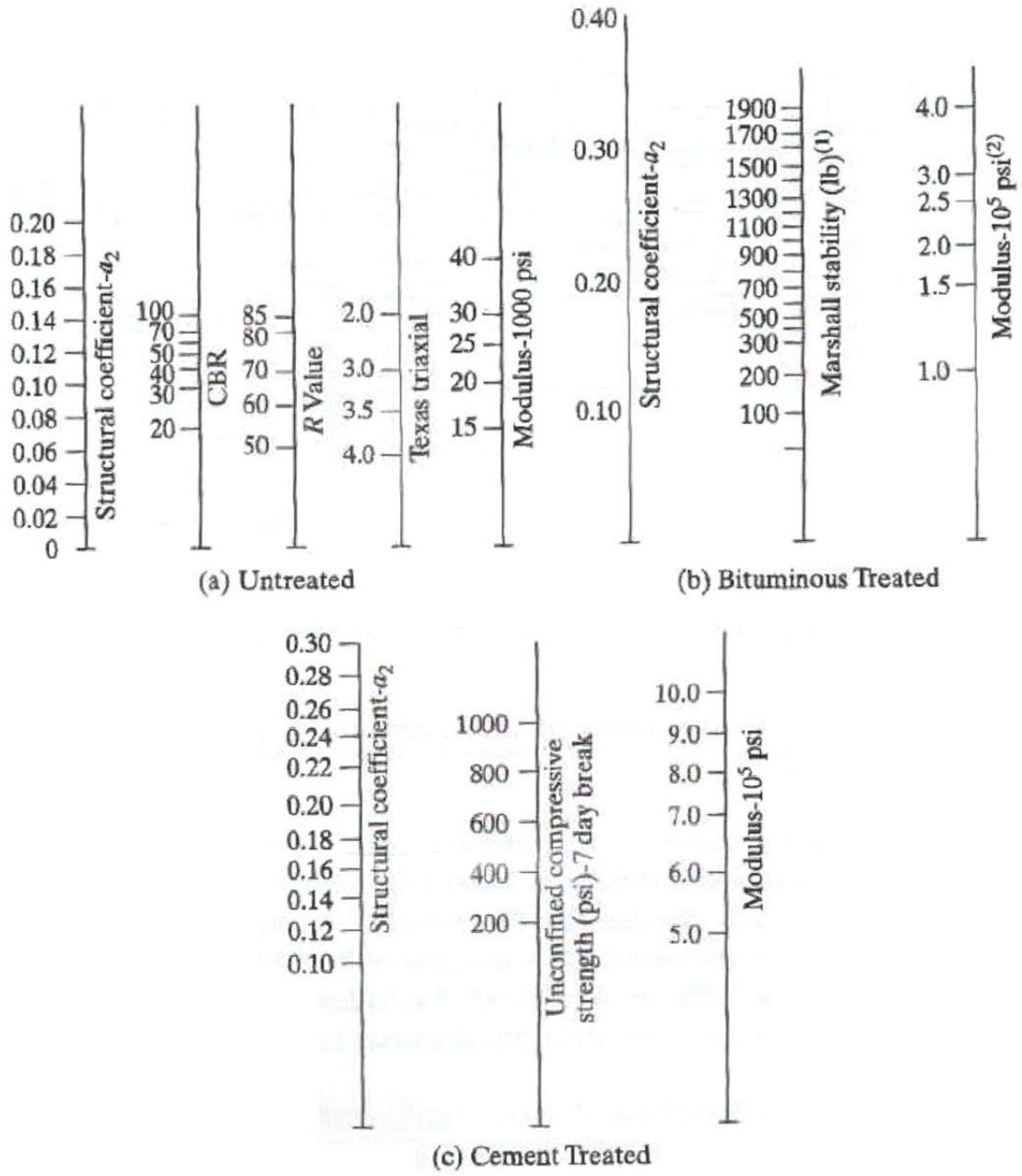

Figure 2-21 AASHTO design guide structural layer coefficient correlation charts (Huang, 2004)

Table 2-5 demonstrates the relationship between structural layer coefficient, Marshall stability, and resilient modulus for a bituminous stabilized base layer. This table can be used in place of the chart shown in Figure 2-21.

Table 2-5 Design guide numerical correlations for structural layer coefficients of bitumen stabilized base materials (FWHA, 2011)

Marshall Stability (lb.)	Structural Coefficient a_2	Modulus ($x10^5$ psi)	Structural Coefficient a_2
1900	0.330	4.0	0.335
1700	0.305	3.0	0.275
1500	0.285	2.5	0.250
1300	0.260	2.0	0.220
1100	0.240	1.5	0.190
900	0.215	1.0	0.125
700	0.190		
500	0.170		
300	0.145		
200	0.125		
100	0.090		

Wirtgen Group (2010) does not recommend using this method for pavements with a design traffic above 10 million ESALs because there is no way of controlling the modular ratio between adjacent layers with this design method. The modular ratio describes the relative stiffness of one layer relative to its supporting layer. Jooste & Long (2007) described the effect of having a stiff layer supported by a soft base, which would result in the overlying layer bending into the supporting layer and lead to the development of tensile and shear forces. Although bituminous stabilized materials are relatively cohesive, and therefore tend to be more tolerant of high modular ratios, it is still ideal to take the modular ratio of the supporting layers into consideration when designing high volume roadways.

2.4.3.2 Pavement Number Approach

The Asphalt Academy (2009) developed the Pavement Number (PN) approach which is summarized in this section, and presented in extensive detail in their published design

guide. The PN approach is a variation of the AASHTO Structural number method. Rather than using a structural coefficient for each layer, an Effective Long Term Stiffness (ELTS) value is used. ELTS is a measure of the stiffness decrease the material will experience due to seasonal variations and deterioration from traffic loads. ELTS also takes into account the placement of the layer within the structural system, and incorporates modular ratio limits to maintain a pavement balance. The PN design method is a knowledge based approach, meaning it utilizes values and limits based on material classifications and past experience.

Jooste & Long (2007) described the design procedure, which begins by estimating the layer thicknesses that the pavement system will have. Using tables provided in the Asphalt Academy (2009) Design Guide, the subgrade is assigned a basic stiffness value based on the material classification. This value is subsequently modified to account for climate conditions and depth of cover of the layer from the surface, and this modified value is used as the ELTS for the subgrade layer. The design then proceeds through the upper layers with modular ratio and stiffness limits, based on past experience and provided in tables, being used to assign an ELTS to each layer. This process is shown graphically in Figure 2-22, with the referenced tables and material classifications being those applicable in the Asphalt Academy (2009) Design Guide.

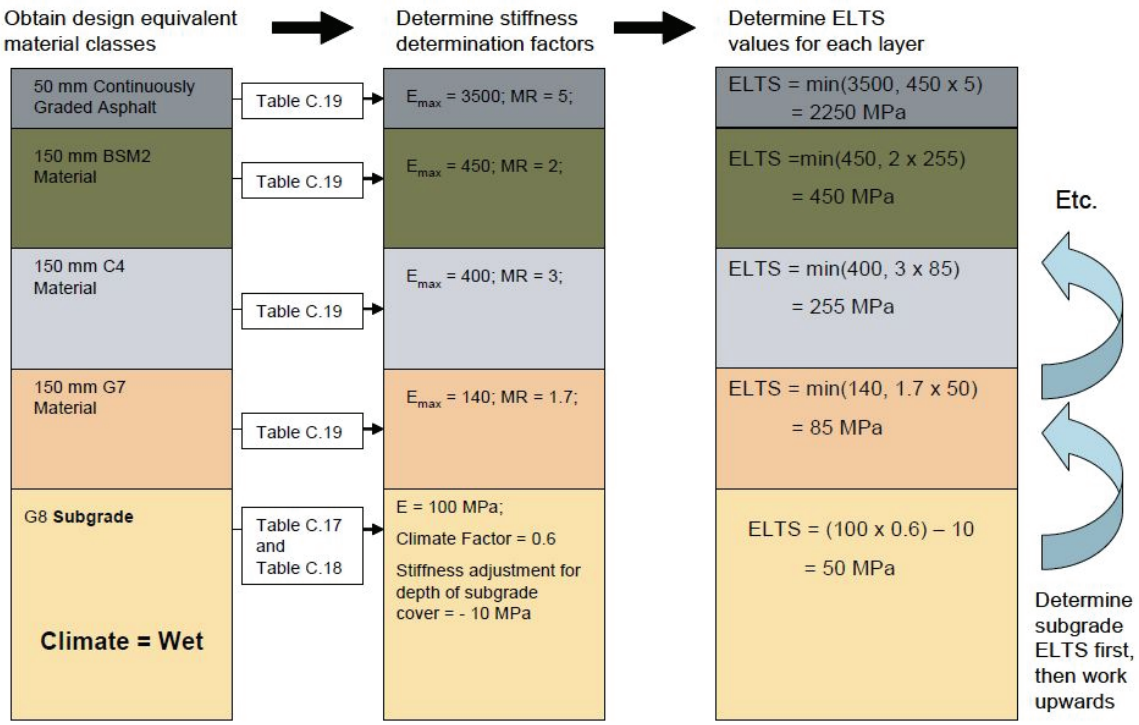

Figure 2-22 Pavement Number design method (Jooste & Long, 2007)

After assigning an ELTS to each layer, Equation 2.16 can be used to determine pavement number. From this value, an estimate of the structural capacity can be determined using a chart and equation presented in the Asphalt Academy (2009) Design Guide.

$$PN = \sum D_i(ELTS)_i \qquad \textbf{[2.16]}$$

where:

PN = Pavement Number
D_i = thickness of layer i (mm)
$ELTS_i$ = effective long term stiffness value of layer i (MPa)

This method is relatively easy to use, and therefore it is ideal for design. Wirtgen Group (2010) suggested that this method be limited to pavements with a design traffic less than 30 million ESALs, an 80 kN axle limit, and having a minimum subgrade CBR of 3 percent.

2.4.3.3 Deviator-Stress Ratio Method

The deviator-stress ratio method for Bitumen Stabilized Materials (BSM) was presented by Wirtgen Group (2010) for use with pavements having design traffic greater than 30 million ESALs. This method uses the theory that the rate of permanent deformation in a BSM layer is a function of the ratio of applied deviator stress to maximum deviator stress to cause failure, and is recommended for high volume designs. The deviator-stess ratio can be calculated using Equation 2.17. Stress at failure is determined through testing, while the applied stresses are calculated from a Mechanistic-Empirical analysis.

$$\text{Deviator} - \text{stress ratio} = \frac{\sigma_1 - \sigma_3}{\sigma_{1.f} - \sigma_3} \quad \textbf{[2.17]}$$

where:

σ_1 = major principal stress applied to BSM layer from mechanistic-empirical analysis

σ_3 = minor principal stress applied to BSM layer from mechanistic-empirical analysis

$\sigma_{1.f}$ = major principal stress at failure from triaxial testing of BSM

A deviator-stress ratio limit is chosen based on the importance of the road and the expected traffic loads. A typical value for the deviator-stress ratio limit is between 35 and 40 percent (Wirtgen Group, 2010). The deviator-stress ratio is then used to predict the service life of the section using transfer functions available in the Asphalt Academy (2009) Design Guide.

2.4.3.4 Set Thickness Approach

Stroup-Gardiner (2011) reported that the set thickness approach is used by a number of state agencies. With this method, a predetermined thickness for recycled materials is used as a means of simplifying the design process. This is often used on lower volume roadways which are not expected to experience high loads (Griggs, 2009).

2.5 Construction

The FDR construction process involves pulverizing the materials, mixing them with a binding agent, and recompacting them. Once the FDR layer has been completed, a suitable wearing surface is constructed. Depending on the equipment used and other considerations, the entire reclamation and stabilization process may be done in one pass, or divided into several individual steps. These stages are further detailed in the following sections.

2.5.1 Climatic Considerations

Consideration should be given to weather conditions at the time of construction. Cold weather and rain can negatively impact different stabilizers. Table 2-6 lists recommendations by Kearney & Huffman (1999) on the environmental limitations of different stabilizers.

Table 2-6 Climatic limitations of FDR stabilizers (adapted from Kearney & Huffman, 1999)

Type of Stabilizer	Climatic Limitation for Construction
Fly Ash with lime	• Reclaimed material cannot be frozen • Air temperature in shade above 4°C and rising • Stabilization complete at least 1 month before first hard freeze • Minimum 2 weeks of warm to hot weather desirable after construction
Portland Cement	• Reclaimed material cannot be frozen • Air temperature in shade above 4°C and rising • Stabilization complete at least 1 month before first hard freeze
Asphalt Emulsion or Expanded Asphalt	• Reclaimed material cannot be frozen • Air temperature in shade above 15°C and rising • Cannot be performed in high humidity conditions • Warm to hot dry weather preferred for optimal results
Calcium Chloride	• Reclaimed material cannot be frozen • Air temperature in shade above 4°C and rising • Stabilization complete at least 1 month before first hard freeze

2.5.2 Pulverization and Preparation

Kandhal & Mallick (1997) stated that initial pulverization and size reduction is done with either a motor grader or a dozer with front or rear mounted ripper teeth. The number of passes required depends on multiple factors. More than one pass may be required for thicker pavements, or to achieve required gradations (Portland Cement Association, N.D.). The gradation from pulverization is affected by the degree of cohesion in the original bound material, as well as the advance speed of the recycler and rotation speed of the blades. The pulverized material will be coarser if the recycler is advancing too fast, or the blades are rotating too slowly (Wirtgen Group, 2010).

Barnes et al. (2012) stated that the thickness of the asphalt concrete, and subsequent effect on the pulverization process must be monitored during construction. If the HMA layer is too thin relative to the pulverization depth, pieces tend to lift vertically, and slightly backwards, breaking into large pieces. This is caused by the upward cutting motion of the pulverization machine cutting tools. Alternatively, if the HMA layer is too thick, this may affect the cooling of the cutting tools on the pulverization machine, which depend in part on moisture in the underlying granular materials to stay cool.

An important aspect of the pulverization process is the control of the blend ratio. The blend ratio is the percentage, by thickness, of reclaimed asphalt to total material pulverized. In an effort to maintain a consistent blend ratio, the depth of pulverization may be adjusted to compensate for variations in pavement thickness. The method in which the pavement layer thicknesses are determined could have an effect on the consistency of the blend ratio achieved. Barnes et al. (2012) identified two common approaches to determining the existing pavement layer thicknesses:

1. The first approach involves using data from cores or test pits. The pavement thickness at these sample locations is used to either specify a constant pulverization depth based on average thicknesses, or specify specific pulverization depths at various sections, reflecting the pavement thickness determined at the nearest core location.

2. A second approach is to use a retroactive depth control method. In this method, the asphalt concrete thickness is measured during construction at the edge of the pulverized material, behind the pulverization process. This measurement is used as an estimate of the asphalt concrete thickness in front of the pulverizing machine, and the pulverization depth is adjusted in an attempt to maintain the specified blend ratio.

The study by Barnes et al. (2012) found that the common approaches to maintaining a consistent blend ratio were not necessarily the most reliable methods, and could lead to large variations in the quality of the reclaimed materials. In cases where there were large variations in asphalt concrete thickness over a short distance, these methods resulted in large differences in the observed blend ratio.

A new approach being studied to control the blend ratio involves using a GPR survey to determine the layer thicknesses in the pavement before construction. With this approach, asphalt concrete thickness throughout the section could be determined beforehand, and pulverization depths specified within appropriate subsections to reflect the true variation in thickness. Determining whether this approach would lead to more consistent results was one of the objectives of this research project.

Following pulverization, corrective aggregate and water may be added. If material is too wet, it is allowed to aerate until it has reached the optimum moisture content. The stabilization method depends on the additive being used, as well as other considerations. Chemical stabilizers are often spread dry over the surface of the road, or added as a slurry to improve uniformity and prevent the loss of additive due to environmental factors such

as wind (Sebesta et al., 2011). Bituminous stabilizers are often added in hot liquid form through the reclaiming machine (Kearney & Huffman, 1999).

2.5.3 Mixing and Compaction

The reclaimed material is mixed with the additive by the reclaiming machine. Wirtgen Group (2010) identified different types of mixing machines that have been developed including:

- tyre-mounted recyclers
- track mounted recyclers

The type of machine used can have an impact on the final quality of the recycled materials. Although further information on the different types of mixing machines is outside the scope of this report, Wirtgen Group (2010) and the Asphalt Academy (2009) have published design guides that extensively detail the FDR construction equipment.

After mixing, the stabilized material is spread and shaped to the desired geometry. It is important that placement be completed as quickly as possible so that compaction can begin. Compaction must meet two general guidelines covering the amount of time between mixing and compaction, as well as the level of compaction. Bang et al. (2008) reported that the level of compaction is generally specified at 95 percent or higher of the maximum dry density as determined from standard or modified Proctor effort compaction tests.

Materials should be compacted as soon as possible after mixing. The amount of time available for compaction varies depending on the additive and must be determined prior to construction. Kearney & Huffman (1999) described a typical rolling pattern sequence followed beginning with initial breakdown rolling using a vibratory padfoot roller, or vibratory single or tandem drum roller. The initial breakdown rolling is done with the goal of compacting the bottom of the layer.

After this compaction is completed, the section may be re-graded to maintain the proper geometry. Intermediate rolling is then completed with a pneumatic-tired roller, which compacts the mid to upper part of the layer. Finish rolling is then done with tandem static steel-wheeled rollers to eliminate tire marks from the pneumatic tired rollers, and bring the material to maximum density.

The compaction process, and the ability to achieve high levels of compaction, is affected by the lift thickness, type of roller, and most importantly the moisture content of the material (Kandhal & Mallick, 1997). As described in Section 2.2.1.2, the moisture content of the material has a large impact on the ability to achieve sufficient compaction levels.

2.5.4 Curing and Surface Construction

To prevent structural damage, heavy trucks should be kept off the FDR layer during the curing period following construction. Bituminous stabilized materials can be opened up for traffic almost immediately. In comparison, Halsted (2008) stated that curing time for a chemically stabilized material varies between 1.5 and 7 days depending on the stabilizer used.

Proper curing procedures must be followed as required with each additive. Chemically stabilized materials may need to be kept moist, which is done by adding moisture or asphalt sealing to maintain as-built moisture content. Light rolling with a pneumatic-tired roller can also be done to keep a tight surface (Kearney & Huffman, 1999). The optimal curing method will however depend on a variety of factors, which must be investigated on a project by project basis.

Sebesta (2006) described a process to reduce the risk of shrinkage cracking in cement-stabilized layers, known as microcracking, which can be completed one to three days after construction. Microcracking is done using a steel drum vibratory roller set to maximum vibration amplitude. This creates a series of fine cracks which enable

distributed shrinkage stress relaxation, thereby minimizing the risk of larger cracks developing. The microcracking process temporarily reduces the stiffness of the layer by approximately 40 to 60 percent. The material recovers, and exceeds its strength at this early age through continued hydration (Sebesta & Scullion, 2004). Figure 2-23 shows an example of a microcracked surface after construction.

Figure 2-23 Cement treated material after microcracking (Sebesta & Scullion, 2004)

The final step is to construct a surface layer to act as a wearing course. Options for a wearing surface include

- HMA
- chip seal or other surface treatment

As with curing methods, the type of wearing surface, time delay before construction, and other factors should be determined on a per project basis. Bitumen stabilized materials for example can withstand traffic loads much sooner than chemically stabilized materials. Traffic loads and environmental factors must also be considered in selecting the most appropriate wearing surface.

2.6 Performance Evaluation

It is common practice in pavement engineering to perform service life predictions by estimating the number of load cycles to cause fatigue failure and failure due to excess permanent deformation (Huang, 2004). There is however a gap in published literature, specifically with regards to bitumen stabilized FDR materials, which have no standard transfer functions available. Wirtgen Group (2010) stated that fatigue is not a failure criterion in stabilized materials since they behave like granular materials, relying on inter particle friction to resist load. With these pavements, a permanent deformation issue such as rutting is the main mode of distress.

Studies in South Africa and presented in the Asphalt Academy (2009) Design Guide evaluated bitumen stabilized materials against failure, however the equations derived were based on limited data, and could not be reliably used for other materials. The Mechanistic-Empirical Pavement Design Guide mentions bitumen stabilized materials, however no transfer functions were included to describe distress in these materials. With no specific equations available, NCHRP (2004) recommended treating stabilized materials as either an unbound aggregate mixture, or in cases where it was produced through a production facility, as an HMA base layer which can then be combined with the HMA surface layer for analysis.

As a result of the lack of guidance on the performance evaluation of most FDR pavements, this section will be limited to a discussion on evaluating the service life of HMA, and granular materials. As these are components of FDR pavement structures, evaluating the service life of these layers must be part of the design process. When combining the treated FDR layer with either the HMA, or unbound granular base layer, the same equations would be used to predict performance in that layer.

2.6.1 HMA Fatigue Life

HMA fatigue life is typically related to the modulus of the mix and the maximum tensile strain developed in the layer. The Mechanistic-Empirical Pavement Design Guide uses a fatigue equation developed by the Asphalt Institute, with modified calibration factors. Equation 2.18, presented by NCHRP (2004), estimates the number of cycles to cause fatigue cracking in an asphalt layer, based on a constant stress condition.

$$N_{f,allow} = 0.00432 * k'_1 * C\left(\frac{1}{\varepsilon_t}\right)^{3.9492}\left(\frac{1}{E}\right)^{1.281} \quad \textbf{[2.18]}$$

where:

$N_{f,allow}$ = allowable number of load applications
k'_1 = layer thickness effect correction factor
C = laboratory to field adjustment factor
ε_t = horizontal tensile strain at the bottom of the HMA layer (inches/inch)
M_R = resilient modulus (psi)

The laboratory to field adjustment factor, C, is calculated using Equation 2.19.

$$C = 10^M \quad \textbf{[2.19]}$$

where:

C = laboratory to field adjustment factor
M = mix factor

The mix factor, M, can be calculated using Equation 2.20. This factor incorporates the effect of asphalt cement content and the air voids in the mix.

$$M = 4.84\left(\frac{V_b}{V_a+V_b} - 0.69\right) \quad \textbf{[2.20]}$$

where:

M	= mix factor	
V_b	= effective asphalt cement content	(%)
V_a	= air voids	(%)

The layer thickness effect correction factor, k'_1, was introduced in the Mechanistic-Empirical Pavement Design Guide to correct for the impact of thickness in the HMA layer. k'_1 can be calculated using Equation 2.21. This equation is for "bottom-up" cracking situations, where the crack initiates at the bottom of the HMA layer due to excessive or repeated loads, and progresses upward to the surface. There is also an equation included in the design guide to correct for "top-down" cracking which has not been included in this report. "Top-down" cracking occurs in thick pavements where there are localized tensile stresses at the pavement surface caused by tire loads, and cracking initiates at the surface of the pavement and progresses downward.

$$k'_1 = \frac{1}{0.000398+\frac{0.003602}{1+e^{(11.02-3.49*h_{ac})}}} \quad \textbf{[2.21]}$$

where:

k'_1	= layer thickness effect correction factor	
h_{ac}	= HMA layer thickness	(inches)

The horizontal tensile strain used in estimating the fatigue life of the HMA material can be found with an elastic layered model, finite element model, or other appropriate analysis.

Fatigue models have been found to be extremely sensitive to the calibration factors and regression constants. Saxena et al. (2010) cautioned that, when using global calibration values, the effect of degradation of the resilient modulus are not properly modeled.

These effects can only be observed if the calibration factors are those from rigorous local calibration, which would take into account the factors that affect degradation in different environments.

2.6.2 Cumulative Permanent Deformation

Although some design models, including the Asphalt Institute and Shell design methods, have based permanent deformation predictions on the vertical compressive strain on the top of the subgrade, Huang (2004) stated that in most situations, this was not a reasonable approach. The rutting observed in pavements is in fact an accumulation of permanent deformation from all the layers within the pavement system. The Mechanistic-Empirical Pavement Design Guide software attempts to address this by taking into consideration the cumulative deformation of all layers. As previously described, there is limited guidance on predicting the rate of rutting in expanded asphalt stabilized FDR layers, therefore this section will be limited to presenting transfer functions to predict the permanent deformation in HMA, and unbound granular and subgrade layers. The rutting depths determined from these equations can then be added together to determine total permanent deformation in the pavement system.

2.6.2.1 HMA

NCHRP (2004) presented a model, shown in Equation 2.22, for predicting the rut depths in HMA layers. This model uses factors based on national calibrations and numerical optimizations.

$$\frac{\varepsilon_p}{\varepsilon_r} = k_1 * 10^{-3.4488} T^{1.5606} N_r^{0.479244} \quad \textbf{[2.22]}$$

where:

ε_p	= accumulated plastic strain at N_r repetitions of load	(inches/inch)
ε_r	= resilient strain of the HMA at the mid depth of the layer	(inches/inch)
k_1	= confining pressure correction factor	
T	= temperature	(°F)
N_r	= number of load repetitions	

The confining pressure correction factor, k_1, was introduced to correct for the confining pressures in the HMA experienced at the computational point in the analysis. This factor can be computed using Equation 2.23 (A), (B), and (C).

$$k_1 = (C_1 + C_2 * z) * 0.328196^z \quad \textbf{[2.23A]}$$

$$C_1 = -0.1039 * {h_{ac}}^2 + 2.4868 * h_{ac} - 17.342 \quad \textbf{[2.23B]}$$

$$C_2 = 0.0172 * {h_{ac}}^2 - 1.7331 * h_{ac} + 27.428 \quad \textbf{[2.23C]}$$

where:

k_1	= confining pressure correction factor	
C_1, C_2	= depth factors	
z	= depth of computational point below surface	(inches)
h_{ac}	= HMA layer thickness	(inches)

The accumulated plastic strain, ε_p, determined in Equation 2.22 can be multiplied by the thickness of the HMA layer, in inches, to determine the total deformation in the layer. Conversely, a cumulative strain could be selected, and the number of cycles to reach that strain level subsequently calculated by rearranging the same equation.

2.6.2.2 Unbound Granular and Subgrade Materials

A model for predicting permanent deformation in unbound materials developed by Tseng & Lytton (1989) was used as a starting reference in developing the model used in the Mechanistic-Empirical Pavement Design Guide. The final model, modified and calibrated, was presented by NCHRP (2004) and is shown in Equation 2.24 for all unbound granular, and subgrade materials.

$$\delta_a = \beta_1 \left(\frac{\varepsilon_0}{\varepsilon_r}\right) e^{-\left(\frac{\rho}{N_r}\right)^{\beta_2}} \varepsilon_v * h \qquad \textbf{[2.24]}$$

where:

δ_a	= permanent deformation of the layer	(inches)
β_1	= calibration factor. 1.673 for unbound granular materials, 1.35 for subgrade materials	
$\frac{\varepsilon_0}{\varepsilon_r}$	= material property factor	
ρ	= material property factor	
N_r	= number of load repetitions	
β_2	= material property factor	
ε_v	= vertical strain at the midpoint of the layer	(inches/inch)
h	= layer thickness	(inches)

The description of the factors in Equation 2.24 has been simplified in this report, as a detailed analysis of them is outside the scope of this project. Equation 2.25 (A) through (D) can be used to estimate the material property factors $\frac{\varepsilon_0}{\varepsilon_r}$, ρ, and β_2. These equations take into consideration the resilient modulus of the material, and the predicted water content of the materials, based on the location of the groundwater table.

$$\log \beta_2 = -0.61119 - 0.017638 W_c \quad \textbf{[2.25A]}$$

$$\left(\frac{\varepsilon_0}{\varepsilon_r}\right) = \frac{\left(0.15 * e^{(\rho)^{\beta_2}}\right) + \left(20.0 * e^{(\rho/10^9)^{\beta_2}}\right)}{2} \quad \textbf{[2.25B]}$$

$$\rho = 10^9 \left[\frac{-4.8929}{(1-(10^9)^{\beta_2})}\right]^{\frac{1}{\beta_2}} \quad \textbf{[2.25C]}$$

$$W_c = 51.712 \left[\left(\frac{M_R}{2555}\right)^{\frac{1}{0.64}}\right]^{-0.3586 * GWT^{0.1192}} \quad \textbf{[2.25D]}$$

where:

β_2	= material property factor	
W_c	= water content	(%)
$\frac{\varepsilon_0}{\varepsilon_r}$	= material property factor	
ρ	= material property factor	
M_R	= resilient modulus of material	(psi)
GWT	= ground water table depth	(ft)

The vertical strain at the midpoint of the layer is determined with an elastic layered model, finite element model, or other appropriate analysis.

2.6.3 Service Life Prediction

The service life of an FDR base is predicted by comparing the expected traffic levels to the number of cycles to failure determined from the fatigue and permanent deformation predictive equations. The number of cycles the pavement is expected to experience is determined using Equation 2.11. By comparing the design traffic to the minimum number of cycles to failure, a reasonable estimate of the pavement service life is assumed.

2.7 Summary

The primary recommendation from the findings of this review relates to the quality of the FDR materials. Research must be completed to better understand how the physical properties of the pulverized materials affect the performance of the recycled layer. More specifically, the effect of gradation on FDR and how to accurately control it requires more research. These findings were the basis for the research program described in the following chapter.

CHAPTER 3: RESEARCH PROGRAM

A laboratory research program was established to evaluate a number of properties in the unstabilized and stabilized FDR materials. The purpose of this research program was first to verify the consistency of materials sampled from an FDR project that used a GPR survey as a proactive pulverization depth control method, and secondly to study a mix design method that better reflects construction conditions and could result in a higher quality FDR base layer. Additionally, a study of the effect of construction variability was included as one of the objectives of the project.

The research program included tests commonly used in pavement engineering to evaluate materials, as well as advanced testing procedures which provided fundamental material property information. The first stage of the research program involved field testing with a GPR survey, described in Section 3.1. Test methods to evaluate both the unbound and bound materials were then selected, and are described in Section 3.2 and Section 3.3 respectively. The rationale for selecting these test procedures, the relevance to pavement engineering, and the testing process are described in these sections.

Testing was based on ASTM and AASHTO standards, which have been referenced throughout the chapter. Unless otherwise specified, testing was completed at Dalhousie University.

3.1 Ground Penetrating Radar Survey

GPR is a non-destructive pavement evaluation technique that can be used to evaluate the thicknesses of the various layers in a pavement structure. Saarenketo & Scullion (1994) described the process which begins with either an air-coupled antenna, or ground-coupled dipole antenna emitting an electromagnetic pulse downward into the pavement structure. Although ground-coupled dipole antennas can operate over a much wider range of frequencies, which enable deeper measurements, air-coupled antennas are more common as they can collect useful information at near highway speeds. The pulse travels through

the materials, with a portion of it being reflected back up to the surface when it encounters a material with different electrical properties. The layer thickness of each particular material is a function of the electromagnetic pulse's travel time, and the electrical properties of the material. The reflection concept and travel path of the pulses are shown in Figure 3-1.

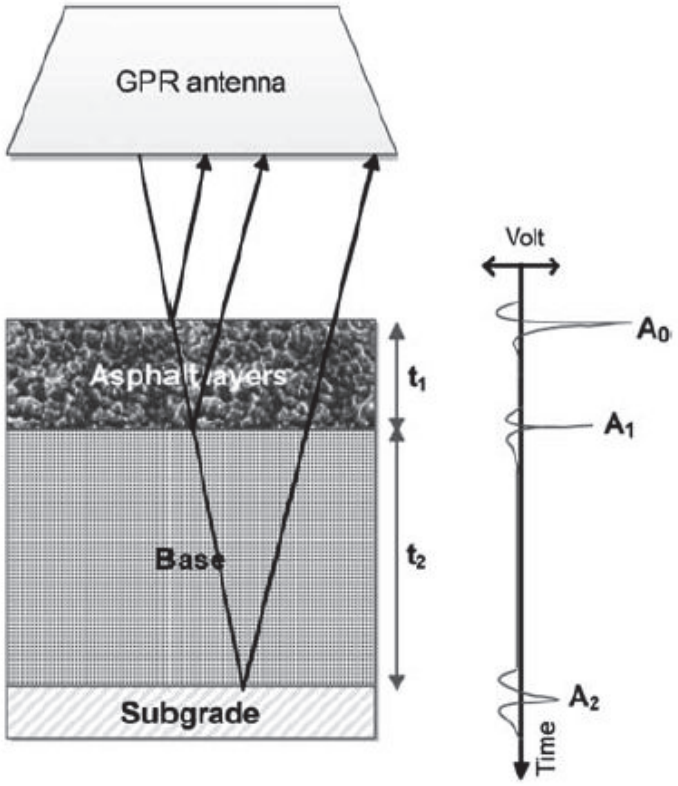

Figure 3-1 GPR electromagnetic pulse reflection concept (Plati & Loizos, 2012)

To perform a GPR analysis, the dielectric properties of the material must be estimated. Loizos & Plati (2006) described the dielectric constant, also referred to as dielectric permittivity, as a measure of the capacity of a material to allow the passage of electromagnetic energy. Different materials exhibit different dielectric constants, and it is the change in dielectric constant when an electromagnetic pulse travels between layers which causes a reflection and identifies the different layers. Daniels (2004) stated that electromagnetic waves travelling through media experience losses due to both electric

fields and magnetic fields. The materials being penetrated in pavement structural systems typically have a very low magnetic response, which are therefore not considered in analysis. Typical dielectric constants for a range of materials are shown in Table 3-1. From these values, it can be noted that the presence of water results in large increases in dielectric constant.

Table 3-1 Typical dielectric constants for different materials (Daniels, 2004)

Material	Dielectric constant
Air	1
Asphalt, dry	2 – 4
Asphalt, wet	6 – 12
Concrete, dry	4 – 10
Concrete, wet	10 – 20
Sand, dry	2 – 6
Shale, dry	4 – 9
Freshwater	81

Plati & Loizos (2012) stated the dielectric constants can be estimated from the GPR data by first calibrating with radar data reflected off a flat copper plate, which is considered to be an ideal electromagnetic reflector. This calibration is done to determine the amplitude of the incidental GPR signal, or proportion of signal reflected off an ideal reflector, which in this case would be 100 percent reflection. With this value, Equation 3.1, presented by Saarenketo & Scullion (2000), can be used to estimate the dielectric constant of the surface layer. This is calculated using the copper plate reflection amplitude, and the amplitude of reflection of the electromagnetic pulse passing from air into the upper layer of the system.

$$\varepsilon_1 = \left[\frac{1+A_1/A_m}{1-A_1/A_m}\right]^2 \quad \textbf{[3.1]}$$

where:

ε_1 = dielectric constant of surface material
A_1 = amplitude of surface reflection
A_m = amplitude of reflection off copper plate

In a similar manner, the dielectric constant of the second layer in the system can be calculated by evaluating the intensity of the surface reflections, and the effect of the materials above the layer. Equation 3.2, presented by Loizos & Plati (2006) can be used to estimate the dielectric constant of the base material.

$$\varepsilon_2 = \varepsilon_1 \left[\frac{1-(A_1/A_m)^2+(A_2/A_m)}{1-(A_1/A_m)^2+(A_2/A_m)}\right]^2 \quad \textbf{[3.2]}$$

where:

ε_2 = dielectric constant of base material
ε_1 = dielectric constant of surface material
A_1 = amplitude of surface reflection
A_m = amplitude of reflection off copper plate
A_2 = amplitude of reflection at surface of base layer

This can be repeated for subsequent layers by adding the effect of each upper layer to the equation. Along with the dielectric constant, the velocity of the electromagnetic pulse through each individual layer must also be calculated. Equation 3.3 is used to calculate this velocity, in metres per nanosecond, which is done by assuming the GPR signal travels at the speed of light in free space (Loizos & Plati, 2006).

$$V = \frac{c}{\sqrt{\varepsilon}} \quad \textbf{[3.3]}$$

where:

V	= electromagnetic pulse velocity through material in question	(m/ns)
c	= speed of light in free space, 0.3 m/ns	
ε	= dielectric constant of material in question	

Finally, the thickness of each layer can be determined based on the velocity of the electromagnetic pulse through each layer, and one half the two-way travel time of the pulse between reflections, as shown in Equation 3.4 (Daniels, 2004).

$$h = \frac{V * t_2}{2} \quad \textbf{[3.4]}$$

where:

h	= layer thickness	(m)
V	= electromagnetic pulse velocity through material in question	(m/ns)
t_2	= two-way travel time	(ns)

To obtain more accurate results, the data from the GPR survey should be assigned a calibration factor based on cores taken from the pavement structure being analyzed. A review by Plati & Loizos (2012) cited multiple reports that have concluded that using GPR to estimate pavement structural layer thicknesses is an effective procedure.

GPR was incorporated into this research project as part of the objective of controlling the consistency of pulverized FDR materials. A GPR survey was completed on a section of Route 790 near Lepreau, New Brunswick which was scheduled to be rehabilitated using expanded asphalt stabilized FDR. Depth measurements were taken at intervals of 10 cm, and the data was correlated to various test pits dug on site.

With the results from the GPR survey, different subsections of pulverization depths were delineated to maintain an approximately consistent blend ratio. Specifying subsections in

which the depth of pulverization would be varied to accommodate the varying pavement thicknesses was expected to lead to consistent quality in the FDR materials.

3.2 Unbound Material Test Procedures

The first phase of testing was done to evaluate the quality and consistency of the unbound, as-received, material. The following tests were completed on the unbound material:

- gradation
- moisture-density relationship
- maximum relative theoretical density
- granular resilient modulus
- direct shear strength
- CBR

With the information from these results, it would be possible to evaluate the quality and consistency of the as-produced Route 790 material.

3.2.1 Gradation

Material gradations are one of the most important physical properties, as the size distribution of the mix affects a number of other properties including density, moisture susceptibility, stiffness, and strength. Given the relatively quick testing time, and the simplicity of the test method, it is commonly used for both initial testing during the mix design stage, as well as following construction as a test against specifications for quality control.

Test procedures outlined in ASTM D6913 were used to determine the gradations of the Route 790 materials. Material was dried at 40°C to constant mass prior to testing. The washed sieve procedure was followed, and material was again dried to constant mass at 40°C after washing. This resulted in a longer testing time, stretching several days, but yielded accurate results. If excess temperatures were used, the recycled asphalt material

would soften and break apart, resulting in gradation results not representative of what was actually constructed. These concerns are similar to the concerns noted in Section 4.1.1 regarding the use of post-extraction gradations.

3.2.2 Moisture-Density Relationship

Moisture-density testing is used during the FDR mix design stage to determine the optimum mixing moisture content, and maximum dry density. The maximum dry density is used as the target density during construction. Optimizing moisture content and density are important as low levels of compaction could lead to problems with excessive permanent deformation, or moisture damage in the constructed base.

With varying density along a section, the quality of the materials could also be expected to vary. This test was used in the research project because having material exhibiting a consistent maximum dry density at all locations would allow this single value to be targeted during construction, with the confidence that achieving that level of compaction would lead to the desired performance.

The moisture-density relationship was determined using procedures outlined in ASTM D698, using standard Proctor effort. Although it is recommended that a modified Proctor test be done for expanded asphalt mix designs, the standard Proctor test was used in order to better collaborate with a research project completed in conjunction with this project, which used standard effort for Proctor tests.

To determine the moisture-density relationship, material was first dried to constant mass at 40°C. Different amounts of water were mixed into each sample, and the material was compacted with standard effort into the Proctor mould, which had a known mass and volume. The compacted sample in the mould is shown in Figure 3-2. The mass of the material and mould were then recorded, and the wet density calculated.

Figure 3-2 Compacted sample in Proctor mould

After recording the mass of the sample and mould, the material was removed from the Proctor mould, and the moisture content was determined by drying the material to constant mass. Knowing the moisture content, the maximum dry density could then be calculated.

3.2.3 Maximum Relative Theoretical Density

The MTD is a measure of the density of the material with no air voids between the particles. Though it is not possible to achieve this density in the field during construction, it is often used to evaluate the amount of air voids in the actual constructed material.

MTD was determined by first drying the materials at 40^{o}C to constant mass, then proceeding with the standard test procedure, outlined in ASTM D2041/2041M. Testing was done at the LVM/Maritime Testing laboratory.

3.2.4 Granular Resilient Modulus

The resilient modulus of a granular material has a large impact on the performance of that material, and its ability to resist load. The higher the resilient modulus, the more load the material can withstand without excessive deformation or failure. Despite the importance of the resilient modulus, it is not routinely performed on granular materials. This is due to the labour-intensive test procedure, and the specialized equipment required doing the test. The results from other tests, such as the CBR, have been correlated to resilient modulus, and are often used as a means of estimating resilient modulus for pavement design.

Testing for resilient modulus was included in the research program in order to compare the stiffness of the materials without relying on the simpler, but less reliable correlations that have been developed. Along with gradation and moisture-density relationship, the granular resilient modulus is one of the most important tests in characterizing the quality of unbound materials.

Resilient modulus of the unbound material was determined using AASHTO T307 procedures. Testing was done on the Instron 8500 loading frame. Samples were first dried to constant mass, and then brought to the optimum moisture content. A cylindrical rubber membrane was placed inside a split steel mould. The material was placed in the mould in five lifts and compacted using an electric rotary hammer. Figure 3-3 shows the just compacted sample, as well as the hammer used.

Figure 3-3 Vibratory compaction of resilient modulus sample

After compaction, the split steel mould was removed, leaving the compacted sample enclosed by the rubber membrane, as shown in Figure 3-4.

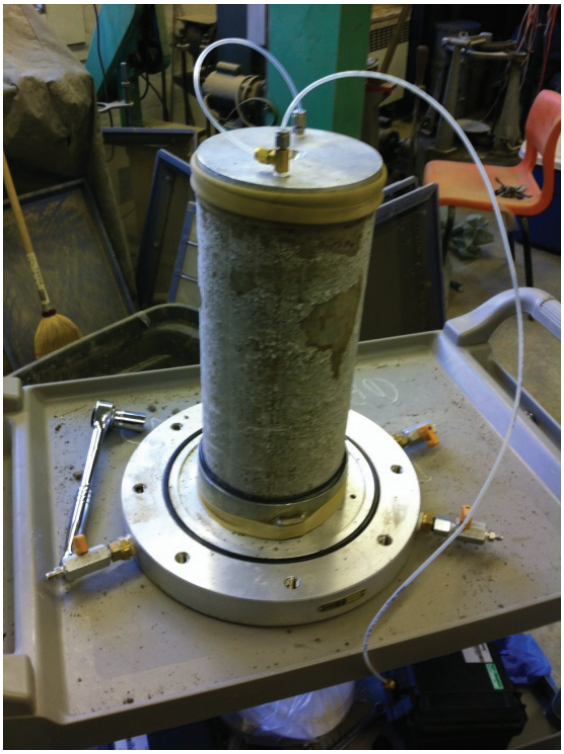

Figure 3-4 Resilient modulus sample enclosed by rubber membrane

The enclosure was then placed over the sample, and the entire triaxial chamber was placed on the Instron loading frame, as shown in Figure 3-5. One of the LVDTs used to record axial deformation can be seen above the chamber.

Figure 3-5 Triaxial chamber setup on load frame

Testing was carried out following the loading sequence given in AASHTO T307. Testing was to be halted either when the sequences were complete, accumulated deformation was too large, or when the sample yielded.

3.2.5 Direct Shear Strength

The direct shear strength test is not commonly done in pavement engineering, however it does measure two important parameters in soil evaluation: shear strength, and friction angle. These values are often estimated in practice, based on material classification. The

direct shear test is important in evaluating the strength of the materials, as well as identifying the level of cohesiveness in the materials. It was included as part of the research program in order to directly compare the strengths of the materials sampled from different locations.

Direct shear strength was determined using ASTM D3080 procedures. Samples were tested at optimum moisture content, and as close as possible to the maximum densities determined from moisture-density testing. A compacted sample is shown in Figure 3-6.

Figure 3-6 Compacted direct shear test sample

The sample was compacted with an impact force using a wooden mallet. The mass of the material and volume of the shear box was known. During compaction, measurements were taken periodically until the material was compacted to the correct density.

3.2.6 CBR

Unlike other test procedures described, the CBR test is an empirical test, which does not measure a fundamental property. The CBR test measures the relative strength of a material compared to that of a standard, well graded crushed material in resisting

penetration from a steel piston. The CBR test is often done in place of resilient modulus testing as it is a relatively simple and quick test to perform, which can be done under soaked or dry conditions. Because this test is commonly done in practice, it was included as part of this research program.

The CBR was determined using ASTM D1883 procedures. Testing was completed to determine CBR under both dry and soaked conditions. Material was first dried at 40°C to constant mass, and then brought to the optimum moisture content. It was compacted using standard effort into the 6 inch diameter mould. Samples for soaked CBR were then immersed in a water bath for 96 hours; samples for dry CBR were tested immediately. Testing was done on the apparatus shown in Figure 3-7.

Figure 3-7 CBR testing machine

Calibration had to first be done to ensure the machine applied load at the proper displacement rate. Testing on the samples was then completed, and the applied load determined from readings from the load gauges.

3.3 Expanded Asphalt Material Mixing and Compaction

The next phase of the testing program involved preparing mix designs for material stabilized with expanded asphalt. Separate mix designs were completed for each material gradation, and followed standard level 1 test procedures. The gradations to be used in this research project were first determined, and the FDR material was prepared. The asphalt cement was then tested to determine optimum mixing conditions, and a mix design was completed for each blend. The testing involved in this phase of the research project will be described in the following section.

3.3.1 FDR material blending

The first step in this phase of the project required establishing material gradations to be tested and compared, which will be explained in Section 4.2.1. This step was similar to what is done in practice, however in practice the materials that are blended together are the RAP and granular materials in set percentages to simulate the proper thickness blend ratio. In this project, the materials were combined by splitting into individual sizes the material collected during construction when the Route 790 section was being pulverized. In an effort to ensure reliability in the consistency of the blended materials, all material was dried to constant mass, and split down into individual sizes using Gilson Company Inc. testing screens, shown in Figure 3-8.

Figure 3-8 Gilson Company Inc. testing screens used to split material by size

The material was then recombined at the proper proportions to ensure the material accurately reflected what was specified in the mix design gradations. Material was split down and recombined in the laboratory facilities at LVM/Maritime Testing.

3.3.2 Asphalt foaming characteristics

When using expanded asphalt, testing must be completed to determine the temperature and water content which maximize the expansion ratio and half-life. Increased expansion ratio allows for better coating, and increased half-life allows for more mixing time. To determine optimum foaming conditions, the asphalt cement was foamed using moisture contents ranging from 2 percent to 4 percent, and at temperatures of 150°C, 155°C, and 160°C. After it was foamed and sprayed into a bucket, a dipstick, shown in Figure 3-9,

was used to measure the peak expansion, and a timer was used to measure half-life. This testing was done using the laboratory facilities and foaming equipment at AMEC.

Figure 3-9 Bucket and dipstick for evaluating asphalt foaming characteristics (Wirtgen Group, 2010)

The optimum temperature and water content added was selected to meet minimum expansion ratio and half-life values. The minimum requirements used in this project called for an expansion ratio of 10, and a half-life of 6 seconds.

3.3.3 Foaming and mixing

The FDR material was mixed and stabilized using a Wirtgen foamer and pugmill mixer, shown in Figure 3-10 and Figure 3-11, in the AMEC laboratory. This equipment is designed to simulate the field construction process. First the Wirtgen WLB10 laboratory scale foamed asphalt plant combined the hot asphalt cement with a set amount of water and air pressure. It then sprayed it out a nozzle into the pugmill mixer. The asphalt cement expanded in the pugmill mixer, already running with the FDR materials, allowing the FDR material to be coated.

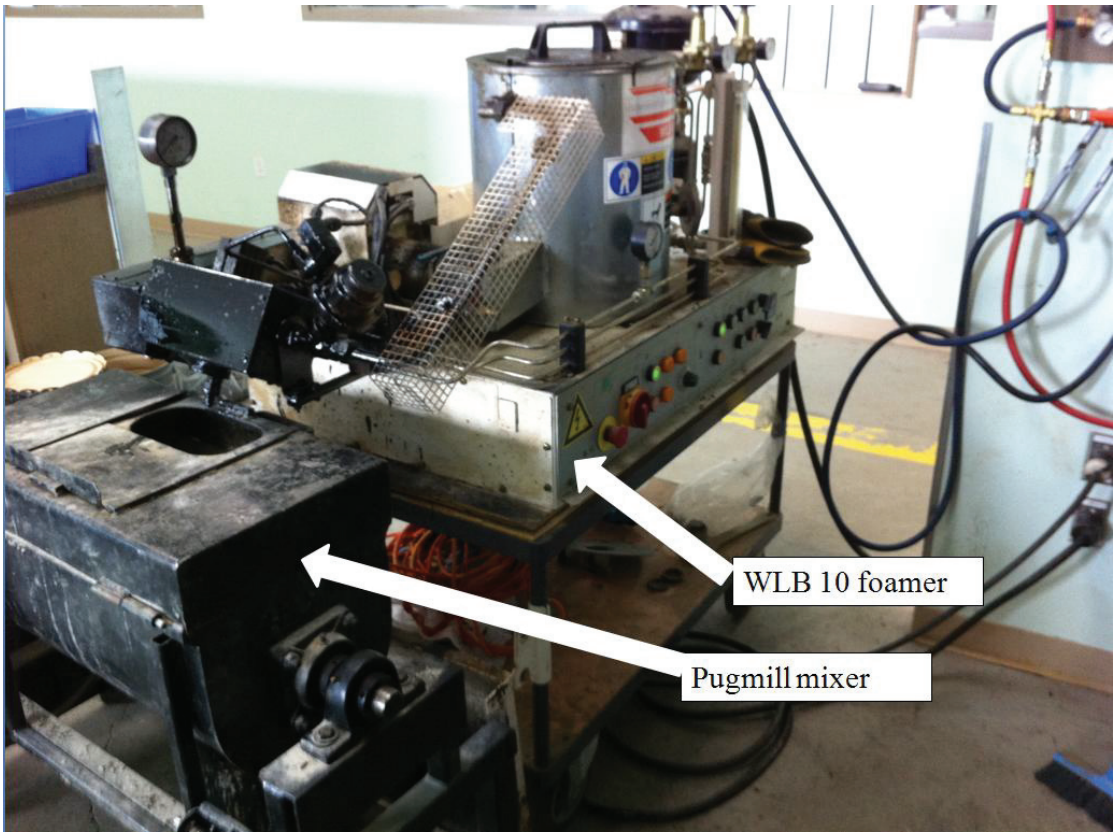

Figure 3-10 Wirtgen WLB 10 laboratory scale foamed asphalt plant with pugmill mixer

Figure 3-11 Wirtgen laboratory scale pugmill mixer

Problems with the pugmill mixer jamming were encountered periodically during mixing. When this happened before the foamed asphalt was added, the jam was cleared and mixing continued. In instances where the jam occurred immediately after the foamed asphalt was added, the batch was discarded. After a batch was successfully mixed, the material was immediately placed in a plastic bag and sealed until it was time for compaction.

3.3.4 Compaction and curing

The type of compaction, and curing procedure used can vary depending on the level of importance of the mix design. A number of compaction options may be used, depending on the goal of the testing. Proctor compaction effort may be used to evaluate the moisture-density relationship of the material, Marshall Compaction may be used for Level 1 testing, or vibratory compaction may be used for more advanced test procedures. Gyratory compaction also shows promise, though there are no standard mix design methods available to date which utilize gyratory compacted specimens.

To meet the requirements of the planned testing program, Marshall size, Proctor size, and gyratory sized samples were fabricated. All samples were compacted on the same day they were mixed, and followed standard Level 1 curing procedures. Compaction and curing was completed in the LVM/Maritime Testing laboratory.

Marshall size

Marshall sized samples, 101 mm in diameter and approximately 63.5 mm tall were made using standard Marshall compaction effort, as described in ASTM D6926. The material was subjected to 75 blows per side with a 4.536 kg mass free falling 457.2 mm, or the equivalent effort when the mechanical hammer was used. A typical Marshall sized sample is shown in Figure 3-12.

Figure 3-12 Marshall sized sample

After compaction, samples were extracted from the compaction mould, and placed in a forced draft oven at 40°C for 72 hours to cure. Some care had to be taken handling these samples as they were somewhat fragile prior to curing.

Proctor size

Proctor sized samples, 101 mm in diameter and approximately 115 mm tall were made with a Proctor hammer using standard effort, as outlined in ASTM D698. The material was compacted in three lifts, 25 blows per lift with a 2.5 kg mass free falling 304.8 mm. A typical proctor sized sample is shown in Figure 3-13.

Figure 3-13 Proctor sized sample

After samples were compacted, difficulties were encountered removing the specimen from the Proctor mould, and handling the specimens. The Proctor compacted samples were fragile, and did not bond together well As a result, all Proctor sized samples were cured, tested for bulk density, and subsequently discarded. Vibratory compaction may have been more effective in fabricating these specimens.

Gyratory size

Gyratory sized samples, shown in Figure 3-14, 152 mm in diameter and approximately 115 mm tall were made with a gyratory compactor, as outlined in ASTM D3387. The material was compacted at a pressure of 600 kPa, and a total of 75 gyrations.

Figure 3-14 Gyratory sized sample

After compaction, samples were extracted from the gyratory compaction mould and placed in a forced draft oven at 40°C for 72 hours to cure. The kneading action of the gyratory compaction resulted in samples which were noticeably more durable than the other samples.

3.4 Stabilized Material Tests

The final phase of testing compared the performance of the materials using three different gradations, and stabilized using expanded asphalt. The following tests were completed on the stabilized material:

- bulk density
- ITS
- resilient modulus
- dynamic modulus
- rutting testing

With the information from this suite of tests, it would be possible to evaluate the effect improving the gradation of the pulverized materials had on the quality of the stabilized FDR materials.

3.4.1 Bulk Density

The bulk density test is a simple volumetric test done in practice to quantify the approximate density of a compacted specimen.

To determine bulk density, measurements of the specimen height were taken using a calliper accurate to 0.01 mm, and using the average of four equally spaced measurements around the specimen. Mass was recorded, accurate to 0.1 grams, and bulk density calculated. Bulk density measurements were taken at the LVM/Maritime Testing laboratory after samples were cured.

3.4.2 Indirect Tensile Strength Test

The ITS test is commonly used for the evaluation of expanded asphalt stabilized FDR mix designs. The results from the ITS test are used for both level 1 and level 2 mix designs. It is a popular test thanks to its simplicity and short testing time. In addition to providing an indirect measure of tensile strength, the test also provides a measure of the

ability of the mix to resist water damage. This is done by testing specimens under dry and saturated conditions, and comparing the results relative to one another. Because this test is often used in pavement engineering, and because of this ability to use the results to evaluate moisture damage, the ITS test was included as part of the research program.

The ASTM D6931 test standard was used in completing ITS testing. A compressive load was applied at a uniform rate of displacement of 50.8 mm/min, and dial readings read from the calibrated proving ring. Testing was done at LVM/Maritime Testing on the testing apparatus shown in Figure 3-15.

Figure 3-15 ITS testing apparatus

Testing was completed at 25°C. In addition to being used to compare the materials under various conditions, ITS testing was also used as the main parameter in selecting optimum asphalt content during the expanded asphalt mix design process.

3.4.3 Resilient Modulus

The resilient modulus is one of the most important parameters in pavement design. Due to the specialized hydraulic loading equipment required, this test is not commonly done on expanded asphalt stabilized FDR samples. When completed, the resilient modulus test provides information on how much deformation a material will exhibit when subjected to a short load pulse. This test was included as part of the research program in order to compare the resilient modulus of the different mixes at a number of temperatures, thereby evaluating the effect of temperature on the strength of the mix.

The resilient modulus test on the stabilized specimens used indirect tension to relate load and displacement. The sample was subjected to a series of short, small loading pulses along the vertical diametrical plane, and resulting horizontal deformation measured. The load applied, a haversine waveform, was approximately 10 to 20 percent of the maximum ITS. LVDT's were initially used to measure horizontal displacement, however small eccentricities in the applied load resulted in a slight rocking motion in the sample, thereby rendering the results unreliable. The original setup using LVDT's can be seen in Figure 3-16.

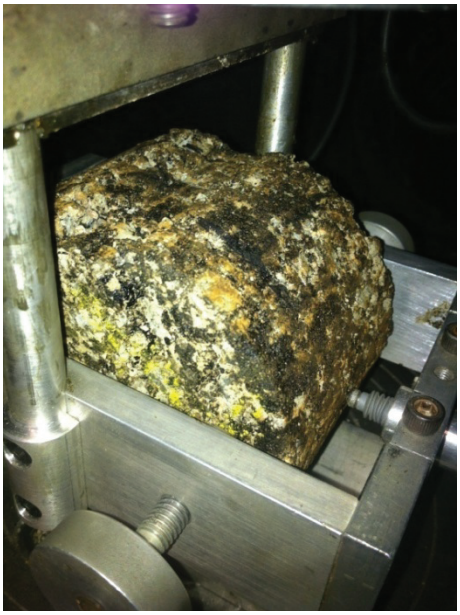

Figure 3-16 Resilient modulus sample setup using LVDTs to record deformation

Dynamic extensometers mounted directly on the sample were instead used, as shown in Figure 3-17. This method of recording horizontal deformation yielded more reliable and consistent results.

Figure 3-17 Dynamic extensometer mounted on resilient modulus sample

This test can be performed at a number of different temperatures, and in order to compare the performance of the materials over a range of temperatures, samples were tested at temperatures of -14°C, -4°C, 6°C, 25°C, and 42°C. The AASHTO T307 test standard was used as a guide in completing this testing.

3.4.4 Dynamic Modulus

The dynamic modulus was included as an input in the NCHRP (2004) Mechanistic-Empirical Pavement Design Guide. It provides more detailed information compared to the resilient modulus test since modulus information is determined for materials loaded over a range of temperatures and frequencies. Although it is required in Mechanistic-Empirical designs, the dynamic modulus is often estimated using equations developed based on past observations. This is done because the dynamic modulus test is a time-consuming test requiring specialized hydraulic loading equipment, and a large amount of data analysis. The test was included in the research program because the information

regarding material performance is useful in comparing the quality of the various FDR mixes tested in this research project.

The AASHTO TP62 test standard was used as a reference in completing dynamic modulus testing, however some variation from the test standard was required. Due to material quantity constraints, three Marshall sized samples were glued together using PL Premium Advanced© to achieve the necessary geometry. This was done because with the amount of material available in this research project for testing, it was not practical to fabricate gyratory specimens greater than 150 mm in height, to be cored and trimmed.

A study by Heritage Research Group, cited by McDaniel et al. (2005), investigated the effect of gluing samples together on the shear stiffness of HMA samples measured using the Superpave Shear Tester. The study found that the glued samples underestimated the stiffness of the specimens when compared to the original samples by an average of 17 percent. For this research project, similar variation was expected in the glued dynamic modulus test samples. Since the goal of the testing was to compare the blends to one another, and they were all tested in the same condition, testing was continued and comparisons made with confidence that the modulus results of the different mixes relative to one another could still be evaluated.

A sulphur end cap, as shown in Figure 3-18, was used to ensure a level, smooth testing surface. The end cap is the same type that is used in testing concrete cylinders for compressive strength. The end cap corrected any height imperfections in the sample, providing a smooth, flat testing surface.

Figure 3-18 Dynamic modulus sample glued and capped

AASHTO TP62 recommends a target air void content of 7.0% for dynamic modulus testing. Given the nature of the materials, and the goals of the project, the samples were tested "as-compacted", meaning after being subjected to 75 blows per side for each Marshall sample.

Testing was done at temperatures of -10°C, 6°C, 22°C, and 41°C. At each temperature, testing was done at load frequencies of 25 Hz, 10 Hz, 5 Hz, 1 Hz, and 0.1 Hz. Although AASHTO TP62 requires testing at 54°C, this was not done since, as a base material insulated by the overlying layer, the FDR layer would be unlikely to reach this temperature in service. Testing was done at the coldest temperature first, and at each individual temperature, testing started at the higher loading frequencies, and proceeded to the lower frequencies. These steps were taken to minimize the effect of permanent deformation in the sample, which experiences greater deformation at higher temperatures and lower load frequencies.

When testing, the cyclic load applied must result in axial strains between 50 and 150 microstrain. Data had to be analyzed immediately after testing, using a Matlab program

on a separate computer. From this analysis, the load was adjusted and sample retested until axial strains were in the allowable range.

3.4.5 Rutting Testing

Although rutting tests have often been done to evaluate the rutting potential of a mix, they are not typically used as a criterion in mix design acceptance. Loaded wheel tracking devices such as the Asphalt Pavement Analyzer may be used to compare the rutting susceptibility of two mixes relative to one another; however Kandhal & Cooley (2002) noted the results cannot be directly correlated to field performance. The rutting test may be used for mix design acceptance in some cases when state agencies set a maximum allowable Asphalt Pavement Analyzer rut depth based on local conditions and past experience (Johnson et al., 2005). The Asphalt Pavement Analyzer rutting test was included in this research program because the objective of the research was not to relate the results to field performance, but rather to compare the rutting potential of the various FDR mixes to one another,.

The AASHTO T340 standard was used as a guide in completing rutting testing. In order to perform a rutting analysis on the materials, samples 150 mm in diameter, and approximately 115 mm high were made using a gyratory compactor. These samples were then trimmed to a height of approximately 75 mm, as shown in Figure 3-19,

Figure 3-19 Gyratory sized sample after cutting for rutting testing.

The trimmed samples were placed in the Asphalt Pavement Analyzer, as shown in Figure 3-20. Testing was to be completed at 40°C, and the chamber was set to this temperature, and samples were left to stabilize for 6 hours before testing. After this waiting period, a hose pressurized to 490 kPa was lowered onto the sample, and a load of 445 N was applied by the loading wheel on to the pressurized hose. The wheel was set to cycle across the hose at a rate of 1 cycle per second either 8000 times, or until a specified failure criterion, a rutting depth of 12.7 mm, had been reached.

Figure 3-20 Two samples for rutting test in the Asphalt Pavement Analyzer

Two samples from the mix were tested simultaneously, with one sample in front of the other, as shown in Figure 3-20. Rut depth measurements were taken from five different locations for each specimen after each cycle, and the information logged in a Microsoft Excel file for analysis.

CHAPTER 4: RESULTS AND DISCUSSION

The following section presents a summary and discussion of the test results. The results and discussion of the unbound material testing are first presented. The expanded asphalt mix designs are then detailed in Section 4.2, followed by a discussion and analysis of the stabilized material testing results in Section 4.3.

4.1 Unbound Material Tests

The first phase of the project involved testing material sampled at six different locations from an FDR project along Route 790 near Lepreau, New Brunswick. A GPR pavement thickness survey was used to divide the section into a series of subsections in which pulverization depth would be varied, in an effort to maintain an approximately consistent blend ratio. The total asphalt concrete thickness and the suggested pulverization depths are shown for the northbound lane in Figure 4-1, and for the southbound lane in Figure 4-2.

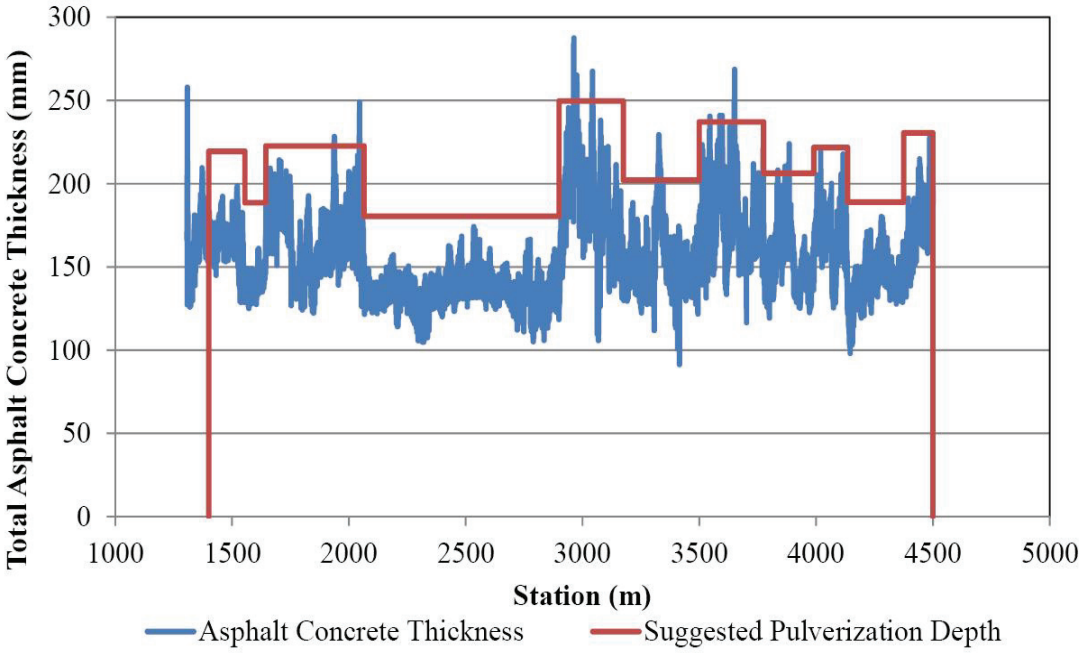

Figure 4-1 Route 790 northbound lane total pavement thickness and suggested pulverization depth

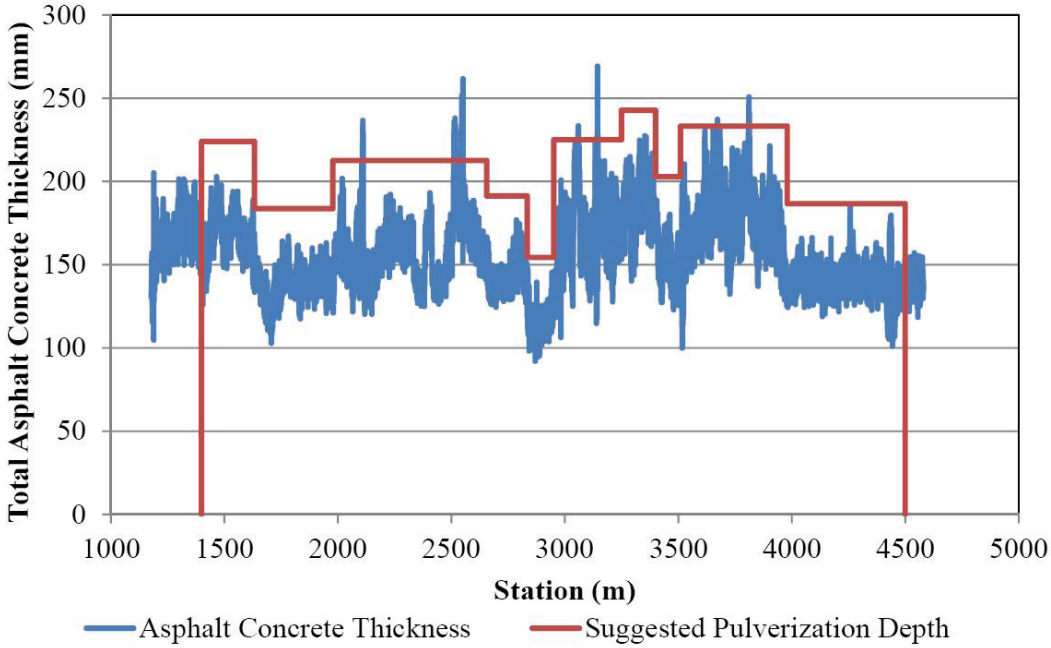

Figure 4-2 Route 790 southbound lane total pavement thickness and suggested pulverization depth

Samples were taken at locations where the blend ratio was almost exactly 0.75, as specified in the job mix formula. Shown in Table 4-1 are the sample locations, and the blend ratio determined at each location based on the GPR survey.

Table 4-1 Route 790 sample locations and blend ratios

Sample Location	Blend Ratio
1+769	0.74
2+185	0.74
2+550	0.75
3+128	0.76
3+446	0.76
4+040	0.76

Given the consistency of the estimated blend ratios, it was expected that the material properties of the FDR samples should exhibit similar consistency. If this was indeed true,

then it might follow that GPR based pulverization depth control may prove to be a valuable method of producing and more readily controlling consistent and higher quality FDR base materials.

4.1.1 Gradation

A sieve analysis was completed on material from each sample location. This was done to compare the gradation of the pulverized material to the gradation specified in the job mix formula. It was also done to evaluate the consistency of the materials in order to demonstrate that by controlling blend ratio, the consistency of the material produced would also be controlled. The results from the sieve analysis completed on material sampled from six locations during construction, as listed in Table 4-1, are shown graphically in Figure 4-3. Also shown is the blended job mix formula for the Route 790 construction project, as provided by the contractor prior to construction. Numerical gradation results can be found in Appendix B.

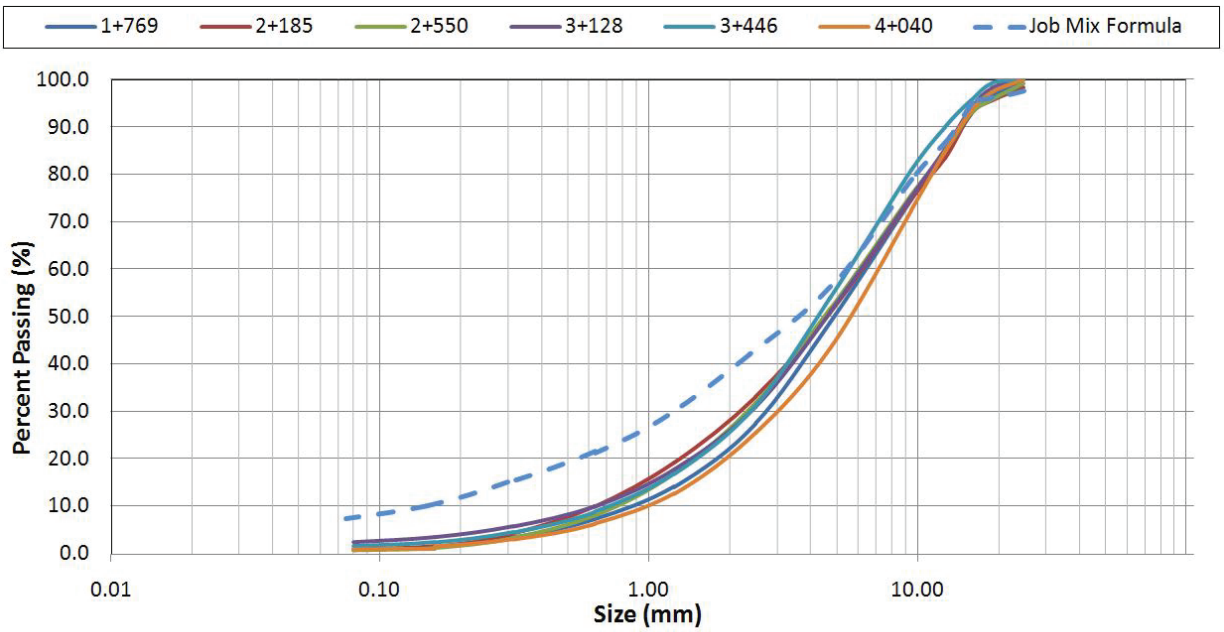

Figure 4-3 Route 790 job mix formula and sample gradations

While the results showed good consistency between the samples, there was a large discrepancy noted between the job mix formula gradation, and the as-built gradations. The as-built material appeared to be relatively lacking in fines, with the average percent passing the 0.080 mm sieve being 1.2 percent, compared to the job mix formula which called for 7.5 percent.

This variation in fines may have been due to the method used during the mix design phase to estimate the fines content. The mixture design approach required the determination of the asphalt cement content within the recycled asphalt concrete fraction of the FDR aggregate in order to provide a basis for determining the amount of virgin liquid asphalt cement added during the stabilization process. The Route 790 job mix formula was based on post-extraction gradations, while the testing on the field collected samples was based on as-produced materials, without extracting the asphalt cement. The pulverization and mixing construction processes are considered to be a cold recycling methodology since the recycled materials are processed in-situ and without additional heat. As a result, the fines bound within the existing asphalt concrete do not become liberated, but instead are pulverized into conglomerate particles of aggregates bound within the aged asphalt cement. The conglomerate particle gradation and densification behaviour differs significantly from the post-extraction gradation of unbound and liberated hot mix asphalt concrete and base aggregates.

To study this further, a sample from location 2+185 was tested by first performing an asphalt extraction, and then doing a sieve analysis on the material. The results of this testing are shown graphically in Figure 4-4, along with the as-produced gradation from that location, as well as the blended job mix formula. Additional fines, expected to be created during multiple passes with the pulverizing machine, were included in the job mix formula. During the course of this research project, it was found that additional fines may not necessarily be produced as a result of these additional passes; however this is an area which requires additional investigation. Numerical gradation results are presented in Appendix B.

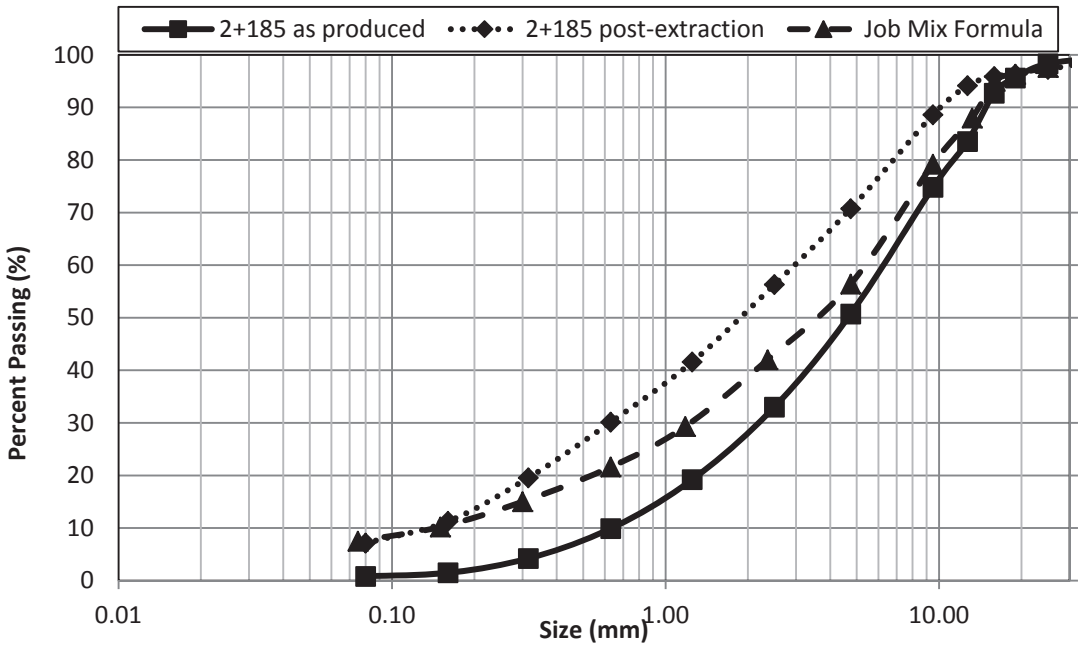

Figure 4-4 Sample location 2+185 material gradations As-Produced compared to Post-Extraction and Job Mix Formula gradations

The results shown in Figure 4-4 confirmed that the Route 790 material had a significant amount of fines that were bound by the old asphalt cement. This is an important point because the FDR process is a cold process, so it is reasonable to conclude there would not enough heat generated during the construction process to heat the material and liberate these fines, which were assumed available in the mix design. These findings would be the basis for the second phase of the study, utilizing a conglomerate particle design approach, described in Sections 4.2 and 4.3.

4.1.2 Other Physical Properties

Shown in Table 4-2 are CBR, MTD, moisture-density relationship, and resilient modulus results. Shown in Table 4-3 are results from direct shear testing. Detailed results for all properties, including graphs where relevant, are included in Appendix B. The resilient modulus values shown are from loading sequence number 2 from the AASHTO T307 test standard, as most samples were only successfully tested up to that sequence, before failing. The compacted resilient modulus samples yielding after only the second testing

sequence suggested that the reclaimed Route 790 aggregates were a poor quality material. Even in a controlled setting, the materials could not withstand increased loads without failing.

Table 4-2 Summary of Route 790 FDR aggregate physical properties

Location	CBR (Unsoaked)	MTD	OMC	Maximum Density (kg/m^3)	Resilient Modulus (MPa)
1+769	3.6	2.491	5.59%	1760	52.8
2+185	3.2	2.504	5.85%	1796	57.8
2+550	3.2	2.509	5.30%	1802	54.2
3+128	4.2	2.505	4.58%	1859	54.1
3+446	2.8	2.486	6.70%	1818	50.6
4+040	2.9	2.487	5.37%	1768	37.0
Mean	3.3	2.497	5.57%	1800	51.1
Standard Deviation	0.5	0.010	0.70%	35.9	7.3

Table 4-3 Direct shear testing results under various normal stress conditions

Location	τ_{max} (50 kPa) (kPa)	τ_{max} (98.1 kPa) (kPa)	τ_{max} (150 kPa) (kPa)	θ
1+769	40.2	85.0	126.4	40.7
2+185	47.1	85.0	122.9	37.2
2+550	41.9	86.2	124.7	39.6
3+128	46.5	85.6	125.2	38.2
3+446	43.7	82.7	122.4	38.2
4+040	45.4	87.3	126.4	39.0
Mean	44.1	85.3	124.7	38.8
Standard Deviation	2.7	1.5	1.7	1.2

There was good consistency between sample locations for all tests. Despite the consistency, the material itself appeared to be a poor quality base material. With CBR values below 5, and the average resilient modulus being just 51.1 MPa, without stabilization this was more characteristic of a weak subgrade material. Wirtgen Group (2010) described a material with CBR values of 3 or less as a "poor" quality subgrade, therefore this material, without stabilization to increase strength, would not be appropriate for use as a base or subgrade material.

Based on the low standard deviations, evident throughout every single test, the research project was advanced to the next stage; a study of the conglomerate particle mix design method, and the effect of gradations.

4.2 Expanded Asphalt Stabilization

The first step of the expanded asphalt mix design was to blend the materials and determine the optimum moisture contents. The foaming characteristics of the asphalt cement were then evaluated, and the materials were stabilized and compacted. Finally, based on recommendations in the Wirtgen Group (2010) design guide, ITS testing was completed to determine optimum asphalt content.

4.2.1 Material Blending

As part of this research project, the Route 790 material was to be compared using three different blends: "As-Is", "Improved", and "Optimum". The materials were blended together following a conglomerate particle design approach. This approach involved using the as-produced gradations, rather than the post-extraction gradations. In the case of the "Improved" and "Optimum" blends, this resulted in the ability to better target the maximum density curve, described in Section 2.1.1. In the case of the "As-Is" blend, it resulted in a more accurate representation of the as-built materials, with the gradation being representative of the field collected samples. To stay consistent with standard

practice at the time, and as used in the actual stabilization process used in the project, 0.5 percent Portland cement (PC) was used as an additive for all mixes.

No changes were made to the "As-Is" materials. The "Improved" blend incorporated the use of a corrective aggregate, 15.6 percent screened crusher dust (CD), resulting in a more suitable gradation that more closely matched the Fuller-Thompson maximum density curve. The "Optimum" blend utilized the Route 790 material with a small amount of corrective aggregate, and the gradation was manipulated to exactly follow the theoretical maximum density line. Figure 4-5 shows the grading curve of each material blend that was tested. Numerical gradation information on the material blends is included in Appendix B.

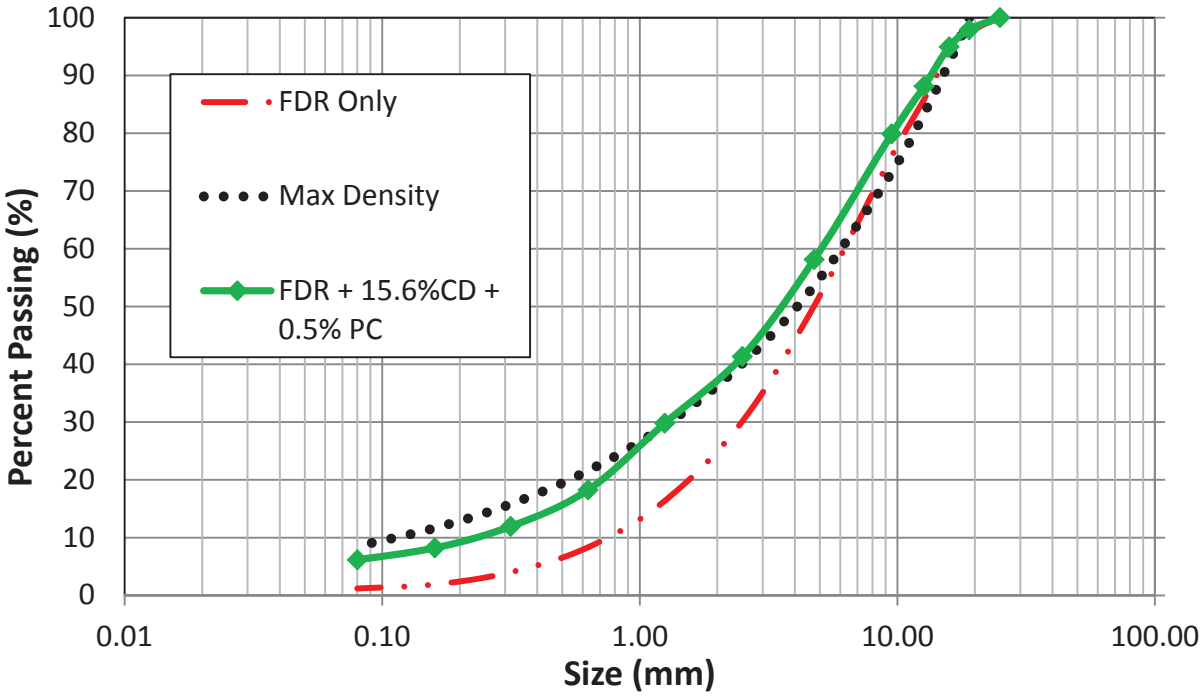

Figure 4-5 Design mix formula gradations for three blends

Material was dried in an oven at 40°C to constant mass, split down into the individual sizes, and then recombined at these specific job mix formula gradations.

4.2.2 Asphalt foaming characteristics

McAsphalt PG58-28 was provided by McAsphalt Industries Ltd. and used to stabilize the FDR materials. Testing was carried out to determine the foaming conditions which would maximize expansion ratio and half-life. Tests were done at temperatures of 150°C, 155°C, and 160°C. Water added ranged between 2 percent and 4 percent of the asphalt mass. The resulting half-life and expansion ratio observed are shown in Table 4-4.

Table 4-4 McAsphalt PG58-28 foaming characteristics

Temperature	**150^{o}C**		**155^{o}C**		**160^{o}C**	
Water Added	**Expansion Ratio**	**Half-Life (s)**	**Expansion Ratio**	**Half-Life (s)**	**Expansion Ratio**	**Half-Life (s)**
2.0 %	6.0	11.90	5.0	16.00	9.4	14.65
2.5 %	8.2	11.46	6.7	15.50	11.0	13.50
3.0 %	8.6	10.37	8.7	12.28	11.2	10.48
3.5 %	10.2	9.53	9.0	9.53	11.6	11.08
4.0 %	11.0	8.55	12.0	10.15	11.8	7.79

From these observations, 160^{o}C and 2.75 percent water addition were selected as optimum asphalt foaming characteristics. Based on a plot of these results, shown in Appendix B, this would provide a half-life of approximately 12.0 seconds, and an expansion ratio of approximately 11.0. This satisfied the minimum requirements recommended by Wirtgen Group (2010), which suggest a minimum expansion ratio of 10 and a minimum half-life of 6 seconds.

4.2.3 Mix Designs

Individual mix designs were completed on all three blends. The first step of the mix design process was to determine the optimum moisture content and maximum dry density of each material blend. The material was compacted using standard effort at a range of

different moisture contents, and the results plotted. From these plots, the optimum moisture content and maximum dry density were determined. The optimum moisture content and maximum dry density of each blend are shown in Table 4-5. It is important to note that the "Improved" and "Optimum" gradations exhibited similar maximum dry densities, which were approximately 75 kg/m^3 higher than that achieved using the "As-Is" gradation. The moisture-density relationship of each blend is shown in Appendix B.

Table 4-5 Optimum moisture contents and maximum dry densities of three material blends

Grading:	Maximum Dry Density (kg/m^3)	OMC (%)
As-Is	1696.3	6.05%
Improved	1869.2	5.23%
Optimum	1872.9	5.35%

After the optimum moisture content was determined, material was mixed at asphalt contents between 2.0 percent and 4.5 percent. Marshall sized samples were made, and cured for 72 hours at 40°C. Three samples for each asphalt content were placed in a 25°C water bath for 24 hours, while three others were set aside. After the 24 hour soak, ITS testing was completed on all samples. Results were plotted, and from these plots the optimum asphalt content was selected. These results are shown for the "As-Is", "Improved", and "Optimum" blends in Figures 4-6, 4-7, and 4-8 respectively. Numerical results are shown in Appendix B.

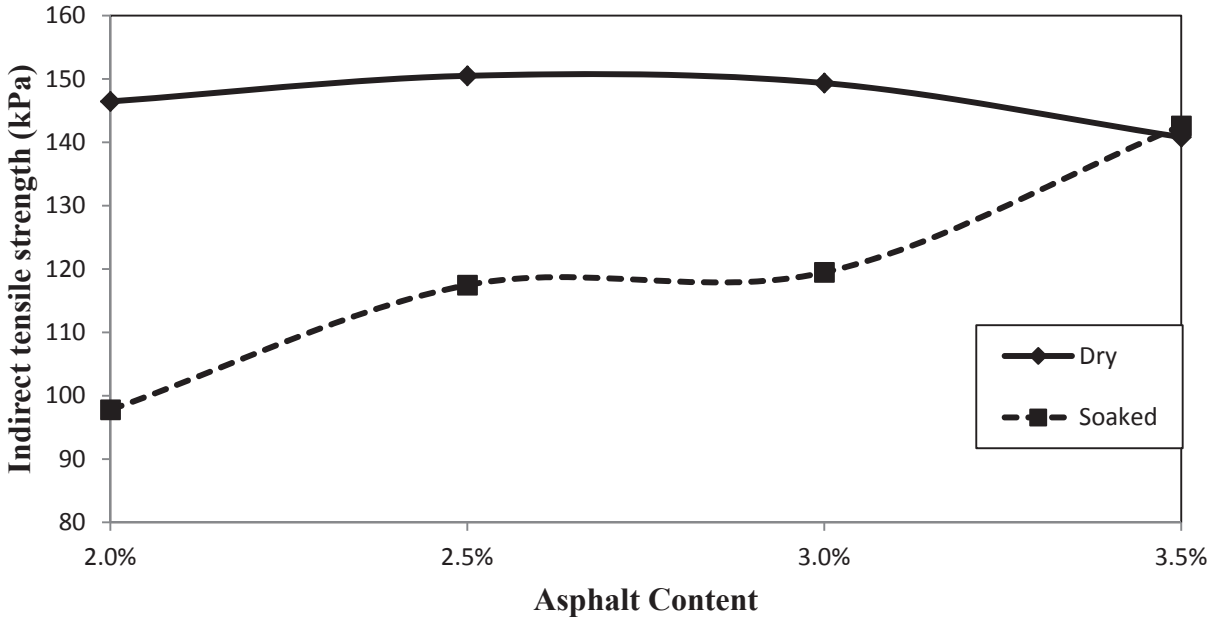

Figure 4-6 "As-Is" blend: ITS vs. asphalt content

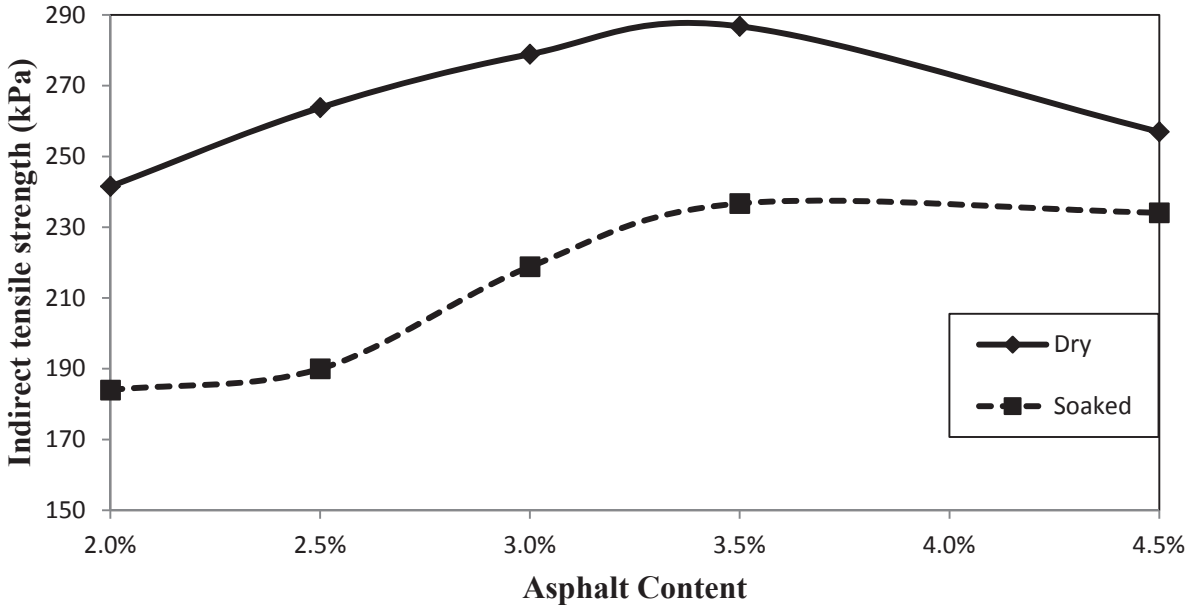

Figure 4-7 "Improved" blend: ITS vs. asphalt content

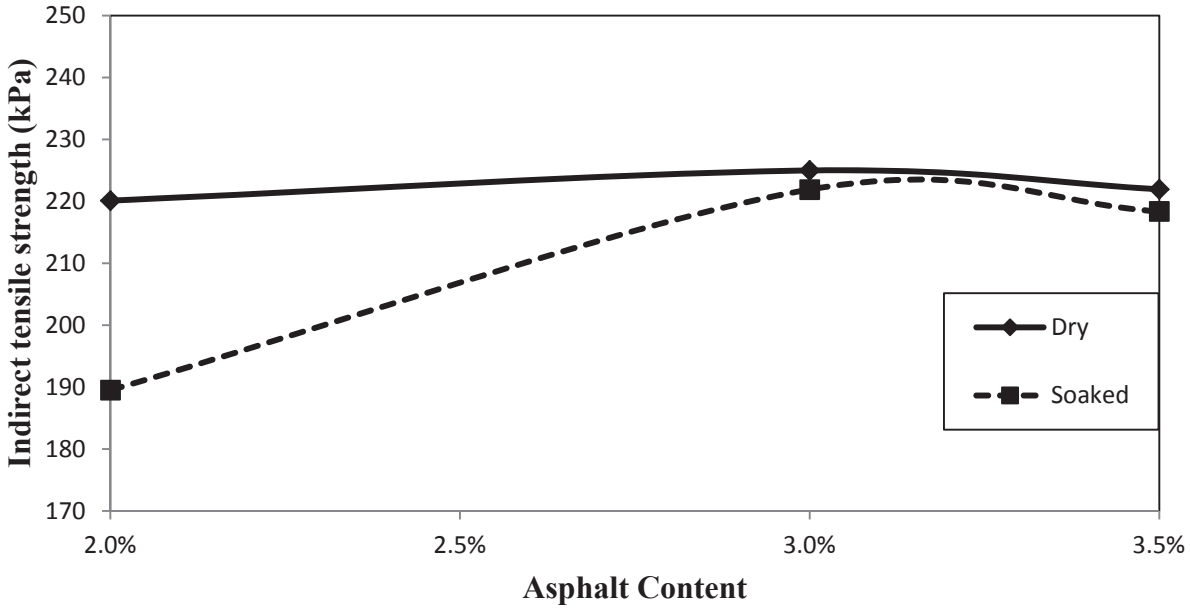

Figure 4-8 "Optimum" blend: ITS vs. asphalt content

The optimum asphalt content was selected based on the ITS results. A standard mix design procedure would require asphalt content be selected as the minimum amount to achieve specified strength requirements. Since these mix designs were completed for research purposes only, the asphalt content was chosen to maximize ITS_{dry}. The optimum mixing conditions determined from mix design testing are listed in Table 4-6. Numerical indirect tensile strength results for each mix are presented in Table 4-9 in Section 4.3.2.

Table 4-6 Expanded asphalt mix design results

Grading	Asphalt Content	Moisture content
As-Is	2.5%	6.05%
Improved	3.5%	5.23%
Optimum	3.0%	5.35%

In addition to testing under these optimum mixing conditions, part of this research project also involved varying the moisture content and asphalt content on the "Improved" blend

to simulate construction variability. From these results, moisture contents of 3.00 percent and 6.60 percent, as well as asphalt contents of 2.5 percent and 4.5 percent were selected as the variable conditions in which the "Improved" blend would be tested.

4.3 Stabilized Material Tests

The next phase of testing entailed evaluating the properties of the stabilized materials. A range of testing was done to simulate the effect that varying gradations and construction variability, in the absence of GPR based pulverization control, would have on performance. Table 4-7 can be used to identify each mix, where they appear in graphs labelled numerically throughout the report. Throughout this thesis, the blends mixed at optimum moisture and asphalt content appear in bold font when compared to other mixes in Tables.

Table 4-7 Numerical identification of each mix

Grading	Asphalt Content	Moisture content	Mix label
As-Is	**2.5 %**	**6.05 %**	**1**
Improved	2.5%	5.23%	2
Improved	3.5%	3.00%	3
Improved	**3.5 %**	**5.23 %**	**4**
Improved	3.5%	6.60%	5
Improved	4.5%	5.23%	6
Optimum	**3.0 %**	**5.35 %**	**7**

Results from the stabilized material tests are detailed in the following sections. These sections present a summary and discussion of the test results obtained from stabilized material testing. Detailed results for each mix have been included in Appendix B.

4.3.1 Bulk Density

The first stage of the testing program consisted of volumetric testing. The bulk density of every compacted sample was calculated, and the average bulk densities for each mix, and sample type, are presented in Table 4-8.

Table 4-8 Bulk density results (kg/m^3)

Grading	Asphalt Content	Moisture content	Marshall	Proctor	Gyratory
As-Is	**2.5 %**	**6.05 %**	**1949.7**	**1781.6**	**2083.5**
Improved	2.5%	5.23%	2007.3	1751.3	2100.7
Improved	3.5%	3.00%	2025.4	1766.4	2095.9
Improved	**3.5 %**	**5.23 %**	**2036.4**	**1764.1**	**2102.5**
Improved	3.5%	6.60%	2031.3	1758.1	2106.9
Improved	4.5%	5.23%	2017.2	1755.7	2098.4
Optimum	**3.0 %**	**5.35 %**	**2006.9**	**1789.8**	**2104.7**

The Proctor samples had bulk densities significantly lower than samples made with other compaction methods. These findings were consistent with qualitative observations of the samples. Based on these results, Proctor compacted samples were discarded from further testing.

Consistent with the moisture-density testing results on the unstabilized material blends, the "As-Is" blend was consistently lower in bulk density compared to other mixes. The "Improved" and "Optimum" blends had very similar densities, with fluctuations occurring with the "Improved" blend densities depending on the asphalt content and mix moisture content. The fluctuations were minor however, and the bulk density did not generally appear to be affected by these variations.

4.3.2 Indirect Tensile Strength

The ITS test was completed on three samples for each condition, soaked and dry. The samples were tested four days after compaction, and ITS results are presented in Table 4-9. Optimum conditions for each blend are in bolded text.

Table 4-9 ITS results for each mix

Grading	Asphalt Content	Moisture content	ITS_{dry} (kPa)	ITS_{wet} (kPa)	TSR
As-Is	**2.5 %**	**6.05 %**	**150.5**	**117.5**	**78.1 %**
Improved	2.5%	5.23%	263.8	190.0	72.0%
Improved	3.5%	3.00%	199.8	157.2	78.7%
Improved	**3.5 %**	**5.23 %**	**286.8**	**236.7**	**82.5 %**
Improved	3.5%	6.60%	245.3	187.8	76.6%
Improved	4.5%	5.23%	257.0	234.1	91.1%
Optimum	**3.0 %**	**5.35 %**	**225.0**	**221.9**	**98.6 %**

A large increase in ITS under soaked and dry conditions was noted between the “As-Is” blend and the “Improved” blend. The ITS of the "Improved" blend was 91 percent higher under dry conditions, and 101 percent higher under soaked conditions.

The results also showed that, though the strength was lower than the “Improved” blend, the “Optimum” blend also performed better than the “As-Is” blend. The “Optimum” blend had a TSR near 100 percent which suggests that the 24 hour soak had little effect on the specimen’s ability to resist load. The results showed a trend in which the TSR increased as the material gradation curve approached the Theoretical Maximum Density curve. It therefore follows that a tighter specification on gradation limits, as well as the use of corrective aggregates to target an optimal gradation, would result in the ability to engineer more durable bases, able to resist moisture damage.

It was noted that moisture content had a greater impact on ITS, more so than asphalt content. Mixing the "Improved" blend at the moisture content below optimum resulted in a strength decrease of just over 30 percent under dry conditions, and 33.6 percent under soaked conditions. There was also a decrease in strength when mixing at increased moisture contents, though not as severe. The loss of strength when mixing at a lower moisture content was likely caused by the lower moisture content leading to a lower density. As described in Section 2.2.1.2, water is required to provide lubrication and reduce surface tension. The lower moisture content may have resulted in a reduced density, and reduced levels of aggregate interlock, thereby reducing strength in the compacted specimens. The increased moisture content would affect compaction since the extra moisture would keep particles apart, again reducing aggregate interlock and strength. In both cases, it would be reasonable to infer that the magnitude of loss in strength would be dependent on the amount of variation in moisture content from optimum conditions.

There was also a decrease in strength with varying asphalt contents, but not as pronounced. The blend mixed at a lower than optimum asphalt content had a decrease in ITS of 8 percent under dry conditions and 19.7 percent under soaked conditions. When mixing at a higher than optimum asphalt content, there was a similar decrease under dry conditions, while there was a minimal decrease under soaked conditions. As expected the mix with higher asphalt content had the better TSR, as ITS_{wet} generally increases with increased asphalt content. The effect of varying moisture contents and asphalt contents from ideal mixing conditions is summarized in Table 4-10.

Table 4-10 Effect of varying moisture and asphalt content on ITS results of "Improved" material blend

		% change in ITS from ideal mixing conditions	
Asphalt Content	**Moisture content**	**ITS_{dry}**	**ITS_{wet}**
2.5%	5.23%	-8.0 %	-19.7 %
4.5%	5.23%	-10.4 %	-1.1 %
3.5%	3.00%	-30.3 %	-33.6 %
3.5%	6.60%	-14.5 %	-20.7 %

The long term ITS of the materials would be higher than the values presented. These were strengths determined 4 days after mixing, and the samples were still gaining strength. These results show that the "Improved" blend had a significantly higher early strength, compared to the "As-Is" blend, meaning it would be better able to withstand traffic loads at an early age.

4.3.3 Resilient Modulus

Resilient modulus results are presented in Table 4-11. These are the average results based on two replicate samples of each mix, and two modulus tests on each individual sample at each temperature. Individual test results are provided in Appendix B.

Table 4-11 Resilient modulus results (MPa)

Mix	Grading	Moisture Content	Asphalt Content	-14°C	-4°C	6°C	25°C	42°C
1	**As-Is**	**6.05%**	**2.5%**	**1950.2**	**1781.1**	**1284.5**	**568.5**	**333.8**
2	Improved	5.23%	2.5%	2664.4	1992.3	1858.0	776.9	335.9
3	Improved	3.00%	3.5%	3066.4	2100.6	1453.7	756.2	227.0
4	**Improved**	**5.23%**	**3.5%**	**3267.7**	**2707.3**	**2185.0**	**1029.5**	**411.6**
5	Improved	6.60%	3.5%	3494.6	2319.5	1675.9	947.2	388.7
6	Improved	5.23%	4.5%	3637.6	2210.0	1987.4	956.9	279.9
7	**Optimum**	**5.35%**	**3.0%**	**2841.9**	**2084.2**	**1501.3**	**1065.4**	**558.3**

Under ideal mixing conditions, the "As-Is" blend had modulus values significantly lower than those of the "Improved" and "Optimum" blends. This indicates that the "As-Is" constructed pavement would perform the poorest. Comparing the "Improved" blend and the "Optimum" blend, the "Improved" blend had higher modulus values at lower temperatures, but comparable, though somewhat lower, values at the increased temperatures. This suggests that at the lower temperatures, the increased asphalt content of the "Improved" blend contributed to the increased modulus. As described in Section 2.2.2.3, as temperature decreases, the viscosity of the asphalt cement increases, thereby increasing the overall stiffness of the mix. The "Improved" blend used 0.5 percent more asphalt cement than the "Optimum" blend, which led to a higher resilient modulus at low temperatures.

At higher temperatures, where the asphalt cement has decreased viscosity and less of an effect, the "Optimum" blend had the best performance. Berg et al. (1996) found that the resilient modulus of a material was dependent in part on the density of that material. In this case, the gradation of the "Optimum" blend, which was the ideal gradation for particle packing, led to a higher resilient modulus than the other blends at increased temperatures.

When comparing the "Improved' blend at different moisture and asphalt contents, the same theory regarding the effects of asphalt content held true. At low temperatures, increased asphalt content resulted in higher modulus values, which subsequently dropped off at higher temperatures. At low temperatures, the mix with the lowest asphalt content had the lowest resilient modulus. With increased temperature, similar to the ITS results, it was the blend mixed under dryer than optimum moisture conditions that had the lowest modulus results. This could once again be attributed to the decreased density which resulted from compacting at the lower than optimum moisture content.

Based on the results, it is evident that in terms of modulus values, the "Improved" blend was more tolerant to increased moisture contents compared to any other variation. The

reason for this is that the moisture content only had the effect of impacting the density of the samples during compaction. Once the material had fully cured, with all moisture removed, the variation in resilient modulus with temperature was primarily due to the change in properties of the asphalt cement in the mix. As stated in Section 2.2.2.3, the resilient modulus is largely dependent on the properties of the asphalt cement, therefore it follows that there would be large variations in the resilient modulus of the samples with different asphalt contents, more so than those with different moisture contents. The poorest performance overall came from the blends mixed at dryer moisture contents and lower asphalt contents.

4.3.4 Dynamic Modulus

Dynamic modulus results are shown in detail in Appendix B. A graph comparing the master curve of each mix at the standardized reference temperature of 21.1°C (70°F) is shown in Figure 4-9. Individual mixes are labelled as described in Table 4-7. From the dynamic modulus testing and analysis, the effect of loading frequency and temperature can be seen.

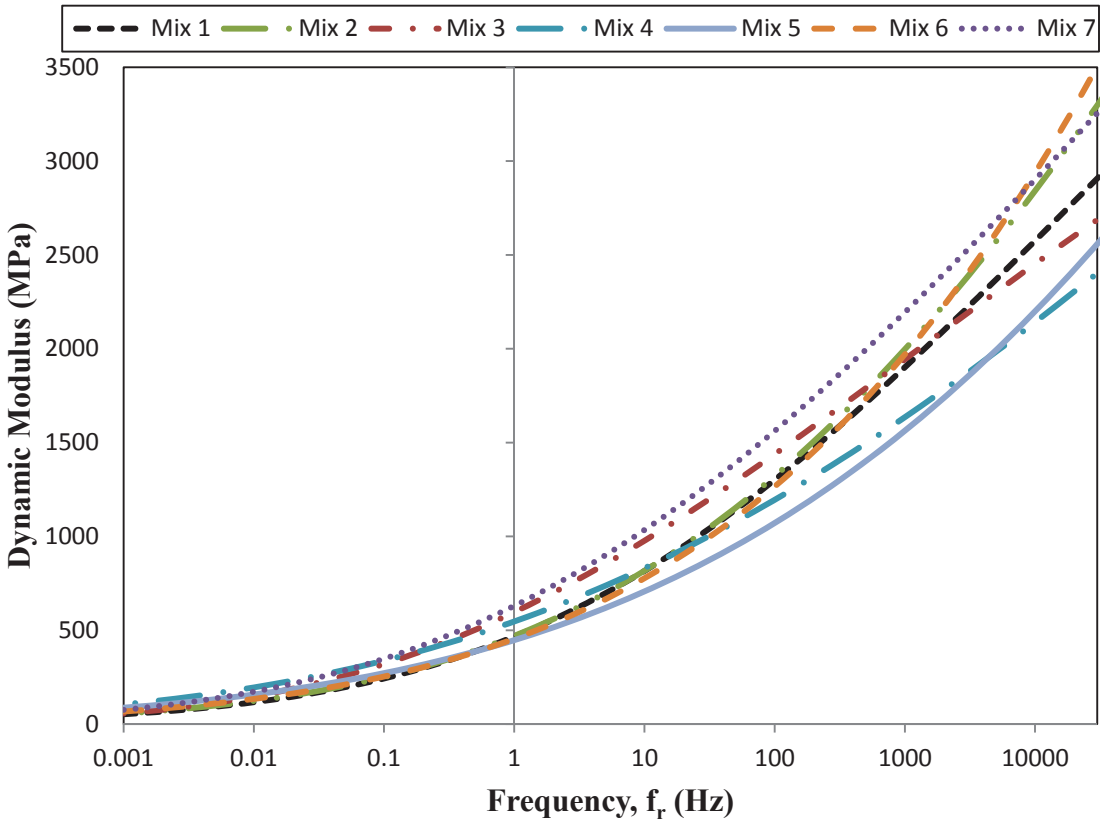

Figure 4-9 Master curve for each mix at 21.1°C reference temperature

The curves presented in Figure 4-9 can be misleading. Although it may appear that some blends performed better than others, dynamic modulus is a function of both temperature and loading frequency, so that may not be the case. Curves such as those shown in Figure 4-9 could be generated, and mixes compared with different results, for any number of temperatures. Therefore to accurately compare the various mixes, the temperature dependency as well as the modulus values at different frequencies must be evaluated.

The temperature dependency of each mix was compared by calculating the shift factor, as defined in Equation 2.11 and correlated for each mix, which would be used to translate modulus from the reference temperature at 21.1°C to temperatures of -10°C, 15°C, and 40°C. The results of these calculations are shown in Table 4-12. When moving to temperatures lower than the reference temperature, the lower the shift factor, the more

temperature dependent the mix. The opposite is true when moving to temperatures higher than the reference temperature, where larger shift factors suggest greater temperature dependency .

Table 4-12 Shift factor relating modulus at 21.6°C to temperatures of -10°C, 15°C and 40°C for each mix

Mix	Grading	Asphalt Content	Moisture content	a(-10)	a(15)	a(40)
1	**As-Is**	**2.5 %**	**6.05 %**	**0.00624**	**0.360**	**25.2**
2	Improved	2.5%	5.23%	0.00542	0.372	18.9
3	Improved	3.5%	3.00%	0.00546	0.353	26.1
4	**Improved**	**3.5 %**	**5.23 %**	**0.00082**	**0.277**	**37.1**
5	Improved	3.5%	6.60%	0.00198	0.307	33.5
6	Improved	4.5%	5.23%	0.00094	0.264	55.1
7	**Optimum**	**3.0 %**	**5.35 %**	**0.00151**	**0.306**	**29.4**

Evaluating the results from Table 4-12, the results generally showed strong correlation between asphalt content and temperature dependency. This is caused by the change, with temperature, in the viscosity of the asphalt cement, with viscosity increasing as temperature decreases. Similar to the resilient modulus, dynamic modulus is largely impacted by the asphalt content of the mix; therefore the mixes with more asphalt cement would exhibit greater variation in dynamic modulus with varying temperatures. Under ideal mixing conditions, the "As-Is" mix was least affected by temperature, likely due to the lower asphalt content of that blend. The "Improved" blend, which had the highest asphalt content of the three blends at 3.5 percent, was the most affected by temperature.

Temperature effects had a large impact on the "Improved" blend evaluated over a range of asphalt contents. There was less of an effect when varying mix moisture contents. Overall, the blend mixed with 4.5 percent asphalt showed a strong relationship between temperature and modulus, while the blend mixed with 2.5 percent was the least affected by temperature. Varying moisture contents also caused some variability in the

temperature effects of the mix however in general, the mixing moisture content had a relatively small impact on the temperature dependency of the mix.

Shifting the dynamic modulus values from the loading frequencies at the 21.1°C reference temperature, the actual performance of the materials could be compared at a number of different temperatures. Using the shift factors from Table 4-12, dynamic modulus values were determined at temperatures of -10°C, 15°C, and 40°C for each mix. Although values could be shifted to any number of temperatures and frequencies, dynamic modulus at a loading frequency of 0.1 Hz and 5 Hz were chosen for comparison, and the results shown in Table 4-13. These frequencies were selected since FDR is most often used on lower volume roads which could be expected to have lower speed limits, and therefore experience lower frequency levels of loading.

Table 4-13 Dynamic modulus results, in MPa, for each mix at specific temperatures and frequencies

	-10°C		**15°C**		**40°C**	
Mix	**0.1 Hz**	**5 Hz**	**0.1 Hz**	**5 Hz**	**0.1 Hz**	**5 Hz**
1	**904.7**	**1839.6**	**328.2**	**877.0**	**84.9**	**297.9**
2	934.7	1970.6	331.1	872.4	100.0	329.6
3	1091.8	1923.7	431.4	1042.1	101.0	387.2
4	**1231.1**	**2029.1**	**445.4**	**916.8**	**138.4**	**361.2**
5	951.1	1801.2	352.5	774.1	116.0	296.8
6	1282.7	2645.8	357.5	894.1	80.7	246.6
7	**1458.7**	**2554.9**	**478.6**	**1136.9**	**119.3**	**403.1**

Both temperature and frequency had a large effect on the dynamic modulus of all mixes. Evaluating the three blends mixed at ideal conditions and loaded at 0.1 Hz, the "As-Is" blend had the lowest modulus values. The "Improved" and "Optimum" blends were higher at 40°C, with a 63 and 41 percent increase respectively over the "As-Is" blend. Overall, the "Optimum" blend generally had the highest performance across all

temperatures, though the "Improved' blend also performed well, especially compared to the "As-Is" blend.

There was less of a change in modulus when loaded at the higher frequency of 5 Hz. The "Optimum" blend was again the consistently better performing material, with the "Improved" blend also performing well. It was noted that the "As-Is" blend performed relatively well when loaded at the higher loading frequency. The higher loading frequency likely contributed to the apparent "masking" of the deficiencies of that blend, with the load being applied over too small a timeframe to expose its weaknesses.

Examining the results of the "Improved" blend mixed at a range of asphalt contents and moisture contents, the results showed relative consistency between the blends. Mix number 6, which had the highest asphalt content, had higher modulus values at low temperatures, but dropped off when temperature increased. This as expected, given the decrease in asphalt cement viscosity that would occur at elevated temperatures. Mix number 2, which had the lowest asphalt content, generally had either lower, or very similar modulus values as the blend mixed under ideal conditions. The mixing moisture content had less of an effect on the modulus. The blend mixed at lower moisture content on average was within 7 percent of the ideal blend. The blend mixed at higher moisture content was generally lower than the ideal blend, but was within 10 percent on average.

4.3.5 Rutting Testing

The Asphalt Pavement Analyzer was used to evaluate the rutting potential of each mix. A graph comparing the average rut depths per load cycle for each mix is shown in Figure 4-10. These rut depth values were determined by taking the average of five depth measurements from each of the two samples tested. Individual mixes are labelled as described in Table 4-7.

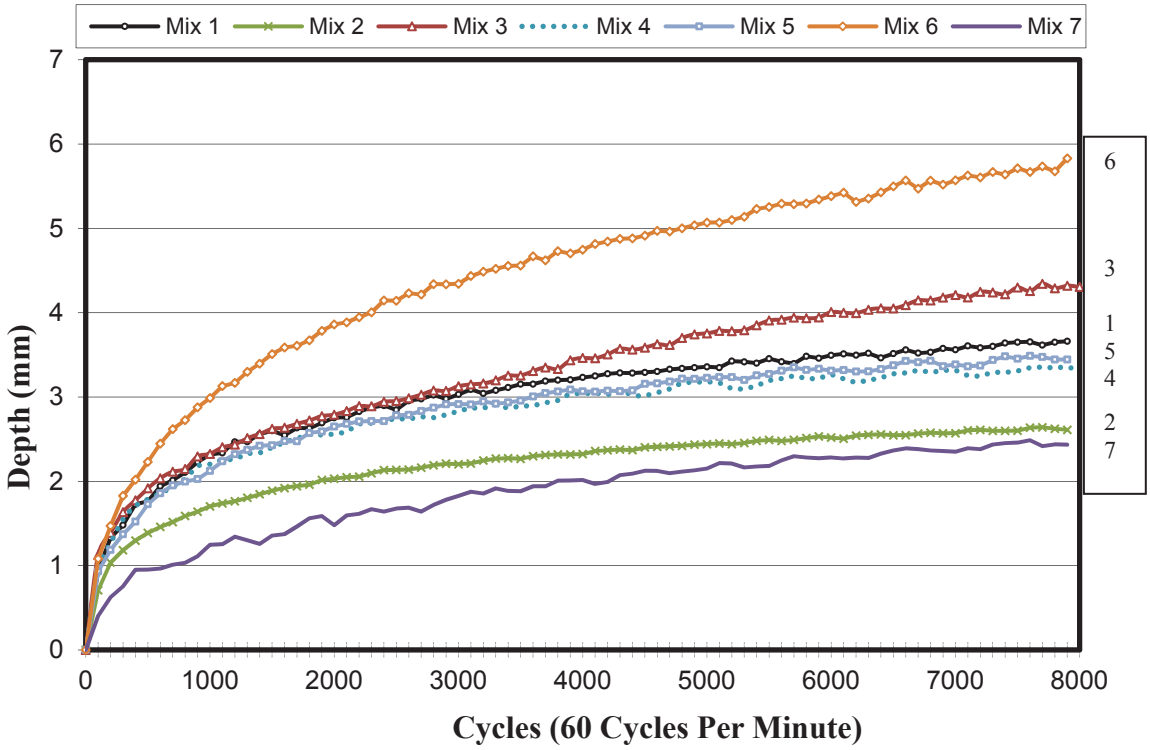

Figure 4-10 Average rut depth per load cycle for each mix

Under ideal mixing conditions, the "As-Is" blend had the highest rut depths after 8000 cycles, with a recorded depth of 3.617 mm. The "Improved" blend performed slightly better with a recorded rut depth of 3.312 mm, and the "Optimum" blend had the best performance with a recorded rut depth of 2.489 mm. As described in Section 2.2.2.5, rutting potential is affected by a number of factors including temperature, density, and asphalt content. The Optimum" blend had the ideal gradation for particle packing, therefore the low rut depths were as expected. The "Improved" blend had 1 percent higher asphalt content compared to the "As-Is" blend, therefore despite the similar rut depths, it demonstrated good performance overall.

Evaluating the "Improved' blend at different moisture and asphalt contents, variation in rut depth could be seen depending on the mixing conditions. With lower asphalt content, the rut depths decreased 20.6 percent after 8000 cycles compared to the blend mixed under ideal conditions, however with the higher asphalt content, rut depth increased 75

percent over the blend mixed under ideal conditions. The variations in moisture content had a negative impact on rutting resistance, with both increased and decreased mixing moisture contents resulting in increased rut depths. Overall, the blend mixed at the higher asphalt content had the poorest performance. Based on a review of literature, this conclusion was as anticipated, however the results also showed that mixing the materials at lower than optimum moisture contents would also have a large detrimental effect on the rutting resistance of the mix.

CHAPTER 5: COMPARATIVE PAVEMENT ANALYSIS

A practical method of describing the effect of the results from Chapter 4 is to relate the increase in performance to potential decreases in layer thicknesses and cost. If a stronger base layer required a thinner HMA overlay, this would result in potentially significant cost savings. The impact of better quality materials would also be notable if the service life of the pavement was extended. To evaluate these two effects, two pavement design methods were used. First, the Structural Number design method according to the 1993 AASHTO Pavement Design Guide was used to design a typical pavement structure with an FDR base layer. Second, a Mechanistic-Empirical design approach was employed to evaluate the service-life, based on fatigue and permanent deformation, on a different pavement structure with an FDR layer.

These analyses were done to compare pavements using each of the 7 mixes evaluated in this research project, and the results are described in the following sections.

5.1 AASHTO Structural Number Pavement Design

To evaluate the quality of the different FDR mixes, the thickness of hot mix asphalt concrete required to achieve a given structural number was determined for a 203.2 mm (8 inch) layer of expanded asphalt stabilized FDR base placed on a typical 37.9 MPa (5500 psi) subgrade soil. For the purposes of this design, the material properties of the FDR layer were varied according to the seven different mixtures evaluated in this research, and the HMA layer thickness was varied according to the design requirements. This hypothetical pavement structure is shown in Figure 5-1.

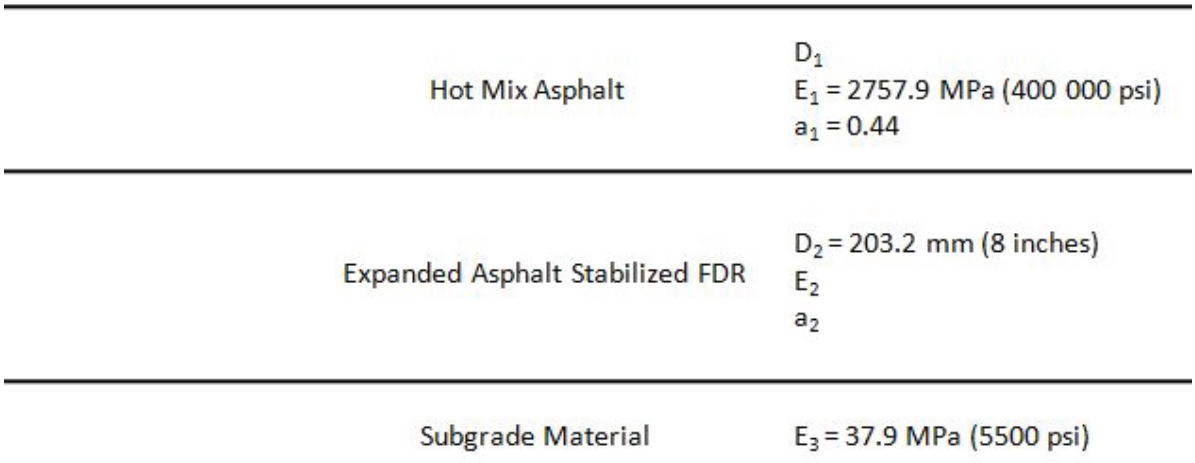

Figure 5-1 Pavement structure to be used for comparison of each FDR blend

The AASHTO structural design method, described in Section 2.4.3.1, was used. A design traffic loading of 100 000 ESALs was arbitrarily selected and typical material properties were assigned for the HMA and the subgrade layer, as shown in Table 5-1.

Table 5-1 Material properties selected for pavement design

Layer	Resilient Modulus (MPa)	Resilient Modulus (psi)	Structural Layer coefficient
HMA	2 757.9	400 000	0.44
Subgrade material	37.9	5500	-

Actual material properties, as determined from the lab testing program, were used for the FDR layer. The structural layer coefficient was determined for each blend based on the resilient modulus using the correlation charts shown in Figure 2-21. To increase accuracy in selecting this layer coefficient, a numerical equivalent to the chart was used, as shown in Table 2-5. From those values, a fourth order polynomial equation was derived to fit the correlation information, allowing for the accurate selection of a structural layer coefficient. Table 5-2 lists the modulus and structural layer coefficient for the FDR blends used. The resilient modulus values determined from laboratory testing at 25°C were chosen for use in design.

Table 5-2 FDR material properties used in structural design

Mix Number	Resilient Modulus (MPa)	Resilient Modulus (psi)	Structural Layer coefficient
1	568.5	82 454.0	0.09
2	776.9	112 679.8	0.15
3	756.2	109 677.5	0.14
4	1029.5	133 536.2	0.19
5	947.2	137 379.7	0.18
6	956.9	138 786.6	0.18
7	1065.4	154 523.2	0.19

The 1993 AASHTO Pavement Design Guide recommends different levels of reliability for various road classifications. This design was done at a 95 percent level of reliability, which is acceptable for urban or rural collector roads. The standard normal deviate (Z_R) was -1.645, and the standard deviation (S_0) was taken to be 0.45 by convention. To simplify the analysis, it was assumed that drainage had no effect, positive or negative, on the pavement structure. This resulted in the drainage coefficients m_2 and m_3 being taken as 1.0. Finally, the initial PSI was defined as 4.2, and terminal PSI was defined as 2.0, as recommended by the AASHTO design guide for low volume highways. Therefore the ΔPSI used in calculations was 2.2.

5.1.1 Design Results

The Structural Number design method was done using a Microsoft Excel spreadsheet. First, the pavement layer information and traffic information was inputted. The minimum structural number for the layer was then determined by using the Microsoft Excel Solver function and solving Equation 2.14. Once the minimum required structural number was determined, Equation 2.15 was used to calculate the minimum layer thickness to meet these requirements. Detailed calculations are included in Appendix C. Table 5-3 lists the thickness results determined for each mix.

Table 5-3 Pavement design results

Mix Number	Grading	Asphalt Content	Moisture Content	FDR Base Thickness (mm)	HMA Overlay Thickness (mm)
1	**As-Is**	**2.5 %**	**6.05 %**	**203.2**	**119.4**
2	Improved	2.5%	5.23%	203.2	91.4
3	Improved	3.5%	3.00%	203.2	94.0
4	**Improved**	**3.5 %**	**5.23 %**	**203.2**	**71.1**
5	Improved	3.5%	6.60%	203.2	76.2
6	Improved	4.5%	5.23%	203.2	76.2
7	**Optimum**	**3.0 %**	**5.35 %**	**203.2**	**71.1**

The "As-Is" blend was the poorest quality, and would require the thickest HMA overlay. For a 203.2 mm FDR base layer, a minimum 119.4 mm HMA overlay would be required to satisfy the design requirements.

The HMA thicknesses required for the various "Improved" blends were in the range of between 71.1 and 94.0 millimetres. Consistent with previous results, the blend mixed under dryer than optimum conditions was the poorest quality. The blend mixed with higher than optimum moisture and asphalt contents resulted in a slightly thicker HMA overlay compared to the mix produced at optimum moisture content. Overall the results indicated that the material performed best when mixed at optimum moisture and asphalt content, but was more tolerant to increases in asphalt and moisture content than to decreases in asphalt or moisture content.

The "Optimum" blend resulted in one of the thinnest minimum HMA overlays required, with the same thickness as required for the "Improved" blend mixed under ideal conditions. Only a 71.1 mm HMA overlay would be required to satisfy the minimum design requirements. This showed that gradation, as previously described, plays an important role in the performance of a material. This blend had the ideal gradation for particle packing, and this led to increased performance in the stabilized material.

5.1.2 Cost Analysis

A basic cost analysis was completed to compare the relative cost of producing the HMA overlay that would be required for each mix, as determined in Section 5.2. This analysis only looked at the cost of producing HMA and did not include other factors such as transportation costs, site preparation, traffic control, etc. As such, while conventional HMA paving costs approximately $113,000/km (Jackson, 2013), values significantly lower were used in this analysis. It is important to note that this is not a life cycle cost analysis. It simply provides information on the relative cost of producing the HMA for construction of the pavement designed in Section 5.2.

Lee (2012) determined that the average competitive unit cost of producing HMA in Nova Scotia between 2008 and 2009 was $49.02 / tonne. Although this value would have risen since then with inflation, and fluctuates according to a number of project variables, it was selected as a reasonable value to use in this cost analysis. Other assumptions made for the cost analysis are shown in Table 5-4. The analysis was based on a hypothetical 1 km long construction project.

Table 5-4 Assumptions made in performing construction cost analysis

Cost of producing HMA	$49.02 / tonne
Length of pavement section considered	1 km
Width of pavement section considered	7 m
Average density of HMA	2350 kg/m^3

Using the assumptions from Table 5-4, and the required overlay thicknesses given in Table 5-3, the cost of producing HMA was determined for a pavement using each FDR mix studied. The result of this cost analysis is given in Table 5-5, and the detailed calculations are included in Appendix C.

Table 5-5 Cost of producing HMA for each pavement design

Mix Number	Grading	Asphalt Content	Moisture content	HMA overlay thickness (mm)	HMA Cost
1	**As-Is**	**2.5 %**	**6.05 %**	**119.4**	**$96 265.53**
2	Improved	2.5%	5.23%	91.4	$73 735.30
3	Improved	3.5%	3.00%	94.0	$75 783.50
4	**Improved**	**3.5 %**	**5.23 %**	**71.1**	**$57 349.67**
5	Improved	3.5%	6.60%	76.2	$61 446.08
6	Improved	4.5%	5.23%	76.2	$61 446.08
7	**Optimum**	**3.0 %**	**5.35 %**	**71.1**	**$57 349.67**

The "Improved" and "Optimum" blends had a significantly lower HMA cost compared to the "As-Is" blend. From the results in Table 5-5, it can be seen that in addition to the better performance of the "Improved" FDR blend, large cost savings would also result from the reduced HMA requirement. In addition, to properly place the HMA, the overlays between 91.4 and 119.4 mm would need to be placed in two separate lifts to achieve proper compaction throughout. This would incur additional costs, above those listed, during construction. Therefore the use of corrective aggregates in this case would have been beneficial and economically justified.

5.2 Mechanistic-Empirical Service Life Predictions

Modern design methods use a Mechanistic-Empirical design approach, in which pavement response is calculated using a linear-elastic, or finite element analysis, and the pavement distress associated with that response over time is estimated using transfer functions developed from past observed pavement performance.

This approach was used to compare the effect of the different FDR mixes tested in this research project on the service life of a pavement structure. A pavement structure, as shown in Figure 5-2, was selected with typical granular base and subgrade properties. The HMA properties were based on dynamic modulus testing reported by Surette et al.

(2010) from a section of Highway 103 near Barrington, Nova Scotia. The HMA was assigned mix properties for air void content and effective asphalt content based on typical mixes. The FDR properties were based on the dynamic modulus testing completed in this research project. Equations 2.9 – 2.11, proposed by Witczak & Bari (2004) and NCHRP (2004), were used to predict the dynamic modulus of the HMA and FDR materials. Although sometimes different from tested values, the predictive equations provided reasonable estimates of the dynamic modulus at different temperatures and frequencies. For this analysis, the ground water table, which impacts the rate of rutting, was assumed to be at a depth of 3.05 m (10 feet).

Hot Mix Asphalt	D_1 = 76.2 mm (3 inches) μ_1 =0.4
Expanded Asphalt Stabilized FDR	D_2 = 152.4 mm (6 inches) μ_2 =0.3
Unbound Granular Base	D_3 = 304.8 mm (12 inches) E_3 = 80 MPa μ_3 =0.35
Subgrade Material	E_4 = 40 MPa μ_4 =0.4

Figure 5-2 Pavement structure to be analyzed to compare service life

The HMA dynamic modulus results were calculated using the Master Curve function shown in Equation 5.1, which was developed by Surette et al. (2010).

$$\log(|E^*|) = -1.5408 + \frac{5.9746}{1+e^{-1.4459+0.3096(\log \omega_r)}} \quad \textbf{[5.1]}$$

where:

$\|E^*\|$	= dynamic modulus	(MPa)
ω_r	= reduced frequency	(Hz)

The shift factor to describe the temperature dependency of the HMA mix was given as shown in Equation 5.2.

$$\log a(T) = -1.16 * 10^{-4} * T^2 - 0.117376 * T + 2.404674 \quad \textbf{[5.2]}$$

where:

a(T)	= shift factor, as a function of temperature	
T	= temperature of interest	(°C)

The structure was analyzed at temperatures of -10°C, 15°C, and 40°C. A loading frequency of 5 Hz was used to determine dynamic modulus. This frequency was selected based on NCHRP (2004) recommendations for predicted vehicle operating speeds on lower volume roads, with a value from the lower end of the range of acceptable frequencies being selected since pavements experience more damage from lower frequency loads. The corresponding dynamic modulus values for the HMA and FDR materials are shown in Table 5-6. The modulus of the unbound granular and subgrade material were held constant for all temperatures, as these layers should not be affected by variations in temperature.

Table 5-6 Dynamic modulus results, MPa, to be used for linear-elastic analysis

	-10°C	15°C	40°C
HMA	5574.4	4212.6	503.0
FDR Mix 1	1839.6	877.0	297.9
FDR Mix 2	1970.6	872.4	329.6
FDR Mix 3	1923.7	1042.1	387.2
FDR Mix 4	2029.1	916.8	361.2
FDRMix 5	1801.2	774.1	296.8
FDR Mix 6	2645.8	894.1	246.6
FDR Mix 7	2554.9	1136.9	403.1

A number of assumptions were made in performing this analysis. The first assumption was that the entire system was at a uniform temperature. In reality, there is a temperature gradient in the material, with the deeper layers being insulated by the surface layer, and therefore not experiencing temperatures, hot or cold, as severe as the surface layer. Poisson's ratio was also assumed to remain constant for the materials at all temperatures, though in reality this value fluctuates with temperature.

Finally, as recommended by NCHRP (2004), the FDR layer was treated as an unbound granular material for the permanent deformation analysis.

As there were numerous assumptions made in this analysis, the results presented are simply for comparison purposes, and would not be reflective of the true behaviour in the field. Since the same assumptions were made for the analysis of the pavement structure with each FDR mix, the results could still adequately be compared relative to one another, which satisfied the purpose of the analysis.

5.2.1 Analysis Results

A linear-elastic analysis was completed using the KENPAVE software. A 40 kN load, which represents one half of a standard ESAL, was applied over a circular loaded tire

contact area assuming a tire pressure of 827.4 kPa (120 psi). The software calculated the mechanistic response of the layers in the pavement, with strain magnitudes given at the points of interest. Specifically, the vertical tensile strain at the bottom of the HMA layer, radial strain at the midpoint of the HMA layer, and the vertical strain at the midpoint of the granular base layer, all at points directly below the load, were used in the analysis.

These strains were used to estimate service life using the transfer functions presented in Section 2.6. The number of cycles to cause fatigue failure in the HMA layer, and to cause a cumulative permanent deformation of 12.7 mm (0.5 inches) were estimated, and are listed in Table 5-7. The detailed results, including the mechanistic analysis results as well as calibration and material factors used, are included in Appendix D.

Table 5-7 Cycles to fatigue and permanent deformation failure for each analyzed pavement at -10°C, 15°C, and 40°C.

	-10°C		15°C		40°C	
FDR Mix	$N_{f,allow}$ HMA fatigue	$N_{r,}$ 12.7 mm rut	$N_{f,allow}$ HMA fatigue	$N_{r,}$ 12.7 mm rut	$N_{f,allow}$ HMA fatigue	$N_{r,}$ 12.7 mm rut
1	1.660×10^{11}	2.090×10^{10}	1.068×10^{10}	1.588×10^{7}	5.164×10^{9}	4 554
2	2.409×10^{11}	2.398×10^{10}	1.048×10^{10}	1.569×10^{7}	9.547×10^{9}	5 145
3	2.108×10^{11}	2.289×10^{10}	2.111×10^{10}	2.274×10^{7}	2.898×10^{10}	6 137
4	2.842×10^{11}	2.539×10^{10}	1.262×10^{10}	1.745×10^{7}	1.758×10^{10}	5 694
5	1.486×10^{11}	2.000×10^{10}	6.826×10^{9}	1.216×10^{7}	5.053×10^{9}	4 533
6	1.609×10^{12}	3.946×10^{10}	1.148×10^{10}	1.655×10^{7}	1.848×10^{9}	3 563
7	1.245×10^{12}	3.753×10^{10}	3.062×10^{10}	2.704×10^{7}	3.934×10^{10}	6 398

In all mixes, the mode of pavement failure was due to excessive permanent deformation. The number of cycles to cause fatigue failure was significantly higher than the number of cycles to cause rutting failure. It was also evident that the performance of each mix was highly dependent on temperature. A typical rural road would be more likely to fail due to

environmental factors before ever reaching the number of cycles to cause failure at the low and midrange temperature. Only the high temperature results demonstrated relatively low cycle counts to cause failure. Despite the generally high number of cycles the pavement could withstand, there were still differences evident when comparing the mixes to one another.

Evaluating the results for the pavement structures with FDR blends mixed at optimum asphalt and moisture contents, the "As-Is" blend had the shortest service life at all temperatures. At -10°C, the "Improved" blend had a 21.5 percent service life increase over the "As-Is" blend, while the "Optimum" blend had a 79.6 percent service increase over the "As-Is" blend. The large difference in service life between the "Improved" blend and the "Optimum" blend was somewhat unexpected given the relatively small difference between the material properties of the two blends; however it followed the differences seen in dynamic modulus testing at that temperature.

Similarly, at 15°C, the "Improved" blend had a 10.0 percent service life increase over the "As-Is" blend, while the "Optimum" blend had a 70.3 percent service increase over the "As-Is" blend. Finally, at 40°C, the "Improved" blend had a 25.0 percent service life increase over the "As-Is" blend, while the "Optimum" blend had a 40.5 percent service increase over the "As-Is" blend. These results showed that the addition of corrective aggregate translated to improvements in the service life of the pavement, which would make the use of these corrective aggregates a worthwhile addition.

The results of the "Improved" blend with variable asphalt and mixing moisture content were generally within 10 percent of those from the blend at optimum moisture and asphalt contents, with a few exceptions. Mix 5, which was mixed at a moisture content above optimum, had a decrease in service life of 21.2, 30.3, and 20.4 percent at -10°C, 15°C, and 40°C respectively. Conversely, Mix 3, which was mixed at moisture content below optimum, had a 30.3 percent improvement in service life at 15°C. It is not clear why this occurred given the overall poor performance of the Mix 3 materials throughout this project. In general, these results showed that a mixing moisture content above

optimum was more detrimental to the mix than mixing at moisture levels below optimum, an observation which is not in agreement with the results from the Asphalt Pavement Analyzer rutting potential test given in Section 4.4.5, which essentially drew the opposite conclusion. This fact shows that the rutting potential of a mix is affected by mixture properties, method of compaction, and the conditions under which the materials are loaded.

Mix 6 also demonstrated variable performance compared to the blend mixed at optimum conditions. This mix had higher than optimum asphalt content, which translated to a high degree of temperature susceptibility. At -10°C, the service life of this mix was 55.4 percent higher than the blend mixed at optimum conditions; however the service life was 37.4 percent lower at 40°C. Since the mode of failure for all pavements was due to excessive permanent deformation, these results were in agreement with all other testing performed in this research project which showed that the asphalt content was highly susceptible to temperature, and increased asphalt content tended to lead to better performance at low temperatures, when the viscosity of the asphalt would be increased.

Overall, the Mechanistic-Empirical analysis demonstrated once again the importance of gradation on the performance of the mix, with increased performance evident in the mixtures using corrective aggregate. The analysis also showed the impact asphalt content and moisture content could have on the service life of a pavement structure, thereby reinforcing the importance of quality control during construction.

CHAPTER 6: CONCLUSIONS

The purposes of this research project was to study a more effective method of designing FDR pavements, and study an approach to better control the quality of the reclaimed materials. To accomplish these objectives, the research program was split into two phases. The first phase of the project involved testing the unbound materials gathered from an FDR project. The second phase of the project involved modifying and testing these materials when stabilized with expanded asphalt.

In the first phase of the research project, materials gathered from an expanded asphalt stabilized FDR project on Route 790 near Lepreau, New Brunswick were subjected to a variety of tests. On this section, an average blend ratio of approximately 0.75 was maintained by varying pulverization depth according to the results of a GPR survey. Samples were taken at locations where the blend ratio was almost exactly 0.75, and the consistency of the materials was then evaluated.

The following tests were completed on these materials to evaluate both physical and mechanical properties.

- gradation
- moisture-density relationship
- maximum relative theoretical density
- granular resilient modulus
- direct shear strength
- CBR

The results from testing of the material taken at six locations during construction showed good consistency in the quality of the materials. The material gradations had low standard deviations at each size, indicating close results. There was however a significant discrepancy noted between the actual gradation results compared to what was specified in the job mix formula. This may be attributed to the method in which the job mix formula gradations were obtained. The job mix formula was based on post-extraction gradations, while the testing on the field collected samples was based on as-

produced materials, without extracting the asphalt cement. As the FDR process is considered a cold recycling process, the fines bound within the existing asphalt concrete do not become liberated, as was predicted during the mixture design process, but rather are pulverized into conglomerate particles bound within the aged asphalt cement. A better approach may be to develop a job mix formula taking into consideration these larger conglomerate particles bound together by asphalt cement from the old pavement, a practice which would lead to the ability to better evaluate the need for corrective aggregates. These findings were part of the motivation in carrying out the second phase of this project.

Apart from the noted poor gradations in the pulverized materials, the material itself appeared to be a poor quality product for use as a base material, with the lack of fines in the material contributing in part to the problem. Despite the consistency, the material had low resilient modulus and low CBR values, which indicated that unstabilized, it would not perform well as a base material. While better quality materials would have been preferable, these results were a good indication of the consistency that could potentially be achieved if the blend ratio of RAP to granular base material pulverized is effectively controlled. Based on these findings, the second phase of the research project was carried out.

The second phase of the research project evaluated the effect of gradation, and using a corrective aggregate on the quality of FDR materials. To do this, FDR material from the Route 790 project was tested using an "As-Is" blend, an "Improved" blend, and an "Optimum" blend. The "As-Is" blend used the material with the gradation as-pulverized. The "Improved" blend incorporated 15.6 percent screened crusher dust into the mix, bringing the gradation curve closer to the theoretical maximum density curve. The "Optimum" blend included a small amount of corrective aggregate, and the gradation of the material was manipulated to exactly follow the theoretical maximum density curve. Mix designs following a conglomerate particle design approach were used, and the material was stabilized using expanded asphalt. The conglomerate particle design approach entailed using gradations as-pulverized; more representative of what would be

produced during construction, rather than after the old asphalt cement had been extracted, as is often done.

Separate expanded-asphalt mix designs were completed for each blend to determine the optimum mixing moisture content and the optimum asphalt content of each mix. The following tests were completed on the stabilized materials for each blend:

- bulk density
- indirect tensile strength
- resilient modulus
- dynamic modulus
- rutting potential

As part of this research project, the effect of construction variability on the "Improved" blend was also evaluated by making and testing samples with mixing moisture and asphalt contents varying from optimum conditions.

Evaluating the three blends mixed under ideal conditions, at optimum moisture and asphalt content, the "As-Is" generally had the poorest performance. ITS testing was completed 4 days after compaction, and was used to evaluate the early strength of the materials, before they had fully cured. The "Improved" blend had the highest ITS under both soaked and dry conditions, though the "Optimum" blend had the highest TSR. The high TSR of the "Optimum" blend, at 98.6 percent, indicated that it was least affected by moisture damage, with the aggregate structure able to resist load regardless of the moisture conditions. The "As-Is" blend had the lowest ITS values, showing it would be the weakest blend under early loading, before full strength has been developed.

To evaluate how each blend performed in cold and warm conditions, the resilient modulus testing was completed over a range of temperatures. As with the ITS testing, the "As-Is" blend had the worst performance, with modulus values lower than the other blends at all temperatures. The "Improved" blend had the highest modulus values at lower temperatures; however it was the "Optimum" blend that had the higher modulus at increased temperatures. This suggested that the increased asphalt content of the

"Improved" blend contributed to the cold temperature resilient modulus. At higher temperatures where the effect of the asphalt cement would be reduced, the "Optimum" blend, with the ideal gradation for particle packing, had the best load transfer abilities. Similar trends were seen in the results from dynamic modulus testing. The "As-Is" blend typically had the worst performance, while the "Optimum" blend typically had the best performance. The development of master curves for each mix also allowed the temperature dependency of each blend to be evaluated. There appeared to be a relationship between asphalt content and temperature dependency, with increased asphalt content leading to increased temperature dependency. The "As-Is" blend had the lowest asphalt content and was least affected by temperature, while the "Improved" blend had the highest asphalt content and was most affected by temperature.

The "As-Is" blend had the poorest performance during rut testing, with specimens from this blend having an average rut depth of 3.617 mm after 8000 cycles. The ideal size distribution of the "Optimum" blend contributed to it having the lowest rut depths of the three blends, with a recorded rut depth of 2.489 mm. The "Improved" blend had a rut depth similar to the "As-Is" blend, at 3.312 mm, however given the increased asphalt content of the "Improved" blend which should have resulted in higher rut depths, this was still considered to be good performance from those specimens. The rutting test was the last test performed on the three blends mixed at optimum moisture and asphalt content.

To study the effects of construction variability, samples were made with the "Improved" blend mixed at moisture contents and asphalt contents above and below the determined optimum conditions.

Moisture content appeared to have a greater effect on ITS than asphalt content. The samples mixed at lower moisture contents had the lowest ITS, with a decrease of approximately 30 percent, while the samples mixed at higher moisture contents had a decrease of 15 to 20 percent. When asphalt content was varied, the dry ITS values were within 10 percent of the optimum, while the soaked ITS values increased as asphalt content increased.

The resilient modulus testing showed that temperature and asphalt content had a large effect on modulus. At lower temperatures, resilient modulus decreased with decreased asphalt content, while the variation in asphalt content had less of an effect at increased temperatures. The samples mixed at dryer than optimum moisture conditions again had the poorest performance, though modulus decreases were also noted with samples mixed at increased moisture contents.

The dynamic modulus testing showed similar trends. The asphalt content of the mix had a large effect on temperature dependency, with the samples at higher asphalt contents being more temperature dependant than the samples at lower asphalt contents. The mixing moisture content appeared to have very little effect on the temperature dependency of the mix.

Asphalt content had the greatest effect on the rutting susceptibility of the mix. Lower asphalt content resulted in the smallest rut depth, while higher asphalt content led to the highest rut depth. The moisture content also had an impact on the rutting resistance of the mix, though the specimens mixed at higher moisture contents were less impacted than those mixed at lower moisture contents. Overall, samples with high asphalt contents were most susceptible to rutting, with those mixed at lower than optimum moisture contents also showing a large increase in rutting susceptibility. The rutting test was the final test to be performed on the stabilized materials.

The following conclusions were drawn from the results of the testing program. In addition to these conclusions, some recommendations based on the results of the study have also been made.

1. Using the GPR survey as a proactive depth control method appeared to lead to extremely good consistency in the properties of the reclaimed materials. Future research investigating the use of a continuous variable depth control technique in which the depth of pulverization was varied continuously according to GPR

survey to maintain blend ratio, could result in extremely consistent, and predictable, pulverized sections.

2. The job mix formula overestimated the fines content of the reclaimed materials significantly, likely leading to reduced performance. A mix design approach taking into account the conglomerate aggregate particles bound by asphalt cement from the old pavement would be more representative of what is achieved in construction. With this approach, the need for corrective aggregate could be more reliably identified.

3. When stabilized with expanded asphalt, significant improvements were noted in the blends utilizing corrective aggregate. This confirms that the gradation of the material plays a large role in the strength and performance of a pavement. This also showed that, when used effectively, corrective aggregates can substantially improve the quality of a pavement.

4. The performance of the "Improved" blend was affected by variations in asphalt content and moisture content. These results show that effective quality control is an important component of the construction process, and that tight specifications on the properties of a constructed expanded asphalt stabilized FDR section would lead to more reliable FDR pavements.

Overall, the FDR process seems to provide a reasonable alternative to conventional rehabilitation methods in damaged pavements. A thorough analysis with consideration of the properties of the pulverized materials, stabilizer used, and construction methods, is extremely important. When using FDR as a rehabilitation strategy, a combination of proper design procedures, construction techniques, and effective quality control are all needed to ensure the effective long term performance of the section. If this is done, it is evident that FDR has the potential to be an excellent option to efficiently reconstruct damaged roads.

REFERENCES

AASHTO. (1993). *AASHTO guide for design of pavement structures (4th edition)*. Retrieved 26 February 2013 from http://www.knovel.com.ezproxy.library.dal.ca/web/portal/browse/display?_EXT_KNOVEL_DISPLAY_bookid=3671&VerticalID=0

AASHTO. (2007a). AASHTO TP62-07 – Standard test method for determining dynamic modulus of hot mix asphalt (HMA). Washington, D.C., USA: American Association of State Highway and Transportation Officials.

AASHTO. (2007b). AASHTO T307-99 (2007) – Standard test method for determining the resilient modulus of soils and aggregate materials. Washington, D.C., USA: American Association of State Highway and Transportation Officials.

American Coal Ash Association. (2003). *Fly ash facts for highway engineers.* Retrieved 22 April 2013 from Federal Highways Administration: http://www.fhwa.dot.gov/pavement/recycling/fafacts.pdf

Asphalt Academy. (2009). *A guideline for the design and construction of bitumen emulsion and foamed bitumen stabilized materials 2nd edition.* Retrieved 9 February 2012 from the Asphalt Academy: http://www.asphaltacademy.co.za/Documents/TG2May09.pdf

ASTM International. (2007a). ASTM D6931– Standard test method CBR (California bearing ratio) of laboratory compacted soils. West Conshohocken, Pennsylvania, USA: ASTM International

ASTM International. (2007b). ASTM D6931– Standard test method for indirect tensile (IDT) strength of bituminous mixtures. West Conshohocken, Pennsylvania, USA: ASTM International

ASTM International. (2009). ASTM D7369– Standard test method for determining the resilient modulus of bituminous mixtures by indirect tension test. West Conshohocken, Pennsylvania, USA: ASTM International

ASTM International. (2011). ASTM D7762 – Standard practice for the design of stabilization of soil and soil-like material with self-cementing fly ash. West Conshohocken, Pennsylvania, USA: ASTM International

Bang, S., Roberts, L., Huft, D., & Johnston, D. (2008). Quality base material produced using full depth reclamation on existing asphalt pavement structure. *ARRA Annual Meeting, February 2008, San Jose del Cabo, Mexico*. Retrieved 6 December 2012 from http://www.aema.org/index.php?option=com_docman&task=doc_view&gid=176&tmpl=component&format=raw&Itemid=46

Barnes, C. (2008). *Evaluating moisture damage in asphalt concrete using surface waves* (Doctoral dissertation). Retrieved from ProQuest Dissertation and Theses database. (NR50288)

Barnes, C. (2010). Forensic investigation of cracking in a Portland cement stabilized full depth recycled pavement. *Annual TAC conference, September 26-29, Halifax, NS*: Transportation Association of Canada.

Barnes, C., Haque, R., Salah, P., Alward, C. (2012). Control of full depth pulverized aggregate production using ground penetrating radar. *Annual TAC conference, October 14-17, Fredericton, NB*: Transportation Association of Canada.

Berg, R.L., Bigl, S.R., Stark, J., Durell, G. (1996). Resilient modulus testing of materials from MN/Road, Phase 1. Retrieved 22 June 2013 from Minnesota Department of Transportation: http://www.mrr.dot.state.mn.us/research/pdf/199621.pdf

Coduto, D.P, (1999). *Geotechnical engineering: Principles and practices*. Upper Saddle River, N.J.: Prentice-Hall, Inc.

Christensen, D.W., Bonaquist, R.F. (2004). Evaluation of indirect tensile test (IDT) procedures for low-temperature performance of hot mix asphalt. Retrieved 24 April 2013 from Transportation Research Board: http://onlinepubs.trb.org/onlinepubs/nchrp/nchrp_rpt_530.pdf

Cross, S. A., Jakatimath, Y. (2007). Determination of dynamic modulus master curves for Oklahoma HMA mixtures: Final Report. Retrieved 23 October 2012 from Oklahoma Department of Transportation: http://www.okladot.state.ok.us/hqdiv/p-r-div/spr-rip/library/reports/rad_spr2-i2177-rpt-final-cross.pdf

Daniels, D.J. (2004). Ground penetrating radar, 2nd edition. Retrieved 25 April 2013 from Google eBook database: http://books.google.ca/books?id=16PV-fhKasoC&source=gbs_navlinks_s

Dewar, J.D. (2002). Computer modelling of concrete mixtures. Retrieved 24 April 2013 from Google eBook database: http://books.google.ca/books?id=gHlmm0fxvlQC&printsec=frontcover&source=gbs_ge_summary_r&cad=0#v=onepage&q&f=false

Dunlavy, J.P., Lipai, M, Baldwin, G. (2009). *Transportation in the North*. Retrieved 4 March 2012 from Statistics Canada:http://www.statcan.gc.ca/pub/16-002-x/2009001/article/10820-eng.htm

Eller, A., Olson, R. (2009). Recycled pavements using foamed asphalt in Minnesota. Retrieved 19 April 2013 from Minnesota Local Road Research Board: http://www.lrrb.org/media/reports/200909.pdf

Federal Highways Administration (FHWA) (2011). *Geotechnical aspects of pavements reference manual*. Retrieved 28 February 2013 from Federal Highways Administration: http://www.fhwa.dot.gov/engineering/geotech/pubs/05037/05c.cfm#f068

Fu, P., Jones, D.J., Harvey, J.T., Halles, F. (2010). An investigation of the curing mechanism of foamed asphalt mixes based on micromechanics principles. *Journal of Materials in Civil Engineering,* 22 *(10)*, 985-999.

Geiger, A., Yuan, D., Nazarian, S., & Abdallah, I. (2007). Effect of pulverization on properties of stabilized bases. Retrieved 30 January 2012 from University of Texas: http://ctis.utep.edu/publications/Reports/Report_0-5223-1-Final.pdf

Griggs, B.E. (2009). *Evaluation of full-depth reclamation on strength and durability of pavement base layers*. MSc Thesis. Retrieved 29 September 2011 from Brigham Young University: http://contentdm.lib.byu.edu/cdm/ref/collection/ETD/id/1700

Halsted, G.E. (2010). Design of full-depth reclamation with Portland cement (FDR-PC) pavements. Retrieved 13 September 2011 from Transportation Association of Canada: http://www.tac-atc.ca/english/resourcecentre/readingroom/conference/conf2010/docs/n1/halsted.pdf

Halsted, G.E. (2008). Long-term performance of failed flexible pavements stabilized with cement. Retrieved 22 September 2011 from Transportation Association of Canada: http://www.tac-atc.ca/english/resourcecentre/readingroom/conference/conf2008/docs/d3/Halsted.pdf

Hensley, T., Jensen, W., & Berryman, C. (2007). Pozzolan stabilized subgrades. Retrieved 27 February 2012 from Nebraska Library Commission: http://nlc1.nlc.state.ne.us/epubs/R6000/B016.0116-2007.pdf

Holt, C., Barnes, C., Sullivan P., & O'Tooke, L. (2009). Full depth remediation of roads using Portland cement. Retrieved 6 December 2011 from Transportation Association of Canada: http://www.tac-atc.ca/english/resourcecentre/readingroom/conference/conf2009/pdf/Holt.pdf

Huang, Y.H. (2004). *Pavement analysis and design (2nd ed.)* Upper Saddle River, NJ: Pearson Prentice Hall.

Jackson, D. (2013, February 28). NS says asphalt plant paying off in pavement savings. *The Chronicle Herald*. pp. A3.

Johnston, A.G., Yeung, K., & Tannahill, D. (2005). Use of asphalt pavement analyzer testing for evaluating premium surfacing asphalt mixtures for urban roadways. *Annual TAC conference*, September 18-21, Calgary, AB. Retrieved 16 April 2013 from Transportation Association of Canada: http://www.tac-atc.ca/english/resourcecentre/readingroom/conferenceconf2005/docs/s4/yeung.pdf

Jones, D., Fu, P., Harvey, J.T., & Halles, F. (2008). Full-depth pavement reclamation with foamed asphalt: Final report. Retrieved 13 December 2012 from California Department of Transportation: http://www.dot.ca.gov/research/researchreports/reports/2008/ucprc-rr-2008-07.pdf

Jones, D., Fu, P., & Harvey, J.T. (2009). Full-depth pavement reclamation with foamed asphalt in California: Guidelines for project selection, design, and construction. Retrieved 2 March 2012 from California Department of Transportation: http://www.dot.ca.gov/research/researchreports/reports/2009/ucprc-gl-2008-01.pdf

Jooste, F., Long, F. (2007). A knowledge based structural design method for pavements incorporating bituminous stabilized materials. Retrieved 23 April 2013 from Gauteng Department of Public Transport, Roads and Works: http://www.gautrans-hvs.co.za/popup/Structural%20Design%20Memo%20FINAL.pdf

Kandhal, P.S., & Cooley, L.A. (2002). Evaluation of permanent deformation of asphalt mixtures using loaded wheel tester. *Asphalt Paving Technology,* (71), 739-753.

Kandhal, P.S., & Mallick, R.B. (1997). Pavement recycling guidelines for State and local governments' participant's reference book. Retrieved 12 January 2012 from Federal Highway Administration: http://www.fhwa.dot.gov/pavement/recycling/98042/

Kearney, E. J., & Huffman, J.E. (1999). Full depth reclamation process. *Transportation Research Record: Journal of the Transportation Research Board, (1684)*, 203-209.

Kim, Y., Lee, H., & Heitzman, M. (2007). Validation of new mix design procedures for cold in-place recycling with foamed asphalt. *Journal of Materials in Civil Engineering* , 1000-1010

Lane, B., Kazmierowski, T. (2012). Long term performance of full depth reclamation with expanded asphalt on the Trans-Canada highway near Wawa, Ontario. *Annual TAC conference*, October 14-17, Fredericton, NB. Retrieved 11 December 2012 from Transportation Association of Canada:http://www.tac-atc.ca/english/annualconference/tac2012/docs/session4/lane.pdf

Lee, G. (2012). Provincial asphalt plant operation. Retrieved 28 February 2013 from Nova Scotia Transportation and Infrastructure Renewal: http://novascotia.ca/tran/highways/pavingplant/Provincial_Asphalt_Plant_Opeations.pdf

Liu, J., Li, P. (2010). Characterization of asphalt treated base course material. Retrieved 28 February 2013 from National Transportation Library: http://ntl.bts.gov/lib/46000/46600/46608/Final_Report_107049.pdf

Loizos, A., Plati, C. (2006). Ground penetrating radar as an engineering diagnostic tool for foamed asphalt treated pavement layers. *International Journal of Pavement Engineering*, 8 (2*)*, 147-155

Luo, R., Lytton, R.L. (2010). Characterization of the tensile viscoelastic properties of an undamaged asphalt mixture. *Journal of Transportation Engineering*, 136 (3*)*, 173-180

Lytton, R.L. (1989). Backcalculation of pavement layer properties. *American Society for Testing and Materials STP 1026*, 7-38

Maher, A., Bennert, T. (2008). Evaluation of Poisson's ratio for use in the mechanistic-empirical pavement design guide (MEPDG). Retrieved 27 April 2013 from State of New Jersey: http://www.state.nj.us/transportation/refdata/research/reports/FHWA-NJ-2008-004.pdf

Marquis, B. (2007). Full depth reclamation with cement along rt. 2A in Reed Plantation. Retrieved 4 March 2013 from Federation of Canadian Municipalities: http://www.fcm.ca/Documents/reports/Danger_Ahead_The_coming_collapse_of_Canadas_municipal_infrastructure_EN.pdf

McDaniel, R.S., Gallivan, V.L., Huber, G.A., Andrewski, D.H, Miller, M. (2005). Use of HMA stiffness results as a referee test in Indiana. *Journal of ASTM International*, 2 (4), 6 pp.

Mishra, S. (N.D.). Dust control, roadbed stabilization, and full depth reclamation with calcium chloride. Retrieved 22 April 2013 from Tetra Chemicals: www.tetrachemicals.com/getFile.asp?File_Content_ID=1027

Mirza, S. (2007). Danger ahead: The coming collapse of Canada's municipal infrastructure. Retrieved 16 September 2011 from MaineDOT: http://www.maine.gov/mdot/tr/documents/pdf/report0506ci1.pdf

Muthen, K.M. (1998). Foamed asphalt mixes – mix design procedure. Retrieved 24 October 2012 from CSIR Transportek: http://asphalt.csir.co.za/FArefs/Muthen%20-%20Mix%20Design.pdf

NCHRP. (2004). Guide for mechanistic-empirical design of new and rehabilitated pavement structures (NCHRP 1-37A). Retrieved 15 February 2012 from Transportation Research Board: http://onlinepubs.trb.org/onlinepubs/archive/mepdg/guide.htm

NSTIR (N.D.). *Monthly weighted average asphalt binder rack price*. Retrieved 1 March 2013 from Nova Scotia Transportation and Infrastructure Renewal: http://novascotia.ca/tran/trucking/rackprice.asp

NSTIR (2012) Full depth reclamation with expanded asphalt stabilization (method spec). Retrieved 4 March 2013 from Nova Scotia Transportation and Infrastructure Renewal: http://www.gov.ns.ca/tran/publications/asphalt/FDR_FoamStabilization_REVMar2012_Method.pdf

Portland Cement Association (N.D.). *Full-depth reclamation with cement*. Retrieved 9 November 2011 from Portland Cement Association: http://www.cement.org/pavements/pv_sc_fdr.asp

Plati, C., Loizos, A. (2012). Using ground-penetrating radar for assessing the structural needs of asphalt pavements. *Nondestructive Testing and Evaluation*, 27 (3*)*, 273-284

Roberts, F. L., Kandhal, P. S., Brown, E. R., Lee, D-Y., & Kennedy, T. W. (1996). *Hot mix asphalt materials, mixture design and construction*. Lanham: National Asphalt Pavement Association Research and Education Foundation.

Ruckel, P.J., Acott, S.M., Bowering, R.H. (1983). Foamed-asphalt paving mixtures: Preparation of design mixes and treatment of test specimens. *Transportation Research Record: Journal of the Transportation Research Board*, (*911)*, 88-95

Saarenketo, T., Scullion, T. (1994). Ground penetrating radar applications on roads and highways. Retrieved 25 April 2013 from Texas Transportation Institute: http://tti.tamu.edu/publications/catalog/record/?id=499

Saarenketo, T., Scullion, T. (2000). Road evaluation with ground penetrating radar. *Journal of Applied Geophysics* (*43)*, 119-138

Saxena, P., Tompkins, D., Khazanovich, L., & Balbo, J. T. (2010). Evaluation of characterization and performance modelling of cementitiously stabilized layers in the "mechanistic-empirical pavement design guide". *Transportation Research Record: Journal of the Transportation Research Board*, (*2186)*, 111-119

Scullion, T. Guthrie, S., Sebesta, S. (2003). Field performance and design recommendations for full depth recycling in Texas. Retrieved 19 September 2011 from Texas Transportation Institute: http://tti.tamu.edu/publications/catalog/record/?id=34016

Sebesta, S. (2006). Microcracking for reduced shrinkage in cement-treated base (Project summary report 0-4502-S). Retrieved 19 September 2011 from Texas Transportation Institute: http://tti.tamu.edu/publications/catalog/record/?id=25931

Sebesta, S., Scullion, T., & Estakhri, C. (2011). Field and lab investigations for full depth reclamation projects(Report No. 0-6271-1). Retrieved 12 September 2011 from Texas Transportation Institute: http://tti.tamu.edu/publications/catalog/record/?id=34016

Sebesta, S. Scullion, T. (2004). Effectiveness of minimizing reflective cracking in cement-treated bases by microcracking. Retrieved 26 September 2011 from Texas Transportation Institute: http://tti.tamu.edu/publications/catalog/record/?id=25930

Stroup-Gardiner, M. (2011). Recycling and reclamation of asphalt pavements using in-place methods. *National Cooperative Highway Research Program (NCHRP) Synthesis of Highway Practice,* 421, 70 pp

Surette, E., Barnes, C., Ali, N. (2010). Use of GPR and MASW to complement backcalculated moduli and design life calculations. *Annual TAC conference, September 26-29, Halifax, NS*: Transportation Association of Canada.

Taylor, P.C., Kosmatka, S.H., Voight, G.F. et al. (2007). *Integrated materials and construction practices for concrete placement: A state-of-the-practice manual*. Retrieved 22 April 2013 from the National Concrete Pavement Technology Center: http://www.cptechcenter.org/publications/imcp/imcp_manual_october2007.pdf

Terrel, R.L, Awad, I.S., & Foss, L.R. (1974). "Technique for characterizing bituminous materials using a versatile triaxial testing system" *Fatigue and Dynamic Modulus Testing of Bituminous Mixtures*. *ASTM STP 561,* 47-66

Texas Department of Transportation (TxDOT) (2005). Guidelines for modification and stabilization of soils and base for use in pavement structures. Retrieved 30 January 2012 from TxDOT: ftp://ftp.dot.state.tx.us/pub/txdot-info/cmd/tech/stabilization.pdf

Tseng, K-H., Lytton, R.L. (1989). Prediction of permanent deformation in flexible pavement materials. *American Society for Testing and Materials STP 1016*, 154-172

University of British Columbia (2011). *Virtual soil lab modules: Soil bulk density*. Retrieved 18 February 2013 from University of British Columbia: http://soilweb.landfood.ubc.ca/labmodules/compaction/soil-bulk-density

Wen, H., Tharaniyil, M. P., Ramme, B., & Krebs, S. (2004). Field performance evaluation of class C fly ash in full-depth reclamation: case history study. *Transportation Research Record: Journal of the Transportation Research Board, (1869)*, 41-46

White, T. D., Haddock, J. E., Hand, A. J. T., Fang, H. (2002). Contributions of pavement structural layers to rutting of hot mix asphalt pavements. Retrieved 22 April 2013 from Transportation Research Board: http://onlinepubs.trb.org/onlinepubs/nchrp/nchrp_rpt_468-a.pdf

Witczak, M. W., Bari, J. (2004). Development of a master curve (E*) database for lime modified asphaltic mixtures. Retrieved 23 October 2012 from the National Lime Association: http://www.lime.org/documents/publications/free_downloads/master-curve.pdf

Wirtgen Group. (2010). *Wirtgen cold recycling technology*. Retrieved 23 September 2011 from Wirtgen GmbH: http://www.wirtgen.de/media/redaktion/pdf-dokumente/03_kaltrecycling_stabilisierung/_allgemein_1/manual/p_manual_e.pdf

Appendix A: Test Standards

A.1 Unbound Material Test Standards

ASTM International Test Standards

ASTM D698	Laboratory Compaction of Soil Using Standard Effort
ASTM D1883	CBR (California Bearing Ratio) of Laboratory-Compacted Soils
ASTM D2041/D2041M	Theoretical Maximum Specific Gravity and Density of Bituminous Paving Mixtures
ASTM D3080	Direct Shear Test of Soils Under Consolidated Drained Conditions
ASTM D6307	Asphalt Content of Hot-Mix Asphalt by Ignition Method
ASTM D6913	Particle-Size Distribution (Gradation) of Soils Using Sieve Analysis

AASHTO Test Standards

AASHTO T307	Resilient Modulus of Soils and Aggregate Materials

A.2 Bound Material Test Standards

ASTM International Test Standards

ASTM D698	Laboratory Compaction of Soil Using Standard Effort
ASTM D3387	Compaction and Shear Properties of Bituminous Mixtures by Means of the U.S. Corps of Engineers Gyratory Testing Machine (GTM)
ASTM D6926	Preparation of Bituminous Specimens Using Marshall Apparatus
ASTM D6931	Indirect Tensile (IDT) Strength of Bituminous Mixtures
ASTM D7369	Resilient Modulus of Bituminous Mixtures by Indirect Tension Test

AASHTO Test Standards

AASHTO T340	Rutting Susceptibility of Hot Mix Asphalt (HMA) Using the Asphalt Pavement Analyzer (APA)
AASHTO TP62	Dynamic Modulus of Hot Mix Asphalt (HMA)

Appendix B: Test Results

Unbound Material Tests

B.1 Route 790 FDR mix design gradations

Table B-1 Route 790 job mix formula developed by Industrial Cold Milling

Material	In-Place Material	Route 790 RAP	Portland Cement		Blend JMF
Size (mm)	% Passing				
50.0	100.0	100.0	100.0		100
25.0	90.4	100.0	100.0		97.6
19.0	85.0	100.0	100.0		96.3.
16.0	79.9	100.0	100.0		95.0
13.2	74.7	92.3	100.0		88.0
9.5	66.0	83.2	100.0		79.2
4.75	51.6	57.1	100.0		56.4
2.36	41.0	41.1	100.0		42.0
1.18	30.5	27.4	100.0		29.3
0.630	720.8	20.3	100.0		21.6
0.300	12.5	14.1	100.0		15.0
0.150	8.1	9.2	100.0		10.2
0.075	6.4	6.0	100.0		7.5

B.2 FDR Gradation Analysis

Table B-2 Gradation analysis of Route 790 pulverized materials

Location	**1+769**	**2+185**	**2+550**	**3+128**	**3+446**	**4+040**		
Size (mm)	% Passing						**Mean**	**Standard Deviation**
50	100	100	100	100	100	100	100	0.0
25	100	98.3	99.2	100	100	100	99.6	**0.7**
19	96.5	95.6	95.8	98.3	99.3	97.4	97.1	**1.4**
15.9	92.8	92.7	93.1	94.1	95.7	93.4	93.6	**1.1**
12.7	84.7	83.5	84.9	85.3	90.1	84.9	85.5	**2.3**
9.5	74.8	74.8	75.8	75.4	81.0	72.5	75.7	**2.8**
4.75	48.9	50.7	51.6	50.9	54.0	43.3	49.9	**3.6**
2.5	27.4	33.0	31.7	31.0	31.2	25.5	30.0	**2.9**
1.25	14.3	19.2	16.9	17.8	16.8	12.8	16.3	**2.4**
0.63	7.2	9.9	8.0	10.0	8.8	6.2	8.3	**1.5**
0.315	3.3	4.2	3.3	5.7	4.5	3.0	4.0	**1.0**
0.16	1.4	1.5	1.2	3.4	2.4	1.5	1.9	**0.8**
0.08	**0.8**	**0.8**	**0.7**	**2.4**	**1.5**	**1.0**	**1.2**	**0.6**
Fineness Modulus:	5.26	5.11	5.16	5.08	5.02	5.38	5.17	**0.13**

B.3 Moisture-Density Relationship: Sta. 1+769

Mass of mould & plate:	4056 g		Mould:	Diameter	101.6 mm	
				Height:	116.4 mm	
				Volume:	9.437E-04 m^3	
Sample No.	1	2	3	4	5	6
Date Tested	17/11/11	18/11/11	19/11/11	20/11/11	14/11/11	14/11/11
mass of sample (g)	2744.9	2639.7	3064.5	2277.8	2129.1	2716.8
% Water added	6.0%	4.0%	7.0%	6.2%	5.0%	6.0%
Mass of water added (g)	164.7	105.6	214.5	141.2	106.5	163.0
Compacted						
Mass of sample + mould + plate (g)	5814.0	5790.0	5807.0	5782.0	5766.0	5778.0
Mass - Wet (for moisture content) (g)	1757.0	1733.2	1747.1	1726.0	1707.6	1719.3
Tare (g)	603.8	337.8	341.2	341.9	337.7	341.5
Mass of dry sample (g)	1665.1	1662.6	1635.7	1627.3	1637.7	1641.7
Actual Moisture Content	5.52%	4.25%	6.81%	6.07%	4.27%	4.73%
Moist Density	1862.9	1837.5	1855.5	1829.0	1812.0	1824.7
Dry density (kg/m^3)	1765.5	~~1762.6~~	1737.2	~~1724.4~~	1737.9	1742.4

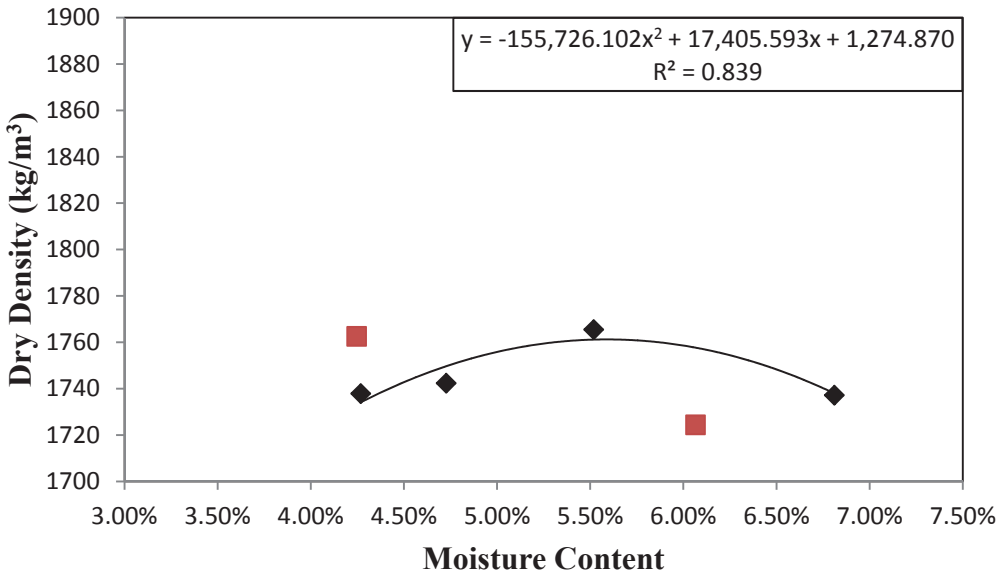

Figure B-1 Sta. 1+769 Moisture Density relationship.
Maximum dry density: 1760 kg/m^3. Optimum moisture content: 5.59%

B.4 Moisture-Density Relationship: Sta. 2+185

Mass of mould & plate:	4056 g		Diameter:	101.6 mm	
			Height:	116.4 mm	
			Volume:	9.437E-04m^3	
Sample No.	1	2	3	4	5
Date Tested	17/10/11	18/10/11	19/10/11	20/10/11	14/11/11
mass of sample (g)	1984.0	2491.3	1974.8	2088.8	2273.2
% Water added	5.0%	6.0%	7.0%	6.1%	6.0%
Mass of water added (g)	99.2	149.5	138.2	127.4	136.4
COMPACTED					
Mass of sample + mould + plate (g)	5803.0	5846.0	5835.0	5821.0	5775.0
Mass - Wet (for moisture content) (g)	1745.5	1787.4	1775.8	1762.9	1714.8
Tare (g)	587.0	342.0	337.6	337.7	583.4
Mass of dry sample (g)	1663.3	1690.1	1665.9	1665.0	1635.4
Actual Moisture Content	4.94%	5.76%	6.60%	5.88%	4.86%
Moist Density	1851.2	1896.8	1885.1	1870.3	1821.6
Dry density (kg/m^3)	1764.1	1793.5	1768.5	~~1766.4~~	1737.2

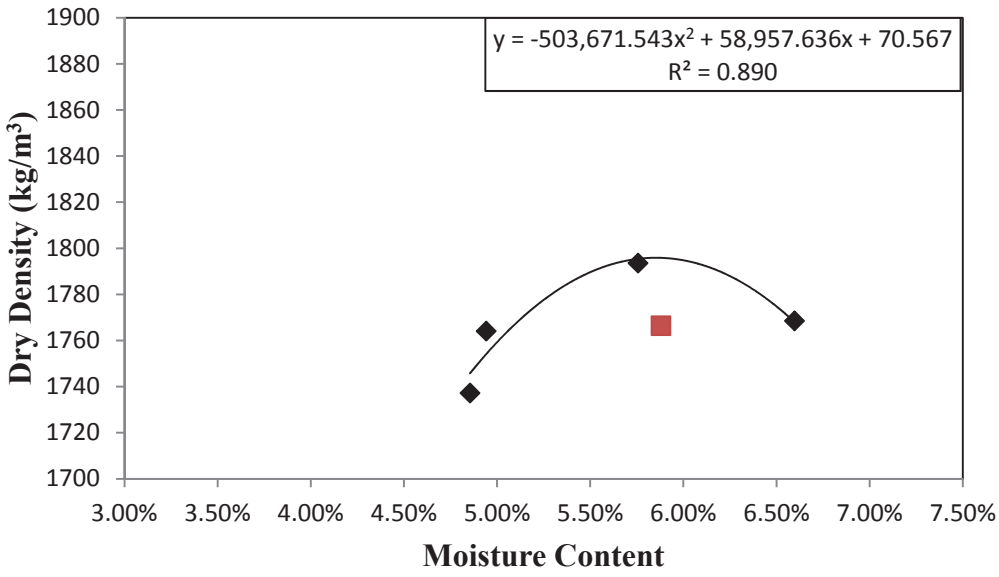

Figure B-2 Sta. 2+185 Moisture Density relationship.
Maximum dry density: 1796 kg/m^3. Optimum moisture content: 5.85%

B.5 Moisture-Density Relationship: Sta. 2+550

Mass of mould & plate:	4056	g	Diameter:	101.6	mm
			Height:	116.4	mm
			Volume:	9.437E-04	m^3

Sample No.	1	2	3	4
Date Tested	17/11/11	18/11/11	19/11/11	20/11/11
dry mass of sample (g)	2364.6	1917.1	1996.8	2369.5
% Water added	7.0%	6.0%	5.0%	4.0%
Mass of water added (g)	165.5	115.0	99.8	94.8
COMPACTED				
Mass of sample + mould + plate (g)	5823.0	5851.0	5828.0	5792.0
Mass - Wet (for moisture content) (g)	1767.0	1792.4	1769.1	1733.6
Tare (g)	340.5	628.0	586.9	1125.0
Mass of dry sample (g)	1653.5	1695.7	1689.9	1666.7
Actual Moisture Content	6.86%	5.70%	4.69%	4.01%
Moist Density	1872.4	1902.1	1877.7	1839.6
Dry density (kg/m^3)	1752.2	1799.5	1793.7	1768.6

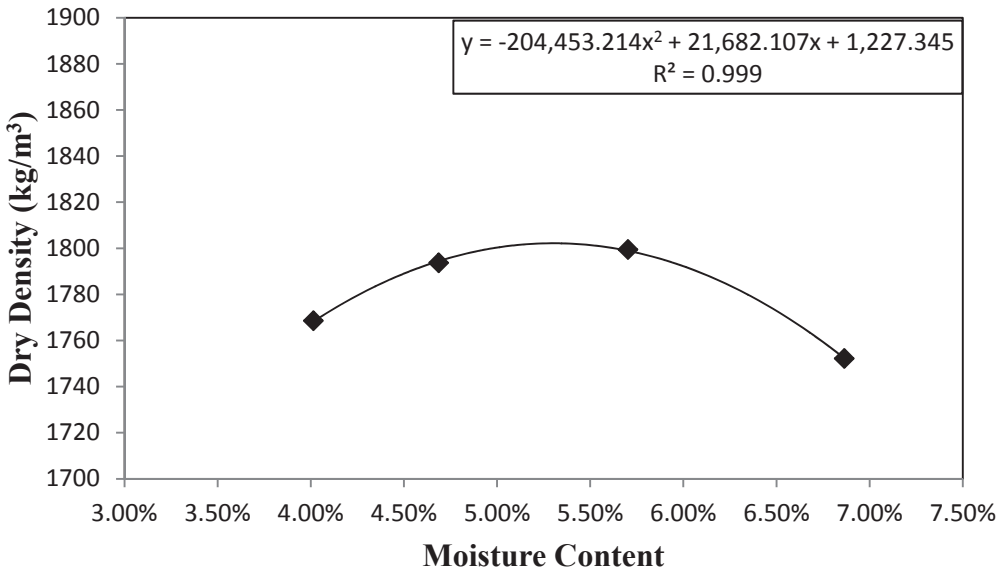

Figure B-3 Sta. 2+550 Moisture Density relationship.
Maximum dry density: 1802 kg/m^3. Optimum moisture content: 5.30%

B.6 Moisture-Density Relationship: Sta. 3+128

Mass of mould & plate:	4056	g	Diameter:	101.6	mm
			Height:	116.4	mm
			Volume:	9.437E-04	m^3

Sample No.	1	2	3	4
Date Tested	17/11/11	18/11/11	19/11/11	20/11/11
mass of sample (g)	2757.7	1893.2	2385.1	2607.7
% Water added	5.0%	4.0%	3.0%	2.5%
Mass of water added (g)	137.9	75.7	71.6	65.2
COMPACTED				
Mass of sample + mould + plate (g)	5871.0	5880.0	5866.0	5825.0
Mass - Wet (for moisture content) (g)	1810.6	1823.7	1809.7	1768.4
Tare (g)	597.5	597.6	604.4	597.7
Mass of dry sample (g)	1708.8	1747.9	1747.2	1710.7
Actual Moisture Content	5.96%	4.34%	3.58%	3.37%
Moist Density	1923.3	1932.8	1918.0	1874.6
Dry density (kg/m^3)	1815.2	1852.5	1851.8	1813.4

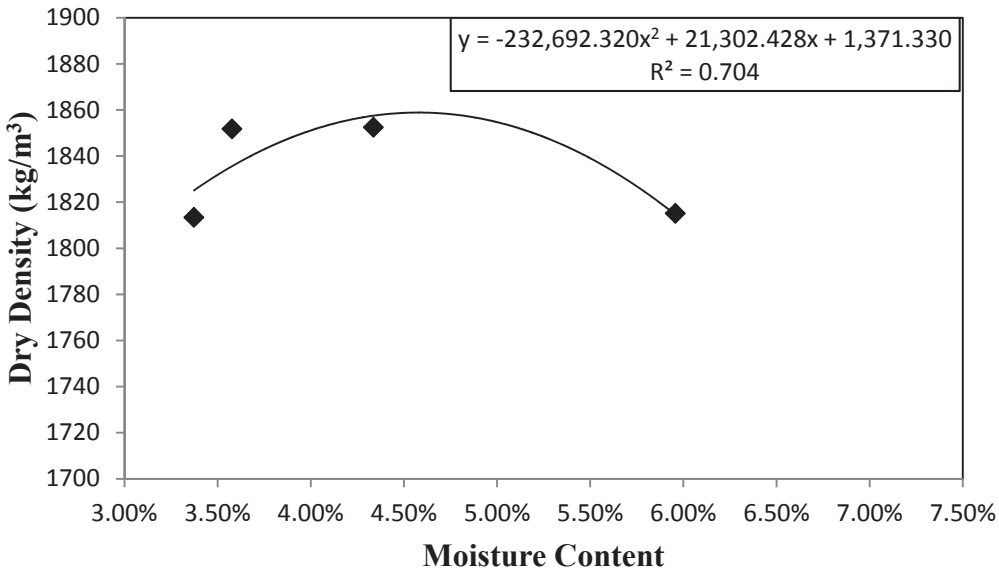

Figure B-4 Sta. 3+128 Moisture Density relationship.
Maximum dry density: 1859 kg/m^3. Optimum moisture content: 4.58%

B.7 Moisture-Density Relationship: Sta. 3+446

Mass of mould & plate:	4056 g		Diameter:	101.6 mm	
			Height:	116.4 mm	
			Volume:	9.437E-04 m^3	

Sample No.	1	2	3	4	5
Date Tested	17/10/11	18/10/11	19/10/11	20/10/11	28/10/11
mass of sample (g)	1921.7	2159.6	1905.2	2631.1	1997.0
% Water added	6.0%	5.0%	7.0%	4.0%	5.5%
Mass of water added (g)	115.3	108.0	133.4	105.2	109.8
COMPACTED					
Mass of sample + mould + plate (g)	5886.0	5831.0	5868.0	5838.0	5783.0
Mass - Wet (for moisture content) (g)	1825.4	1773.3	1807.3	1779.1	1726.1
Tare (g)	337.4	604.4	597.0	604.6	584.4
Mass of dry sample (g)	1708.0	1675.7	1681.9	1694.2	1636.3
Actual Moisture Content	6.87%	5.82%	7.46%	5.01%	5.49%
Moist Density	1939.2	1880.9	1920.1	1888.3	1830.0
Dry density (kg/m^3)	1814.5	1777.4	1786.9	~~1798.2~~	1734.8

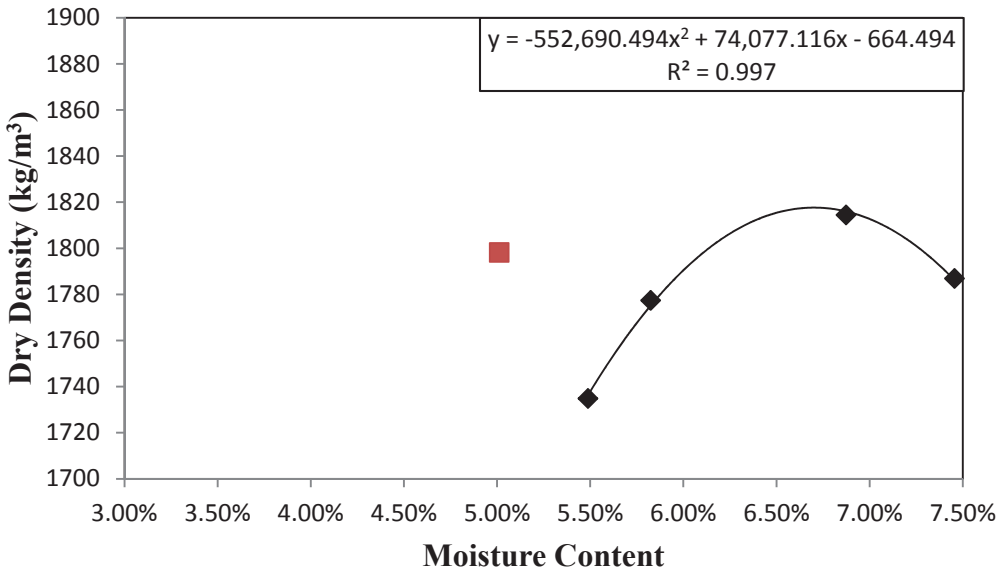

Figure B-5 Sta. 3+446 Moisture Density relationship.
Maximum dry density: 1818 kg/m^3. Optimum moisture content: 6.70%

B.8 Moisture-Density Relationship: Sta. 4+040

Mass of mould & plate:	4056	g	Diameter:	101.6	mm
			Height:	116.4	mm
			Volume:	9.437E-04	m^3

Sample No.	1	2	3	4
Date Tested	17/11/11	18/11/11	19/11/11	20/11/11
mass of sample (g)	1995.4	2354.1	2001.9	2194.4
% Water added	7.0%	5.0%	4.0%	6.0%
Mass of water added (g)	139.7	117.7	80.1	131.7
COMPACTED				
Mass of sample + mould + plate (g)	5785.0	5820.0	5772.0	5799.0
Mass - Wet (for moisture content) (g)	1719.8	1761.4	1714.3	1738.3
Tare (g)	626.6	586.1	1124.4	585.2
Mass of dry sample (g)	1606.6	1674.6	1642.8	1634.2
Actual Moisture Content	7.05%	5.18%	4.35%	6.37%
Moist Density	1832.2	1869.3	1818.4	1847.0
Dry density (kg/m^3)	1711.6	1777.1	1742.5	1736.4

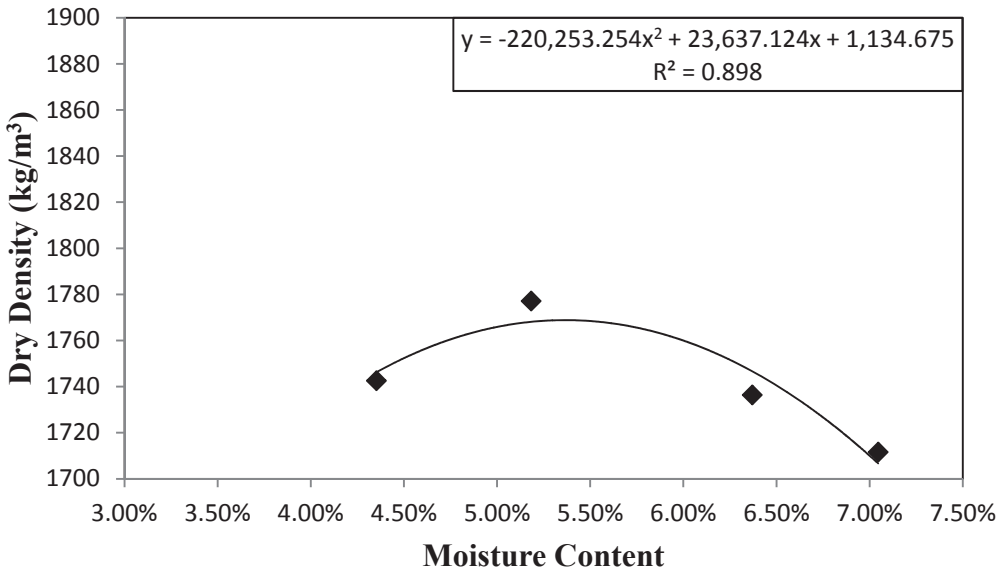

Figure B-6 Sta. 4+040 Moisture Density relationship.
Maximum dry density: 1768 kg/m^3. Optimum moisture content: 5.37%

B.9 Maximum Relative Theoretical Density Results

ASTM D2041/D2041M - 11

Tested by:	P. Salah					
Weighing Flask in water method:						
Station	1+769	2+185	2+550	3+128	3+446	4+040
Direction	SB	SB	NB	NB	SB	NB
Date Tested:	23/09/11					
Mass of sample in air	1650.3	2093.1	2747.3	2670.2	2362.8	1844.7
Mass of flask and sample in water	1531.2	1824.3	2195.8	2147.8	1979.4	1646.4
Mass of flask in water	543.4	567.0	543.4	543.4	567.0	543.4
Mass of sample in water	987.8	1257.3	1652.4	1604.4	1412.4	1103.0
Volume	662.5	835.8	1094.9	1065.8	950.4	741.7
MRTD:	2.491	2.504	2.509	2.505	2.486	2.487

B.10 Granular Resilient Modulus Results

All calculations completed using Matlab program following AASHTO T307 calculation procedures. Modulus values in MPa.

Table B-3 Route 790 sample locations and blend ratios

Sequence	1+769	2+185	2+550	3+128	3+446	4+040
1	51.3	50.1	53.7	45.4	42.8	36.8
2	52.8	57.8	54.2	54.1	50.6	37.0
3		52.4		56.8	50.5	
4				55.2	50.9	
5				50.8	48.7	
6				39.0		
7				44.2		
8				45.8		
9				44.8		
10						
11						
12						
13						
14						

B.11 Direct Shear Test Results: Sta. 1+769

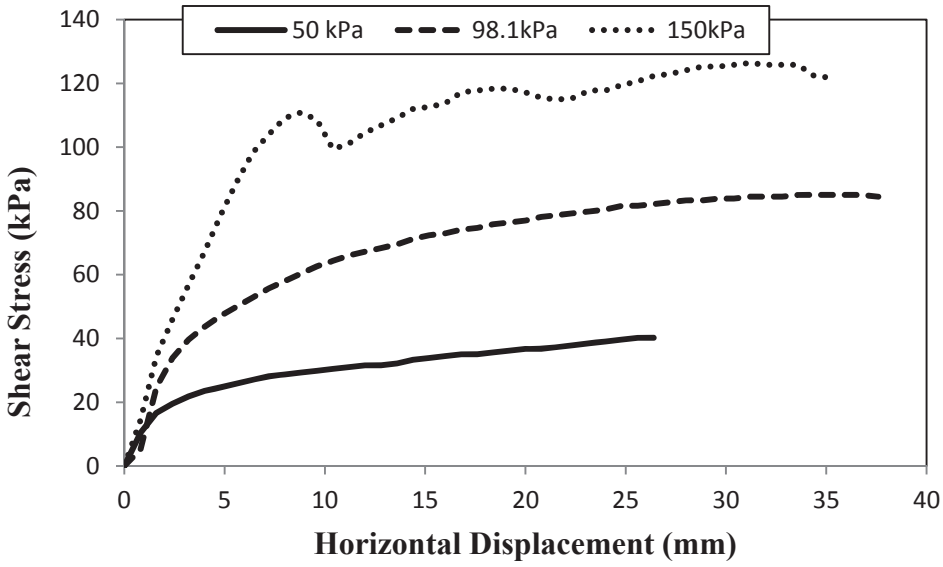

Figure B-7 Sta. 1+769 direct shear test results.

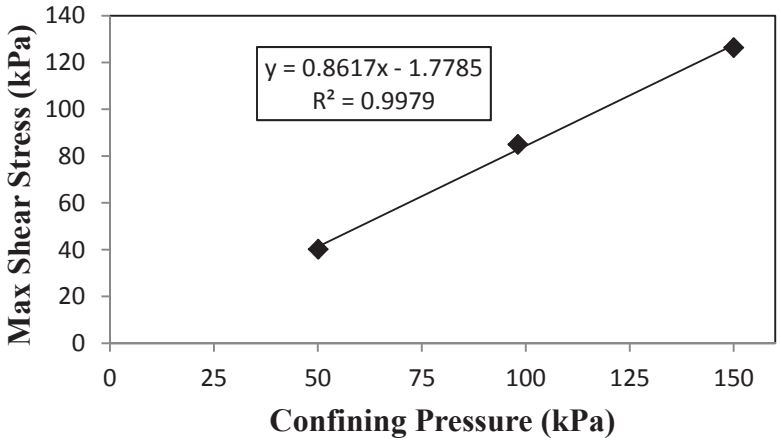

Figure B-8 Sta. 1+769 maximum shear stress versus confining pressure

$\theta = \tan^{-1} 0.861 = 40.7°$

B.12 Direct Shear Test Results: Sta. 2+185

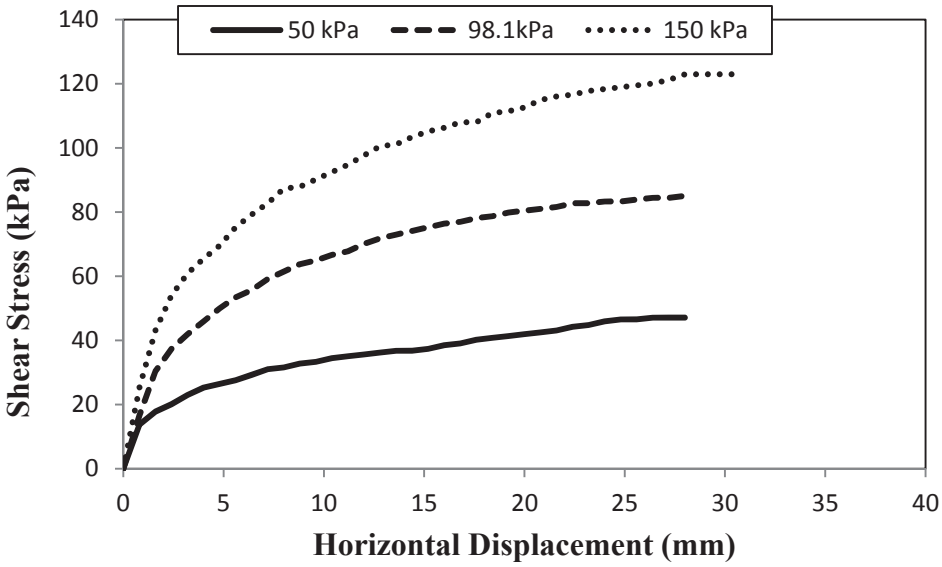

Figure B-9 Sta. 2+185 direct shear test results

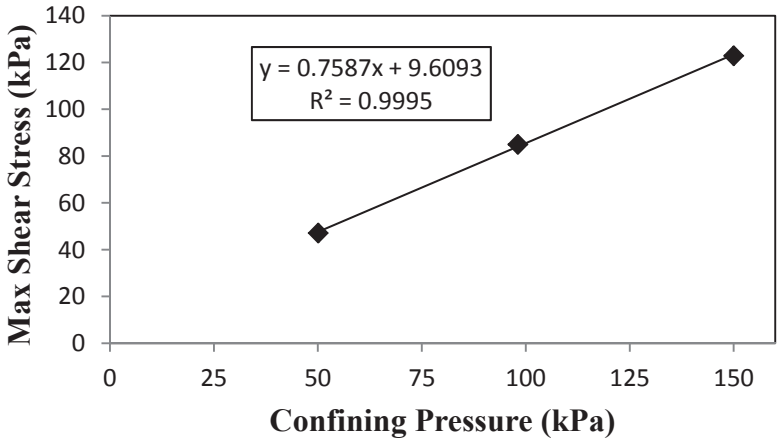

Figure B-10 Sta. 2+185 maximum shear stress versus confining pressure

$$\theta = \tan^{-1} 0.758 = 37.2°$$

B.13 Direct Shear Test Results: Sta. 2+550

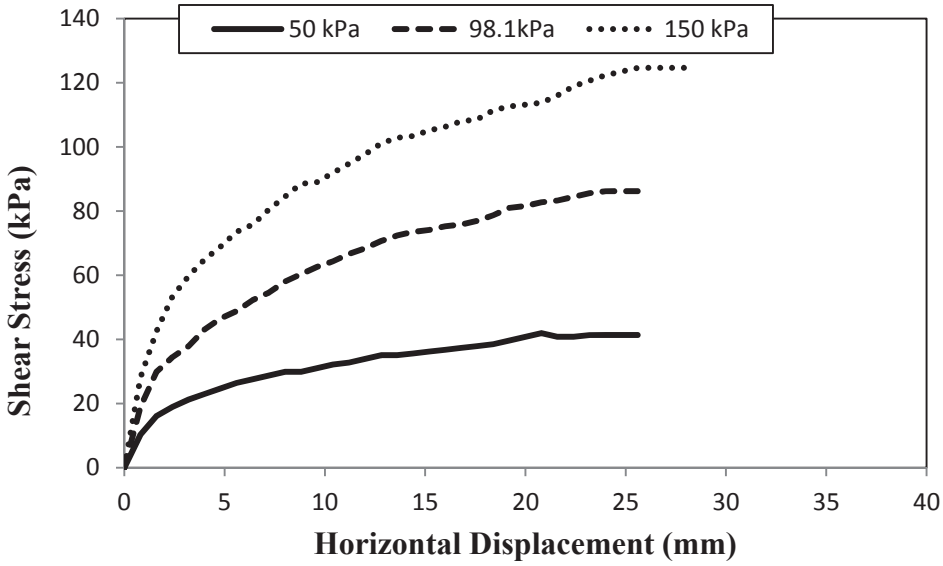

Figure B-11 Sta. 2+550 direct shear test results

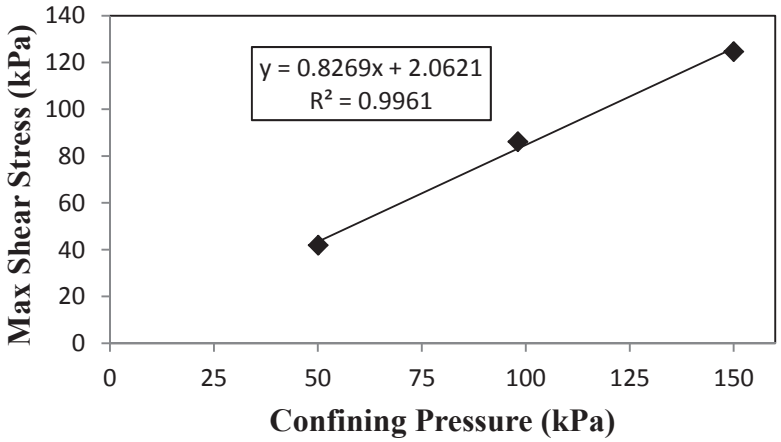

Figure B-12 Sta. 2+550 maximum shear stress versus confining pressure

$\theta = \tan^{-1} 0.826 = 39.6°$

B.14 Direct Shear Test Results: Sta. 3+128

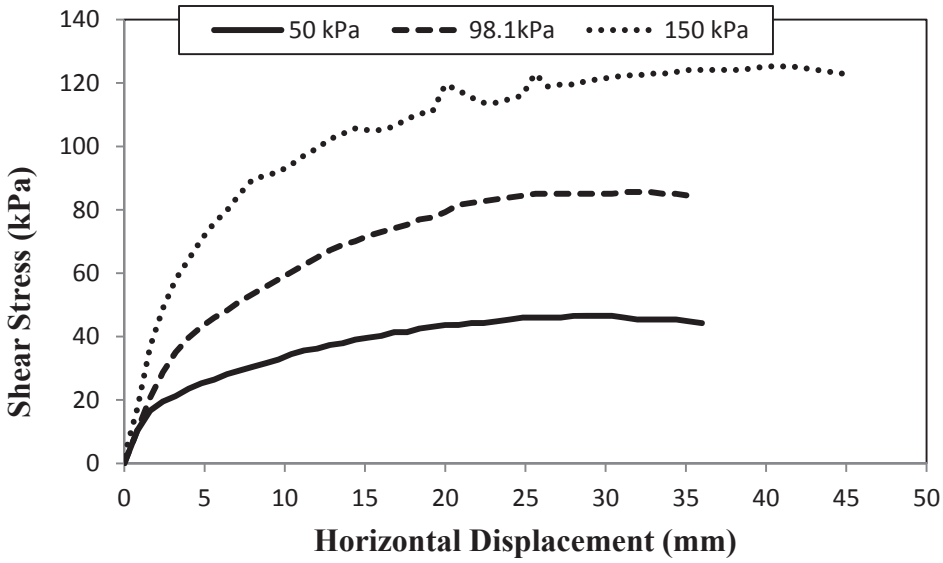

Figure B-13 Sta. 3+128 direct shear test results

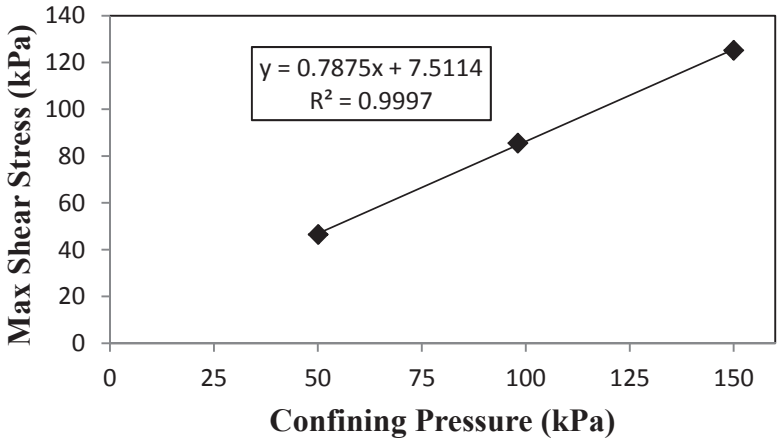

Figure B-14 Sta. 3+128 maximum shear stress versus confining pressure

$\theta = \tan^{-1} 0.787 = 38.2°$

B.15 Direct Shear Test Results: Sta. 3+446

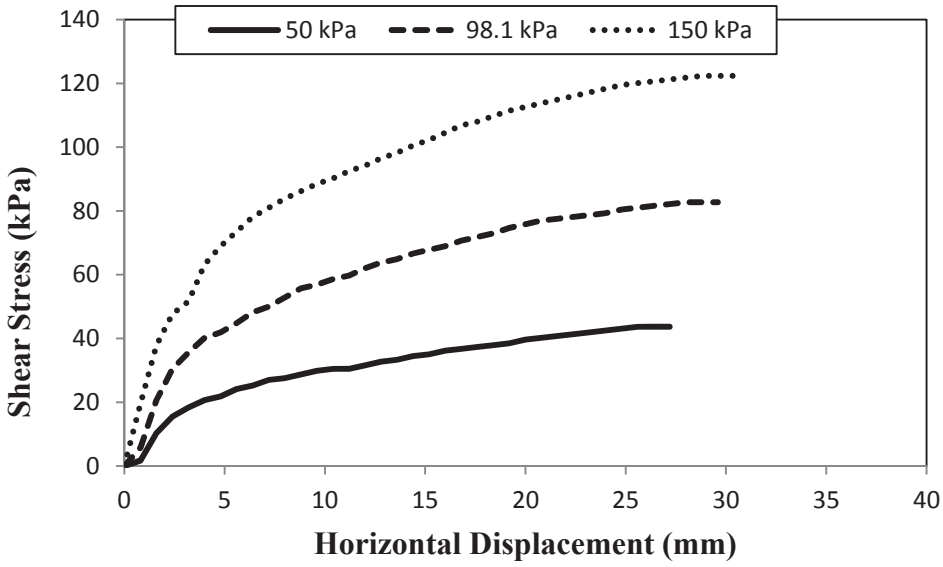

Figure B-15 Sta. 3+446 direct shear test results

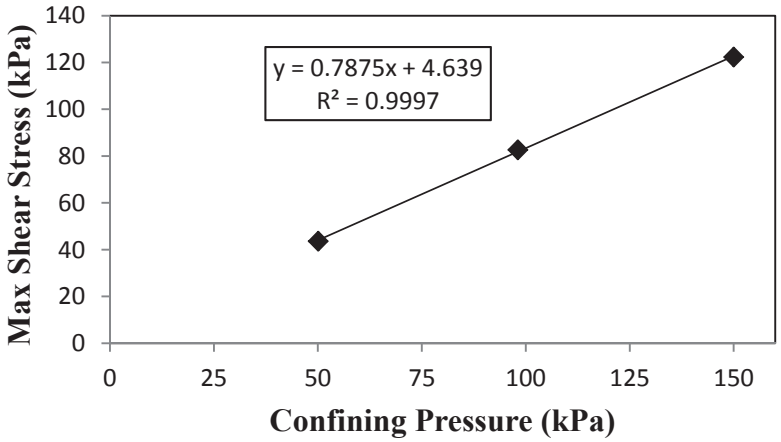

Figure B-16 Sta. 3+446 maximum shear stress versus confining pressure

$\theta = \tan^{-1} 0.787 = 38.2°$

B.16 Direct Shear Test Results: Sta. 4+040

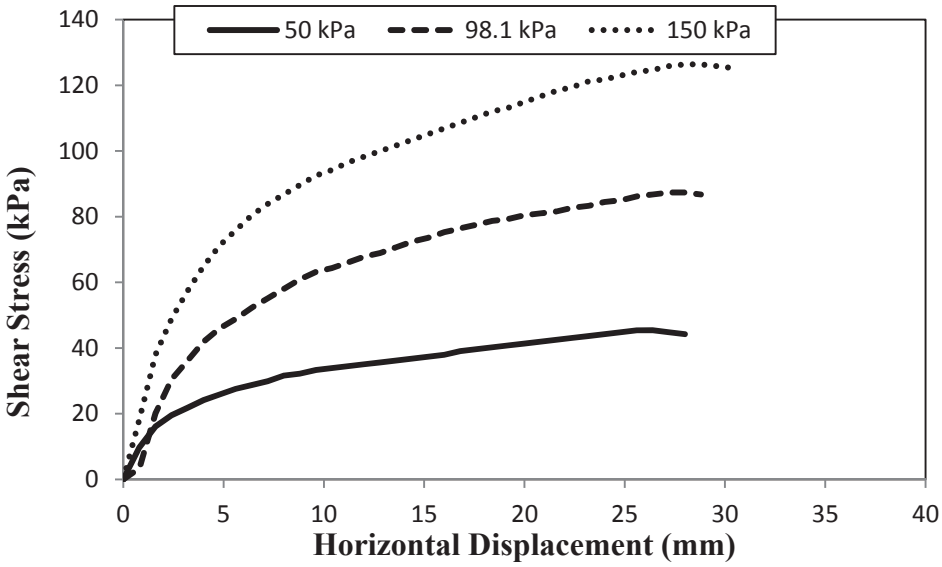

Figure B-17 Sta. 4+040 direct shear test results

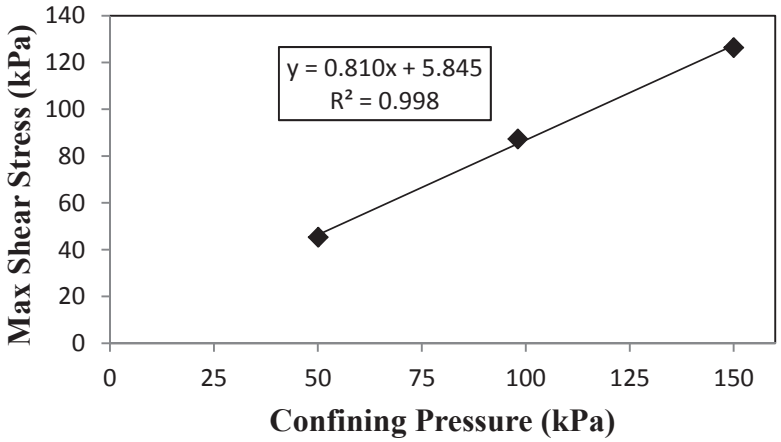

Figure B-18 Sta. 4+040 maximum shear stress versus confining pressure

$$\theta = \tan^{-1} 0.810 = 39.0°$$

B.17 CBR Results: Sta. 1+769

Table B-4 Station 1+769 CBR results

Sample No.	1	1 - Soaked	2	2 - Soaked	3	3 - Soaked
Displacement (inches)	Stress (psi)	Stress (psi)	Stress (psi)	Stress (psi)	Stress (psi)	Stress (psi)
0.025	-	-	3.33	3.33	6.67	6.67
0.05			6.67	6.67	13.34	13.34
0.075			10.00	13.34	20.01	20.01
0.1			13.34	16.67	33.35	26.68
0.125			16.67	20.01	46.69	30.01
0.15			23.34	23.34	56.69	33.35
0.175			30.01	30.01	66.69	40.02
0.2			36.68	33.35	76.70	43.35
0.3			56.69	50.02	113.38	60.03
0.4			80.03	66.69	140.06	76.70
0.5			103.38	83.37	166.74	93.37
CBR at 0.2 inches	-	-	2.6	2.2	4.7	2.7

Average CBR –3.6 Average soaked CBR – 2.4

B.18 CBR Results: Sta. 2+185

Table B-5 Station 2+185 CBR results

Sample No.	**1**	**1 - Soaked**	**2**	**2 - Soaked**	**3**	**3 - Soaked**
Displacement (inches)	Stress (psi)	Stress (psi)	Stress (psi)	Stress (psi)	Stress (psi)	Stress (psi)
0.025	10.00	10.00	6.67	13.34	10.00	10.00
0.05	16.67	20.01	10.00	26.68	20.01	23.34
0.075	23.34	26.68	16.67	40.02	26.68	33.35
0.1	26.68	33.35	26.68	46.69	36.68	43.35
0.125	30.01	40.02	33.35	56.69	43.35	50.02
0.15	33.35	46.69	40.02	66.69	50.02	60.03
0.175	40.02	53.36	46.69	76.70	56.69	66.69
0.2	43.35	60.03	53.36	86.70	63.36	73.36
0.3	60.03	76.70	76.70	113.38	80.03	93.37
0.4	76.70	93.37	93.37	143.39	106.71	113.38
0.5	93.37	110.05	110.05	166.74	130.05	130.05
CBR at 0.2 inches	2.7	3.3	3.2	4.9	3.7	4.0

Average CBR – 3.2 Average soaked CBR – 4.1

B.19 CBR Results: Sta. 2+550

Table B-6 Station 2+550 CBR results

Sample No.	**1**	**1 - Soaked**	**2**	**2 - Soaked**	**3**	**3 - Soaked**
Displacement (inches)	Stress (psi)	Stress (psi)	Stress (psi)	Stress (psi)	Stress (psi)	Stress (psi)
0.025	10.00	10.00	3.33	10.00	6.67	13.34
0.05	16.67	23.34	10.00	23.34	13.34	30.01
0.075	23.34	33.35	16.67	33.35	16.67	40.02
0.1	30.01	43.35	23.34	43.35	23.34	50.02
0.125	36.68	53.36	30.01	53.36	30.01	56.69
0.15	40.02	63.36	36.68	63.36	36.68	63.36
0.175	46.69	70.03	50.02	70.03	43.35	70.03
0.2	50.02	76.70	56.69	80.03	46.69	80.03
0.3	73.36	100.04	86.70	103.38	60.03	103.38
0.4	93.37	126.72	113.38	126.72	76.70	130.05
0.5	110.05	150.06	143.39	150.06	93.37	153.40
CBR at 0.2 inches	3.2	4.4	3.8	4.4	2.7	4.6

Average CBR – 3.2 Average soaked CBR – 4.5

B.20 CBR Results: Sta. 3+128

Table B-7 Station 3+128 CBR results

Sample No.	1	1 - Soaked	2	2 - Soaked	3	3 - Soaked
Displacement (inches)	Stress (psi)	Stress (psi)	Stress (psi)	Stress (psi)	Stress (psi)	Stress (psi)
0.025	13.34	16.67	10.00	13.34	3.33	16.67
0.05	26.68	33.35	20.01	26.68	3.33	30.01
0.075	33.35	46.69	30.01	36.68	6.67	36.68
0.1	40.02	53.36	43.35	43.35	13.34	46.69
0.125	46.69	70.03	53.36	53.36	23.34	56.69
0.15	53.36	80.03	60.03	60.03	33.35	63.36
0.175	60.03	86.70	70.03	66.69	46.69	73.36
0.2	66.69	93.37	83.37	73.36	56.69	80.03
0.3	93.37	126.72	106.71	96.71	93.37	106.71
0.4	116.72	176.74	140.06	113.38	123.39	136.72
0.5	143.39	186.75	163.40	133.39	153.40	166.74
CBR at 0.2 inches	4.1	5.7	4.7	4.1	3.9	4.8

Average CBR – 4.2 Average soaked CBR – 4.8

B.21 CBR Results: Sta. 3+446

Table B-8 Station 3+446 CBR results

Sample No.	1	1 - Soaked	2	2 - Soaked	3	3 - Soaked
Displacement (inches)	Stress (psi)	Stress (psi)	Stress (psi)		Stress (psi)	
0.025	6.67	3.33	6.67	13.34	3.33	10.00
0.05	10.00	13.34	10.00	23.34	6.67	20.01
0.075	13.34	26.68	16.67	33.35	13.34	30.01
0.1	20.01	33.35	23.34	46.69	20.01	40.02
0.125	23.34	40.02	30.01	53.36	26.68	46.69
0.15	26.68	46.69	36.68	60.03	36.68	53.36
0.175	30.01	53.36	46.69	70.03	43.35	63.36
0.2	33.35	60.03	56.69	76.70	50.02	70.03
0.3	50.02	80.03	76.70	106.71	70.03	93.37
0.4	63.36	96.71	93.37	136.72	90.04	113.38
0.5	76.70	116.72	113.38	166.74	106.71	136.72
CBR at 0.2 inches	2.1	3.4	3.2	4.7	3.0	4.0

Average CBR – 2.8 Average soaked CBR – 4.0

B.22 CBR Results: Sta. 4+040

Table B-9 Station 4+040 CBR results

Sample No.	**1**	**1 - Soaked**	**2**	**2 - Soaked**	**3**	**3 - Soaked**
Displacement (inches)	Stress (psi)	Stress (psi)	Stress (psi)	Stress (psi)	Stress (psi)	Stress (psi)
0.025	10.00	6.67	13.34	6.67	3.33	10.00
0.05	16.67	16.67	20.01	13.34	6.67	20.01
0.075	23.34	23.34	26.68	20.01	10.00	30.01
0.1	26.68	30.01	33.35	26.68	13.34	43.35
0.125	33.35	36.68	40.02	33.35	20.01	53.36
0.15	40.02	43.35	46.69	36.68	26.68	60.03
0.175	43.35	50.02	50.02	43.35	30.01	63.36
0.2	46.69	56.69	56.69	50.02	33.35	76.70
0.3	66.69	76.70	76.70	63.36	50.02	100.04
0.4	83.37	103.38	96.71	76.70	70.03	126.72
0.5	100.04	123.39	116.72	93.37	90.04	146.73
CBR at 0.2 inches	2.9	3.5	3.4	2.7	2.3	4.3

Average CBR – 2.9 Average soaked CBR – 3.5

B.23 McAsphalt PG58-28 Foaming Characteristics

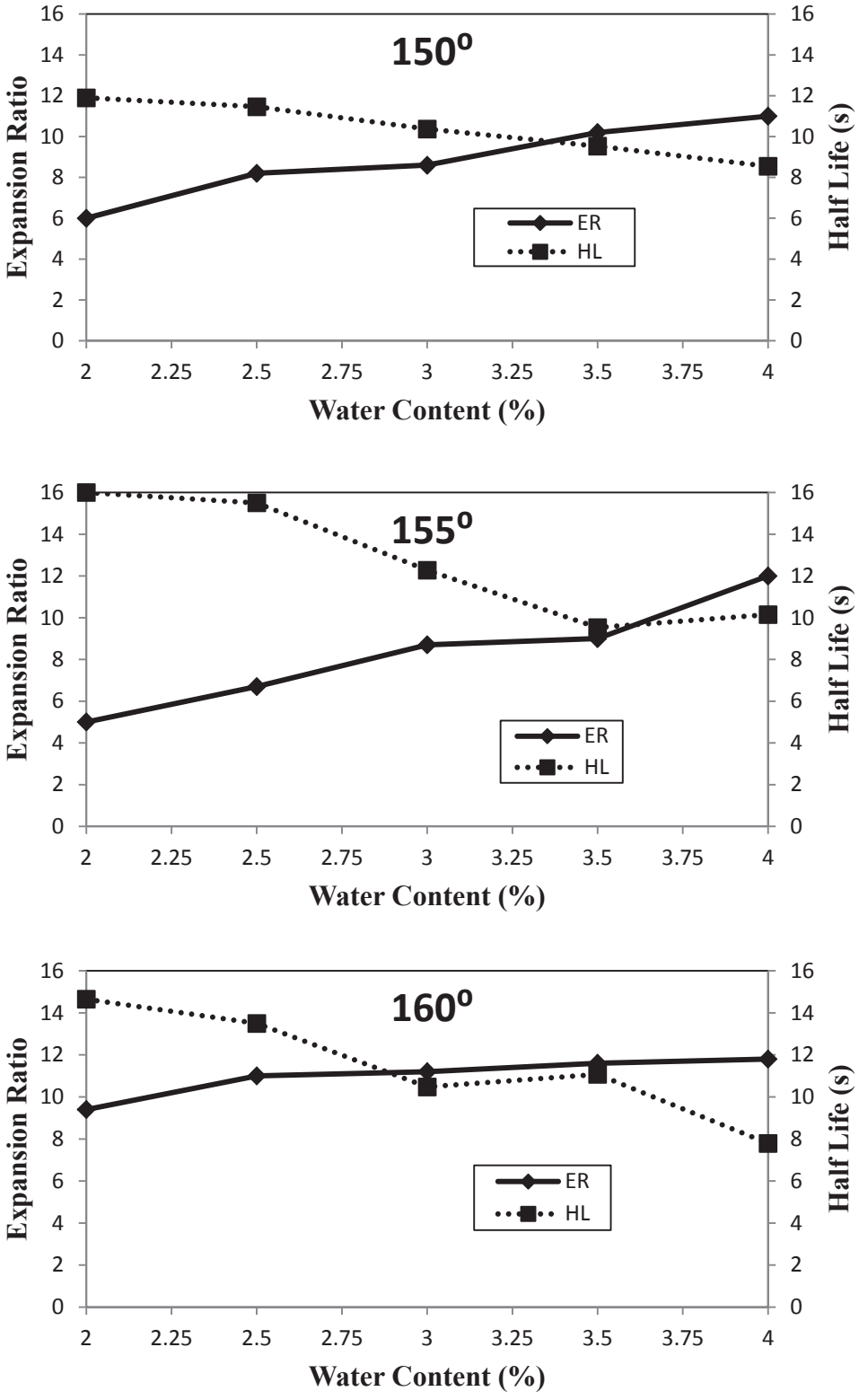

Figure B-19 McAsphalt PG58-28 foaming characteristics at 150°C, 155°C, & 160°C

B.24 Material Job Mix Formulas for three FDR blends.

Table B-10 Individual and combined material gradations

Percent Passing						
Size (mm)	**Route 790 FDR**	**Screened Crusher Dust**	**Portland Cement**	**As-Is JMF**	**Improved JMF**	**Optimum JMF**
25.0	100	100.0	100.0	100	100	100.0
19.0	97.1	100.0	100.0	97.1	97.6	100.0
15.9	93.6	100.0	100.0	93.6	94.6	92.3
12.7	85.5	100.0	100.0	85.6	87.8	83.4
9.5	75.7	100.0	100.0	75.8	79.6	73.2
4.75	49.9	100.0	100.0	50.2	58.0	53.6
2.5	30.0	100.0	100.0	30.4	41.3	40.1
1.25	16.3	100.0	100.0	16.7	29.8	29.4
0.63	8.3	69.1	100.0	8.8	18.2	21.6
0.315	4.0	51.8	100.0	4.5	11.9	15.8
0.16	1.9	39.4	100.0	2.4	8.2	11.7
0.08	1.2	29.8	100.0	1.7	6.2	8.5

B.25 Moisture-Density Relationship: "As-Is" FDR Blend

Mass of mould & plate:	4212	g		Diameter	101.6	mm
				Height:	116.4	mm
				Volume:	9.437E-04	m^3

Sample No.	1	2	3	4
Date Tested	30/04/12	30/04/12	30/04/12	03/05/12
Air dry mass of sample (g)	2000.0	2000.0	2000.0	2000.0
% Water added	5.0%	6.0%	7.0%	6.0%
Mass of water added (g)	100.0	120.0	140.0	120.0
Mass of sample + mould + plate (g)	5840.0	5899.0	5908.0	5886.0
Mass - Wet (for moisture content) (g)	1688.7	1683.8	1690.3	1669.5
Tare (g)	598.4	582.3	1124.5	584.6
Mass of dry sample (g)	1613.7	1596.4	1582.9	1582.7
Actual Moisture Content	4.65%	5.47%	6.79%	5.48%
Moist Density	1725.1	1787.7	1797.2	1773.9
Dry density (kg/m^3)	1648.5	1694.9	1683.0	1681.7

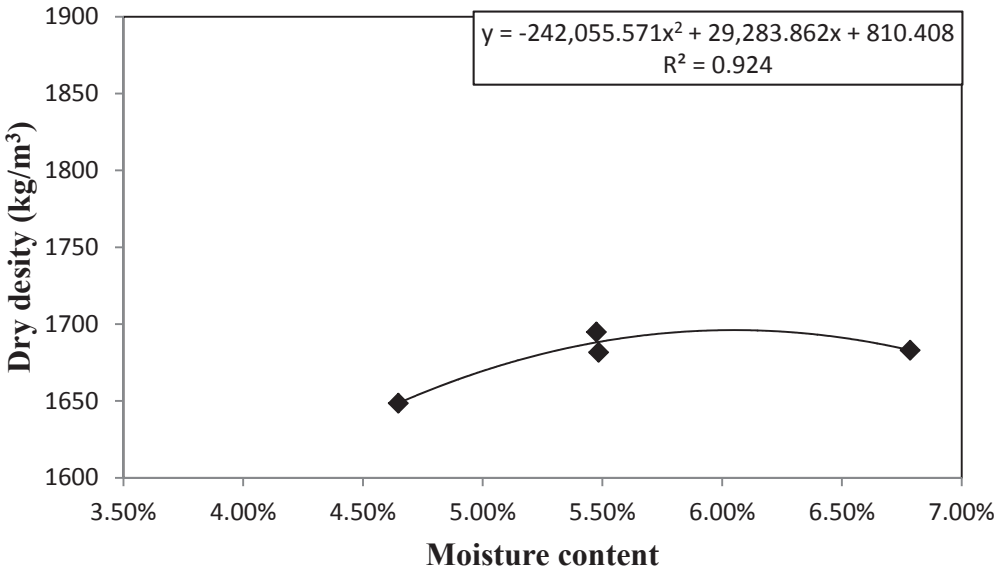

Figure B-20 "As-Is" blend Moisture Density relationship.
Maximum dry density: 1696 kg/m^3. Optimum moisture content: 6.05%

B.26 Moisture-Density Relationship: "Improved" FDR Blend

Mass of mould & plate:	4212	g		Diameter	101.6	mm
				Height:	116.4	mm
				Volume:	9.437E-04	m^3

Sample No.	1	2	3	4	5
Date Tested	30/04/12	30/04/12	30/04/12	30/04/12	03/05/12
mass of sample (g)	2000.0	2000.0	2000.0	2000.0	2000.0
% Water added	4.0%	5.0%	6.0%	7.0%	6.2%
Mass of water added (g)	80.0	100.0	120.0	140.0	124.0
COMPACTED					
Mass of sample + mould + plate (g)	6031.0	6055.0	6079.0	6007.0	6052.0
Mass - Wet (for moisture content) (g)	1815.8	1840.8	1865.4	1791.4	1835.6
Tare (g)	625.0	589.7	595.9	625.5	338.1
Mass of dry sample (g)	1742.3	1755.1	1766.4	1679.8	1731.6
Actual Moisture Content	4.22%	4.88%	5.60%	6.64%	6.01%
Moist Density	1927.5	1953.0	1978.4	1902.1	1949.8
Dry density (kg/m^3)	1849.5	1862.0	1873.4	1783.6	1839.3

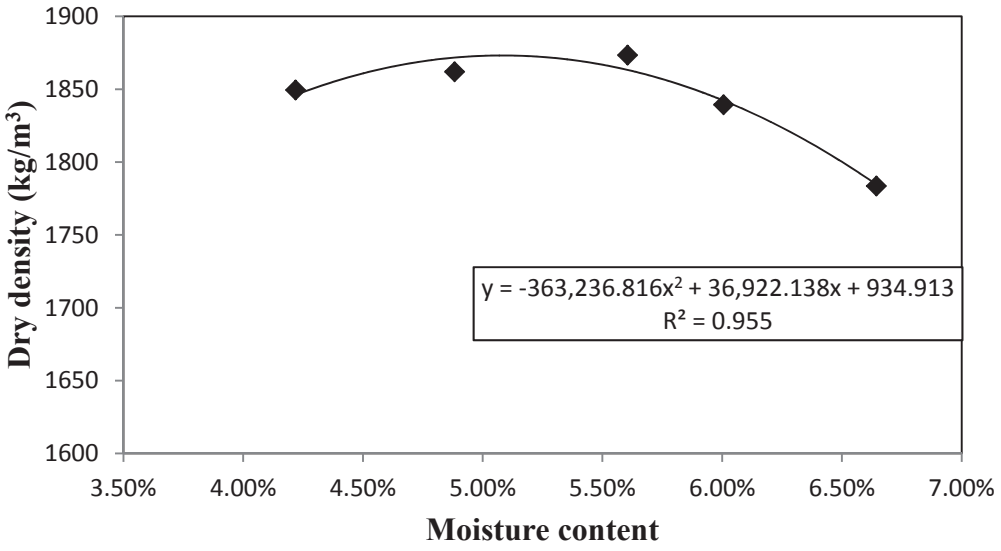

Figure B-21 "Improved" blend Moisture Density relationship.
Maximum dry density: 1869 kg/m^3. Optimum moisture content: 5.23%

B.27 Moisture-Density Relationship: "Optimum" FDR Blend

Mass of mould & plate:	4212	g		Diameter	101.6	mm
				Height:	116.4	mm
				Volume:	9.437E-04	m^3

Optimum

Sample No.	1	2	3	4
Date Tested	30/04/12	30/04/12	30/04/12	03/05/12
Air dry mass of sample (g)	2000.0	2000.0	2000.0	2000.0
% Water added	4.0%	5.0%	7.0%	6.0%
Mass of water added (g)	80.0	100.0	140.0	120.0
COMPACTED				
Mass of sample + mould + plate (g)	5987.0	6065.0	6061.0	6063.0
Mass - Wet (for moisture content) (g)	1771.8	1849.4	1842.9	1845.0
Tare (g)	337.5	598.2	1138.2	598.4
Mass of dry sample (g)	1705.4	1766.7	1729.6	1746.2
Actual Moisture Content	3.89%	4.68%	6.55%	5.66%
Moist Density	1880.9	1963.6	1959.3	1961.4
Dry density (kg/m^3)	1810.4	1875.8	1838.9	1856.4

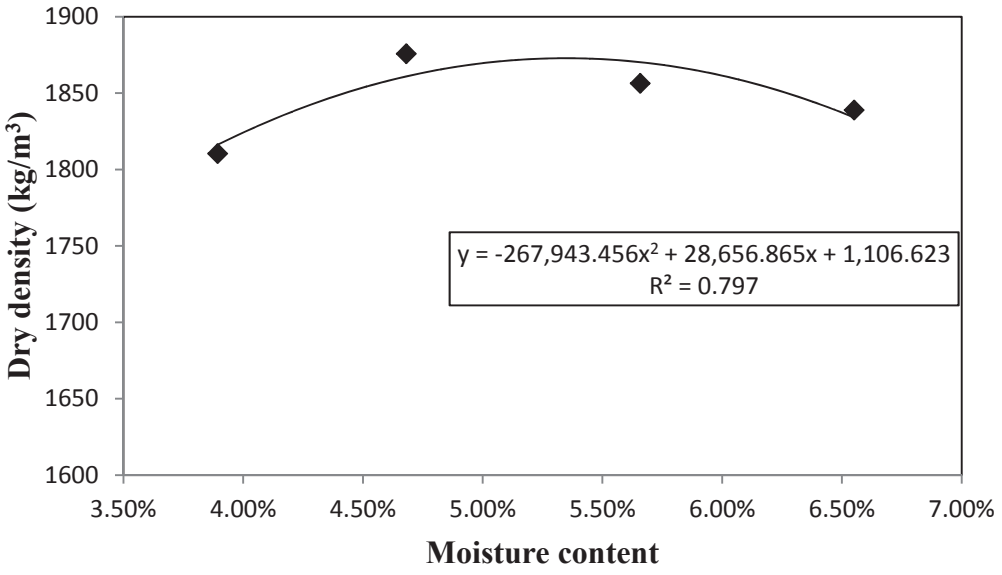

Figure B-22 "Optimum" blend Moisture Density relationship.
Maximum dry density: 1873 kg/m^3. Optimum moisture content: 5.35%

Table B-11 "As-Is" Blend Mix Design **B.28**

AC %		Sample No:	Mass (g)	Height (mm)	Diameter (mm)	Bulk Density	Dial Reading	Load (N)	ITS (kPa)	Average ITS (kPa)	TSR
2.0%	Soaked	1	999.8	64.05	101.6	1925.4	22	1068.2	104.50	97.79	66.8%
		2	978.9	63.77	101.6	1893.4	21	1021.1	100.33		
		3	948.7	62.27	101.6	1879.2	18	879.9	88.54		
	Dry	4	1058.6	69.08	101.6	1890.2	27	1303.4	118.23	146.45	
		5	939.2	59.93	101.6	1933.0	34	1632.8	170.72		
		6	1086.1	69.99	101.6	1914.1	35	1679.9	150.40		
2.5%	Soaked	7	1083.6	70.53	101.6	1895.0	28	1350.5	119.98	117.46	78.1%
		8	1100.6	71.33	101.6	1903.2	28	1350.5	118.63		
		9	1009.2	66.60	101.6	1869.1	25	1209.3	113.77		
	Dry	10	1077.2	70.45	101.6	1886.0	31	1491.7	132.67	150.49	
		11	1065.0	69.44	101.6	1891.7	37	1774.0	160.08		
		12	1130.9	73.75	101.6	1891.4	39	1868.1	158.72		
3.0%	Soaked	13	1059.3	69.93	101.6	1868.4	28	1350.5	121.01	119.47	80.0%
		14	1044.7	68.10	101.6	1892.2	32	1538.7	141.58		
		15	963.1	63.69	101.6	1865.2	20	974.0	95.82		
	Dry	16	1089.8	71.30	101.6	1885.3	31	1491.7	131.09	149.35	
		17	1053.0	68.02	101.6	1909.5	36	1727.0	159.09		
		18	1090.4	70.41	101.6	1910.2	37	1774.0	157.87		
3.5%	Soaked	22	1116.8	71.73	101.6	1920.4	35	1679.9	146.75	142.59	101.3%
		20	1032.7	65.72	101.6	1938.2	35	1679.9	160.17		
		21	1037.9	67.58	101.6	1894.3	27	1303.4	120.85		
	Dry	23	1014.8	65.70	101.6	1905.2	31	1491.7	142.27	140.82	
		24	1063.4	69.18	101.6	1896.0	32	1538.7	139.37		

Table B-12 "Improved" Blend Mix Design **B.29**

AC %		Sample No:	Mass (g)	Height (mm)	Diameter (mm)	Bulk Density	Dial Reading	Load (N)	ITS (kPa)	Average ITS (kPa)	TSR
2.0%	Soaked	51	1102.7	66.60	101.6	2042.2	42	2009.3	189.04	183.98	76.2%
		52	1091.1	65.78	101.6	2045.9	39	1868.1	177.95		
		53	1108.6	68.07	101.6	2008.8	42	2009.3	184.96		
	Dry	55	1142.1	69.39	101.6	2030.2	57	2711.6	244.86	241.53	
		56	1104.7	66.33	101.6	2054.3	56	2665.0	251.75		
		57	1087.5	66.85	101.6	2006.6	51	2432.3	227.98		
2.5%	Soaked	58	1113.0	68.97	101.6	1990.5	46	2197.6	199.65	189.98	72.0%
		59	1102.9	67.55	101.6	2013.9	44	2103.4	195.11		
		60	1091.9	66.82	101.6	2015.6	39	1868.1	175.18		
	Dry	64	1100.0	67.98	101.6	1995.9	63	2990.8	275.67	263.80	
		65	1116.4	68.26	101.6	2017.2	59	2804.6	257.44		
		66	1099.7	68.04	101.6	1993.6	59	2804.6	258.28		
3.0%	Soaked	70	1109.3	67.67	101.6	2022.0	49	2338.7	216.55	218.83	78.5%
		71	1113.6	68.75	101.6	1997.9	47	2244.6	204.58		
		72	1096.7	67.23	101.6	2012.1	53	2525.4	235.37		
	Dry	73	1105.8	68.24	101.6	1998.8	60	2851.2	261.80	278.90	
		74	1084.8	66.90	101.6	2000.1	62	2944.2	275.76		
		75	1081.2	65.57	101.6	2033.9	66	3130.4	299.14		
3.5%	Soaked	77	1118.2	68.62	101.6	2010.0	56	2665.0	243.35	236.71	82.5%
		78	1097.8	67.18	101.6	2015.6	52	2478.9	231.21		
		79	1113.6	68.41	101.6	2007.9	54	2571.9	235.57		
	Dry	80	1099.9	67.58	101.6	2007.5	64	3037.3	281.62	286.77	
		81	1092.6	66.06	101.6	2040.1	66	3130.4	296.93		
		82	1095.3	67.54	101.6	2000.3	64	3037.3	281.78		

Table B-13 "Optimum" Blend Mix Design **B.30**

AC %		Sample No:	Mass (g)	Height (mm)	Diameter (mm)	Bulk Density	Dial Reading	Load (N)	ITS (kPa)	Average ITS (kPa)	TSR
2.0%	Soaked	25	1132.5	69.50	101.6	2009.9	44	2103.4	189.64	189.52	86.1%
		26	955.1	57.88	101.6	2035.4	34	1632.8	176.76		
		27	1019.4	62.28	101.6	2018.9	42	2009.3	202.15		
	Dry	28	1153.4	71.10	101.6	2000.9	51	2432.3	214.36	219.99	
		29	1022.1	62.51	101.6	2016.8	43	2056.4	206.13		
		30	1016.0	61.43	101.6	2040.0	40	1915.2	195.35		
		31	1086.9	67.15	101.6	1996.5	53	2525.4	235.65		
		32	1069.0	63.69	101.6	2070.3	53	2525.4	248.45		
3.0%	Soaked	34	1058.5	65.31	101.6	1999.1	47	2244.6	215.35	221.91	98.6%
		35	972.4	60.44	101.6	1984.5	44	2103.4	218.06		
		36	983.4	60.54	101.6	2003.6	47	2244.6	232.32		
	Dry	37	996.9	61.55	101.6	1997.8	43	2056.4	209.35	225.10	
		38	1110.3	67.93	101.6	2016.1	50	2385.8	220.07		
		39	1042.7	64.55	101.6	1992.4	45	2150.5	208.75		
		33	1040.8	65.90	101.6	1948.1	58	2758.1	262.25		
3.5%	Soaked	41	1042.6	64.79	101.6	1984.9	49	2338.7	226.18	218.37	98.3%
		42	1096.4	68.70	101.6	1968.5	49	2338.7	213.31		
		43	1051.9	63.86	101.6	2031.7	46	2197.6	215.63		
	Dry	44	1050.5	65.03	101.6	1992.5	47	2244.6	216.28	222.04	
		45	1074.9	67.01	101.6	1978.6	45	2150.5	201.09		
		46	1054.8	64.91	101.6	2004.4	41	1962.3	189.43		
		47	1096.3	67.64	101.6	1999.2	64	3037.3	281.37		

B.31 "Improved" blend indirect tensile strength results

Table B-14 ITS Results for "Improved" blend with variable mixing moisture content

Grading	Moisture Content	AC %		Sample No:	Mass (g)	Height (mm)	Diameter (mm)	Bulk Density	Dial Reading	Load (N)	IDT (kPa)	Average IDT (kPa)	TSR
Improved	3.00%	3.5%	Soaked	117	1106.2	67.19	101.6	2030.7	36	1727.0	161.05	157.25	78.7%
				118	1101.6	67.73	101.6	2006.2	34	1632.8	151.06		
				119	1106.2	67.79	101.6	2012.8	36	1727.0	159.63		
			Dry	120	1086.8	66.49	101.6	2016.1	46	2197.6	207.10	199.85	
				121	1076.7	65.89	101.6	2015.6	38	1821.1	173.18		
				122	946.4	57.42	101.6	2033.0	42	2009.3	219.26		

Grading	Moisture Content	AC %		Sample No:	Mass (g)	Height (mm)	Diameter (mm)	Bulk Density	Dial Reading	Load (N)	IDT (kPa)	Average IDT (kPa)	TSR
Improved	6.60%	3.5%	Soaked	144	972.8	59.48	101.6	2017.3	37	1774.0	186.88	187.84	76.6%
				148	927.9	56.03	101.6	2042.7	~~44~~	~~2103.4~~	~~235.23~~		
				149	1047.6	63.56	101.6	2033.0	40	1915.2	188.81		
			Dry	145	1032.8	62.45	101.6	2039.9	54	2571.9	258.05	245.35	
				146	1061.0	64.04	101.6	2043.6	52	2432.3	237.99		
				151	976.2	59.83	101.6	2012.5	48	2291.7	240.01		

B.32 Resilient Modulus Sample Calculations

Sample #: 138 Side: A Temperature: 25°C

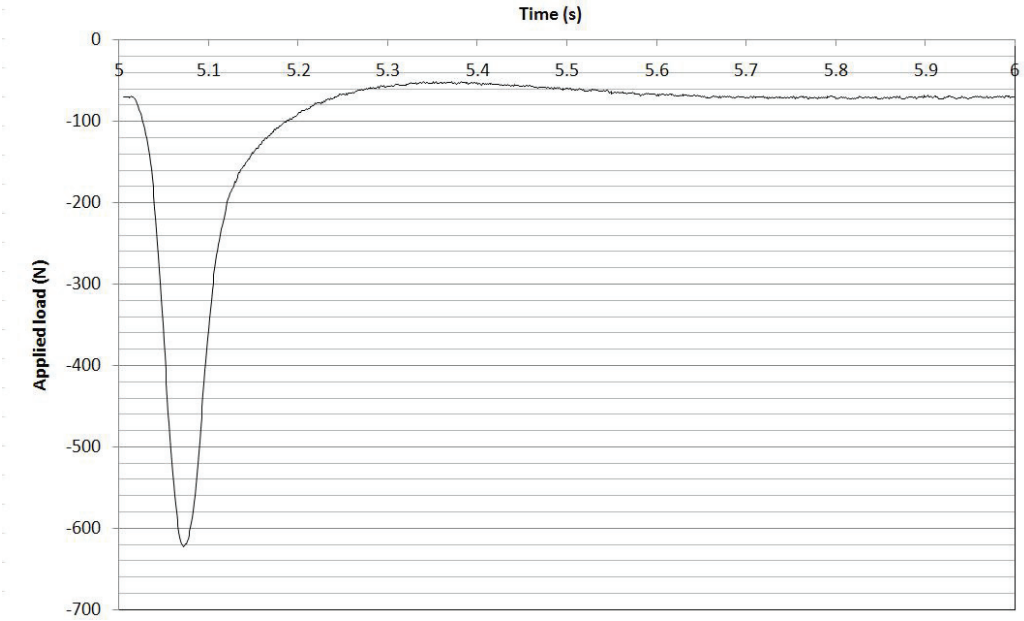

Figure B-23 Sample 138, Side A: Load vs. Time curve at 25°C

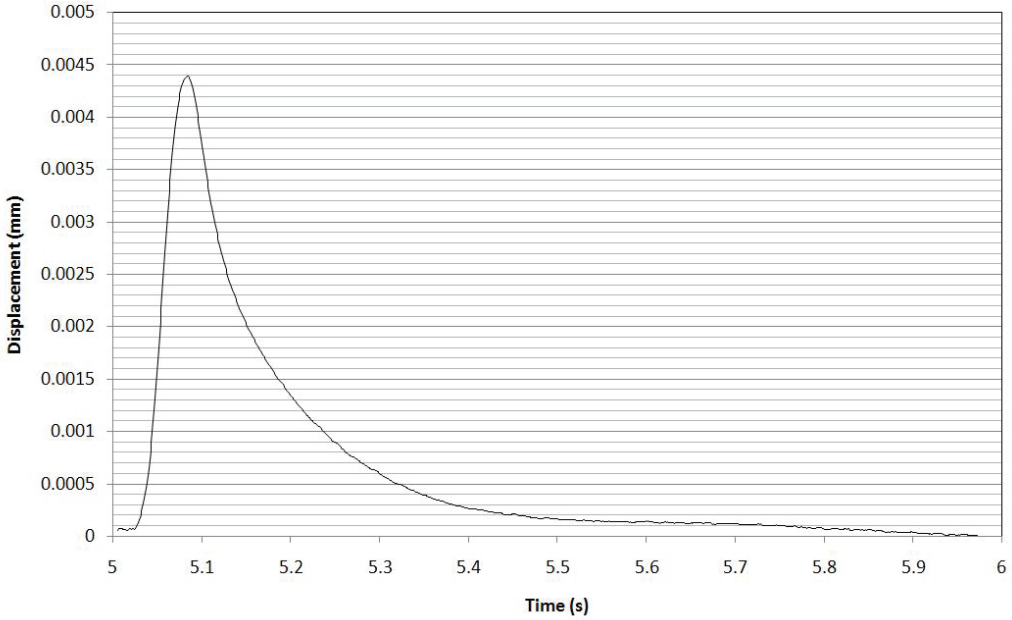

Figure B-24 Sample 138, Side A: Displacement vs. Time curve at 25°C

B.33 Resilient Modulus Sample Calculations (continued)

Sample 138 thickness: 60.23 mm

μ: 0.30

P_{cyclic}: 561.7 N

δ_h: 0.0037981 mm

I_1: 0.199157

I_2: -0.655247

$$M_R = \frac{561.7}{0.0037981 * 60.23} * [.199157 - (-0.655247) * 0.3]$$

M_R = 971.6 MPa

B.34 Resilient Modulus Results:

Table B-15 Resilient modulus results (MPa)

Mix Number	Sample No.	Temp (°C)	-14	-4	6	25	42
1	93	A	1421.9	1933.3	818.8	528.9	329.8
		B	2478.4	1628.9	1750.2	608.0	337.8
		Average	1950.2	1781.1	1284.5	568.5	333.8
	Mix 1 Overall Averages		**1950.2**	**1781.1**	**1284.5**	**568.5**	**333.8**
2	186	A	3806.8	2438.6	1853.9	771.5	334.3
		B	1522.0	1546.0	1862.1	782.3	337.5
		Average	2664.4	1992.3	1858.0	776.9	335.9
	Mix 2 Overall Averages		**2664.4**	**1992.3**	**1858.0**	**776.9**	**335.9**
3	124	A	1882.2	2041.3	1091.0	395.2	266.3
		B	4130.7	1842.5	1896.9	1167.1	248.0
		Average	3006.5	1941.9	1494.0	781.2	257.2
	128	A	4728.7	2267.6	1065.4	809.4	226.1
		B	1524.0	2250.9	1761.4	652.9	167.7
		Average	3126.4	2259.3	1413.4	731.2	196.9
	Mix 3 Overall Averages		**3066.4**	**2100.6**	**1453.7**	**756.2**	**227.0**
4	138	A	2753.6	3066.0	1933.8	971.6	303.9
		B	3781.7	3021.9	2458.2	869.7	294.4
		Average	3267.7	3044.0	2196.0	920.7	299.2
	Mix 4 Overall Averages		**3267.7**	**3044.0**	**2196.0**	**920.7**	**299.2**
5	147	A	3567.8	2238.2	~~3031.7~~	873.5	465.5
		B	2847.3	2190.8	~~2226.1~~	1160.8	448.1
		Average	3207.6	2214.5	~~2628.9~~	1017.2	456.8
	154	A	3864.9	2185.0	1675.9	786.0	353.1
		B	3698.2	2663.9	~~2399.4~~	968.4	288.2
		Average	3781.6	2424.5	1675.9	877.2	320.7
	Mix 5 Overall Averages		**3494.6**	**2319.5**	**1675.9**	**947.2**	**388.7**

B.35 Resilient Modulus Results (cont)

Table B-15 (cont) Resilient modulus results (MPa)

Mix Number	Sample No.	Temp (°C)	-14	-4	6	25	42
6	158	A	4109.1	2326.6	2206.4	971.2	375.8
		B	4524.7	1906.7	2081.8	981.4	410.3
		Average	4316.9	2116.7	2144.1	976.3	393.1
	160	A	2958.2	2144.3	1991	1019.7	130.4
		B		2462.3	1670.2	855.3	202.9
		Average	2958.2	2303.3	1830.6	937.5	166.7
	Mix 6 Overall Averages		**3637.6**	**2210.0**	**1987.4**	**956.9**	**279.9**
7	99	A	3121.9	1983.0	1002.8	1192.7	540.4
		B	2686.0	1986.2	1826.0	1183.1	324.9
		Average	2904.0	1984.6	1414.4	1187.9	432.7
	100	A	1577.6	3085.4	1255.6	878.0	694.5
		B	3981.9	2183.8	1920.8	1007.7	673.4
		Average	2779.8	2183.8	1588.2	942.9	684.0
	Mix 7 Overall averages		**2841.9**	**2084.2**	**1501.3**	**1065.4**	**558.3**

B.36 Dynamic Modulus Results

Table B-16 Dynamic modulus results (MPa)

-10°C	Modulus Values													
Mix No.	1		2		3		4		5		6		7	
	A	B	A	B	A	B	A	B	A	B	A	B	A	B
25Hz	2491.2	2173.8	1739.4	3286.2	3537.5	1352.9	3459.2	1929.4	-	2481.9	3851.8	2704.1	2719.0	3622.1
10Hz	2177.6	1962.3	1517.6	2661.9	3073.2	1127	2959.7	1565	-	2002.9	3327.8	2392.0	2334.7	3198.0
5Hz	1984.5	1862.2	1387.1	2614.3	2892.4	922.2	2672.3	1386	-	1753.6	3132.3	2226.0	2130.2	2963.3
1Hz	1646.9	1584.7	1176.1	2209.4	2450.5	721.3	2174.1	1094.1	-	1397.2	2690.1	1892.7	1829.5	2547.7
0.1Hz	1238.0	1183.7	687.1	1683.7	1884.4	430.8	1616	799.1	-	890.2	2092.3	1449.7	1238.1	1887.2

6°C	Modulus Values													
Mix No.	1		2		3		4		5		6		7	
	A	B	A	B	A	B	A	B	A	B	A	B	A	B
25Hz	1782.3	1601.8	-	1827.3	1968.4	1427.9	1918.9	1181.1	-	1438.0	2113.8	1596.1	1511.3	2417.2
10Hz	1420.4	1304.0	935.4	1457.3	1593.2	1188.7	1615	889.7	-	1122.6	1599.1	1185.0	1236.1	2015.2
5Hz	1219.0	1153.5	715.5	1276.8	1381.1	1005.4	1333.8	809.4	-	973.4	1406.7	1057.1	1070.2	1843.4
1Hz	902.7	894.9	537.9	981.4	1057.2	758.2	1029.2	638.7	-	753.1	1098.7	820.9	872.8	1442.0
0.1Hz	579.0	564.1	370.7	602.6	722.5	492.2	666.2	419.4	-	500.8	741.3	463.3	524.6	873.1

22°C	Modulus Values													
Mix No.	1		2		3		4		5		6		7	
	A	B	A	B	A	B	A	B	A	B	A	B	A	B
25Hz	1106.5	1117.1	842.6	1167.4	1115.4	1239.3	1369.8	697.8	-	935.1	895.9	926.4	1145.9	1337.6
10Hz	834.1	860.4	633.1	889.8	838.7	1188.3	976.3	538.7	-	679.6	649.6	693.8	912.8	1049.2
5Hz	701.7	707.4	537.2	745.6	703.4	987.6	796.2	403.0	-	525.6	508.0	549.2	754.0	910.8
1Hz	466.8	508.1	343.1	477.8	477.8	725.6	505.3	263.9	-	343.6	322.3	368.1	541.2	655.6
0.1Hz	251.6	280.5	193.2	247.0	252.9	387.9	264.5	133.7	-	182.8	152.7	180.4	352.9	395.4

B.37 Dynamic Modulus Results (cont)

Table B-16 (cont) Dynamic modulus results (MPa)

41°C	Modulus Values													
Mix Number:	1		2		3		4		5		6		7	
	A	B	A	B	A	B	A	B	A	B	A	B	A	B
25Hz	453.3	495.2	476.1	623.4	553.6	613.4	745.8	541.1	-	601.2	489.2	470.5	583.0	704.8
10Hz	305.5	386.1	338.1	445.8	423.3	467.2	521.4	361.4	-	408.6	338.3	326.0	411.4	506.6
5Hz	245.8	324.4	277.0	365.0	343.6	376.5	408.2	286.6	-	332.4	270.0	260.5	332.2	408.6
1Hz	139.9	206.6	182.7	241.1	214.3	232.4	249.5	181.8	-	215.2	170.7	163.2	212.3	264.4
0.1Hz	60.7	100.0	78.2	111.3	85.6	98.0	119.4	90.6	-	104.0	75.1	70.5	102.6	114.5

B.38 Mix Number 1 Results Summary

- Grading: "As-Is"
- Asphalt Content: 2.5 %
- Moisture Content: 6.05 %

Bulk Density

- Marshall compacted specimens B_D: 1949.7 kg/m^3
- Proctor compacted specimens B_D: 1781.6 kg/m^3
- gyratory compacted specimens B_D: 2083.5 kg/m^3

Indirect Tensile Strength

- ITS_{wet}: 117.5 kPa
- ITS_{dry}: 150.5 kPa
- TSR: 78.1 %

Resilient Modulus

Table B-17 Resilient modulus of mix 1 at each test temperatures

Temperature	-14°C	-4°C	6°C	25°C	42°C
Resilient Modulus (MPa)	1950.2	1781.1	1284.5	568.5	333.8

An approximate straight line relationship can be observed by plotting resilient modulus versus test temperature, as shown in Figure B-25.

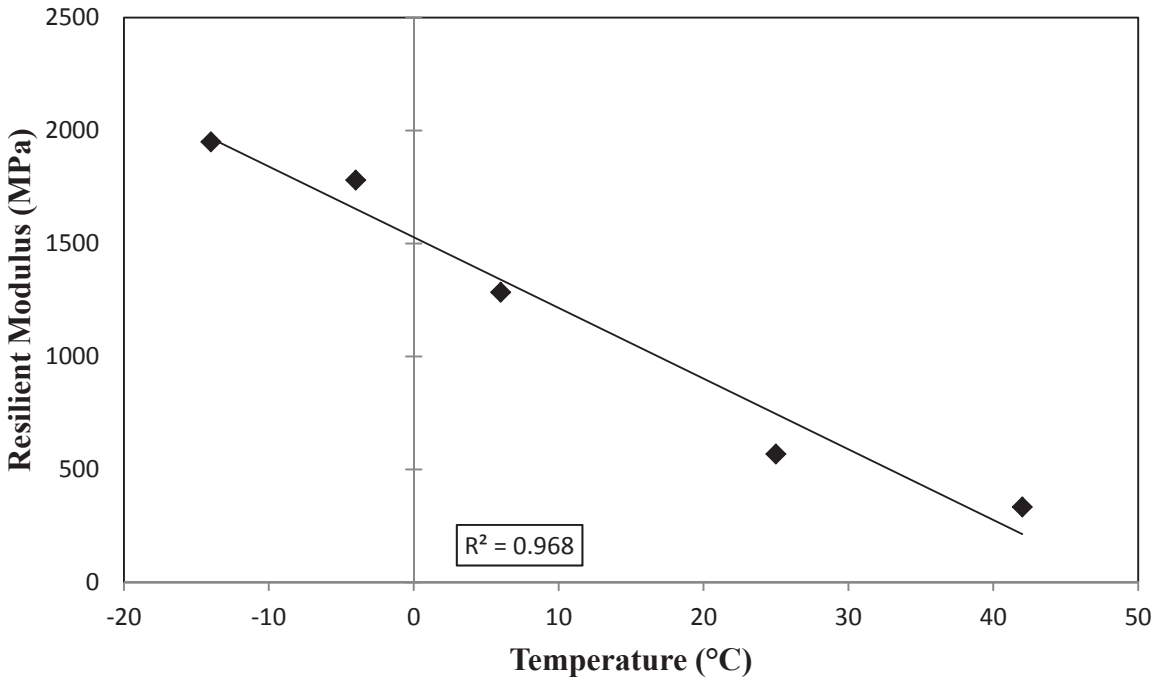

Figure B-25 Mix number 1 resilient modulus versus test temperature

Dynamic Modulus

Table B-18 Dynamic modulus of mix 1 at each test temperature and frequency

	-10°C	6°C	22°C	41°C
Frequency	**Dynamic modulus (MPa)**			
25 Hz	2332.5	1692.1	1111.8	474.3
10 Hz	2070.0	1362.2	847.3	345.8
5 Hz	1923.4	1186.3	704.6	285.1
1 Hz	1615.8	898.8	487.5	173.3
0.1 Hz	1210.9	571.6	266.1	80.4

With this modulus data, an analysis was done to develop the master curve at a reference temperature of 21.1°C (70°F). The test data was plotted and shifted to form a smooth curve, shown in Figure B-26.

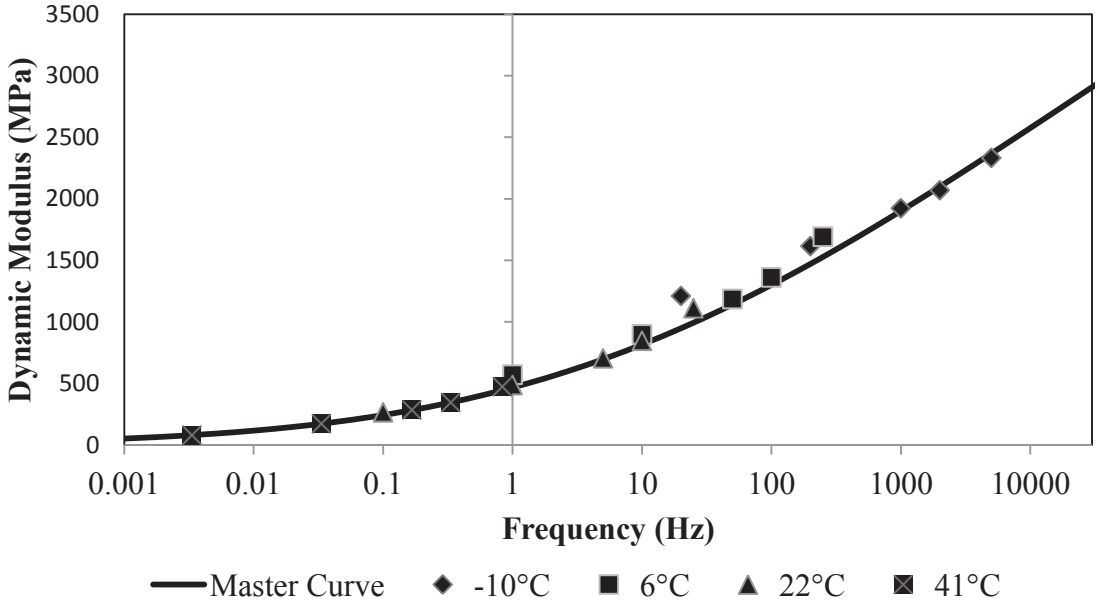

Figure B-26 Mix number 1 dynamic modulus master curve at 21.1°C reference temperature

The sigmoidal function developed to describe the master curve is given in Equation B.1.

$$\log(|E^*|) = -1.2167 + \frac{5.0683}{1+e^{-1.1896+0.2904(\log \omega_r)}} \quad \textbf{[B.1]}$$

where:

$\|E^*\|$	= dynamic modulus	(MPa)
ω_r	= reduced frequency	(Hz)

The shift factor to describe the temperature dependency of the mix is given in Equation B.2.

$$\log a(T) = -2.051 * 10^{-5} * T^2 + 0.0376 * T - 2.7360 \quad \textbf{[B.2]}$$

where:

a(T) = shift factor, as a function of temperature
T = temperature of interest (°F)

The sigmoidal function given in Equation B.1, and the shape factor equation given in Equation B.2 resulted in a log error of the sum of squares equal to 0.0363, showing that there was good correlation between the test data and the derived functions.

Rutting Test

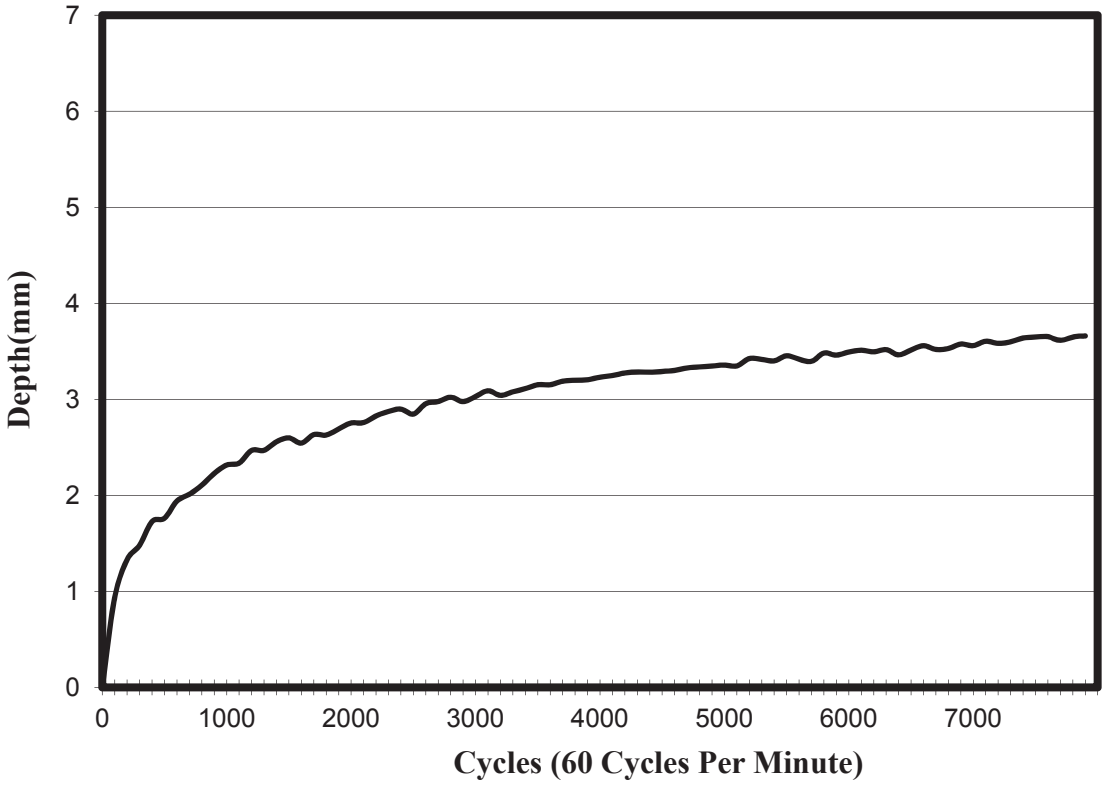

Figure B-27 Mix 1 average rut depth per load cycle

Figure B-28 Mix 1, Sample 1 rutted sample

Figure B-29 Mix 1, Sample 2 rutted sample

B.39 Mix Number 2 Results Summary

- Grading: "Improved"
- Asphalt Content: 2.5 %
- Moisture Content: 5.23 %

Bulk Density

- Marshall compacted specimens B_D: 2007.3 kg/m^3
- Proctor compacted specimens B_D: 1751.3 kg/m^3
- gyratory compacted specimens B_D: 2100.7 kg/m^3

Indirect Tensile Strength

- ITS_{wet}: 190.0 kPa
- ITS_{dry}: 263.8 kPa
- TSR: 72.0 %

Resilient Modulus

Table B-19 Resilient modulus of mix 2 at each test temperature

Temperature	-14°C	-4°C	6°C	25°C	42°C
Resilient Modulus (MPa)	2664.4	1992.3	1858.0	776.9	335.9

An approximate straight line relationship can be observed by plotting resilient modulus versus test temperature, as shown in Figure B-30.

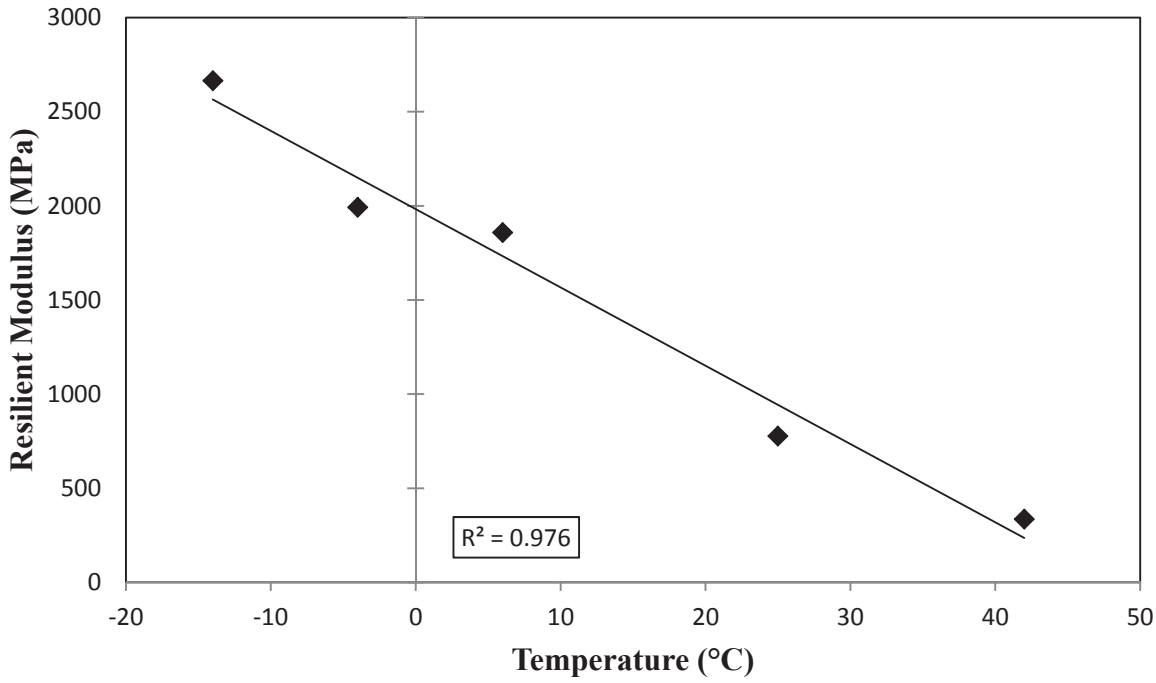

Figure B-30 Mix number 2 resilient modulus versus test temperature

Dynamic Modulus

Table B-20 Dynamic modulus of mix 2 at each test temperature and frequency

	-10°C	**6°C**	**22°C**	**41°C**
Frequency	**Dynamic modulus (MPa)**			
25 Hz	2512.8	1827.3	1005.0	549.8
10 Hz	2089.8	1196.4	761.5	392.0
5 Hz	2000.7	996.2	759.7	486.7
1 Hz	1692.8	759.7	410.5	211.9
0.1 Hz	1185.4	486.7	220.1	94.8

With this modulus data, an analysis was done to develop the master curve at a reference temperature of 21.1°C (70°F). The test data was plotted and shifted to form a smooth curve, shown in Figure B-31.

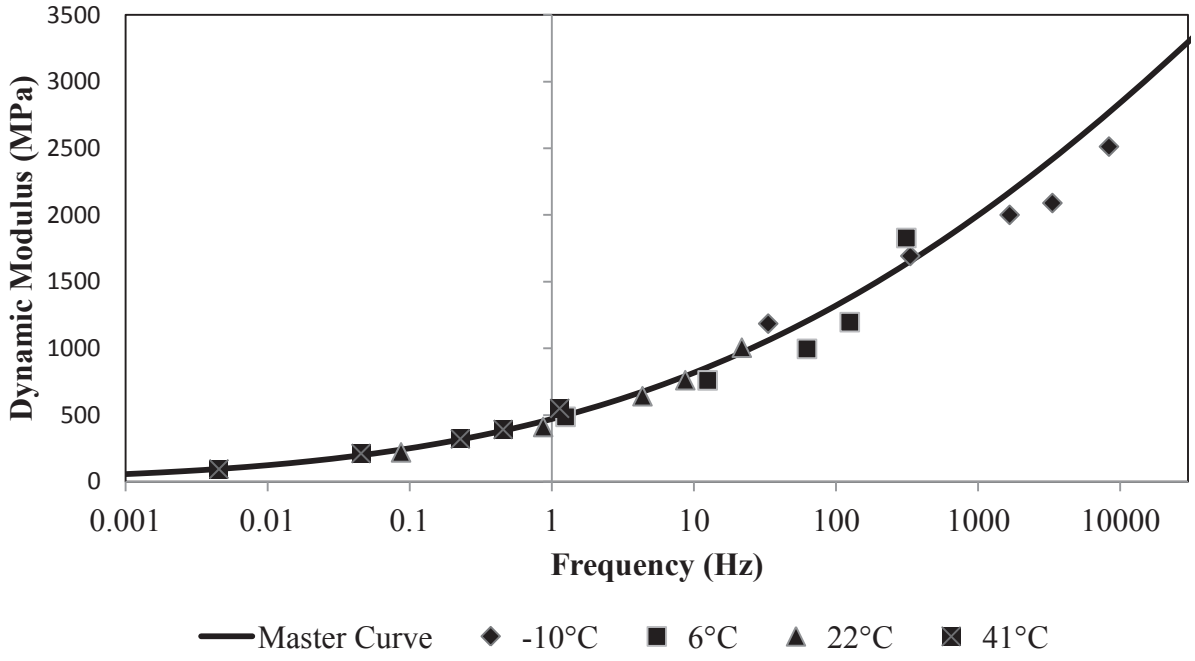

Figure B-31 Mix number 2 dynamic modulus master curve at 21.1°C reference temperature

The sigmoidal function developed to describe the master curve is given in Equation B.3.

$$\log(|E^*|) = -4.3870 + \frac{8.6033}{1+e^{-1.5196+0.2026(\log \omega_r)}} \quad \textbf{[B.3]}$$

where:

$\|E^*\|$	= dynamic modulus	(MPa)
ω_r	= reduced frequency	(Hz)

The shift factor to describe the temperature dependency of the mix is given in Equation B.4.

$$\log a(T) = -3.227 * 10^{-5} * T^2 + 0.0432 * T - 2.8636 \quad \textbf{[B.4]}$$

where:

a(T) = shift factor, as a function of temperature
T = temperature of interest (°F)

The sigmoidal function given in Equation B.3, and the shape factor equation given in Equation B.4 resulted in a log error of the sum of squares equal to 0.0373, showing that there was good correlation between the test data and the derived functions.

Rutting Test

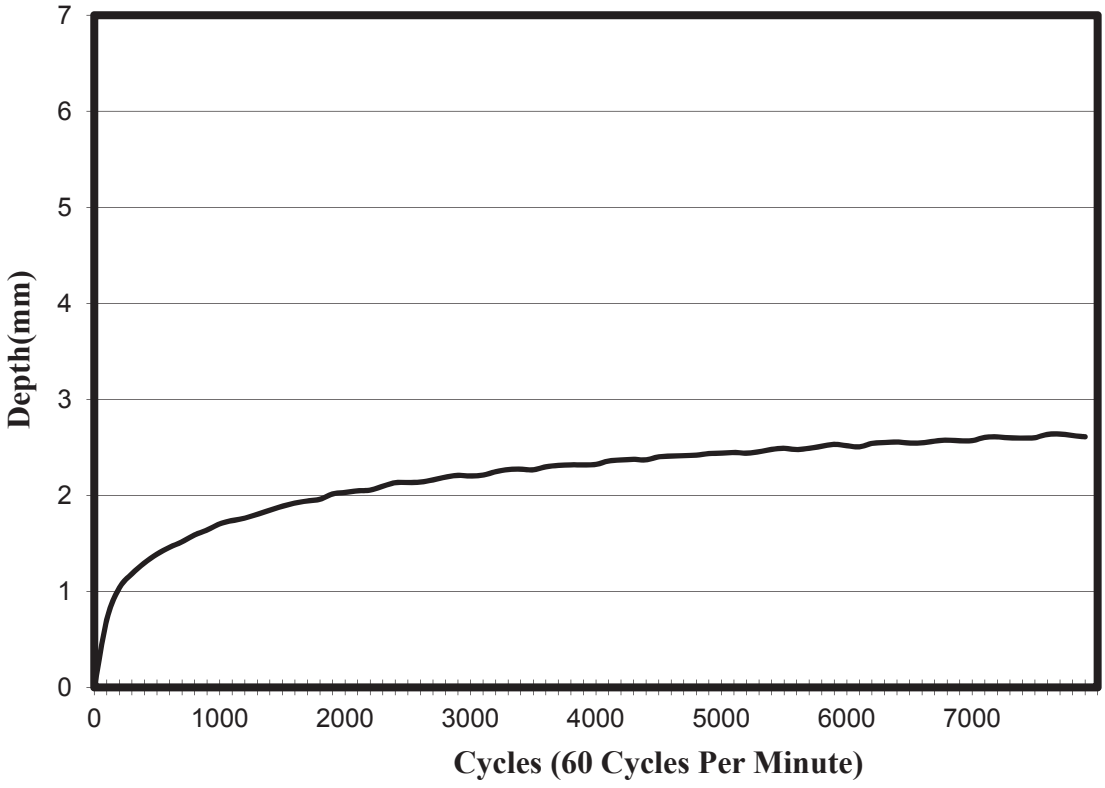

Figure B-32 Mix 2 average rut depth per load cycle

Figure B-33 Mix 2, Sample 1 rutted sample

Figure B-34 Mix 2, Sample 2 rutted sample

B.40 Mix Number 3 Results Summary

- Grading: "Improved"
- Asphalt Content: 3.5 %
- Moisture Content: 3.00 %

Bulk Density

- Marshall compacted specimens B_D: 2025.4 kg/m^3
- Proctor compacted specimens B_D: 1766.4 kg/m^3
- gyratory compacted specimens B_D: 2095.9 kg/m^3

Indirect Tensile Strength

- ITS_{wet}: 157.3 kPa
- ITS_{dry}: 199.9 kPa
- TSR: 78.7 %

Resilient Modulus

Table B-21 Resilient modulus of mix 3 at each test temperature

Temperature	-14°C	-4°C	6°C	25°C	42°C
Resilient Modulus (MPa)	3066.4	2100.6	1453.7	756.2	227.0

An approximate exponential relationship can be observed by plotting resilient modulus versus test temperature, as shown in Figure B-35.

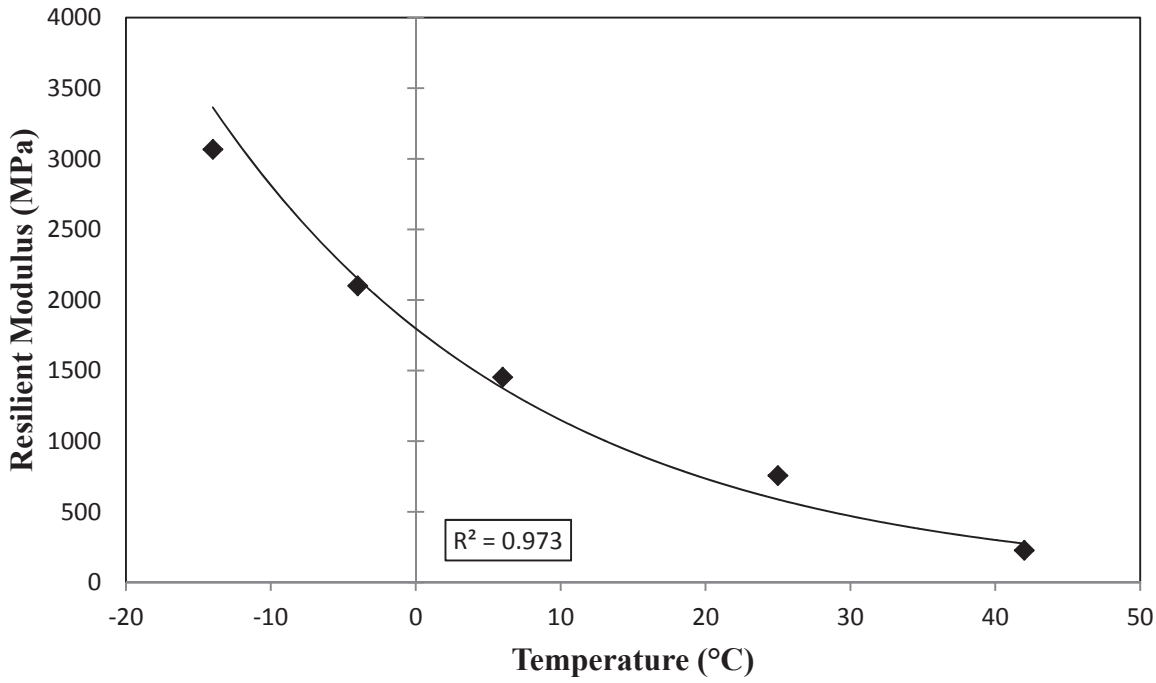

Figure B-35 Mix number 3 resilient modulus versus test temperature

Dynamic Modulus

Table B-22 Dynamic modulus of mix 3 at each test temperature and frequency

	-10°C	**6°C**	**22°C**	**41°C**
Frequency	**Dynamic modulus (MPa)**			
25 Hz	2445.2	1698.2	1177.4	583.5
10 Hz	2100.1	1391.0	1013.5	445.3
5 Hz	1907.3	1193.3	845.5	360.1
1 Hz	1585.9	907.7	601.7	223.4
0.1 Hz	1157.6	607.4	320.4	91.8

With this modulus data, an analysis was done to develop the master curve at a reference temperature of 21.1°C (70°F). The test data was plotted and shifted to form a smooth curve, shown in Figure B-36.

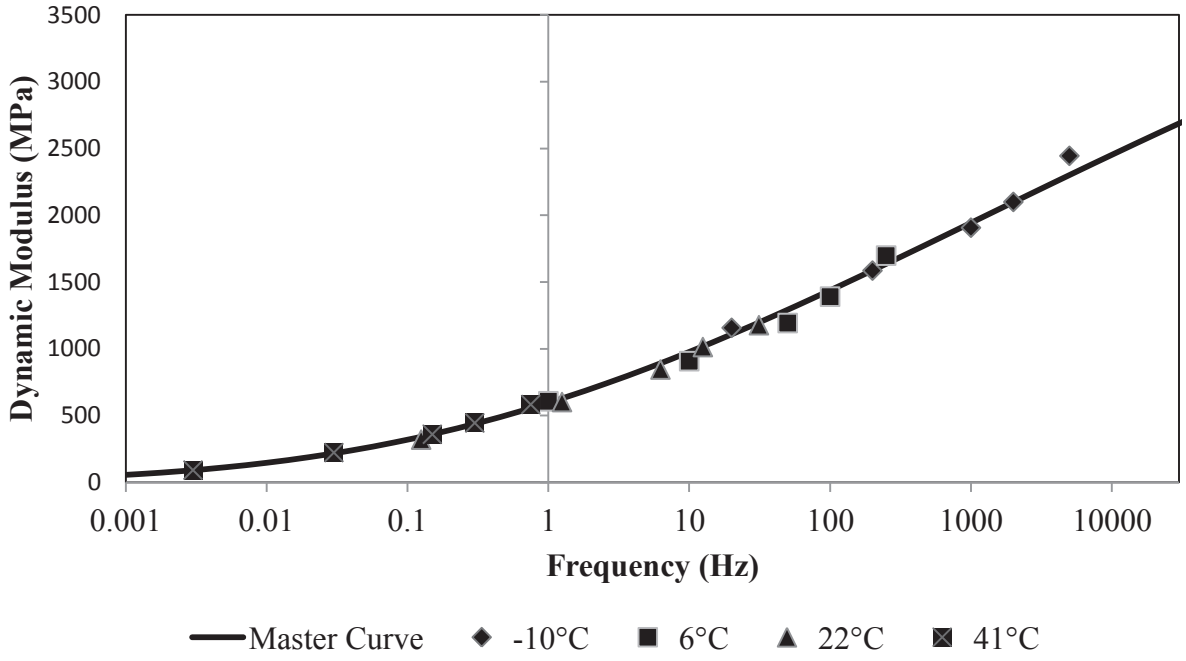

Figure B-36 Mix number 3 dynamic modulus master curve at 21.1°C reference temperature

The sigmoidal function developed to describe the master curve is given in Equation B.5.

$$\log(|E^*|) = -8.6042 + \frac{12.3226}{1+e^{-2.4908+0.2764(\log \omega_r)}} \quad \textbf{[B.5]}$$

where:

$\|E^*\|$	= dynamic modulus	(MPa)
ω_r	= reduced frequency	(Hz)

The shift factor to describe the temperature dependency of the mix is given in Equation B.6.

$$\log a(T) = -1.390 * 10^{-5} * T^2 + 0.0392 * T - 2.8147 \quad \textbf{[B.6]}$$

where:

a(T) = shift factor, as a function of temperature
T = temperature of interest (°F)

The sigmoidal function given in Equation B.5, and the shape factor equation given in Equation 4.6 resulted in a log error of the sum of squares equal to 0.0109, showing that there was good correlation between the test data and the derived functions.

Rutting Test

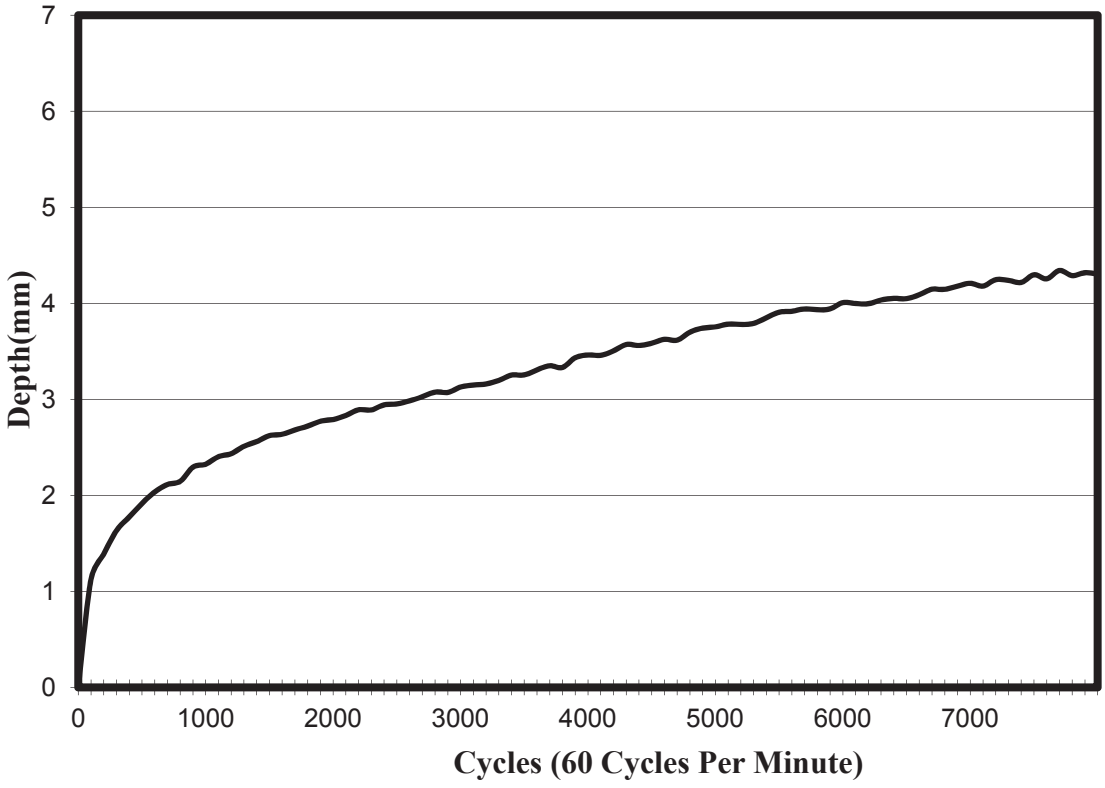

Figure B-37 Mix 3 average rut depth per load cycle

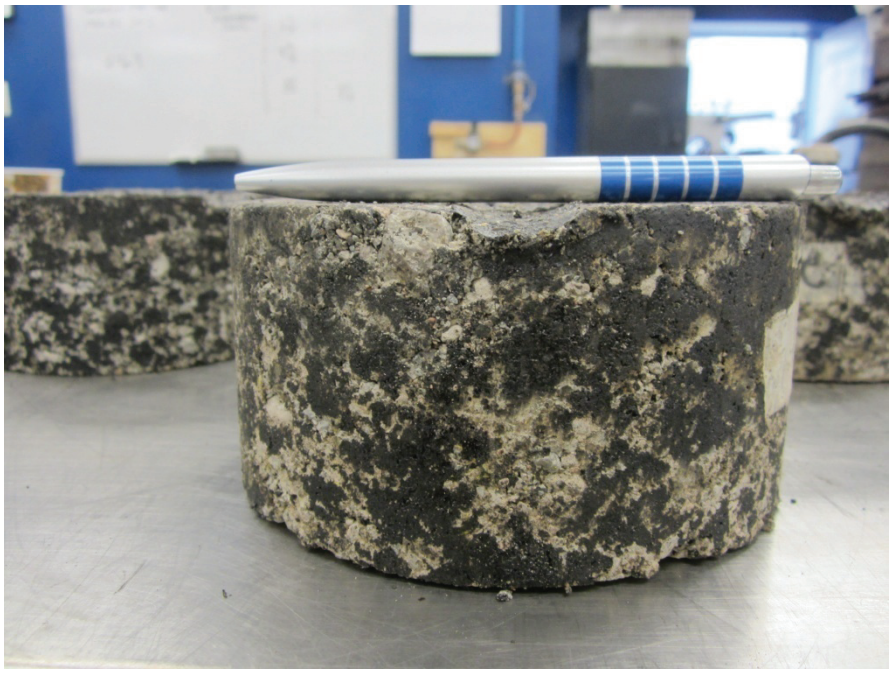

Figure B-38 Mix 3, Sample 1 rutted sample

Figure B-39 Mix 3, Sample 2 rutted sample

B.41 Mix Number 4 Results Summary

- Grading: "Improved"
- Asphalt Content: 3.5 %
- Moisture Content: 5.23 %

Bulk Density

- Marshall compacted specimens B_D: 2036.4 kg/m^3
- Proctor compacted specimens B_D: 1764.1 kg/m^3
- gyratory compacted specimens B_D: 2102.5 kg/m^3

Indirect Tensile Strength

- ITS_{wet}: 236.7 kPa
- ITS_{dry}: 286.8 kPa
- TSR: 82.5 %

Resilient Modulus

Table B-23 Resilient modulus of mix 4 at each test temperature

Temperature	-14°C	-4°C	6°C	25°C	42°C
Resilient Modulus (MPa)	3267.7	2707.3	2185.0	1029.5	411.6

An approximate straight line relationship can be observed by plotting resilient modulus versus test temperature, as shown in Figure B-40.

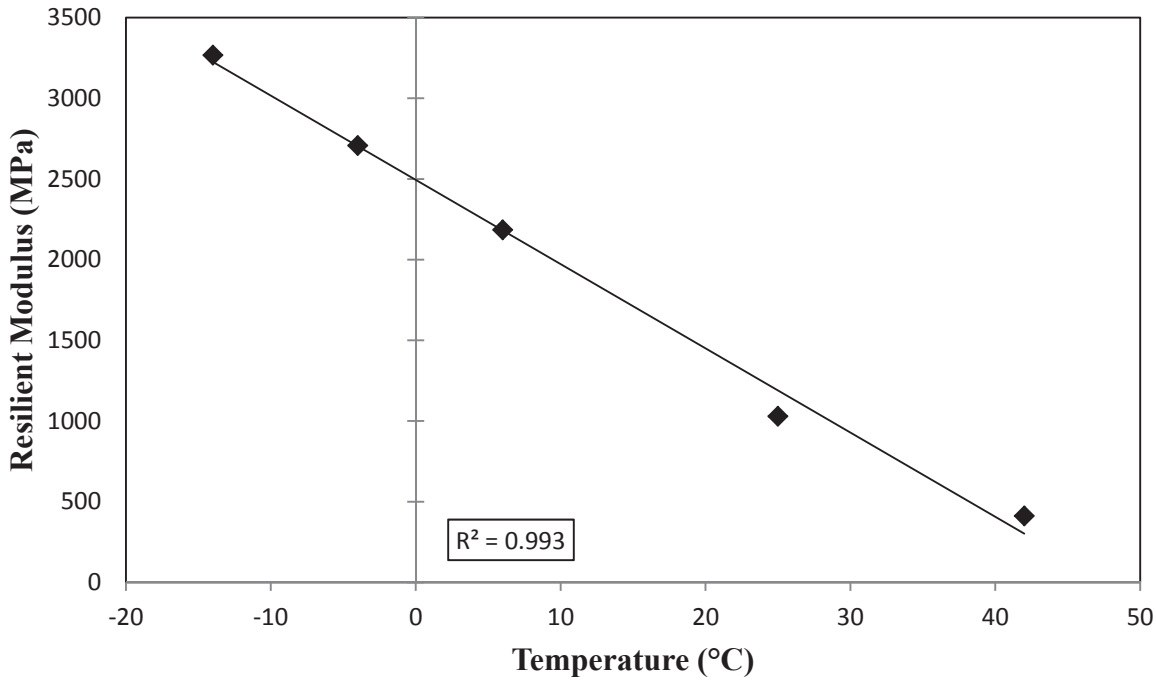

Figure B-40 Mix number 4 resilient modulus versus test temperature

Dynamic Modulus

Table B-24 Dynamic modulus of mix 4 at each test temperature and frequency

	-10°C	**6°C**	**22°C**	**41°C**
Frequency	**Dynamic modulus (MPa)**			
25 Hz	2694.3	1550.0	1033.8	549.8
10 Hz	2262.4	1252.4	757.5	441.4
5 Hz	2029.2	1071.6	599.6	347.4
1 Hz	1634.1	834.0	384.6	215.7
0.1 Hz	1207.6	542.8	199.1	105.0

With this modulus data, an analysis was done to develop the master curve at a reference temperature of 21.1°C (70°F). The test data was plotted and shifted to form a smooth curve, shown in Figure B-41.

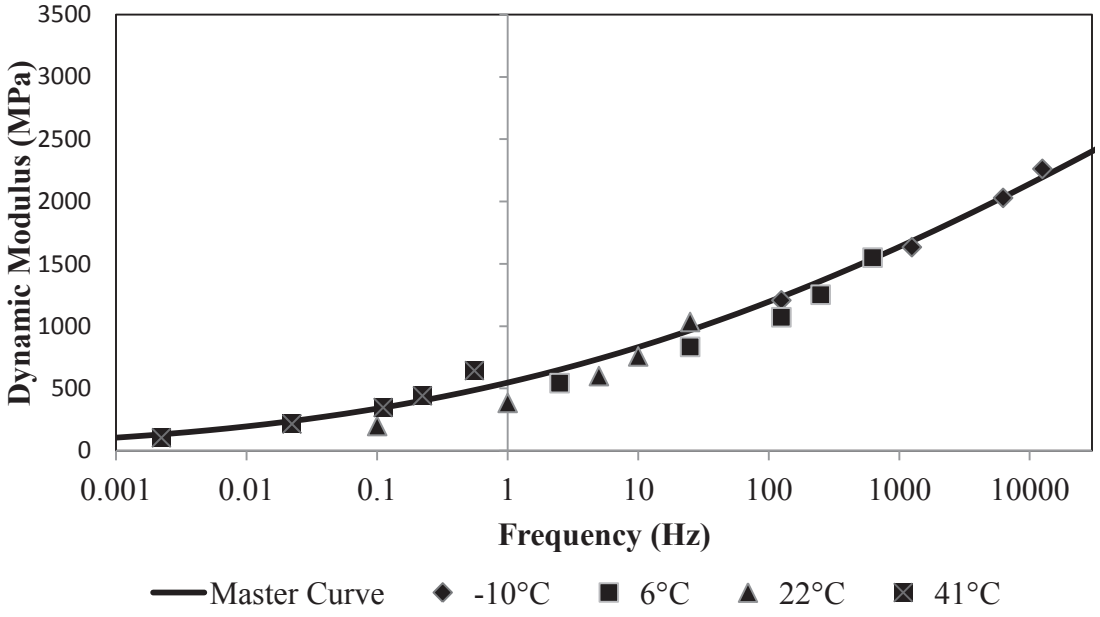

Figure B-41 Mix number 4 dynamic modulus master curve at 21.1°C reference temperature

The sigmoidal function developed to describe the master curve is given in Equation B.7.

$$\log(|E^*|) = -8.4279 + \frac{12.4220}{1+e^{-2.1846+0.1726(\log \omega_r)}} \quad \textbf{[B.7]}$$

where:

$\|E^*\|$	= dynamic modulus	(MPa)
ω_r	= reduced frequency	(Hz)

The shift factor to describe the temperature dependency of the mix is given in Equation B.8.

$$\log a(T) = -1.001 * 10^{-4} * T^2 + 0.0636 * T - 3.9586 \quad \textbf{[B.8]}$$

where:

a(T) = shift factor, as a function of temperature
T = temperature of interest (°F)

The sigmoidal function given in Equation B.7, and the shape factor equation given in Equation B.8 resulted in a log error of the sum of squares equal to 0.1198, showing that there was good correlation between the test data and the derived functions.

Rutting Test

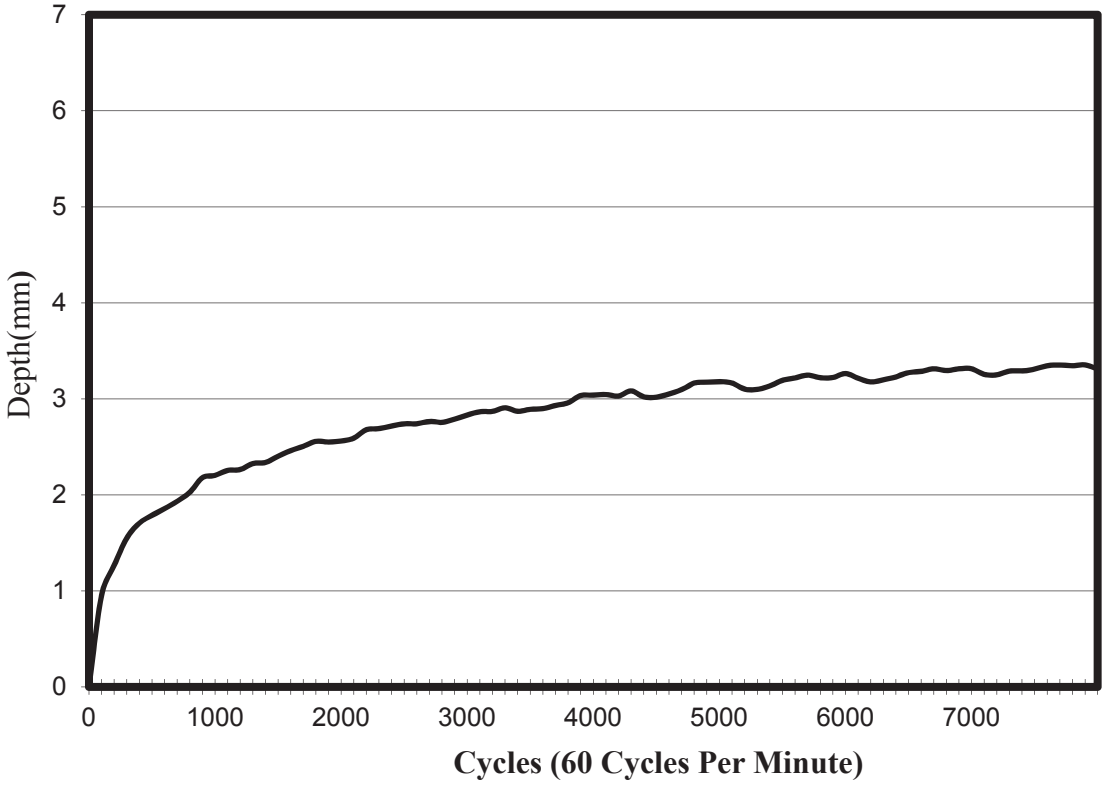

Figure B-42 Mix 4 average rut depth per load cycle

Figure B-43 Mix 4, Sample 1 rutted sample

Figure B-44 Mix 4, Sample 2 rutted sample

B.42 Mix Number 5 Results Summary

- Grading: "Improved"
- Asphalt Content: 3.5 %
- Moisture Content: 6.60 %

Bulk Density

- Marshall compacted specimens B_D: 2031.3 kg/m^3
- Proctor compacted specimens B_D: 1758.1 kg/m^3
- gyratory compacted specimens B_D: 2106.9 kg/m^3

Indirect Tensile Strength

- ITS_{wet}: 187.8 kPa
- ITS_{dry}: 245.4 kPa
- TSR: 76.6 %

Resilient Modulus

Table B-25 Resilient modulus of mix 5 at each test temperature

Temperature	-14°C	-4°C	6°C	25°C	42°C
Resilient Modulus (MPa)	3494.6	2319.5	1675.9	947.2	388.7

An approximate exponential relationship can be observed by plotting resilient modulus versus test temperature, as shown in Figure B-45.

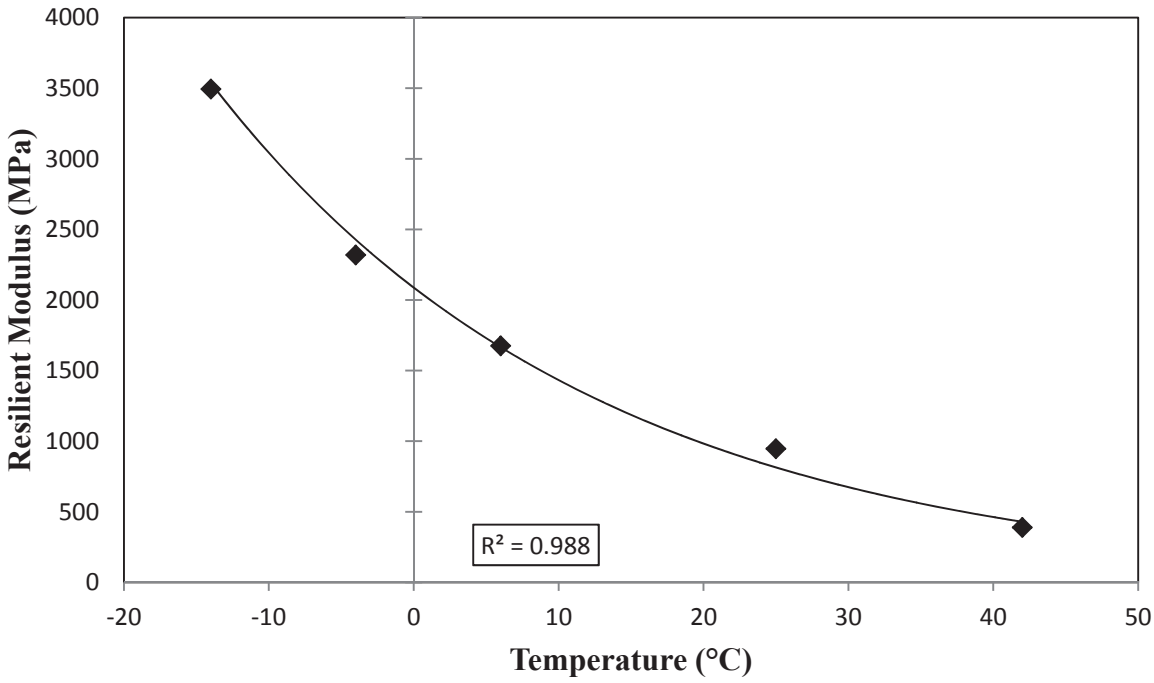

Figure B-45 Mix number 5 resilient modulus versus test temperature

Dynamic Modulus

Table B-26 Dynamic modulus of mix 5 at each test temperature and frequency

	-10°C	**6°C**	**22°C**	**41°C**
Frequency	**Dynamic modulus (MPa)**			
25 Hz	2481.9	1438.0	935.1	601.2
10 Hz	2002.9	1122.6	679.6	408.6
5 Hz	1753.6	973.4	525.6	332.4
1 Hz	1397.2	753.1	343.6	215.2
0.1 Hz	890.2	500.8	182.8	104.0

With this modulus data, an analysis was done to develop the master curve at a reference temperature of 21.1°C (70°F). The test data was plotted and shifted to form a smooth curve, shown in Figure B-46.

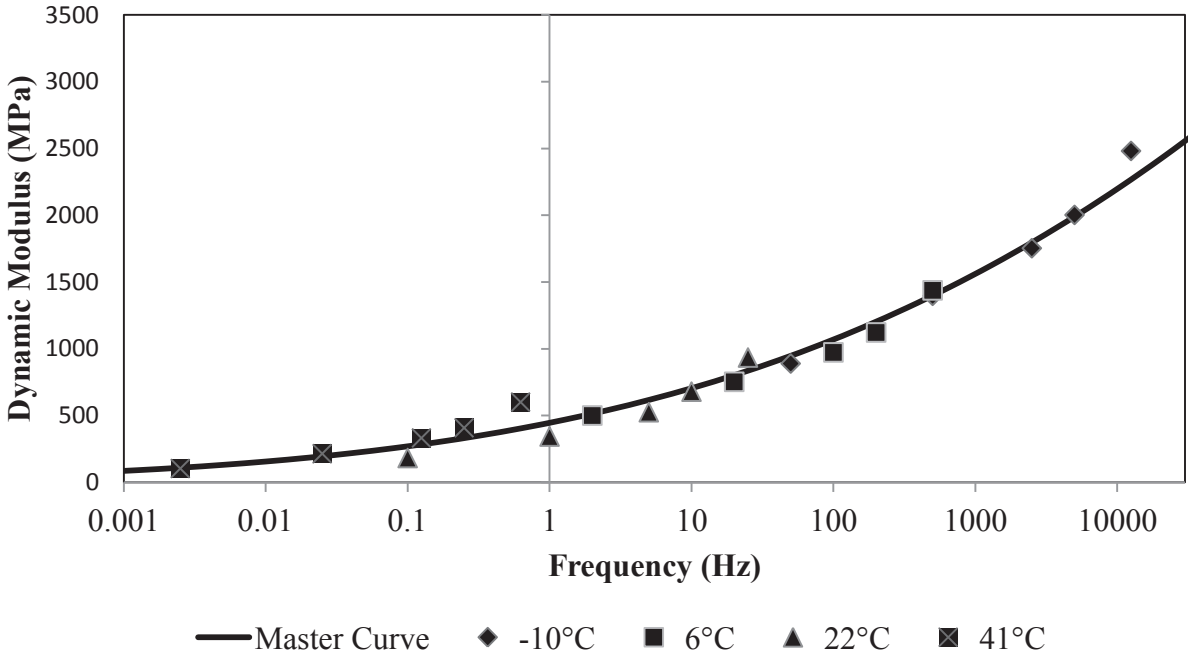

Figure B-46 Mix number 5 dynamic modulus master curve at 21.1°C reference temperature

The sigmoidal function developed to describe the master curve is given in Equation B.9.

$$\log(|E^*|) = -8.6974 + \frac{13.2657}{1+e^{-1.7779+0.1266(\log \omega_r)}} \quad \textbf{[B.9]}$$

where:

$\|E^*\|$	= dynamic modulus	(MPa)
ω_r	= reduced frequency	(Hz)

The shift factor to describe the temperature dependency of the mix is given in Equation B.10.

$$\log a(T) = -3.791 * 10^{-5} * T^2 + 0.0515 * T - 3.4171 \quad \textbf{[B.10]}$$

where:

a(T) = shift factor, as a function of temperature
T = temperature of interest (°F)

The sigmoidal function given in Equation B.9, and the shape factor equation given in Equation B.10 resulted in a log error of the sum of squares equal to 0.0906, showing that there was good correlation between the test data and the derived functions.

Rutting Test

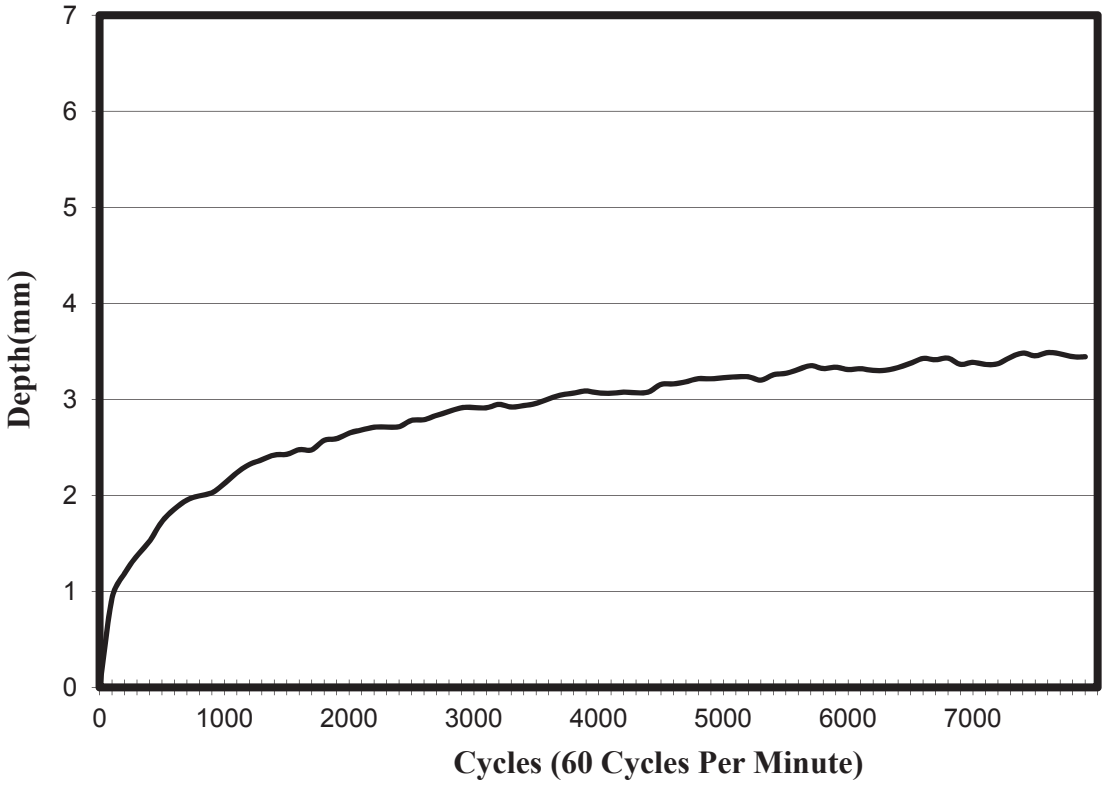

Figure B-47 Mix 5 average rut depth per load cycle

Figure B-48 Mix 5, Sample 1 rutted sample

Figure B-49 Mix 5, Sample 2 rutted sample

B.43 Mix Number 6 Results Summary

- Grading: "Improved"
- Asphalt Content: 4.5 %
- Moisture Content: 5.23 %

Bulk Density

- Marshall compacted specimens B_D: 2017.2 kg/m^3
- Proctor compacted specimens B_D: 1755.7 kg/m^3
- gyratory compacted specimens B_D: 2098.4 kg/m^3

Indirect Tensile Strength

- ITS_{wet}: 234.1 kPa
- ITS_{dry}: 257.0 kPa
- TSR: 91.1 %

Resilient Modulus

Table B-27 Resilient modulus of mix 6 at each test temperature

Temperature	-14°C	-4°C	6°C	25°C	42°C
Resilient Modulus (MPa)	3637.6	2210.0	1987.4	956.9	279.9

An approximate exponential relationship can be observed by plotting resilient modulus versus test temperature, as shown in Figure B-50.

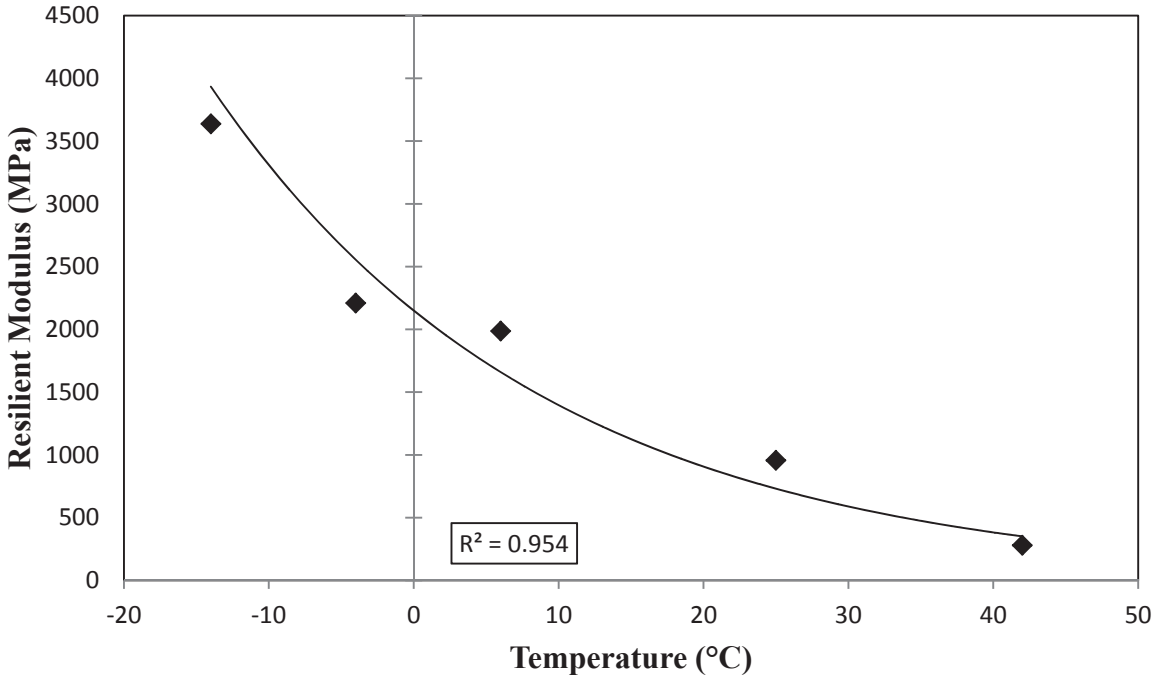

Figure 4-50 Mix number 6 resilient modulus versus test temperature

Dynamic Modulus

Table B-28 Dynamic modulus of mix 6 at each test temperature and frequency

	-10°C	6°C	22°C	41°C
Frequency	**Dynamic modulus (MPa)**			
25 Hz	3278.0	1855.0	911.2	479.9
10 Hz	2859.9	1392.1	671.7	332.2
5 Hz	2679.2	1231.9	528.6	265.3
1 Hz	2291.4	959.8	345.2	167.0
0.1 Hz	1771.0	602.3	166.6	72.8

With this modulus data, an analysis was done to develop the master curve at a reference temperature of 21.1°C (70°F). The test data was plotted and shifted to form a smooth curve, shown in Figure B-51.

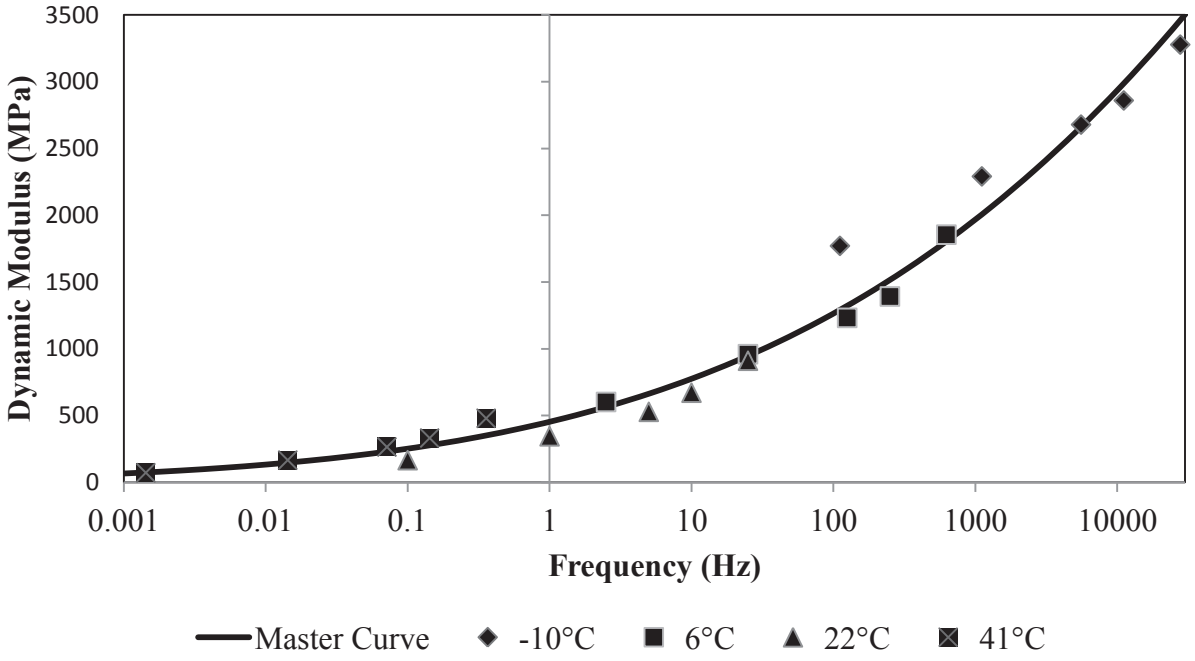

Figure B-51 Mix number 6 dynamic modulus master curve at 21.1°C reference temperature

The sigmoidal function developed to describe the master curve is given in Equation B.11.

$$\log(|E^*|) = -8.5497 + \frac{13.4030}{1+e^{-1.6301+0.1326(\log \omega_r)}} \quad \textbf{[B.11]}$$

where:

$\|E^*\|$	= dynamic modulus	(MPa)
ω_r	= reduced frequency	(Hz)

The shift factor to describe the temperature dependency of the mix is given in Equation B.12.

$$\log a(T) = -3.194 * 10^{-5} * T^2 + 0.0568 * T - 3.8174 \quad \textbf{[B.12]}$$

where:

a(T) = shift factor, as a function of temperature
T = temperature of interest (°F)

The sigmoidal function given in Equation B.11, and the shape factor equation given in Equation B.12 resulted in a log error of the sum of squares equal to 0.1001, showing that there was good correlation between the test data and the derived functions.

Rutting Test

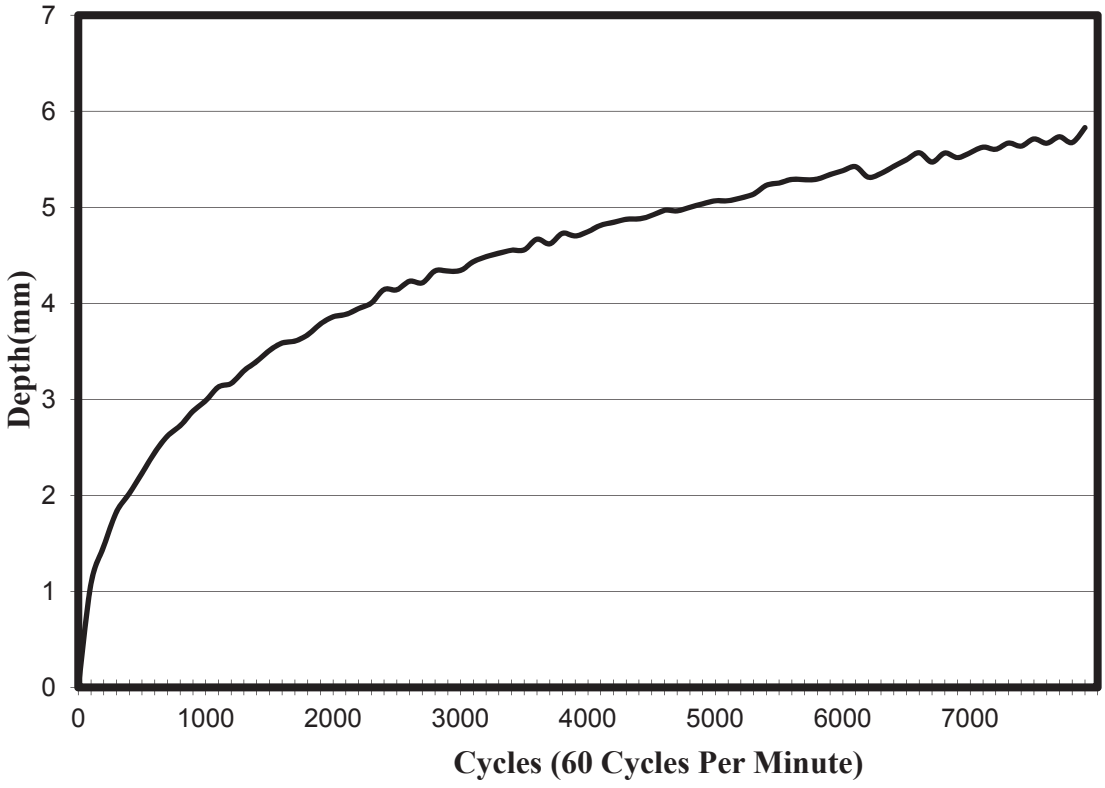

Figure B-52 Mix 6 average rut depth per load cycle

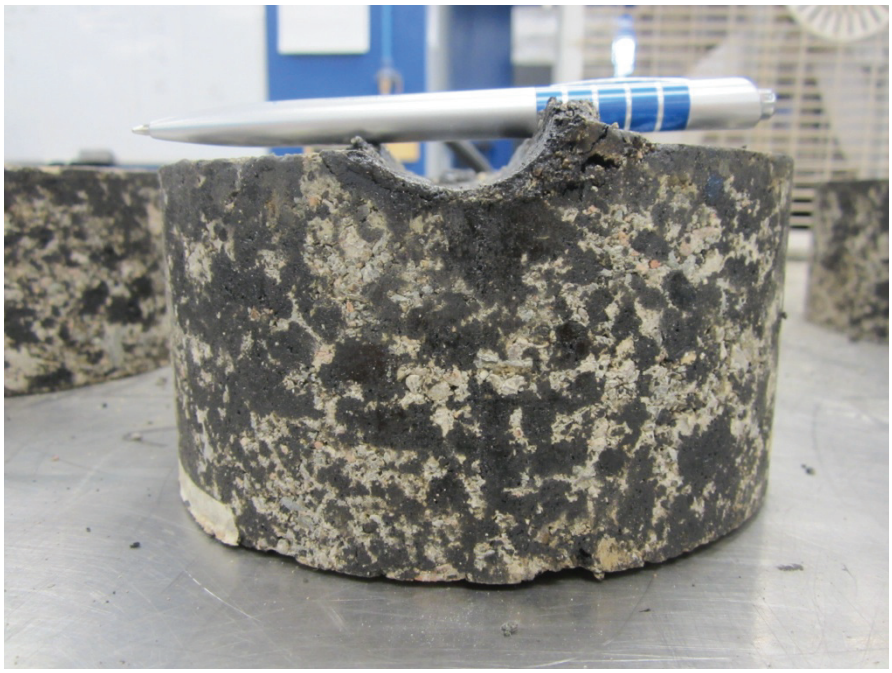

Figure B-53 Mix 6, Sample 1 rutted sample

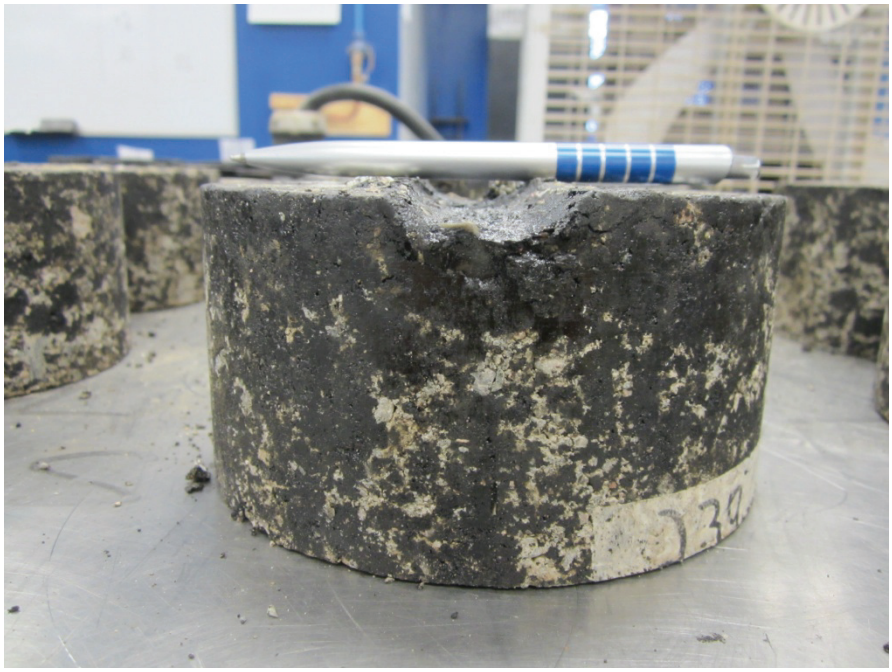

Figure B-54 Mix 6, Sample 2 rutted sample

B.44 Mix Number 7 Results Summary

- Grading: "Optimum"
- Asphalt Content: 3.0 %
- Moisture Content: 5.35 %

Bulk Density

- Marshall compacted specimens B_D: 2006.9 kg/m^3
- Proctor compacted specimens B_D: 1789.8 kg/m^3
- gyratory compacted specimens B_D: 2104.7 kg/m^3

Indirect Tensile Strength

- ITS_{wet}: 221.9 kPa
- ITS_{dry}: 225.0 kPa
- TSR: 98.6 %

Resilient Modulus

Table B-29 Resilient modulus of mix 7 at each test temperature

Temperature	-14°C	-4°C	6°C	25°C	42°C
Resilient Modulus (MPa)	2841.9	2084.2	1501.3	1065.4	558.3

An approximate exponential relationship can be observed by plotting resilient modulus versus test temperature, as shown in Figure B-55.

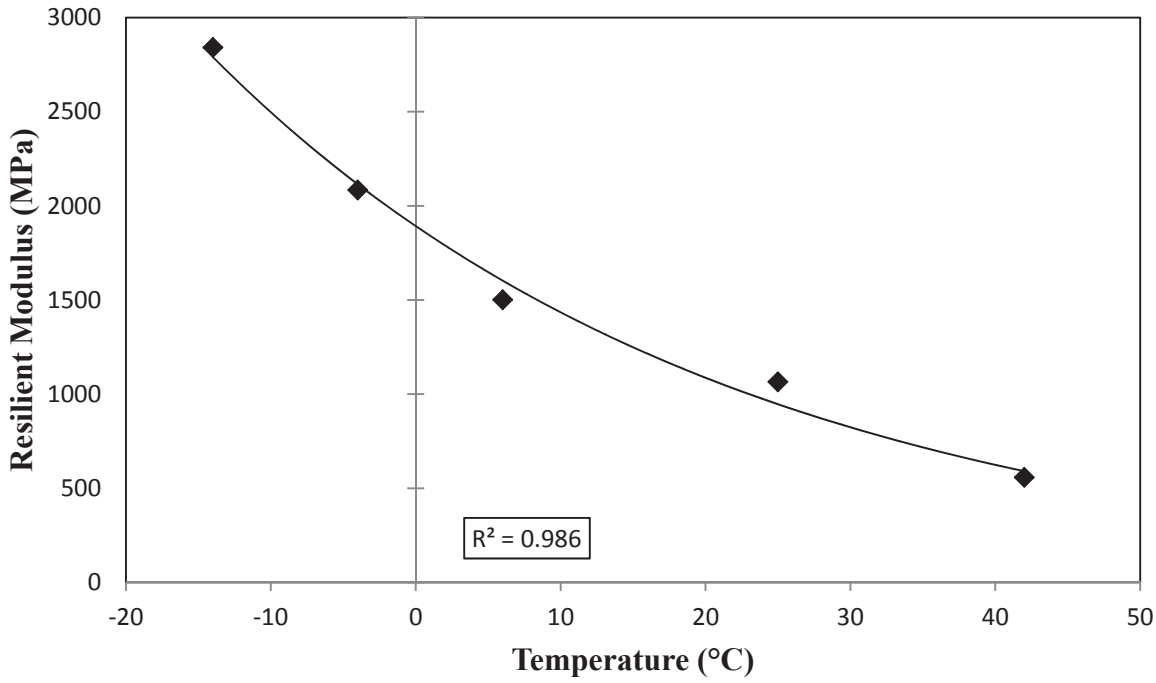

Figure B-55 Mix number 7 resilient modulus versus test temperature

Dynamic Modulus

Table B-30 Dynamic modulus of mix 7 at each test temperature and frequency

	-10°C	**6°C**	**22°C**	**41°C**
Frequency	**Dynamic modulus (MPa)**			
25 Hz	3170.6	1964.3	1241.8	643.9
10 Hz	2766.4	1625.7	981.0	459.0
5 Hz	2546.8	1456.8	832.4	370.4
1 Hz	2188.6	1157.4	598.4	238.4
0.1 Hz	1562.7	698.9	374.2	108.6

With this modulus data, an analysis was done to develop the master curve at a reference temperature of 21.1°C (70°F). The test data was plotted and shifted to form a smooth curve, shown in Figure B-56.

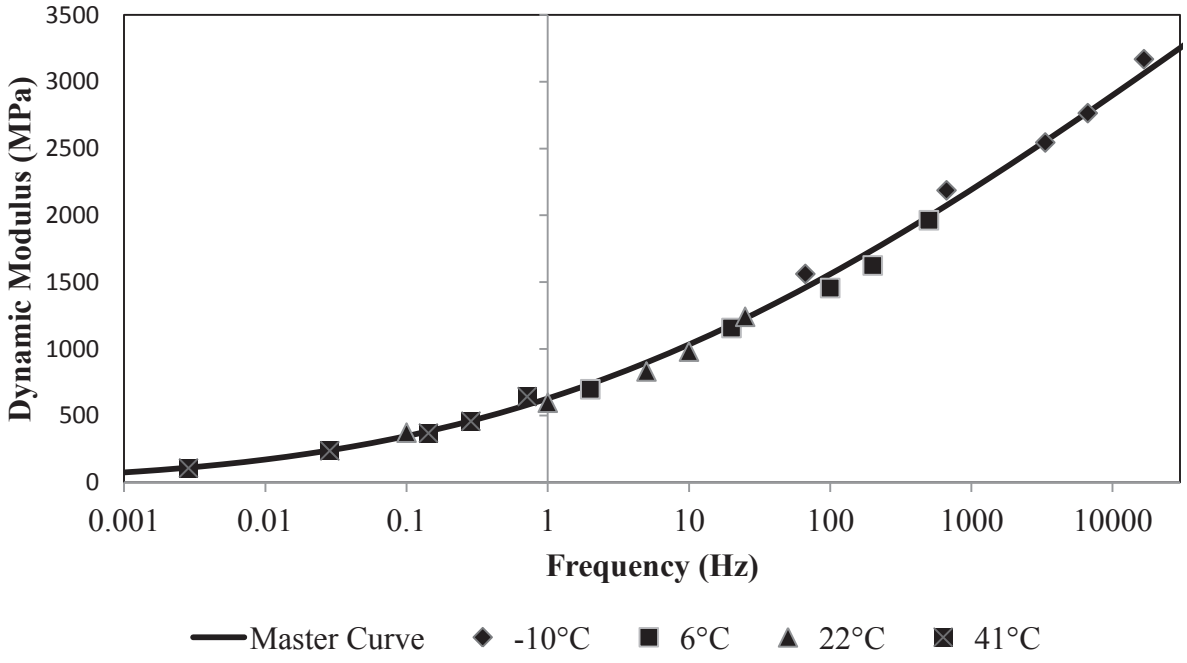

Figure B-56 Mix number 7 dynamic modulus master curve at 21.1°C reference temperature

The sigmoidal function developed to describe the master curve is given in Equation B.13.

$$\log(|E^*|) = -9.0312 + \frac{13.0172}{1+e^{-2.2996+0.2183(\log \omega_r)}} \quad \textbf{[B.13]}$$

where:

$\|E^*\|$	= dynamic modulus	(MPa)
ω_r	= reduced frequency	(Hz)

The shift factor to describe the temperature dependency of the mix is given in Equation B.14.

$$\log a(T) = -8.002 * 10^{-5} * T^2 + 0.0571 * T - 3.6046 \quad \textbf{[B.14]}$$

where:

a(T) = shift factor, as a function of temperature
T = temperature of interest (°F)

The sigmoidal function given in Equation B.13, and the shape factor Equation given in Equation B.14 resulted in a log error of the sum of squares equal to 0.0103, showing that there was good correlation between the test data and the derived functions.

Rutting Test

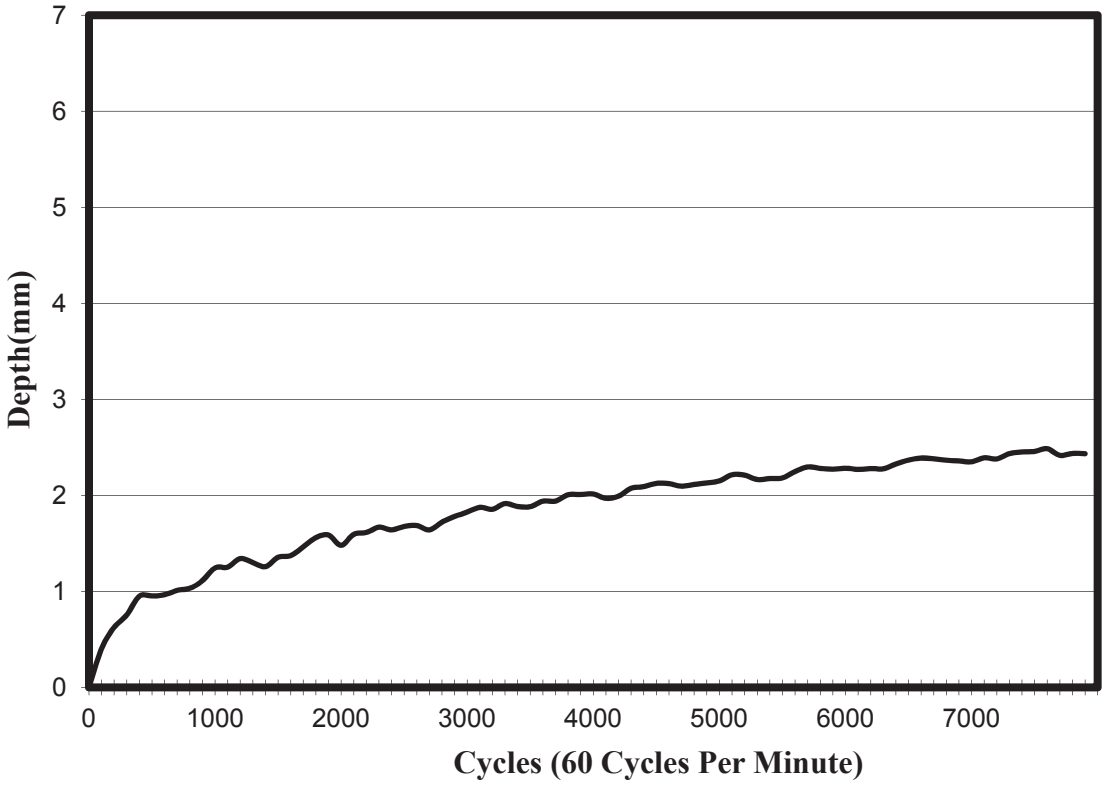

Figure B-57 Mix 7 average rut depth per load cycle

Figure B-58 Mix 7, Sample 1 rutted sample

Figure B-59 Mix 7, Sample 2 rutted sample

Appendix C: AASHTO Structural Design

AASHTO Structural Coefficient Method

C.1 Mix 1 AASHTO Structural Design

a_1:	0.44			E1	430000	psi
a_2:	0.09	m_2	1	E2	82454.0	psi
				E3	5500	psi

ΔPSI: 2.2

Asphalt

ESAL: 100000 ΔPSI: 2.2

Z_R: -1.645 M_{R2}: 82454 psi

S_0: 0.45

SN_1: 0 .9

Solve Equation 2.14 by setting left side equal to right side and using Solver analysis to set that cell equal to 0 by changing SN

LHS: 5.000 RHS: 5.000

LHS - RHS = 0.0

D1 > SN_1/ a_1

D1> 2.04 Use D_1 = 4.7 inches

FDR Base

ESAL: 100000 ΔPSI: 2.7

Z_R: -1.645 M_{R3}: 5500 psi

S_0: 0.45

SN_2: 2.8

Solve Equation 2.14 by setting left side equal to right side and using Solver analysis to set that cell equal to 0 by changing SN_2 and D_1, with the constraint that D_2 = 8 inches and D_1 be greater than the minimum required D_1 determined in previous calculations.

LHS: 5.000 RHS: 4.999

LHS - RHS = 0

D2 > $(SN_2 - a_1D_1)/ a_2m_2$

D2> 8.0 Use D_2 = 8.0 inches

C.2 Mix 2 AASHTO Structural Design

a_1:	0.44			E1	430000	psi
a_2:	0.15	m_2	1	E2	112679.8	psi
				E3	5500	psi
ΔPSI:	2.2					

Asphalt

ESAL:	100000	ΔPSI:	2.2	
Z_R:	-1.645	M_{R2}:	112680	psi
S_0:	0.45			

SN_1:	0.8

Solve Equation 2.14 by setting left side equal to right side and using Solver analysis to set that cell equal to 0 by changing SN

LHS:	5.000	RHS:	5.000
LHS - RHS =	0.0		

D1 > SN_1 / a_1

D1>	1.72	Use D_1 =	3.6	inches

FDR Base

ESAL:	100000	ΔPSI:	2.2	
Z_R:	-1.645	M_{R3}:	5500	psi
S_0:	0.45			

SN_2:	2.8

Solve Equation 2.14 by setting left side equal to right side and using Solver analysis to set that cell equal to 0 by changing SN_2 and D_1, with the constraint that D_2 = 8 inches and D_1 be greater than the minimum required D_1 determined in previous calculations

LHS:	5.000	RHS:	4.999
LHS - RHS =	0		

D2 > $(SN_2 - a_1 D_1) / a_2 m_2$

D2>	8	Use D_2 =	8.0	inches

C.3 Mix 3 AASHTO Structural Design

a_1:	0.44			E1	430000	psi
a_2:	0.14	m_2	1	E2	109677.5	psi
				E3	5500	psi
ΔPSI:	2.2					

Asphalt

ESAL:	100000	ΔPSI:	2.1	
Z_R:	-1.645	M_{R2}:	109678	psi
S_0:	0.45			

SN_1: 0.8

Solve Equation 2.14 by setting left side equal to right side and using Solver analysis to set that cell equal to 0 by changing SN

LHS: 5.000 RHS: 5.000

LHS - RHS = 0.0

D1 > SN_1/ a_1

D1> 1.75 Use D_1 = 3.7 inches

FDR Base

ESAL:	100000	ΔPSI:	2.1	
Z_R:	-1.645	M_{R3}:	5500	psi
S_0:	0.45			

SN_2: 2.8

Solve Equation 2.14 by setting left side equal to right side and using Solver analysis to set that cell equal to 0 by changing SN_2 and D_1, with the constraint that D_2 = 8 inches and D_1 be greater than the minimum required D_1 determined in previous calculations

LHS: 5.000 RHS: 4.999

LHS - RHS = 0

D2 > $(SN_2 - a_1D_1)/ a_2m_2$

D2> 8 Use D_2 = 8.0 inches

C.4 Mix 4 AASHTO Structural Design

a_1:	0.44			E1	430000	psi
a_2:	0.19	m_2	1	E2	149316.4	psi
				E3	5500	psi

ΔPSI: 2.2

Asphalt

ESAL: 100000 ΔPSI: 2.2

Z_R: -1.645 M_{R2}: 149316 psi

S_0: 0.45

SN_1: 0.6

Solve Equation 2.14 by setting left side equal to right side and using Solver analysis to set that cell equal to 0 by changing SN

LHS: 5.000 RHS: 5.000

LHS - RHS = -1.7E-05

D1 > SN_1/ a_1

D1> 1.45 Use D_1 = 2.8 inches

FDR Base

ESAL: 100000 ΔPSI: 2.1

Z_R: -1.645 M_{R3}: 5500 psi

S_0: 0.45

SN_2: 2.8

Solve Equation 2.14 by setting left side equal to right side and using Solver analysis to set that cell equal to 0 by changing SN_2 and D_1, with the constraint that D_2 = 8 inches and D_1 be greater than the minimum required D_1 determined in previous calculations

LHS: 5.000 RHS: 4.999

LHS - RHS = 0

D2 > $(SN_2 - a_1D_1)/ a_2m_2$

D2> 8.000001 Use D_2 = 8.0 inches

C.5 Mix 5 AASHTO Structural Design

a_1:	0.44			E1	430000	psi
a_2:	0.18	m_2	1	E2	137379.7	psi
				E3	5500	psi
ΔPSI:	2.2					

Asphalt

ESAL:	100000	ΔPSI:	2.1	
Z_R:	-1.645	M_{R2}:	137380	psi
S_0:	0.45			

SN_1:	0.7

Solve Equation 2.14 by setting left side equal to right side and using Solver analysis to set that cell equal to 0 by changing SN

LHS:	5.000	RHS:	5.000
LHS - RHS =	0.0		
D1 >	SN_1/ a_1		
D1>	1.53	Use D_1 =	3.0 inches

FDR Base

ESAL:	100000	ΔPSI:	2.2	
Z_R:	-1.645	M_{R3}:	5500	psi
S_0:	0.45			

SN_2:	2.8

Solve Equation 2.14 by setting left side equal to right side and using Solver analysis to set that cell equal to 0 by changing SN_2 and D_1, with the constraint that D_2 = 8 inches and D_1 be greater than the minimum required D_1 determined in previous calculations

LHS:	5.000	RHS:	4.999
LHS - RHS =	0		
D2 >	$(SN_2 - a_1D_1)/ a_2m_2$		
D2>	8	Use D_2 =	8.0 inches

C.6 Mix 6 AASHTO Structural Design

a_1:	0.44			E1	430000	psi
a_2:	0.18	m_2	1	E2	138786.6	psi
				E3	5500	psi
ΔPSI:	2.2					

Asphalt

ESAL:	100000	ΔPSI:	2.2	
Z_R:	-1.645	M_{R2}:	138787	psi
S_0:	0.45			

SN_1:	0.7

Solve Equation 2.14 by setting left side equal to right side and using Solver analysis to set that cell equal to 0 by changing SN

LHS:	5.000	RHS:	5.000

LHS - RHS = 0.0

D1 > SN_1/ a_1

D1>	1.52	Use D_1 =	3.0	inches

FDR Base

ESAL:	100000	ΔPSI:	2.2	
Z_R:	-1.645	M_{R3}:	5500	psi
S_0:	0.45			

SN_2:	2.8

Solve Equation 2.14 by setting left side equal to right side and using Solver analysis to set that cell equal to 0 by changing SN_2 and D_1, with the constraint that D_2 = 8 inches and D_1 be greater than the minimum required D_1 determined in previous calculations

LHS:	5.000	RHS:	4.999

LHS - RHS = 0

D2 > $(SN_2 - a_1D_1)/ a_2m_2$

D2>	8	Use D_2 =	8.0	inches

C.7 Mix 7 AASHTO Structural Design

a_1:	0.44			E1	430000	psi
a_2:	0.19	m_2	1	E2	154523.2	psi
				E3	5500	psi
ΔPSI:	2.2					

Asphalt

ESAL:	100000	ΔPSI:	2.2	
Z_R:	-1.645	M_{R2}:	154523	psi
S_0:	0.45			

SN_1:	0.6

Solve Equation 2.14 by setting left side equal to right side and using Solver analysis to set that cell equal to 0 by changing SN

LHS:	5.000	RHS:	5.000
LHS - RHS =	0.0		

D1 > SN_1 / a_1

D1>	1.42	Use D_1 =	2.8	inches

FDR Base

ESAL:	100000	ΔPSI:	2.2	
Z_R:	-1.645	M_{R3}:	5500	psi
S_0:	0.45			

SN_2:	2.8

Solve Equation 2.14 by setting left side equal to right side and using Solver analysis to set that cell equal to 0 by changing SN_2 and D_1, with the constraint that D_2 = 8 inches and D_1 be greater than the minimum required D_1 determined in previous calculations

LHS:	5.000	RHS:	4.999
LHS - RHS =	0		

D2 > $(SN_2 - a_1 D_1) / a_2 m_2$

D2>	8	Use D_2 =	8.0	inches

C.8 HMA Cost Analysis

Average price of producing HMA:	$49.02 / tonne	1 tonne = 1000 kg
Average HMA density:	2350 kg/m^3	
Pavement length:	1 km	
Pavement width (2 lane):	7 m	

Cost / mm HMA thickness

$$2350\ \frac{kg}{m^3} * 1000\ m * 7\ m * \frac{\$49.02}{1000\ kg} * \frac{1\ m}{1000\ mm} = \frac{\$806.38}{mm\ thickness}$$

Table C-1 HMA cost determination for each mix

Mix	HMA thickness (inches)	HMA thickness (mm)	Cost
1	**4.7**	**119.38**	**$96 265.53**
2	3.6	91.44	$73 735.30
3	3.7	93.98	$75 783.50
4	**2.8**	**71.12**	**$57 349.67**
5	3.0	76.20	$61 446.08
6	3.0	76.20	$61 446.08
7	**2.8**	**71.12**	**$57 349.67**

Appendix D: Mechanistic-Empirical Service Life Analysis

D.1 HMA Service Life Analysis Factors

Analysis completed based on Equations 2.18 – 2.23. Values have been converted from SI units, and are presented in Imperial units

Table D-1 Factors and properties used to evaluate fatigue life of HMA layer

V_b = 5.0 %	k'_1 = 582.8037
V_a = 4.0 %	E_{-10} = 808 503.8 psi
h_{ac} = 3 inches	E_{15} = 610 979.0 psi
M = -0.65071	E_{40} = 72 960.4 psi
C = 0.223506	

Table D-2 Factors and properties used to evaluate permanent deformation of HMA layer

h_{ac} = 3 inches	C_1 = -10.8167
z = 1.5 inches	C_2 = 22.3835
K_1 = 4.279022	

D.2 FDR Permanent Deformation Analysis Factors

Analysis completed based on Equations 2.24 – 2.25. Values have been converted from SI units, and are presented in Imperial units

Table D-3 Dynamic modulus, in psi, for each mix at three analysis temperatures

FDR Mix	14 °F (-10°C)	59°F (15°C)	104°F (40°C)
1	266 811.4	127 198.1	43 206.7
2	285 811.4	126 530.9	47 804.4
3	279 009.1	151 143.8	56 158.6
4	294 296.1	132 970.6	52 387.6
5	261 242.0	112 273.7	43 047.2
6	383 740.8	129 678.2	35 766.3
7	370 556.9	164 893.4	58 464.7

Table D-4 Material water content as a percentage, calculated from Equation 2.25D, with ground water table at depth of 10 feet.

FDR Mix	14 °F (-10°C)	59°F (15°C)	104°F (40°C)
1	1.68	2.90	6.43
2	1.60	2.91	5.97
3	1.63	2.55	5.30
4	1.56	2.81	5.58
5	1.71	3.18	6.45
6	1.28	2.86	7.39
7	1.32	2.39	5.14

D.3 FDR Permanent Deformation Analysis Factors (cont)

Table D-5 Material property factor, β_2, calculated from Equation 2.25A.

FDR Mix	14 °F (-10°C)	59°F (15°C)	104°F (40°C)
1	0.22866	0.21760	0.18855
2	0.22943	0.21750	0.19212
3	0.22916	0.22068	0.19740
4	0.22975	0.21843	0.19518
5	0.22841	0.21515	0.18842
6	0.23235	0.21796	0.18133
7	0.23204	0.22211	0.19865

Table D-6 Material property factor, ρ, calculated from Equation 2.25C.

FDR Mix	14 °F (-10°C)	59°F (15°C)	104°F (40°C)
1	1077.4	1552.4	5057.4
2	1051.7	1557.8	4283.5
3	1060.5	1396.6	3390.4
4	1041.4	1508.5	3734.3
5	1085.7	1692.8	5089.8
6	961.5	1532.9	7232.8
7	970.7	1331.3	3214.9

D.4 FDR Permanent Deformation Analysis Factors (cont)

Table D-7 Material property factor, $\varepsilon_0/\varepsilon_r$, calculated from Equation 2.25B.

FDR Mix	14 °F (-10°C)	59°F (15°C)	104°F (40°C)
1	20.8829	21.1191	22.1107
2	20.8684	21.1215	21.9501
3	20.8734	21.0473	21.7357
4	20.8626	21.0993	21.8226
5	20.8875	21.1799	22.1170
6	20.8159	21.1104	22.4802
7	20.8214	21.0157	21.6889

Table D-8 Other factors used to evaluate FDR Permanent Deformation

$\beta_1 = 1.673$
GWT = 10 ft
h = 6 inches

D.5 Unbound Granular Base Permanent Deformation Analysis Factors

Table D-9 Factors and properties used to evaluate permanent deformation of unbound granular base

$\beta_1 = 1.673$	$W_c = 16.95$
h = 12 inches	$B_2 = 0.1230$
GWT = 10 ft	$\rho = 782\ 337.7$
$M_R = 11\ 603.0$ psi	$\varepsilon_0/\varepsilon_r = 30.2825$

D.6 Results of KENPAVE Mechanistic Analysis and Predicted Service Life

Table D-10 Mechanistic analysis results, and predicted cycles to fatigue and permanent deformation failure for pavement structure at -10°C

-10°C

Mix:	$\varepsilon_{t,\ HMA}$	$\varepsilon_{r,\ HMA}$	$\varepsilon_{v,\ FDR}$	$\varepsilon_{v,\ SB}$	$N_{f,allow\ HMA}$	$N_{r,0.5in\ PD}$	$\delta_{a\ HMA}$	$\delta_{a\ FDR}$	$\delta_{a\ SB}$	δ_{total} (in)
1	7.595E-05	1.223E-05	1.8360E-04	3.469E-04	**1.660E+11**	**2.090E+10**	0.3031	0.0380	0.1585	0.50
2	6.911E-05	1.166E-05	1.7380E-04	3.377E-04	**2.409E+11**	**2.398E+10**	0.3087	0.0360	0.1551	0.50
3	7.149E-05	1.185E-05	1.7720E-04	3.409E-04	**2.108E+11**	**2.289E+10**	0.3068	0.0367	0.1563	0.50
4	6.628E-05	1.143E-05	1.6970E-04	3.339E-04	**2.842E+11**	**2.539E+10**	0.3110	0.0351	0.1536	0.50
5	7.811E-05	1.242E-05	1.8680E-04	3.497E-04	**1.486E+11**	**2.000E+10**	0.3014	0.0386	0.1596	0.50
6	4.273E-05	9.850E-06	1.3640E-04	3.010E-04	**1.609E+12**	**3.946E+10**	0.3310	0.0283	0.1405	0.50
7	4.560E-05	1.001E-05	1.4050E-04	3.052E-04	**1.245E+12**	**3.753E+10**	0.3285	0.0291	0.1423	0.50

D.7 Results of KENPAVE Mechanistic Analysis and Predicted Service Life (cont.)

Table D-11 Mechanistic analysis results, and predicted cycles to fatigue and permanent deformation failure for pavement structure at 15°C

	15°C									
Mix:	$\varepsilon_{t,\ HMA}$	$\varepsilon_{r,\ HMA}$	$\varepsilon_{v,\ FDR}$	$\varepsilon_{v,\ SB}$	$\mathbf{N_{f,allow\ HMA}}$	$\mathbf{N_{r,0.5in\ PD}}$	$\delta_{a\ HMA}$	$\delta_{a\ FDR}$	$\delta_{a\ SB}$	δ_{total} (in)
1	1.666E-04	3.042E-05	3.4220E-04	4.778E-04	**1.068E+10**	**1.588E+07**	0.2277	0.1269	0.1456	0.50
2	1.674E-04	3.051E-05	3.4360E-04	4.787E-04	**1.048E+10**	**1.569E+07**	0.2271	0.1273	0.1457	0.50
3	1.402E-04	2.771E-05	2.9980E-04	4.496E-04	**2.111E+10**	**2.274E+07**	0.2463	0.1126	0.1412	0.50
4	1.597E-04	2.970E-05	3.3080E-04	4.705E-04	**1.262E+10**	**1.745E+07**	0.2326	0.1231	0.1445	0.50
5	1.866E-04	3.254E-05	3.7600E-04	4.986E-04	**6.826E+09**	**1.216E+07**	0.2143	0.1379	0.1485	0.50
6	1.636E-04	3.010E-05	3.3720E-04	4.746E-04	**1.148E+10**	**1.655E+07**	0.2299	0.1252	0.1452	0.50
7	1.276E-04	2.645E-05	2.8010E-04	4.358E-04	**3.062E+10**	**2.704E+07**	0.2555	0.1058	0.1388	0.50

D.8 Results of KENPAVE Mechanistic Analysis and Predicted Service Life (cont.)

Table D-12 Mechanistic analysis results, and predicted cycles to fatigue and permanent deformation failure for pavement structure at 40°C

	40°C									
Mix:	$\varepsilon_{t,\ HMA}$	$\varepsilon_{r,\ HMA}$	$\varepsilon_{v,\ FDR}$	$\varepsilon_{v,\ SB}$	**$N_{f,allow\ HMA}$**	**$N_{r,0.5in\ PD}$**	$\delta_{a\ HMA}$	$\delta_{a\ FDR}$	$\delta_{a\ SB}$	δ_{total} (in)
1	3.990E-04	6.179E-04	1.1960E-03	8.944E-04	**5.164E+09**	**4554**	0.2247	0.1928	0.0827	0.50
2	3.415E-04	6.135E-04	1.0890E-03	8.734E-04	**9.547E+09**	**5145**	0.2366	0.1805	0.0831	0.50
3	2.578E-04	6.093E-04	9.3640E-04	8.402E-04	**2.898E+10**	**6137**	0.2557	0.1613	0.0831	0.50
4	2.926E-04	6.115E-04	9.9950E-04	8.545E-04	**1.758E+10**	**5694**	0.2475	0.1694	0.0831	0.50
5	4.012E-04	6.181E-04	1.2000E-03	8.952E-04	**5.053E+09**	**4533**	0.2243	0.1932	0.0827	0.50
6	5.176E-04	6.277E-04	1.4240E-03	9.338E-04	**1.848E+09**	**3563**	0.2030	0.2159	0.0815	0.50
7	2.386E-04	6.082E-04	9.0170E-04	8.319E-04	**3.934E+10**	**6398**	0.2603	0.1567	0.0831	0.50